SOME MIXING FLOWS
OF
INDUSTRIAL RELEVANCE

by

Vinaben Bodalia B.Sc.

Thesis submitted to the C.N.A.A. in partial fulfilment of the requirements for the degree of Doctor of Philosophy

The collaborating establishment was

Unilever Research Ltd.

Department of Chemical Engineering and Mathematics and Computer Science

The Polytechnic of Wales

Pontypridd

December 1986

To Mum and Dad

CERTIFICATE OF RESEARCH

This is to certify that, except where specific reference is made, the work described in this thesis is the result of the investigation carried out by the candidate.

Candidate V Bodalia

Director of Studies W H Granville

DECLARATION

This is to certify that neither this thesis nor any part of it has been presented or is being concurrently submitted in candidature for any other degree than the degree of Doctor of Philosophy of the C.N.A.A.

Candidate V Bodalia .....

ACKNOWLEDGEMENTS

I wish to express my gratitude to my Director of Studies, Dr. W. H. Granville and to my supervisors Dr. R. W. Williams, Dr. D. G. Knight and Dr. T. H. Hammond for their invaluable guidance and encouragement throughout the period of investigation.

I am particularly indebted to the Technical Staff of the Chemical Engineering Department for their assistance during the research period, to the Computer Centre Staff for the advice given in the course of computational work and to the Staff of the Media Resources unit for the use of their video facilities.

Appreciation is also tendered to Dr. P. R. Williams of University College, Swansea for carrying out rheological tests on one of the fluids used for this research.

Thanks are due to Neal, Angela, Philip and the Porters of the Polytechnic for their friendship and unfailing support. Sincere thanks are especially extended to my Parents, for without their support, everlasting patience and encouragement this work could not have been accomplished.

Finally, I would like to express special thanks to my fiancé Mahesh for undertaking the difficult task of typing this thesis.

SUMMARY

In this thesis, theoretical and experimental investigation is undertaken into the steady mixing flows generated by rotating cylindrical and disc stirrers in Newtonian and non-Newtonian fluids. No mixing study is carried out.

In Chapter 1, we briefly discuss the importance of the low speed mixing of fluids together with the processes involved and the different types of agitators and fluids found in common industrial applications.

The literature reviewed in Chapter 2 covers previous work in flow visualisation techniques, power consumption of stirrers, fluid particle velocities and theoretical studies of flows. The chapter ends with an outline of the advantages and disadvantages of the techniques used by other investigators and the reasons for developing new methods for the purpose of this research.

In Chapter 3, a description is given of the experimental arrangement and the flow visualisation technique used for this study. The procedure adopted along with the choice of the particular rotors and fluids studied are outlined. Also described are the methods used for characterisation of the test fluids and the mode in which various parameters were calculated.

The theoretical and numerical methods which are employed in this work to simulate the experimental flows are detailed in Chapter 4. Numerical results obtained from these methods are compared with those of other workers for similar arrangements in Chapter 5.

Experimental and theoretical results obtained for primary flows are presented and compared in Chapter 6 with the corresponding results for secondary flows discussed in Chapter 7. Couple values, Power numbers and discharge efficiencies obtained numerically are given in Chapter 8, together with a comparison of the theoretical and experimental couple values for the geometries investigated. All diagrams showing the results for Chapters 5, 6, 7 and 8 are given at the end of each chapter, while others are shown in the text.

Finally, Chapter 9 outlines the conclusions reached from the work carried out and presents suggestions for possible future improvements and developments of the computer and experimental methods. Listings of some of the computer programs used for experimental and theoretical work and a copy of a published paper containing results of our preliminary investigations are given in the appendices.

CONTENTS

			PAGE
		ACKNOWLEDGEMENTS	
		SUMMARY	
CHAPTER 1		INTRODUCTION	1
	1.0	Background	1
	1.1	The Mixing Process	1
	1.2	Types of Agitators	5
	1.3	Types of Fluids	5
	1.4	Understanding Mixing	8
CHAPTER 2		LITERATURE SURVEY	11
	2.0	Introduction	11
	2.1	Mixing	11
	2.2	Flow Visualisation Techniques	13
	2.2.1	Trace Particle Techniques	13
	2.2.2	Air Entrainment Techniques	15
	2.2.3	Dye Techniques	15
	2.2.4	Miscellaneous Techniques	16
	2.3	Experimental Power Consumption	16
	2.4	Fluid Particle Velocities	17
	2.5	Birefringence	19
	2.6	Theoretical Studies of Flows	19
	2.6.1	Analytical Studies	20
	2.6.2	Numerical Studies	21
	2.7	Conclusion	23

CHAPTER 3		EXPERIMENTAL WORK	25
	3.0	Introduction	25
	3.1	Description of Initial Apparatus	25
	3.1.1	Flow Visualisation Technique	31
	3.2	Materials	32
	3.3	Choice of Stirrers	36
	3.4	Familiarisation and Experimental Procedure	37
	3.4.1	Couple Measurements	41
	3.4.2	Viscometric Experiments	41
	3.5	Modification of Apparatus	44
	3.6	Primary Flows	46
	3.7	Secondary Flows	50
CHAPTER 4		MATHEMATICAL MODELLING	56
	4.0	Introduction	56
	4.1	Equations	56
	4.2	Primary Flow Simulation	59
	4.2.1	Cylindrical Stirrer	59
	4.2.2	Couple on the Cylindrical Stirrer	63
	4.2.3	Disc Stirrer	63
	4.2.4	Couple on the Disc Stirrer	65
	4.2.5	Power Number	66
	4.2.6	Finite Difference Approximation and Paddon's Method	66
	4.2.7	Pao's Method	70
	4.3	Secondary Flow Simulation	74
	4.3.1	Cylindrical Stirrer	74
	4.3.2	Discharge Efficiency	82
	4.3.3	Disc Stirrer	83
	4.4	Conclusion	85

CHAPTER 5	JUSTIFICATION OF THE MATHEMATICAL METHOD AND THE COMPUTER PROGRAMS	86
5.0	Introduction	86
5.1	Results from the Finite Difference and Finite Element Methods	87
5.2	Results from Pao's and Paddon's Methods	87
5.3	Comparison of our Results with those of Pao	88
5.4	Results for the Cylindrical and Near-Cylindrical Disc Stirrers	89
5.5	Comparison of our Results with those of Spragg	90
5.6	Comparison With Other Work	92
5.7	Conclusion	93
CHAPTER 6	PRIMARY FLOW RESULTS	110
6.0	Introduction	110
6.1	Results From Viscometric Experiments	110
6.2	Flow Patterns	111
6.3	Angular Velocity Distributions	112
6.4	Shear Rate Distributions	114
6.5	Conclusion	116
CHAPTER 7	SECONDARY FLOW RESULTS	137
7.0	Introduction	137
7.1	Flow Patterns	137
7.2	Angular Velocity Distributions	138
7.3	Shear Rate Distributions	141
7.4	Streamlines	142
7.5	Vorticity Results	146
7.5.1	Incompressibility Results	148
7.6	Conclusion	148

CHAPTER 8		FURTHER RESULTS	167
	8.0	Introduction	167
	8.1	Variation of Numerical Couple and Power Number with Gap Size y_b	167
	8.2	Variation of Numerical Couple and Power Number with Step Size h	168
	8.3	Variation of Couple with Reynolds Number	168
	8.4	Numerical Discharge Efficiencies	170
	8.5	Comparison of Theoretical Couples with Experimental Couples	171
	8.6	Conclusion	172
CHAPTER 9		CONCLUSIONS AND SUGGESTIONS FOR FUTURE WORK	183
	9.0	Conclusions	183
	9.0.1	Comparison of Theoretical Results with Experimental Results	185
	9.0.2	Couple Values, Power Numbers and Discharge Efficiencies	186
	9.1	Suggestions for Future Work	187
LIST OF REFERENCES			189
NOMENCLATURE			196
APPENDICES			199

CHAPTER 1

INTRODUCTION

1.0 Background

This thesis is concerned with the study of the flows generated by the mixing or blending of liquids. Mixing is perhaps the most common operation in the chemical processing and allied industries. For example, it is of vital importance in the mining, food, petroleum, chemical, biochemical - for the fermentation of broths, pharmaceuticals and power industries and also in municipal and industrial waste treatment. However, it has received very little study and has proved intractable to a rigid theoretical analysis. Therefore, in comparison with the more theoretically developed chemical engineering operations, such as multicomponent distillation, mixing is still regarded as something of an art.

Mixing is a process which has been used by man as far back as he can remember; using simple tools, such as a wooden spoon or fork or even one's hand to achieve the final product of the required consistency. Even at home a simple industrial mixer is used for mixing cement and the advent of the Kenwood mixer has proved extremely beneficial and quick for the busy housewife.

1.1 The Mixing Process

Quillen [75] defined mixing as the 'intermingling of two or more dissimilar portions of a material resulting in the attainment of a desired level of uniformity, either physical or chemical in the final product'. Without external forces, mixing in liquids occurs by natural diffusion and is relatively slow. Therefore, liquid mixing is most commonly accomplished by utilizing the mechanical energy, or power, generated by

rotating an agitator, or stirrer, in the liquid. However, it is important that the correct type of agitator is used to avoid wastage of this energy.

When a stirrer is rotating in a confined liquid mass (Fig. 1.1) it generates liquid streams of high speeds in the vicinity of the stirrer. These move towards the stagnant or slower moving regions of liquid which in turn replace the void created by the fast moving liquid, hence creating a form of pumping action. This process eventually results in uniform mixing by momentum transfer. A high degree of mixing occurs when the entire liquid mass is under fast moving and disordered flow conditions. The quantity of mechanical energy required to give this condition is dependent upon the vessel and agitator geometry and on the physical properties, such as the viscosity, or thickness, of the liquids being mixed. For more viscous liquids, for example non-drip paints the mixing process is more difficult. Viscosity is the property of a liquid to resist the flow through internal forces and molecular attraction. These forces retard the high velocity streams and confine them to the immediate vicinity of the stirrer only, hence leaving regions where mixing does not occur. Therefore, in general the thicker the liquid the greater is the energy required to produce mixing.

When low viscosity liquids are mixed at high speeds vortexing may develop. This is when the liquid which swirls in the direction of the agitator rotation causes a drop in liquid level around its shaft (Fig. 1.2), hence generating a whirlpool type effect. This type of flow is undesirable since it gives poor mixing. However, it may be minimised by the installation of baffles, which take the form of thin vertical strips mounted against the walls of the vessel and help to reduce vortexing. For high viscosity liquids the need for baffles is relatively less.

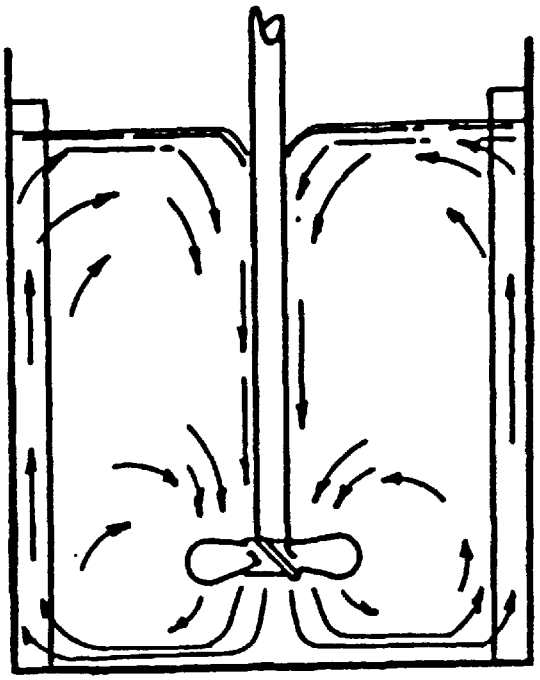

Figure 1.1 Liquid flow generated by a rotating stirrer.

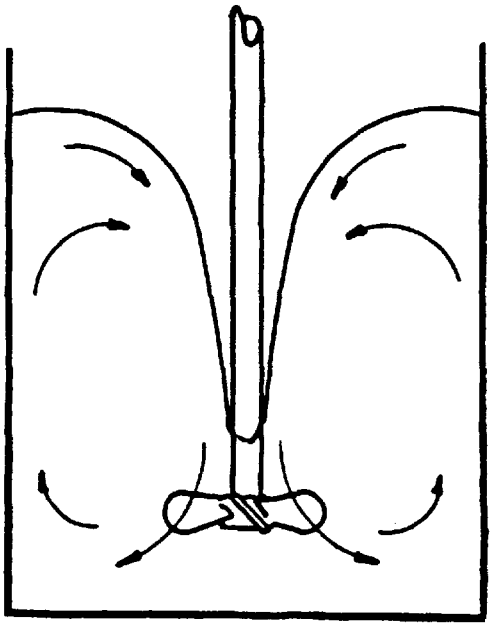

Figure 1.2 Vortex formation in an unbaffled vessel.

There are essentially three regimes of flow in mixing. These are shown in Figure 1.3, which is a plot of the Power number (representing the power drawn by an agitator) versus the Reynolds number Re (representing the speed of the flow). At low speeds, the viscous or laminar regime occurs where the inertial forces are negligible and the liquid moves in more or less closed loops determined by the geometry of the mixer. This is also known as primary flow. Velocity gradients between adjacent fluid particles exist in the vessel which give rise to shear and stretching deformations. The movement of a layer of molecules relative to parallel adjacent layers is known as shear. Mixing under laminar flow conditions is highly inefficient since both shearing and stretching as well as molecular diffusion are very slow processes. At slightly higher speeds the flows become more unstable with these processes becoming more pronounced and the transition or streamline regime occurs. This is also known as secondary flow and is superimposed over the primary flow.

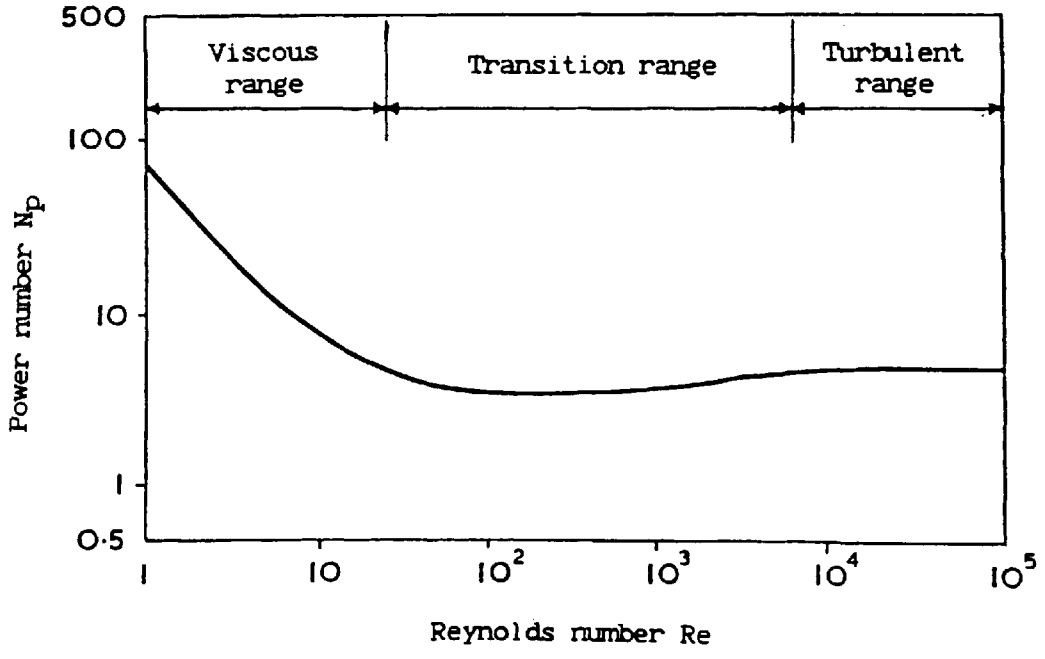

Figure 1.3 A Power curve for a typical mixing configuration

At very high speeds, the flow breaks down into the turbulent regime. This is when the flow is random and more efficient mixing occurs. For the purpose of this research, we shall restrict ourselves to orderly non-turbulent flows.

1.2 Types of Agitators

In general, agitators may be classified into the following two groups :-

(i) Agitators with a small blade area which rotate at high speeds. These include Rushton turbines, such as the six-blade flat blade turbine and marine type propellers (Fig. 1.4). They are used to mix low to medium viscosity liquids, such as oils, resins and syrups.

(ii) Agitators with a large blade area which rotate at low speeds. These include anchors, gates, paddles, helical ribbons and helical screws (Fig. 1.5). They are used to mix relatively high viscosity liquids such as stiff pastes and putties.

More details of the various types of agitators available and their uses may be found in standard texts [36, 58, 64].

1.3 Types of Fluids

Liquids may be classified into two main groups :-

(i) Newtonian Fluids

The viscosities of these fluids do not change with either time or any applied forces or deformations. Water, syrup and glycerol are typical examples.

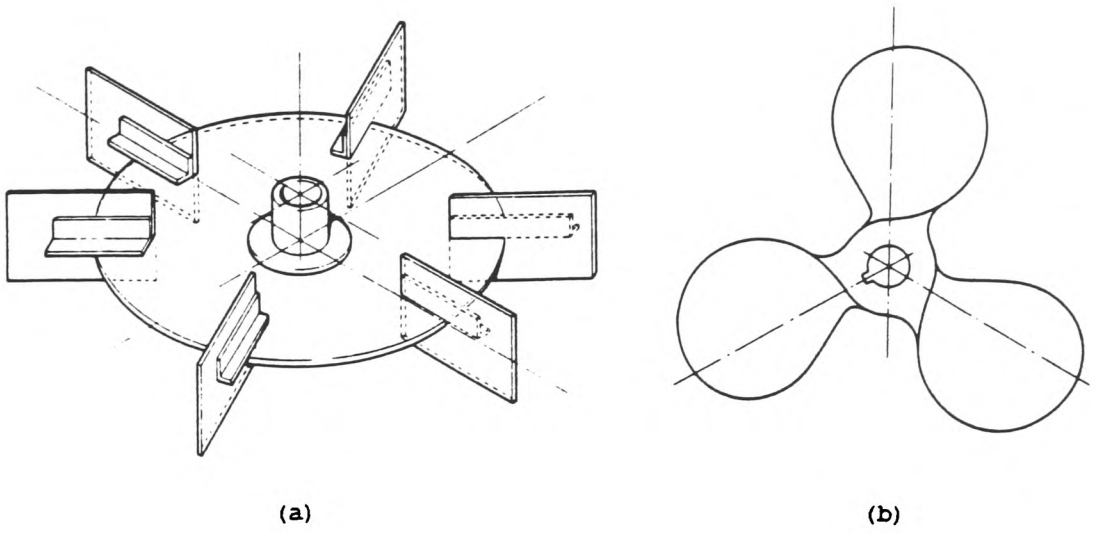

Figure 1.4 A six blade flat blade turbine (a) and a marine propellor (b).

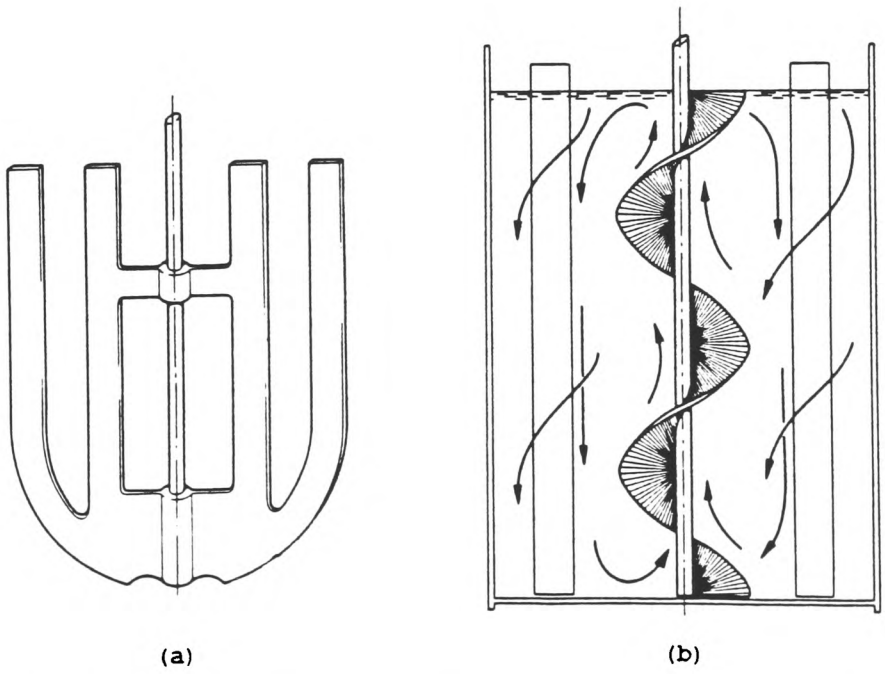

Figure 1.5 A gate type anchor agitator (a) and a helical screw agitator (b).

(ii) Non-Newtonian Fluids

The viscosities of these fluids change with either time or any applied forces. This group may further be divided into the following :-

(a) Pseudoplastic (or shear-thinning) fluids whose viscosities decrease with shear forces. They are the most common type of non-Newtonian fluids and include various body fluids, pharmaceuticals and liquid food products, soaps and detergents and many more.

(b) Dilatant (or shear thickening) fluids whose viscosities increase with shear forces. Various concentrations of starch slurries exhibit this property.

(c) Thixotropic fluids whose viscosities decrease with time but there is no change with any applied forces. Non-drip paints show this property.

(d) Rheopectic fluids which are rare and whose viscosities increase with time include latex solutions.

(e) Viscoelastic fluids which exhibit an elastic type effect. These include some doughs and egg white.

(f) Plastic fluids which have the property of being able to suspend abrasive particles. They possess a property known as the 'apparent' yield stress. Jif is a typical example.

We shall only deal with Newtonian and pseudoplastic liquids and shall not be concerned with the other liquids mentioned above due to their inherent complexity.

The combination of the various agitators, fluids and types of flows involved all complicate the problems encountered in mixing.

1.4 Understanding Mixing

In order to understand the mixing phenomena in stirred vessels, it is essential to make accurate observation of the fluid mechanics. This is because a wide range of interactions can occur and observations allow a quick assessment of the quality of mixing in relation to the required condition. However, observations alone are not sufficient and certain experimental measurements are also necessary. Furthermore, experimental observations and quantities need to be complimented by theoretical investigations as is discussed below.

It seems appropriate here to mention that theoretical analysis of mixing flows is by no means straightforward. For example, consider the commonly used geometry of a six-bladed Rushton Turbine (Fig. 1.4) mounted coaxially on a shaft in a cylindrical baffled vessel. Attempts by many workers (which are referenced by Spragg [85]) have been made to predict the flow of a Newtonian fluid in this relatively complex geometry. However, there is much uncertainty attached to the mathematical modelling of fluid flows in such geometries and, therefore, it seems only sensible to carry out work on simpler systems involving laminar or slow flows which can more easily be examined both experimentally and theoretically. Encouraging results on simple mixing systems may then lead to work on more complicated systems.

If mathematical models closely describe experimental work carried out on simple geometries on the small scale, predictions of mixing parameters, such as the degree of mixing and power consumption on more complex geometries on the larger scale may be made. This is extremely important in the chemical industries, since without the basic experimental work and mathematical modelling predictions would not easily be possible. This would inevitably lead to a wastage of time, money and effort as

one would need to resort to experimentation at all scales, large and small, by trial and error alone. From the above discussion we can see that there is a clear need to undertake some basic research work enabling a better comprehension of the flows involved in mixing. It is, therefore, the intention of this research project to contribute to the understanding of the flows involved in the low speed mixing of viscous fluids.

Initial investigations are carried out on the flows induced by a finite cylinder rotating in a cylindrical vessel containing the fluid. Both experimental and theoretical studies are performed on this system. This then leads to investigations on the relatively more complicated flows generated by a finite disc rotating under similar conditions. The finite disc forms a rather simple version of the common Rushton Turbine except that it has no blades. Therefore, successful work on the disc may eventually be extended to include the Rushton Turbine.

A novel flow visualisation technique is developed for the purpose of observing the flows induced in the above geometries (see Chapter 3 for full details). From this technique quantitative measurements are carried out and certain parameters associated with mixing flows calculated.

Power consumption of the mixing system is an important quantity, since in industrial applications the most efficient mixing system together with the least power input is required. Therefore , this quantity is also determined.

Furthermore, theoretical values of the mixing parameters are obtained using computer techniques. These are compared with the experimentally determined values and the results are discussed in the latter part of this thesis.

It is hoped that the flow visualisation and theoretical techniques developed in this project will help to provide a 'stepping stone' for further work in the field of mixing. The work carried out here may be extended to include the study of more complicated rotors and fluids and also of colour band mixing. Even the more complex flows generated by the inclusion of baffles may eventually be studied. Thus, there is much work to be carried out before the phenomenon of mixing is fully understood.

CHAPTER 2

LITERATURE SURVEY

2.0 Introduction

It is of great benefit, and therefore important, to study previous work carried out in the field of mixing. This is because it would enable one to become familiar with experimental and theoretical techniques which have already been developed and also enable one to decide whether to use the ideas behind these methods or not. Furthermore, if it is known which mixing systems and types of flows have already been investigated, then no repetition will occur and investigations may be carried out on new systems, thus making progress in the field.

Therefore, with the above in mind a literature survey was carried out and is reviewed in this chapter. The review covers work in :-

(i) Mixing

(ii) Flow visualisation techniques

(iii) Power consumption

(iv) Fluid particle velocities

(v) Birefringence

(vi) Theoretical studies of flows

2.1 Mixing

A host of literature on mixing, either in the form of papers or books is available. A very comprehensive review of the field of mixing was carried out by Quillen [75] who has had many years of practical experience in this field. He compiled a descriptive review of the principal kind of mixers that exist and their many applications. Rushton [78] in a later article also gave a review on mixing.

He covered literature on not only the mixing of liquids, but also on the mixing of pastes and solids. Literature on the mechanical mixing of elastic liquids was summarised by Ulbrecht [89] who also commented briefly on scale up. In their recent paper, Collias and Prud'homme [18] also survey work on mixing of elastic fluids.

Books such as that by Nagata [58], Oldshue [64] and others [19, 36, 39] deal with the phenomena of mixing in general. They cover the numerous types of agitators that are available and the conditions under which they are utilised. Different kinds of liquids are characterised into general groups according to their properties and discussions on power requirement and scale-up are also carried out. In most cases, mixing is based on experimental work and design methods upon empirical correlations rather than on comprehensive theoretical analysis.

Spragg et al [85] are perhaps the first to carry out a theoretical analysis of actual mixing. In their recent paper, they discuss a theoretical approach to the investigation of the streamline flow and mixing induced by a disc rotating in a vessel containing the fluid. Equations are developed to predict the concentration of a band of coloured tracer fluid as it is transported through the mixing vessel. These equations are then solved using computer simulation techniques enabling mixing rates and concentrations to be determined.

In general, it can be concluded from the above review that much work, both experimentally and theoretically, needs to be carried out on actual mixing to be of any help in industry. Of course, basic work in mixing flows should be carried out initially before proceeding to more complicated flows which are encountered in 'real mixing'. This project aims to make a contribution to the field of mixing by studying the mixing flows induced by simple stirrers.

2.2 Flow Visualisation Techniques

As mentioned in Chapter 1, it is important to be able to make accurate observations of the flows involved in mixing. Being able to see what is happening inside the mixing vessel helps tremendously in the comprehension of the mixing phenomenon and is far more meaningful than only speculative predictions. Therefore, it is essential to review literature on flow visualisation to see which techniques are available.

A number of flow visualisation techniques (from simple camera to more complicated laser techniques) have been used to study the flow patterns of fluids around various types of agitators and fluid flows in general. These may be classified into four groups and are discussed below.

2.2.1 Trace Particle Techniques

Many scientists have used trace particles, for example aluminium, highly reflective titanium oxide coated mica (Timica) or polystyrene to follow the flow induced by rotating agitators. Many variations of this technique have been used and have proved very popular, since not only can flow patterns be determined, but in some cases also the velocities and other parameters. The fluids under investigation have usually been transparent enabling the particles to be seen clearly.

There are essentially two methods of illuminating the flows under investigation; either a relatively simple light source or a more complicated laser light source. The 'light-streak' technique developed by Sach [79] was used by Metzner and coworkers [51 - 54] to study flows generated by rotating turbine impellers. The technique utilized a relatively simple arc lamp. Cairncross and Hansford [10] used a halogen projector lamp to study the flows due to rotating spheres and

discs, while Peters and Smith [70 - 72] made use of fluorescent and theatrical spot lamps to illuminate the flows induced by rotating anchors. No mention of special lighting systems is made and, therefore, it is assumed that uncomplicated types of light sources were used by other investigators, such as: Sato [80] who observed flows in rectangular mixing vessels; Kuriyama et al [46] for visualising flows induced by rotating anchors and by Kuwahara et al [47] for investigating flows past an elliptic cylinder started impulsively. In the latter case aluminium dust together with electrolysis methods were used.

A more recent method of illuminating the flow field under investigation is that utilising a helium-neon laser light source [18, 27]. This method although expensive and more complicated than those mentioned above is fairly populer and has widely been used. Both the 'laser-speckle' technique used by Binnington et al [6] and the 'laser-doppler' technique used by Cochrane et al [16, 17] and Poulter and Snaddon [69] make use of lasers as a light source.

Being able to just visualise the flows at the time of experimentation is not enough. Permanent records which may be studied at a later date are important, as this enables a closer study of the flows to be carried out. Perhaps the most popular and simple method of recording flow patterns is via a view camera [10, 51 - 54] or cine camera [70 - 72]. However, a more modern technique utilises a video camera [24, 60] which gives records of flows which may be replayed more easily. Most of the flow visualisation techniques discussed in this section used one of these methods of recording the fluid flows.

A different method of flow visualisation was that used by Dijkstra and Van Heijst [23]. The path of small particles in the fluid was

visualised by means of a stroboscope and their positions determined by stereophotography with two cameras being used for recording the flows.

2.2.2 Air Entrainment Techniques

This is a very simple and effective technique for obtaining flow patterns. It has been used by Nienow et al [60] and Shan-Sheng [82] to study fluid flows in various geometries. The secret behind this method is that the fluid must be moving at fast speeds to enable air bubbles to be entrained in it.

2.2.3 Dye Techniques

Another method of flow visualisation which is very popular is the dye technique used by White et al [106, 107] to look at flow patterns around a number of different agitators. The dye is injected into the fluid under investigation via a hypodermic needle and the flows are recorded by a camera. This technique as a means of flow visualisation was used by Griffiths et al [29] to study flows around a finite rotating disc; by Walters and Savins [97] to look at flows due to a rotating solid sphere; by Ulbrecht [89, 90] to determine the flow patterns generated by rotating spheres and discs; by Hill et al [33] to observe flows in the disc and cylinder system and by Mena et al [50] to study the flow through oscillating pipes. Townsend et al [88], Gad-el-Hak [27] and Collias and Prud'homme [18] all used similar dye techniques to study flows while a photochromic dye technique was used by Dembek [21]. This latter method allowed reversible colouring without contamination of the fluid.

2.2.4 Miscellaneous Techniques

Although not a very popular technique, the electrochemical method has been used by certain scientists. Quraishi [76] used this method together with analytical indicators to study fluid flow while Jaksic [40] used an electrochemical method whereby zinc was deposited enabling the flow to be seen.

A relatively new technique was developed by Mann and Kynsh [49] to study flows. Acid and alkali tracers were introduced simultaneously into the fluid at different positions within the vessel. Visualisation of the acid and alkali reacting were achieved by shading back-mixed cells with hatchings equal to the pH. Computer simulations of these shaded diagrams were then output directly into a 16 mm movie film.

Finally, most of the techniques discussed so far have dealt essentially with flows in transparent liquids. Ultrasound techniques have been used for visualising flows in opaque fluids, such as in the medical field, to observe the development of a foetus in a pregnant woman.

2.3 Experimental Power Consumption

Very often when too much power or energy is input into a system and is not necessary to achieve the desired quantity of mixing, it is obviously a waste of both energy and more importantly money. On the other hand if too little power is input, the required pumping may not be achieved and thus more time may be required to give mixing, again with loss of money. Therefore, it is essential to have an optimum mixing system with the least power input to avoid wastage of time and money.

Both experimental and theoretical studies have been carried out on the determination of the power consumption of stirrers. In this section, the experimental techniques used to determine the power required is reviewed. Theoretical studies enabling predictions to be made of the power needed in the mixing systems is reviewed in section 2.6.

A number of methods exist to determine the power required in mixing. The most common, however, is probably that in which the torque or couple exerted on the stirrer is measured via a dynamometer. From this the power may then be calculated. Peters [70], Metzner and Taylor [54], Walters and Savins [97], Chavan et al [11], Griffiths et al [29], Pasquali et al [68], Nienow et al [59] and Hocker et al [34] all used variations of the dynamometer method to obtain power measurements.

Collias and Prud'homme [18], Ayazi Shamlou and Edwards [2], Foresti and Liu [25], Honji et al [35], Kuwahara et al [47], Metzner and Otto [51, 52], Nienow and Coworkers [60], O'Kane [62], and Sato [80] all used variations of the strain gauge method to obtain power consumption in their respective mixing geometries.

Sestak et al [81] obtained torque measurements using a rotational rheometer Rheotest, while Walters [96] utilised a Contraves balance rheometer. Cheng [13], however, used a Brabender Plastograph which provided torque measuring facilities.

2.4 Fluid Particle Velocities

Fluid particle velocities are important in mixing flows as they may be used to determine other quantities, such as shear rates and mixing times. However, very little work has been carried out to determine the necessary speeds.

Metzner and Taylor [54] used the 'light-streak' technique whereby a view camera was utilised to photograph trace particles for known exposure times. From the photographs, the lengths of the trace particle streaks were measured enabling the fluid velocities and local shear rates to be determined. Cairncross and Hansford [10] and Kuriyama et al [46] used a very similar method of obtaining velocity profiles and shear rates (see Chapter 3).

Peters and Smith [71] recorded the movement of tracer particles using a cine-camera. A projector was used to 'throw' the film frame by frame onto fixed tracing paper and successive positions of the particles marked on it. Knowing the camera filming speeds and the distance the particle travelled in a fixed time enabled the local fluid velocities and shear rates to be calculated.

Desouza [22] determined velocities in high and low velocity regions of his geometry using a pitot tube and a hot-wire anemometer respectively.

A more expensive technique is that of laser-speckle photography used by Binnington et al [6] to determine fluid velocities in flows. A similar Laser-Doppler Velocimeter technique was used by Cochrane et al [16] to obtain point velocity measurements in fluids.

The method of stereophotography together with tracer particles was used by Dijkstra and Van Heijst [23] to obtain velocities in three-dimensions. The particle motion was visualised by means of a stroboscope. Again knowing the distance travelled by the particle and the time between two successive points, the local fluid velocities were determined.

2.5 Birefringence

Laser techniques [86, 91] have been used to experimentally determine the birefringence or stresses in simple two-dimensional flows only. In this research we are concerned with more complicated three-dimensional flows for which the determination of birefringence is far more difficult and, therefore, is not carried out.

2.6 Theoretical Studies of Flows

It was mentioned earlier that without theoretical models prediction of flows for complex geometries would not be easy as any design procedures, scale up methods etc. would need to be based purely on experimentation at all levels, by trial and error alone. However, a number of scientists have carried out theoretical studies in the field of mixing flows.

The theoretical equations due to the flow of various fluids around different types of stirrers have been solved mathematically both by analytical and numerical methods. Generally speaking, analytical methods have been used to solve the equations related to the flows of Newtonian fluids around simple stirrers, such as the rotation of spheres. As the geometry becomes more complicated, the flow faster and the fluids non-Newtonian, the flows become extremely complex mathematically. Analytical predictions of these flows fail and numerical procedures need to be used. In this section, the theoretical work carried out on the rotation of stirrers together with the conditions (that is, type of fluid and Reynolds number Re) under which they have been studied, has been reviewed. Since Reynolds number is a

representation of the speed of the rotor the higher the speed the higher is the Reynolds number. The objective is to summarize whether the laminar or streamline flows under consideration have been solved by analytical or numerical methods. Turbulent flows are not considered. The details of the technique used is not given as full details may be found in the reference.

2.6.1 Analytical Studies

Fluids flowing with $Re \rightarrow 0$ (Primary Flow)

The flow of Newtonian fluids in various geometries has been studied analytically and solutions for the fluid velocities together with equations for couple values may be found in a standard text [95]. Analytic methods were also used by Jeffrey [41] to solve the equations due to Newtonian fluids flowing around a number of different rotating stirrers of ellipsoidal shape.

Van Wazer [92] and Borne [9] both used analytical techniques to solve for the flows of non-Newtonian fluids between concentric cylinders of infinite length and concentric spheres respectively. Theoretical couple values were also calculated.

Fluids flowing with $Re < 10$ (Streamline Flow)

Fosdick and Kao [26], Thomas and Walters [87], Walters [96], Walters and Waters [98] and Wein [103] all used an analytical approach to solve the equations governing the flow of an elastic fluid between two concentric spheres. Work by Fosdick and Kao and Walters and coworkers was based on the solution obtained when starting with a Newtonian fluid. Wein however, based his work on that carried out for a power

law fluid (see Chapter 3). Again couple values were also determined. Waters and King [101] and Waters and Gooden [102] investigated the flow of elastic fluids around various stirrers of ellipsoidal shape and solved the equations analytically with great difficulty. Giesekus [28] and Walters and Waters [99] used an analytical method to solve for the flows due to a Cone-and-Plate geometry.

Fluids flowing with $10 < Re < 1000$

No analytical work was found for fluids flowing with Reynolds numbers between 10 and 1000.

Fluids flowing with $Re > 1000$

The flow of various non-Newtonian fluids at high Reynolds numbers has been investigated analytically for parallel plates by Kale et al [42] and Williams [108]. Their work was based on the 'Von Karman' type of flow with $Re \approx 1000$ [94]. An analytical approach was also taken by Mitchka and Ulbrecht [56, 90] and Shih and Hwang [83] to solve the equations due to the flow of power law and inelastic fluids around rotating cones and spheres. Theoretical torque values were also determined.

2.6.2 Numerical Studies

Fluids flowing with $Re \rightarrow 0$ (Primary Flow)

The mathematical equations describing the flow of a Newtonian fluid due to the slow steady rotation of various stirrers [29, 30, 46] have been solved numerically. Solutions for the fluid velocities and shear rates [29, 46] were obtained and in some cases the couple or power consumption for the stirrer was also determined [30, 46, 48].

Wein [103, 104] and Williams [110] carried out a numerical analysis of the flows induced by the rotation of ellipsoidal and disc stirrers in non-Newtonian liquids. Griffiths and Walters [30], Paddon and Walters [66] and Keentok et al [43] all used numerical procedures to determine the flows due to rotating cones, cylinders and vanes respectively. Couple values [30, 66] were also determined.

Fluids flowing with Re < 10

Griffiths et al [29] extended their work on Newtonian fluids to include the numerical study of elastic fluids flowing with Re < 10 around rotating discs. Paddon [65, 66] however, investigated the flow of elastic fluids in the cone-and-plate geometry and solved the governing Oldroyd [63] type equations numerically, while Williams [109] carried out work on flows around finite rotating discs and cylinders and also spheres and thin discs [111].

Fluids flowing with 10 < Re < 1000

Various Newtonian and non-Newtonian fluids flowing with Reynolds number between 10 and 1000 have been studied by several investigators. The equations due to the flows generated by rotating disc stirrers in the fluids have been solved by Dijkstra and Van Heigst [23], Spragg et al [85] and Wang and Yang [100] using numerical methods and computer techniques. The fluid velocities, shear rates and streamlines were determined. Pao [68], Bartela and Gori [4], Nirschl and Stewart [61] and Kramer and Johnson [45] all used numerical techniques to solve the theoretical equations due to the flow of fluids in a rotating cover or disc geometry. The torque was also determined by Bartela and Gori.

Fluids flowing with Re > 1000

Very little work on laminar flow of fluids with Reynolds numbers greater than 1000 has been carried out. Pao [67] and Hyun [38] both used numerical procedures to solve the equations governing the flow in their respective disc-cylinder geometries. We are not concerned with turbulent flows and, therefore, previous work carried out in this area has not been reviewed.

2.7 Conclusion

From the above review, it can be seen that most of the flow visualisation techniques which have been used in previous work determine flow patterns in various geometries in two dimensions only. The only exception to this is the work carried out by Dijkstra and Van Heijst [23] who used two cameras simultaneously to give instantaneous three-dimensional pictures of the flows.

Small particles in the form of a powder [54] or air bubbles [59] (which are very difficult to track individually) and dyes have all been used to follow the flows. Powder and dye techniques have the disadvantage that the fluid cannot be reused. The air entrainment technique is only successful for fast flows and allows qualitative determination of flow patterns rather than enabling quantitative study can be carried out.

Many workers have determined fluid velocities in two- or three-dimensions and the methods used have either been expensive and complicated (laser techniques [6, 16]) or simple but extremely tedious and time-consuming ('light-streak' technique [54]). The method of stereophotography [23] is also a fairly complex technique for obtaining fluid velocities.

The aim of this research was to obtain simultaneous three-dimensional images with the aid of tracer particles, to obtain a permanent record of the flows and also to determine various mixing parameters by using a technique which was both simple and within the limits of our budget (approximately £2000). To achieve this a novel flow visualisation technique was developed, the details of which may be found in Chapter 3. Couple or torque measurements were carried out via the measuring head of a Haake Rotovisco RV2 viscometer (see section 3.4.1). Although the complete methods of other scientists proved unsuitable for our purpose for the reasons outlined above, the ideas behind the techniques and the experience of these investigators were taken into consideration and utilised where necessary.

For mathematical modelling of the flows it was necessary to take a numerical approach to solve the equations. Although, a simple concentric cylinder geometry was studied initially and analytical techniques could have been used with difficulty to model the flows, our aim was to use a technique which could be used for both simple and eventually more complex geometries. As mentioned earlier, analytical techniques fail when more complicated flows are involved. With this in mind, Paddon's numerical method [67] (see section 4.2.1) was initially used for modelling primary flows in concentric cylinders. However, this method did not work very well for modelling secondary flows, so a different method by Pao [68] was adopted and was used to model flows generated by a rotating cylindical stirrer and the slightly more complex flows due to a rotating disc stirrer. It is hoped that the technique used here will help in the future to model more complex flows.

CHAPTER 3

EXPERIMENTAL WORK

3.0 Introduction

It was concluded in the last chapter that there was a need to develop an experimental technique which was cheap, which proved fairly simple and from which the required experimental data could be obtained. In this chapter, the method of flow visualisation together with the experimental procedure required to achieve this and the way in which various parameters were calculated for this research are described. The factors affecting the choice of geometry and fluids used are also given. Furthermore, the problems encountered during experimentation and how these were overcome are outlined.

3.1 Description of Apparatus

A global view of the apparatus is shown in Photograph 3.1. The experimental arrangement consisted of a solid aluminium cylindrical stirrer (Photograph 3.2a) rotating via a Haake Rotovisco viscometer in a perspex cylindrical vessel containing the fluid under investigation. The stirrer was painted black to ensure that no light was reflected from it, and that the tracer particles inserted in the fluid could be seen against the black background. The cylindrical vessel was placed in a square bottomed perspex vessel containing colourless liquid paraffin. This minimised horizontal optical distortion caused by the curvature of the inner cylindrical vessel. No vertical distortion was observed and, therefore, vertical measurements were unaffected. This outer vessel was not really necessary as the radial measurements were taken from the view of the bottom where no observed distortion occurred,

Photograph 3.1

Experimental arrangement
used for preliminary work.

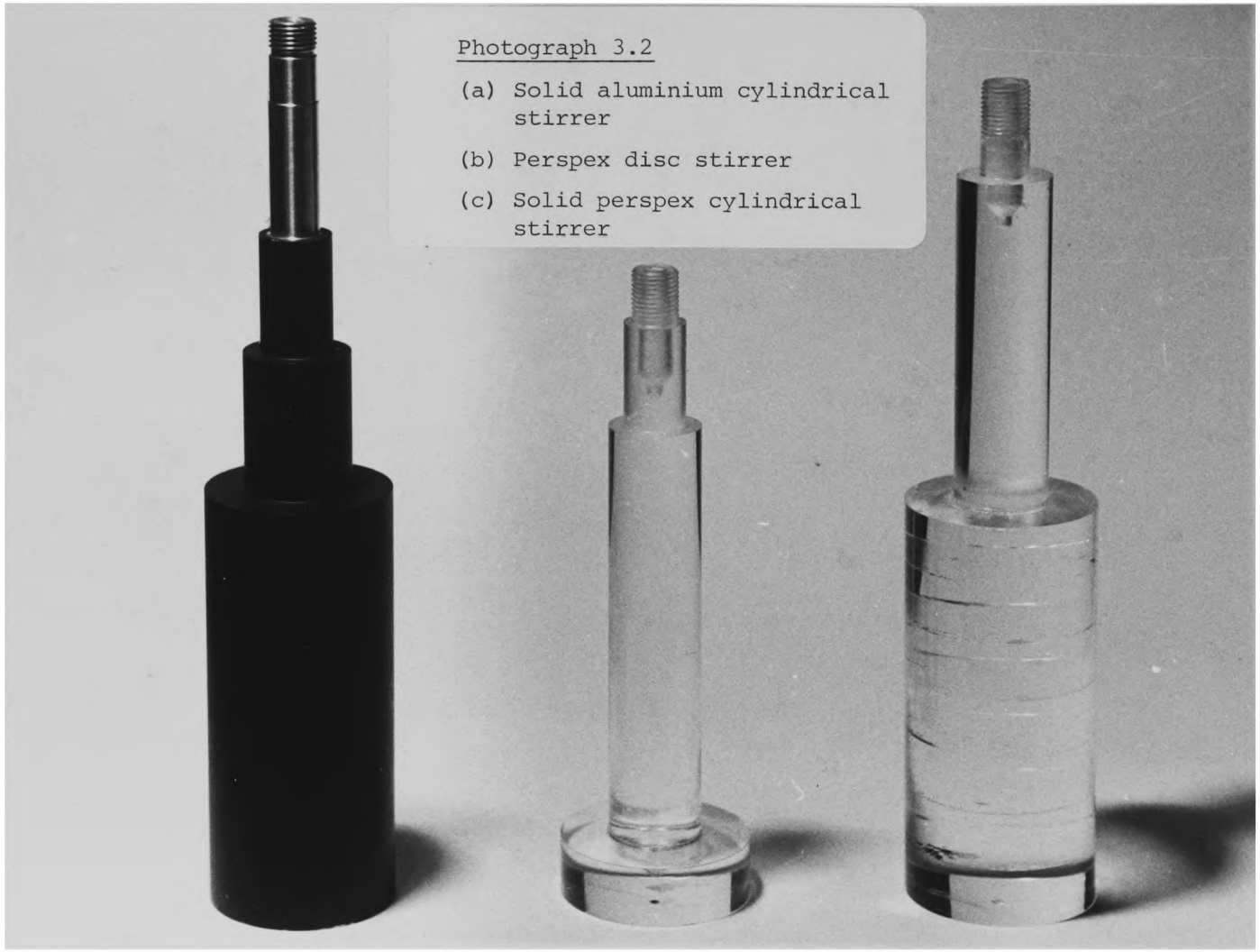

Photograph 3.2

(a) Solid aluminium cylindrical stirrer

(b) Perspex disc stirrer

(c) Solid perspex cylindrical stirrer

(a) (b) (c)

since the bottom of the vessel was flat. However, the paraffin enhanced the light reflected from the particles enabling them to be seen more clearly. In the absence of paraffin, the particles could still be seen but with less definition. Therefore, it seemed sensible to include the vessel containing the paraffin to give a better resolution of the particles and at the same time correct the horizontal view.

Acetate sheets on which fine grid lines were drawn were stuck to the front and outside bottom of the square vessel (Photograph 3.3). Since the diameter of the tracer particles used was approximately 2 mm, a grid size of 4 mm X 4 mm was taken. This ensured that not only was the grid visible, but also that particle positions could be determined as accurately as possible. Red reference lines in the form of a cross drawn on the bottom grid were used mainly for centering the apparatus and also for determination of particle positions with reference to the centre. Black card was permanently stuck on the back of the square vessel and placed temporarily on top during each run, thus enhancing the clarity of the front and bottom views respectively. White card was found not to be so effective. Scales stuck on the shaft of the rotating cylinder and also on the outer perspex cylinder enabled the gap size z_b and height of the fluid z_c in the apparatus to be determined (Fig. 3.1).

A digital watch on front of the apparatus was used for timing purposes. Two semi-circular perspex flat plates were used as a centralising device to ensure that the stirrer was placed in the centre of the cylindrical vessel as accurately as possible, hence ensuring symmetry. A plane mirror inclined at an angle of 45° was placed underneath the apparatus and the reflection of the bottom view of flows as seen in the mirror recorded via a video camera. More details of the flow visualisation method used may be found in the next section.

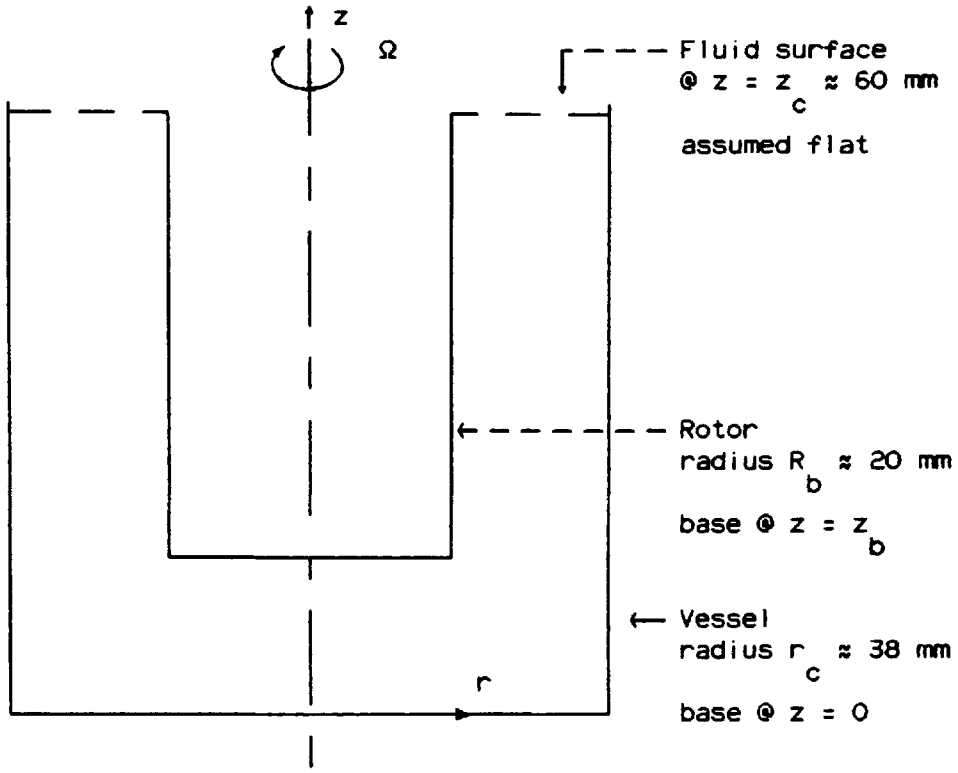

Figure 3.1 Cylindrical Rotor

A camera was not placed directly underneath the apparatus, as camera focussing was found to be more difficult.

Different coloured tinsel strands tied into small knots to give almost spherical particles were used to follow the flow. It was essential to use few particles for clarity and to enable them to be individually tracked.

An optimum illuminating arrangement was found by trial and error. This consisted of two 100 W tungsten filament lamps placed on either side to light the apparatus and a small 60 W lamp placed in front to light up the watch. Black card was placed over all the laboratory windows to stop any external light from impinging on the apparatus. A darkened room was necessary again to ensure visual clarity of the flows.

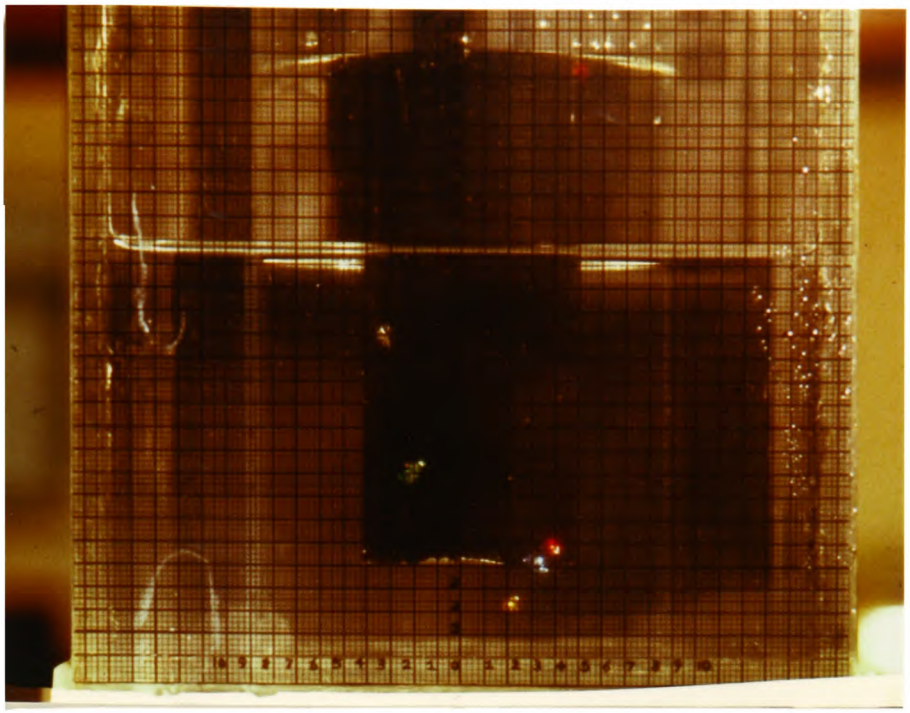

(a)

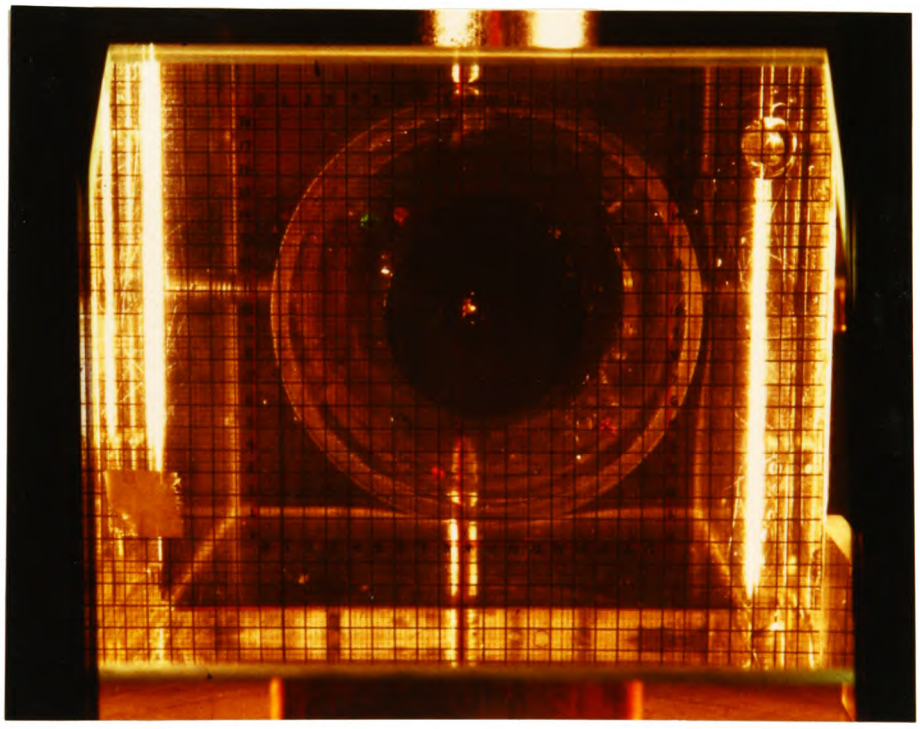

Photograph 3.3

Front (a) and bottom (b)
views of the apparatus.

3.1.1 Flow Visualisation Technique

The flow visualisation technique developed involved the tracking of tracer particle positions as functions of time using two video cameras, one viewing the front and the other the bottom of the apparatus via its reflection in the plane mirror (Photograph 3.4). This ensured that instantaneous three-dimensional views of the flows were obtained as opposed to most previously discussed techniques giving two-dimensional views only. Both views were recorded simultaneously on a split image visual display unit using the JVC 2000 and VHS colour video cameras together with a VHS video recorder and an Electrocraft Vision Mixer (Photograph 1). The best resolution of the flows was found when the VHS camera was focussed on the front view and the JVC camera on the mirror.

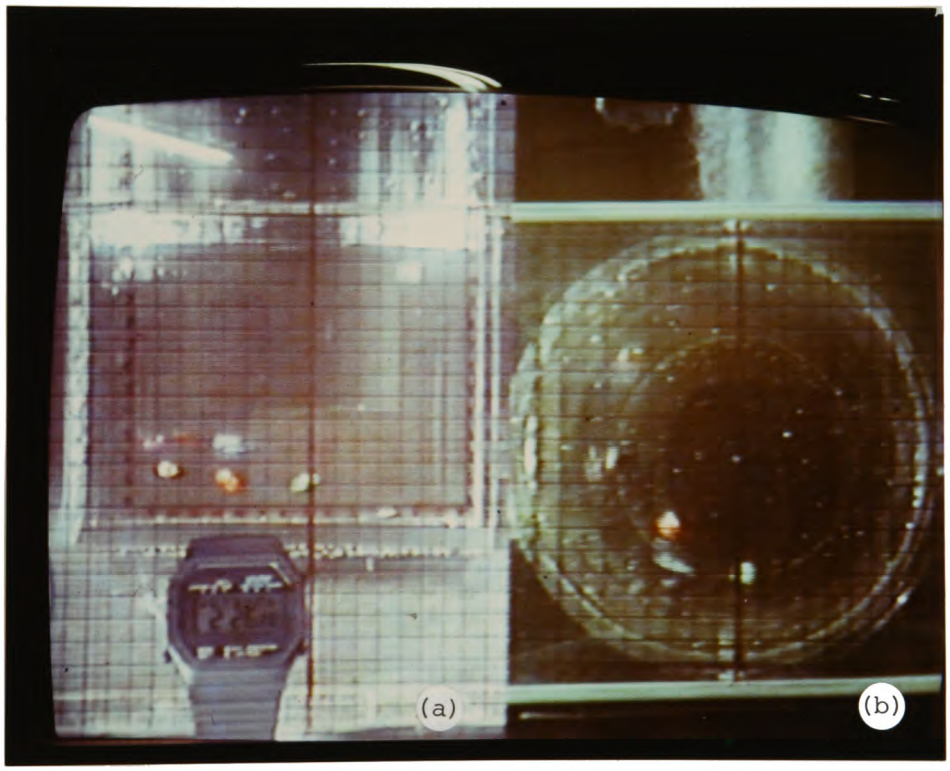

Photograph 3.4

Front (a) and bottom (b) views of the apparatus as seen on the monitor.

The technique of utilizing video equipment to record the flows proved advantageous in many ways. The film which was stored on a VHS video cassette could be played forwards or backwards as many times as was required and with great flexibility. This together with the 'freeze-frame' facility, which enabled the film to be played frame by frame could be used within experimental errors, to determine accurate particle positions and timing of flows. Various parameters, such as fluid velocities could then be calculated at a later date. The video tape allowed many recordings to be stored on it thus reducing costs. Furthermore, the flows could be analysed at some later stage at leisure, rather than at the time of experimentation. Generally, good clear pictures were obtained except when the 'freeze-frame' facility was used for fast flows. In this case, the particles appeared blurred.

It should be noted here that the above apparatus (Photograph3-1) was used for preliminary experimentation only, the results of which may be found in reference [8] and are included in Appendix 1. Further experiments on the cylindrical stirrer and the disc stirrer were performed after improvement of the apparatus (see section 3.5).

3.2 Materials

A nominal 1.1 Pas glycerol-water solution and 0.2% aqueous solution of Goodrich Carbopol 910 of nominal viscosity 0.9 Pas were used for this investigation. Glycerol, which is a simple Newtonian fluid with good flow visualisation properties, was used for the preliminary work and for testing the mathematical model. The work was then extended to include Carbopol 910, which is a simple negligibly elastic, shear-thinning fluid with no time dependent (i.e. no thixotropic) or 'apparent' yield stress behaviour. It is a copolymer of acrylic acid and was

recommended for this study by Dr. H. A. Barnes of Unilever Research [3] as a good representation of products, such as soaps and detergents manufactured by Unilever Research and also of other industrial products.

For research work, it is important to use fluids which can represent the properties of products used in everyday life rather than 'ideal' fluids to be of any benefit. Therefore, a good reason for choosing Carbopol 910 for this study is that it is shear-thinning like many everyday products. Furthermore, like glycerol, Carbopol 910 has the advantage of being transparent for easy viewing and flow visualisation. The procedure for obtaining a solution of Carbopol 910 together with its inherent properties are given in the instruction manual "Carbopol-Water Soluble Resins" supplied by B. F. Goodrich, Chemical (U.K.) Limited [5]. A solution of Carbopol 910 was stored under airtight conditions to ensure that no dehydration occurred leaving a thick jelly-like substance. Other non-Newtonian fluids, such as, polyacrylamide, carboxymethylcellulose and xanthan were found to be unsuitable for this work, since they either exhibited thixotropic, elastic, apparent yield stress or cloudy properties. It was hoped that a third fluid exhibiting only simple shear-thinning behaviour could be used to test with and which would also serve as a check for the reliability of the experimental and theoretical techniques used here. Therefore, solutions of various concentrations (3.6%, 4.3%, 6.8%) of polyvinylpyrolidone (PVP) were made up and tested using the Haake Rotovisco viscometer in its standard viscometric mode (Fig. 3.2) (see section 3.4.2). PVP a colourless liquid, was referenced by Ulbrecht et al [90] as being a simple inelastic fluid with good optical properties. However, it was found to be virtually Newtonian and, therefore, was not used for experimentation. Similarly, 0.5% solution of Methocel HG90 [15] although

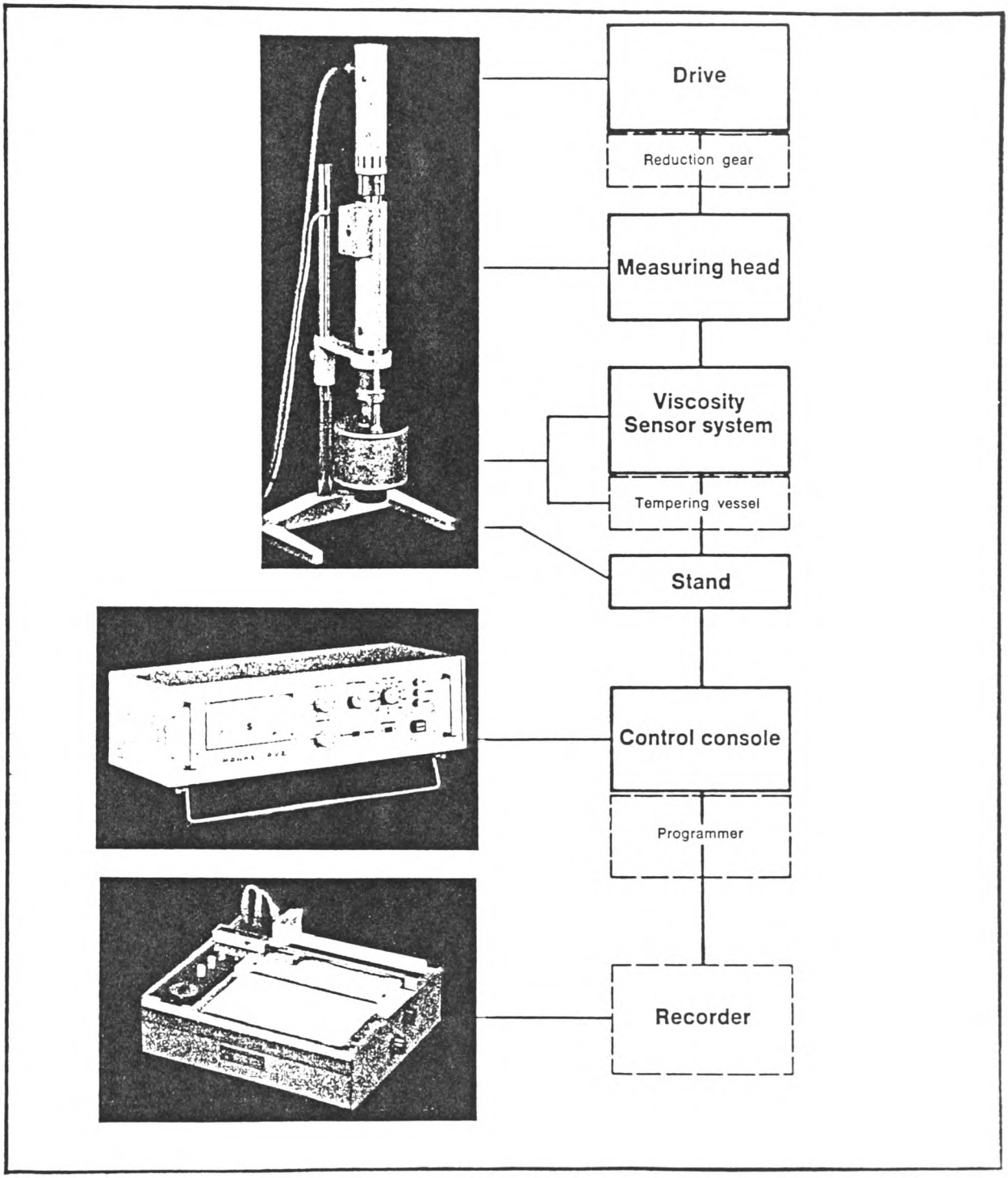

Figure 3.2 A Haake Rotovisco viscometer in its standard viscometric mode

colourless was also found to be almost Newtonian and Carbopol 940, which is another copolymer of acrylic acid appeared to be a cloudy solution in which tracer particles were difficult to track. These latter two fluids were also, therefore, unsuitable for our purpose.

Water, many different concentrations of sugar solutions and various grades of paraffin were tried out as a correction fluid to counteract the distortion caused by the cylindrical perspex vessel. Both water and sugar solutions were found to be ineffective for this purpose. It was concluded that 'heavy' liquid paraffin, a colourless liquid was the best fluid to use to counteract the distortion. The reasons for using perspex for the apparatus was that the flows could easily be seen through it and because it is more durable and resilient than glass.

Various coloured tinsel strands tied into small knots to give almost spherical particles were found to be the most suitable for following the flow. Tying tinsel strands into knots was a lengthy process since they kept disravelling. The light could be reflected from all angles even when the particle was rotated and ensured that it could be filmed both from the front and from the reflection of the bottom view via the mirror. The problem with flat untied tinsel segments was that they could be rotated in the light plane which was perpendicular to the line of sight from the camera in such a way that the light would not be reflected from it during the full time of recording. A typical tinsel particle was not solid having air entrained between the strands and when immersed in the test fluid, the air was replaced by the fluid making the particle neutrally bouyant. The large surface area exhibited by the particle also played an important part in keeping it neutrally bouyant. It is, therefore, assumed as with work by others e.g. Metzner and Taylor [54], that the particle

was of the same density as the fluid and hence moved in essentially the same way as the fluid. Furthermore, these particles, had the advantage that they were non-invasive i.e. the fluid could be reused.

Many other particles, such as nylon 66, polyvinylchloride (PVC), polypropylene, polystyrene, rubber, wool, polyether-ether ketone (PEEK) to name a few, were examined for use as tracer particles, but it was found that they either floated or sank in the fluid within seconds of starting the rotor or generally behaved in an undesirable fashion. Therefore, they were not suitable for following the flow. Also, most of the particles were either colourless (PVC), dull grey (PEEK) or brown in colour which made visualisation very difficult. Painting these particles with fluorescent paint did not help either. It must be stressed here that the task of trying to find a tracer particle which was both buoyant in the fluid and could be seen and tracked easily proved to be both laborious and time-consuming. Incidentally, some of the particles were supplied by either Courtaulds Ltd., Coventry [20] or Hydraulics and Supreme Plastics Engineering Ltd., Coventry [37].

3.3 Choice of Stirrers

For initial investigations, a finite cylindrical stirrer (Fig. 3.1 and Photograph 3.2) was chosen, since only limited previous work [107] had been carried out on this particular geometry. It also proved a relatively simple geometry for carrying out preliminary experimental work [8] and for mathematically modelling primary flows which were then extended to include the secondary flow regime.

Once work was completed for the cylindrical rotor, similar experimental and theoretical analysis were carried out for the relatively

more complex flows generated by a finite disc stirrer (Fig. 3.3 and Photograph32b). This is a slightly more complex version of the cylinder and a relatively simple version of the widely used Rushton Turbine. It seemed sensible to study the disc, so that the common Rushton Turbine could eventually be modelled.

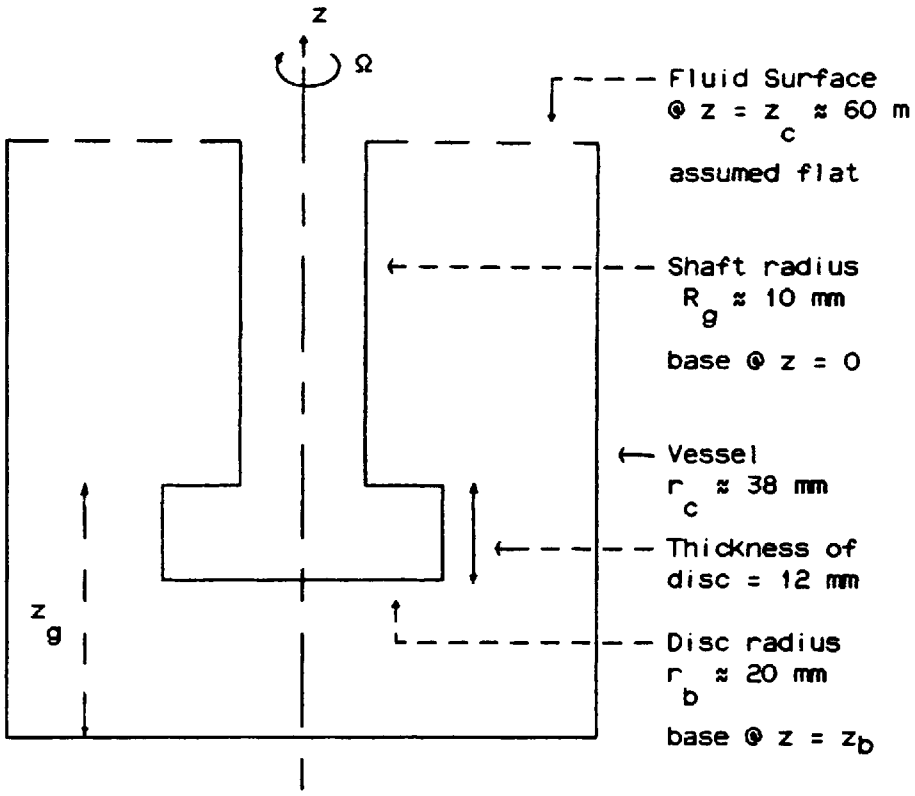

Figure 3.3 Disc Rotor

3.4 Familiarisation and Experimental Procedure

As with any experimental work, it is essential to gain familiarity with the various instruments used for the research. With this in mind, work was carried out to give an understanding of how the apparatus operated. Also, many trial and error experiments were performed to give the optimum experimental arrangement.

The Haake Rotovisco viscometer, which is an instrument for measuring viscosity, was used in its standard viscometric mode (Fig. 3.2) to determine the characteristic flow curves for various test fluids (see section 3.4.2). The flow curve which is a plot of the speed of rotor versus scale reading from the viscometric dial could be plotted either automatically using a chart recorder or manually. These initial experiments proved extremely useful for characterising the fluids that were used for the research at a later stage.

When the apparatus was set up as discussed in section 3.1, much time and effort was spent in trying to obtain the best arrangement and technique for experimentation. The laboratory windows needed to be covered with black card to darken the room and lights were placed at various angles until the best resolution of the particles was obtained. Cameras were also tested out in various positions until the optimum arrangement was found. Initial familiarisation experiments were carried out on the rotating cylinder in the following way and results are given in reference [8]. Problems encountered during these experiments were rectified before continuation of further work. The improvements are given in section 3.5.

The fluid under investigation, either glycerol or Carbopol 910 was poured into the perspex cylinder. The free surface of the fluid at z_c was observed to be essentially flat during a run. After addition of the tinsel particles, the stirrer was carefully lowered into it. As many bubbles as possible were dislodged from the fluid using a thin wire rod bent at approximately 90° at the end. Heavy liquid paraffin was carefully poured into the square bottomed vessel and air bubbles dislodged in the same way.

After ensuring that the rotor was centralised using the special device, the tracer particles were positioned in the fluid at various heights using a glass rod. Black card was then carefully placed on top of the apparatus ensuring that the particles could be seen clearly from the bottom.

Several speeds were used and it was found that generally speeds below 16 rpm (1.68 radians/second) were too slow for the particles to remain suspended in the fluid for more than five minutes. Above 16 rpm weak secondary flow was observed as well as primary flow. Therefore, a speed of 16 rpm was used to give primary flows. At 64 rpm (6.72 radians/second), more pronounced secondary flow could be seen superimposed on the primary flow. Between 64 rpm and 128 rpm which is the next speed setting on the standard Haake Rotovisco RV2 viscometer, the programmer PG 112, an auxiliary unit, was used which when connected to the viscometer permitted the selection of additional six speeds within the range 0.1 - 1000 rpm. However, it was found that a speed of 128 rpm (13.44 radians/second) was sufficient to give good secondary flows and, therefore, this unit was only used for test purposes for various speeds between 64 rpm and 512 rpm (i.e. 6.72 and 53.76 radians/second respectively). Above 128 rpm the flow was too fast for it to be seen clearly even when using the freeze-frame facility.

Arbitrarily chosen gap sizes z_b of 12 mm (small gap) and 21 mm (large gap) with a fluid height z_c of 60 mm were taken. Several runs were carried out for each gap size, speed and fluid. To differentiate between each run a card giving all the essential details was used (Fig. 3.4).

Each time a new arrangement was used accurate positioning and focussing of the cameras had to be carried out to ensure that symmetrical views of the front and bottom were obtained. This took about four

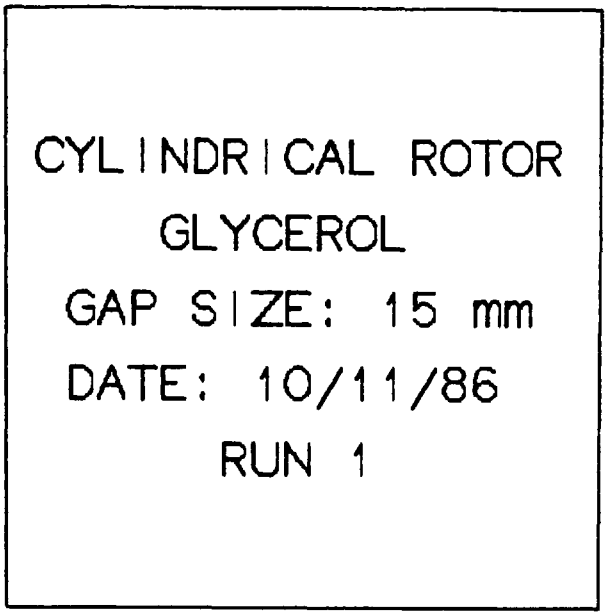

Figure 3.4 Sample card showing details of an experimental run.

hours and was carried out with the lamps switched on. During the first run it was found that the heating effect from these lamps affected the fluid under investigation in a very unusual way making some of the tracer particles float on the surface and others sink to the bottom in the first few seconds of starting the rotor. In previous trial experiments which were carried out under normal room lighting this unusual behaviour did not occur. Therefore, once the visualisation equipment i.e. cameras, video recorder, vision mixer, lamps, plane mirror etc. were all placed in position for experimentation, the fluid was allowed to cool overnight and the experimental runs carried out on the following day.

On the following day, after ensuring that all the experimental equipment was still intact and the rotor still centralised, the lamps and rotor were switched on, the stop watch started and a recording of the flow taken for approximately three minutes. Between each run the lamps were switched off to minimise heating of the fluid and the

temperature of the fluid taken. A fan was also used to control the temperature of the fluid. Once improvements on the apparatus were carried out experimentation was found to be far easier (see section 3.5).

3.4.1 Couple Measurements

Further experiments were carried out for each fluid whereby scale readings from the viscometer were taken for various speeds of the rotor. Using these readings, experimental couple values were obtained by using the spring constant of the dynamometer. These were compared with theoretical values and various graphs representing couples were drawn which are presented later.

3.4.2 Viscometric Experiments

It is important to know the viscosity of a liquid so that it may be used in the mathematical equations which are solved to give theoretical values of various parameters and for eventual scale-up purposes. The viscosity is also required to calculate the theoretical couple on the stirrer.

For the viscometric experiments, the Haake Rotovisco viscometer was calibrated and used in its standard mode of concentric cylinders (Fig. 3.2) [14, 92]. Scale readings at various speeds of the rotor for both glycerol and Carbopol 910 at 296 K and 294 K respectively were obtained. From these readings, the viscometric curves were drawn and are presented later in Figures 6.1 and 6.2.

The Haake viscometer is designed essentially to enable the viscosity of Newtonian fluids to be easily calculated. When the speeds and

scale readings are multiplied by certain instrument constants, the gradient of the line gives the viscosity which is always constant. However, this need not be the case with shear-thinning fluids such as Carbopol 910, in which a non-linear dependence of stress on the rate of strain is observed. If the concept of the viscosity is to carry over to liquids showing non-linear dependence of the stress on the rate of strain, then the viscosity is no longer a constant. Therefore, an 'apparent viscosity' is defined which is dependent on the shear rate.

Generally, when the apparent viscosity is measured over a range of shear rates Newtonian behaviour is often indicated at very low and high shear rates (Fig. 3.5). At low shear rates, the shear stress is proportional to the shear rate and viscosity approaches a constant value η_0 known as the zero shear viscosity or the 'lower Newtonian viscosity'. At higher shear rates the viscosity decreases as shear rate increases. This is known as the power law region and is the dominating region. Finally, at very high rates of shear, the viscosity may again become independent of shear rate and approach infinite shear viscosity η_∞, otherwise known as the 'upper Newtonian viscosity'.

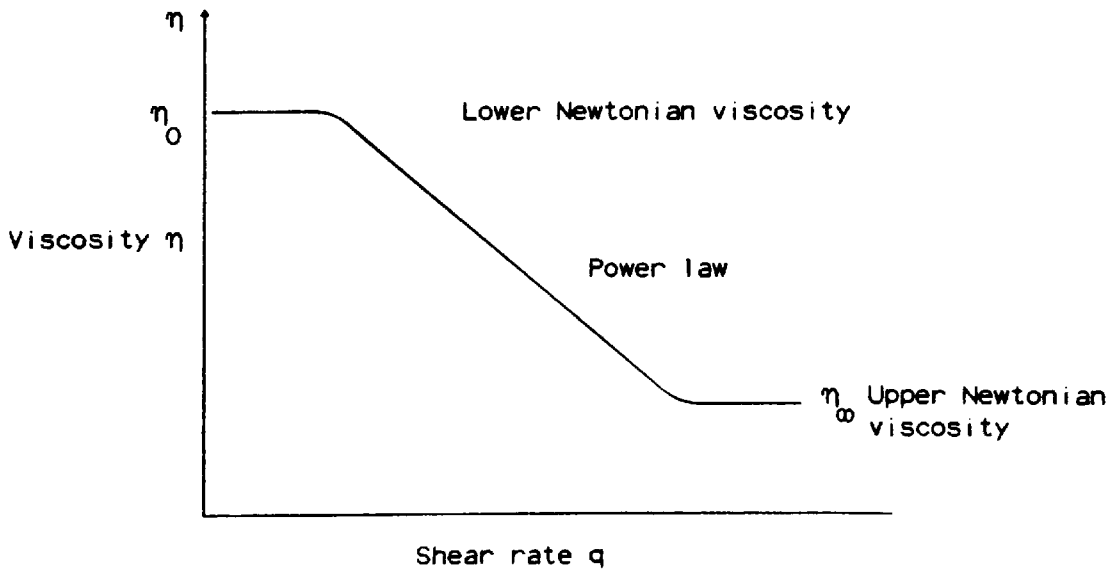

Figure 3.5 A common form for the viscosity as a function of strain rate for pseudoplastic fluids.

Thus, once the viscometric data for Carbopol 910 was obtained, a fluid model had to be fitted to it which described the behaviour of the fluid for mathematical modelling purposes. The Cross and Carreau [7, 12] models were chosen, the equations of which may be found in Chapter 4. These models closely represent the behaviour described above. It is not easy to obtain the zero (η_0) and infinite (η_∞) shear viscosities and the constants n and λ required in the theoretical equations. Therefore, a non-linear minimization technique [58] was used to determine both the parameters and the type of model, Cross or Carreau, which fitted the viscometric data for Carbopol 910.

A computer program was developed which used the above technique together with the NAG routines E04GEF and F04ASF [58] to give the required parameters. Each speed and scale reading was input into the program together with the dimensions of the standard viscometer concentric cylinders and the spring constant of the dynamometer. For each point, the shear rate (q), stress (τ) and viscosity (η) were determined and the following non-linear quantity was minimised

$$\sum_{i=1}^{N} \left[\eta \left[q_i \right] - \eta_i \right]^2 \qquad (3.1)$$

where N is the number of data points

The Cross and Carreau models were then fitted to the data and the one with the least error was taken to be the best model for representing Carbopol 910 (see section 6.1).

3.5 Modification of Apparatus

It was required that the experiment be carried out under isothermal or constant temperature conditions. However, the tungsten filament lamps posed a heating problem. Not only did the fluid under investigation rise in temperature, but the tracer particles behaved in an unusual way as mentioned in section 3.4. Therefore, for subsequent work these lamps were replaced by unidirectional fluorescent lamps (Photograph 3.5). The new lamps provided a bright light required to see the tracer particles but gave no apparent heating effect. Thus it was possible to keep the temperature of the glycerol at 296 K and that of Carbopol 910 at 294 K. A fan was no longer required.

The JVC 2000 video camera was replaced by a new Hitachi FP-5 video camera. This new camera had the added facility of a built-in clock and therefore the need for a stop watch and the 60 W lamp used to light up the watch were no longer necessary.

For convenience, the arbitrarily chosen gap sizes of 12 mm and 21 mm were changed to 15 mm and 25 mm i.e. 0.8 and 1.3 in dimensionless form (see Chapter 4) respectively.

The above modifications made experimentation a great deal easier in that there was no longer any need to leave the apparatus overnight to cool down after setting it up or to let it cool down between each run. Moreover, the built-in stop clock in the camera ensured that no setting up of the watch had to be carried out which was awkward in itself.

In the preliminary work, a solid aluminium cylinder was used. The tracer particles could not be seen from the front view when they

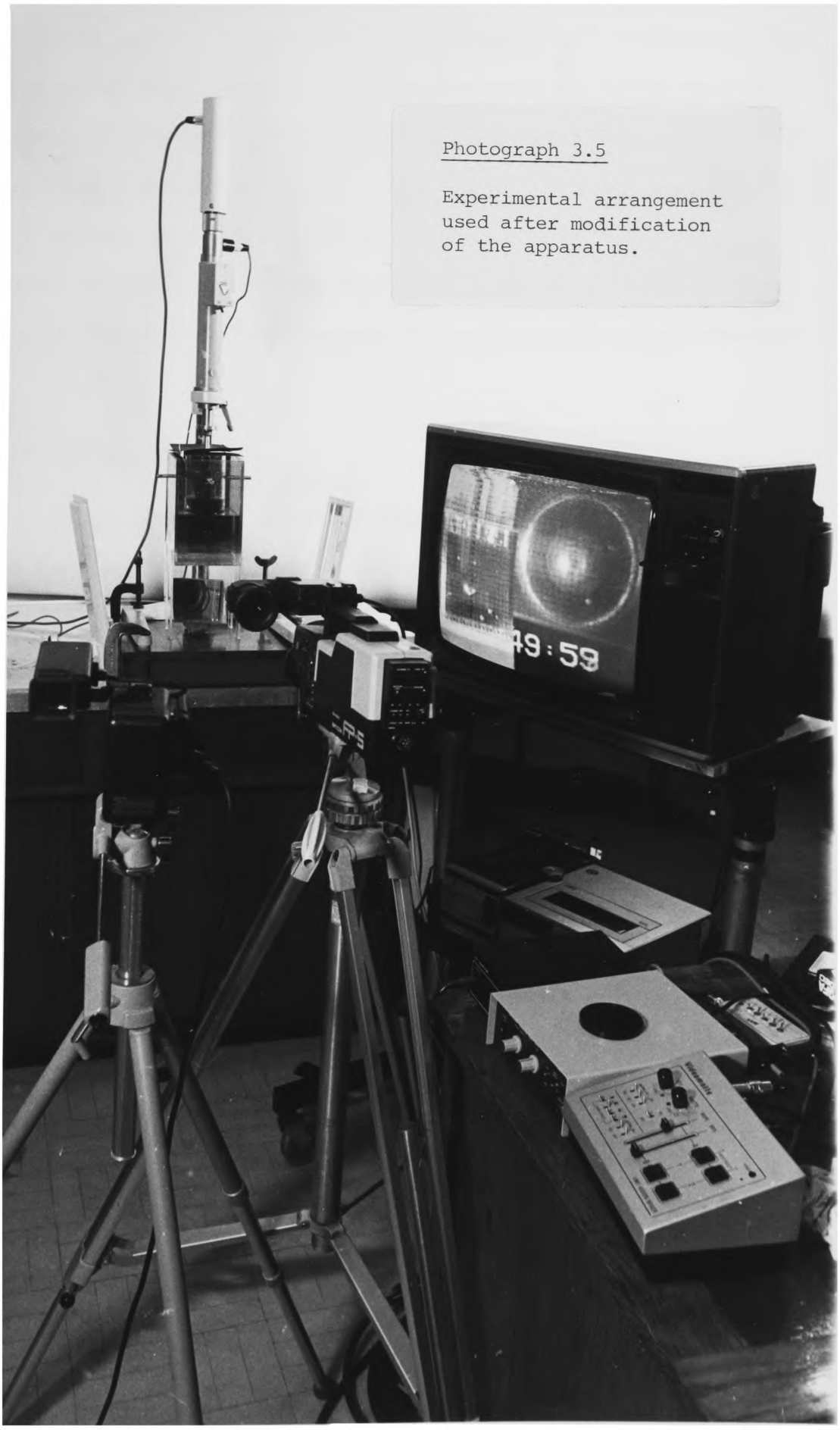

Photograph 3.5

Experimental arrangement used after modification of the apparatus.

were behind the rotor. For primary flow this factor was not important, since the particle remained at the same height as it travelled round in a closed loop. However, in secondary flows the height does not remain the same and it is important that the particles be seen at all positions even when behind the rotor. Thus, the solid aluminium stirrer was replaced by a solid clear perspex cylindrical stirrer through which the particles could be seen (Photograph32c). Similarly, the finite disc stirrer was also made from solid perspex (Photograph32b).

3.6 Primary Flows

In primary flow, the fluid travelled in essentially the same way as the rotor (see Chapter 6) i.e. in circular paths and, therefore, it was relatively easy to take measurements for determining the various primary flow parameters. The positions of the tracer particles as functions of time were taken from the video recordings using a monitor and the freeze-frame facility on the video recorder in the following way. The recording was allowed to play and each time a particle crossed the -y' axis (Fig. 3.6) the 'pause' button was pressed hence 'freezing' the film. The position of the particle from both the front and bottom views were noted together with the time. The 'pause' button was released and the film allowed to play until the particle crossed the -x' axis. Its position from the bottom view was noted. This was repeated until each particle crossed the +y', +x' and the -y' axis again. At this point the time and position from the front view were also noted. All distance measurements were taken to the nearest 0.5 mm and time measurements to the nearest 0.01 second.

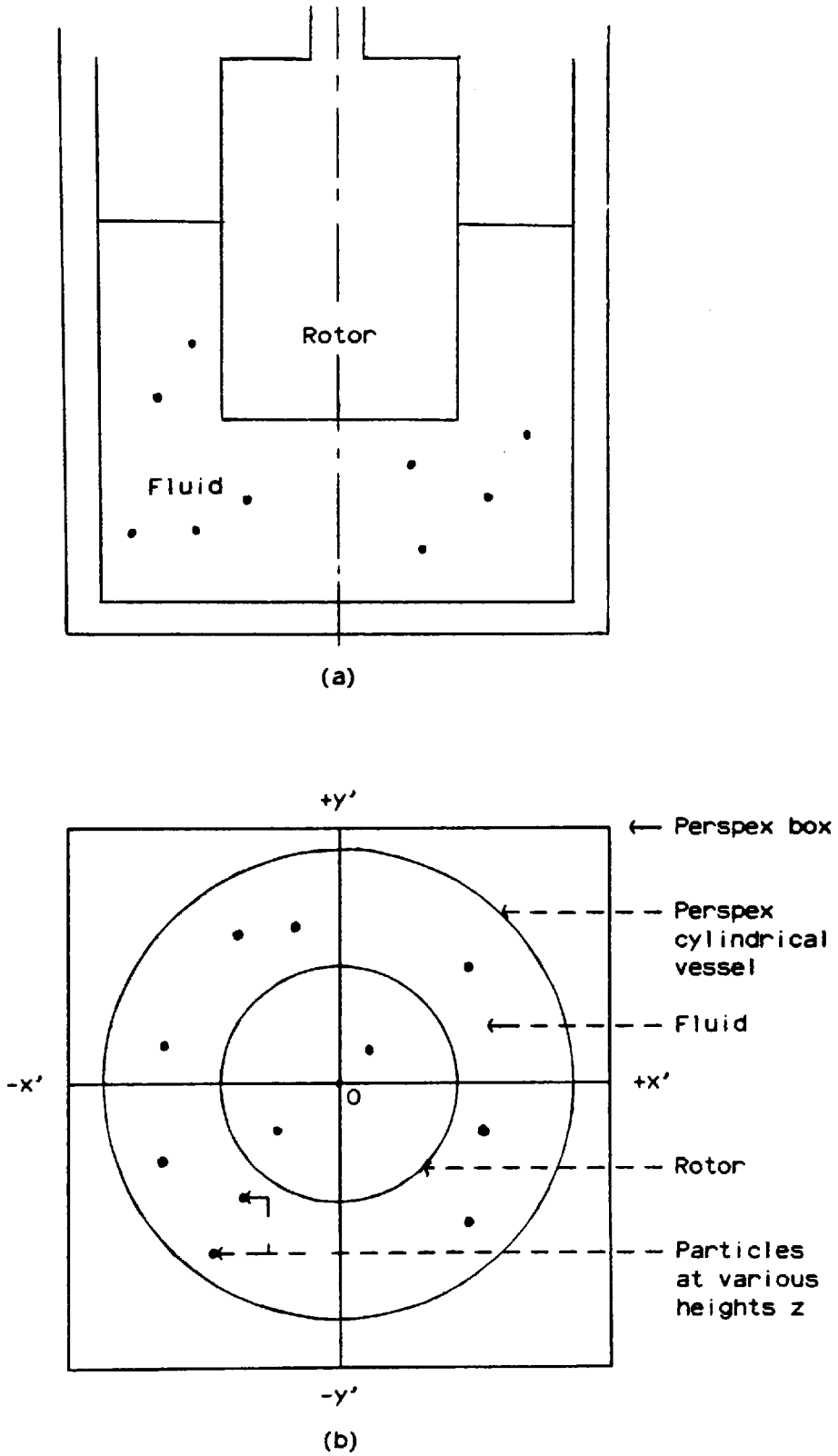

Figure 3.6 Front (a) and bottom (b) views of apparatus.

A computer program PRI (see Appendix 2) was developed for calculating experimental values of the various parameters. The 'raw' data was used as data input for this program and the height (z) of the particle from the bottom of the perspex cylinder, the radius (r) of the circle along which the particle was travelling and the time taken for each particle to complete one revolution were calculated. The height and radius were both non-dimensionalised by dividing by the radius of the stirrer r_b, thus becoming y and x respectively (Fig. 3.7). The reason for using dimensionless values was to ensure smaller numbers which are easier to handle and to enable the parameters to be compared with their respective theoretical values which were also non-dimensionalised. Furthermore, this would enable a variety of geometries to be modelled relatively easily and it would also help scale up. The above values were then used within the program to give the angular velocities and shear rates at various points in the fluid.

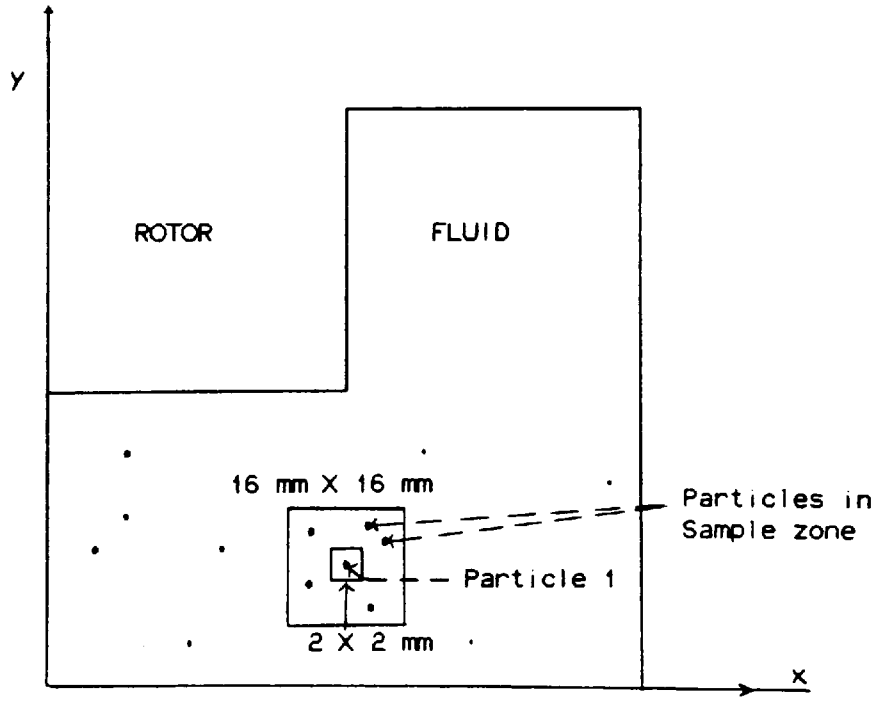

Figure 3.7

The strain rates were obtained using the following method. Since the apparatus was symmetrical we may represent it as one half as shown in Figure 3.7. The strain rate of each particle is calculated in turn. Consider particle 1 as shown in Figure 3.7. A 2 mm to 8 mm sample zone was taken around this particle. The computer program was written in such a way so as to search through all the particles to find all those which lay in the sample zone of the particle under consideration. All particles in the zone were considered individually with reference to particle 1 and their strain rates ($\dot{\gamma}$) determined using the following

$$\dot{\gamma} = x \left[\left[\frac{\Delta u}{\Delta x} \right]^2 + \left[\frac{\Delta u}{\Delta y} \right]^2 \right]^{1/2} \qquad (3.2)$$

where Δu = difference in angular velocities between reference particle and particle under consideration

Δx = difference in radius between reference particle and particle under consideration

Δy = difference in height between reference particle and particle under consideration

x = dimensionless radius

The average of all these strain rate values was taken to be the one required for particle 1. This process was repeated for all the particles in the same way. To carry out these calculations by hand would have been extremely laborious and time-consuming. Therefore, the computer proved very useful in saving time and effort. Incidentally the DEC-20 mainframe computer was used for all computer analysis.

The computer program (Appendix 2) was also used for comparing experimental values with those obtained theoretically (see Chapter 4), by determining the percentage difference between them. Standard deviation and mean values of these percentage differences for strain rates (GDIFF) and angular velocities (UDIFF) were also determined.

An example of a typical printout obtained from the computer showing all the above values is given in Appendix 3. The results are discussed in Chapter 6.

3.7 Secondary Flows

For secondary flows, the fluid motion is much more complicated as it occurs in the radial (r), vertical (z) and angular (θ) directions. The equations which enable the speed in these directions to be determined are more complex as well. The speeds in the radial (V_x) and vertical (V_y) directions are expressed in terms of a stream function α. Full details are given in Chapter 4 and only the method used for calculating the values of u, V_x, V_y, α and vorticity χ experimentally is given here. These experimental values are compared with the corresponding theoretical values in Chapter 7.

To determine the above values experimentally, the video recordings were analysed, again using the monitor and the freeze-frame facility on the video recorder. After noting the initial position and time of a tracer particle, the subsequent positions of the particle were noted every 0.4 second for convenience until it reached its initial starting point hence completing one cycle. Again the time and positions of the particle were noted. The flow pattern for secondary flow is more fully described in Chapter 7.

A computer program was developed for determining various secondary flow parameters. From this program, x and y values were calculated in a similar way to that for primary flows and the angle θ through which the particle moved every 0.4 second was also determined. A plot of x against y may be drawn. Although it is not shown here, the closed fluid particle path is seen to be unsmooth. This may be due to experimental

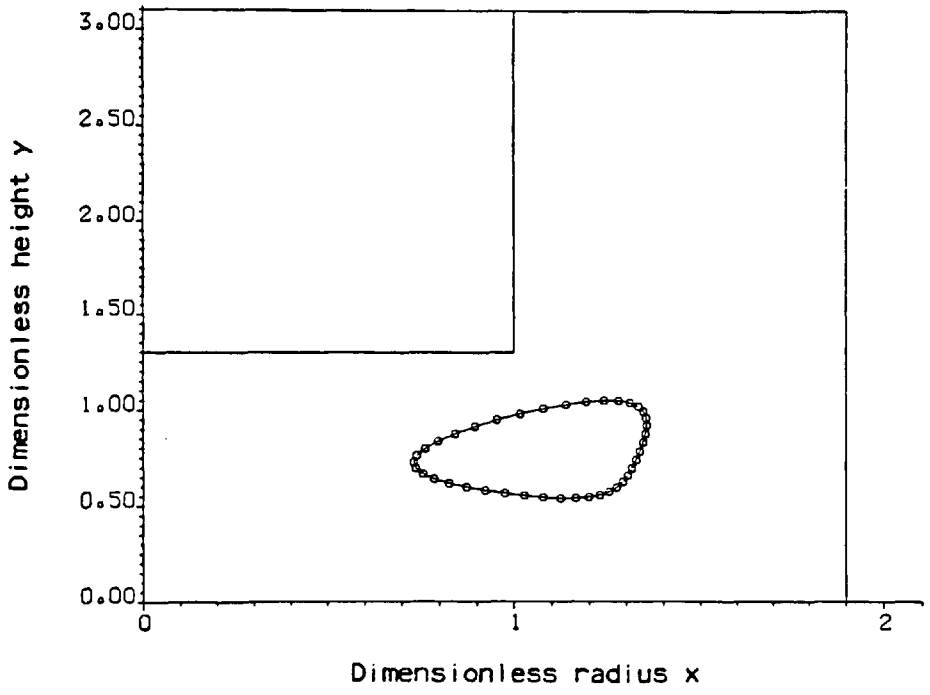

Figure 3.8 A typical 'smoothed' secondary flow streamline after treatment of the raw data.

errors, such as slight 'wobble' in the rotor and inaccurate timing of flows and determination of particle positions. The data was, therefore, treated using a Fourier analysis [32] to give 'smoothed' values of x and y from which the best smooth streamline could be drawn (Fig. 3.8). The θ values were also treated to give smoother values.

The Fourier expansion of a periodic function F(t) is given by,

$$F(t) = \frac{1}{2} a_0 + \sum_{N=1}^{\infty} \left[a_N \cos \left[\frac{N\pi t}{T} \right] + b_N \sin \left[\frac{N\pi t}{T} \right] \right] \qquad (3.3)$$

where F(t) is the variable to be smoothed

t is the time

T time to complete one cycle of stream pattern

$$a_N = \frac{2}{T} \int_0^T F(t) \cos \left[\frac{N\pi t}{T} \right] dt \qquad (3.4)$$

$$b_N = \frac{2}{T} \int_0^T F(t) \sin \left[\frac{N\pi t}{T} \right] dt \qquad (3.5)$$

The Trapezium rule was used together with equations 3.4 and 3.5 to estimate a_N and b_N respectively for x, y and θ which were then used in equation 3.3 to determine the smoothed values of x, y and θ. Although the upper limit of N on the summation in equation 3.3 is normally infinity, for computation purposes a finite value is required. In order to avoid errors by over smoothing resulting in 'kinks' in the streamlines, the least possible value of N was obtained, by trial and error, which gave satisfactory smoothing. A value of 3 or 4 depending on the number of data points was found to be appropriate. The smoothed values of x, y and θ were then used in all subsequent calculations.

For each x,y point in the fluid, the corresponding θ value was differentiated using equation 3.3 with respect to time to give the angular velocity u. The x and y values were differeniated to give the velocities V_x and V_y in the x and y directions respectively.

For a particular arrangement, knowing the values of x, y, u, V_x and V_y, the strain rates $\dot{\gamma}$ were calculated for all x,y points in the fluid using the following equation

$$\dot{\gamma} = \left[2 \left[\left[\frac{\Delta V_x}{\Delta x} \right]^2 + \left[\frac{\Delta V_y}{\Delta y} \right]^2 + \left[\frac{V_x}{x} \right]^2 \right] + x^2 \left[\left[\frac{\Delta V}{\Delta x} \right]^2 + \left[\frac{\Delta V}{\Delta y} \right]^2 \right] + \left[\frac{\Delta V_x}{\Delta y} + \frac{\Delta V_y}{\Delta x} \right]^2 \right]^{1/2} \qquad (3.6)$$

and a similar method of sample zones as that used for determining the primary flow strain rates.

For each x,y point in the fluid, the vorticity χ and incompressibility I were calculated together with the above method of sample zones where χ and I given by

$$\chi = \frac{\Delta V_x}{\Delta y} - \frac{\Delta V_y}{\Delta x} \qquad (3.7)$$

and

$$I = \left[\frac{x \left[\frac{\Delta V_x}{\Delta x} + \frac{\Delta V_y}{\Delta y} \right] + V_x}{x \left[\left| \frac{\Delta V_x}{\Delta x} \right| + \left| \frac{\Delta V_y}{\Delta y} \right| \right] + |V_x|} \right] * 100 \qquad (3.8)$$

respectively.

The reason for determining incompressibility values was to check if the method for determining experimental quantities gave accurate results. Ideally, the incompressibility should be zero for all points in the fluid. However, this is not the case in practical because some experimental error is always present.

The values of the stream function α were determined using the following equation as

$$\alpha_q = \alpha_p + \frac{x_p}{2}\left[(V_{xq} + V_{xp})\Delta y - (V_{yq} + V_{yp})\Delta x\right] + \frac{\Delta x}{2}\left[V_{xp}\Delta y - V_{yp}\Delta x\right] + O(\Delta)^3 \qquad (3.9)$$

in the method below.

Consider the outer streamline in Figure 3.9 , the value of which was determined initially. The shortest distance e.g. PQ between this streamline and the outer boundries was taken to minimise errors and the points on either end considered. Since the velocities in the x and y directions at the two points are known, the value of α at Q may be obtained by substituting the various values in equation 3.9 in obvious notation. This procedure was repeated for the next inner streamline e.g. R and instead of considering the outer boundaries, the outer streamline nearest to R i.e. Q was considered. Similarly, the technique was repeated for all other streamlines.

Having determined all the experimental values of the various parameters required for both primary and secondary flows, the percentage difference between the experimental and theoretical values of u (UDIFF), γ (GDIFF) and χ (VDIFF) were determined. The mean values of UDIFF, GDIFF and VDIFF and the standard deviations from these values were also calculated.

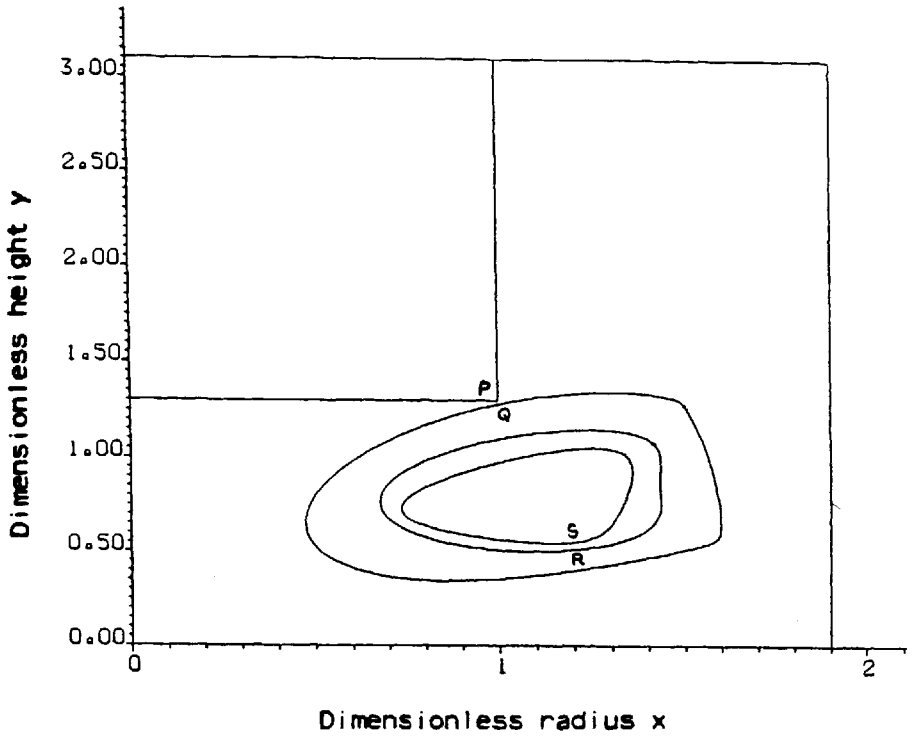

Figure 3.9 Typical 'smoothed' secondary flow streamlines for determination of stream functions (α).

3.8 Conclusion

A novel flow visualisation technique has been developed which is relatively cheap, simple and flexible for obtaining good, clear three-dimensional pictures of fluid flows around rotating stirrers. Two views (horizontal and vertical) can be obtained simultaneously, enabling visualisation and measurements to be carried out relatively easily in three-dimensions. The method allows a permanent record of the flows to be taken which may be studied at leisure at a later date. It also enables flow patterns to be determined as well as the parameters associated with both primary and secondary flows.

CHAPTER 4

MATHEMATICAL MODELLING

4.0 Introduction

As mentioned in an earlier chapter a theoretical model describing the flows generated in simple mixing systems would help a great deal in predicting the flows for more complex industrial mixers. Scale-up would be easier and both time and money could be saved.

In this chapter, the equations associated with the flows due to the stirrers rotating under both primary and secondary flow conditions and the mathematical methods developed to solve them are outlined. The differential equations describing the flows were developed by Dr. Williams [112] and the computer program used to solve the equations for the cylindrical stirrer using numerical methods was developed by Dr. Knight [44]. It is hoped that the theoretical techniques used here will help to contribute to any future work in this field.

4.1 Equations

There are essentially three types of equations which were used to describe the flows induced by the rotating cylinder and the rotating disc. These are given below.

(i) The Stress Equations of Motion

These are also known as the Cauchy Equations and describe for Newtonian and non-Newtonian fluids, the balance between the inertial forces, the pressures and the stresses due to the liquid itself. Due to the cylindrical nature of the geometry studied, it is convenient to use cylindrical polar co-ordinates

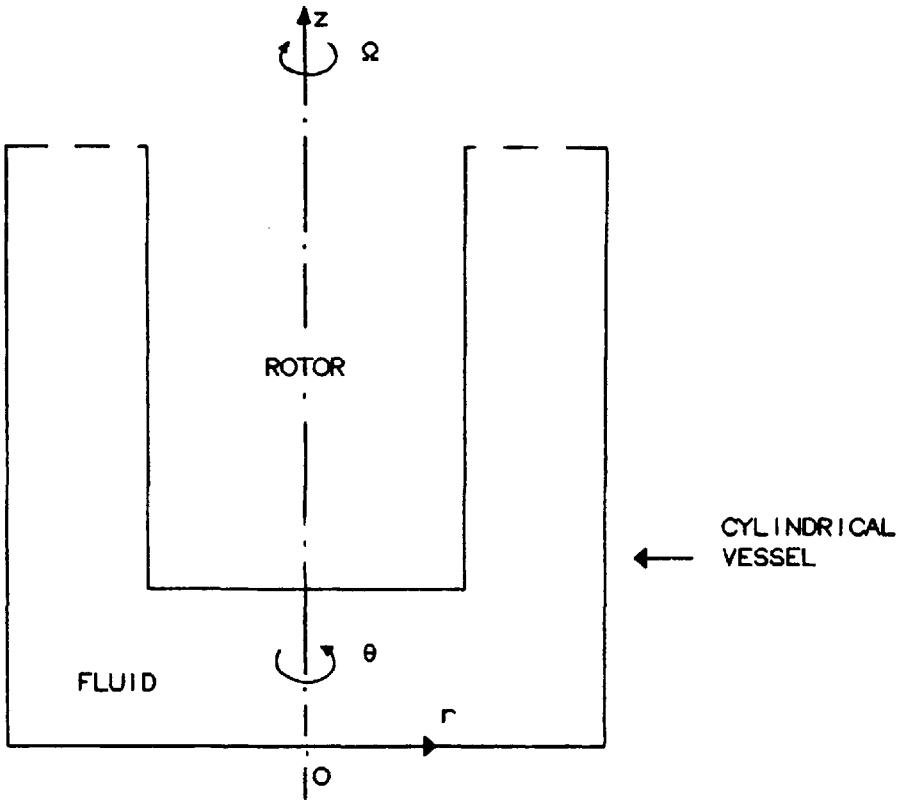

Figure 4.1 Diagram showing cylindrical co-ordinates

r, θ, z with the z-axis along the axis of rotation (Fig. 4.1). The equations are presented in terms of the stress in the r, θ and z directions. We consider only steady (i.e. $\partial/\partial t = 0$), isothermal flows with the density of the fluid taken as constant and assume that the flow is axi-symmetric with no changes occurring in the θ direction (i.e. $\partial/\partial\theta = 0$). Therefore, the equations of motion are reduced to the following.

$$\rho\left[V_r\frac{\partial V_r}{\partial r} - \frac{V_\theta^2}{r} + V_z\frac{\partial V_r}{\partial z}\right] = \left[\frac{1}{r}\frac{\partial(r\tau_{rr})}{\partial r} + \frac{\partial(\tau_{zr})}{\partial z} - \frac{\tau_{\theta\theta}}{r}\right] - \frac{\partial p}{\partial r} \qquad (4.1)$$

$$\rho\left[V_r\frac{\partial V_\theta}{\partial r} + \frac{V_r V_\theta}{r} + V_z\frac{\partial V_\theta}{\partial z}\right] = \left[\frac{1}{r^2}\frac{\partial(r^2\tau_{r\theta})}{\partial r} + \frac{\partial(\tau_{z\theta})}{\partial z}\right] \qquad (4.2)$$

$$\rho\left[V_r\frac{\partial V_z}{\partial r} + V_z\frac{\partial V_z}{\partial z}\right] = \left[\frac{1}{r}\frac{\partial(r\tau_{rz})}{\partial r} + \frac{\partial(\tau_{zz})}{\partial z}\right] - \frac{\partial p}{\partial z} - \rho g \qquad (4.3)$$

where τ_{ij} are the physical components of the extra stress tensor due to the structure of the fluid

V_r, V_θ, V_z are the velocities in the r, θ and z directions respectively.

p is an arbitrary isotropic pressure

ρ is the density of the fluid

g is the gravitational constant

(ii) The Continuity Equation

This equation describes the conservation of mass. After considering the assumptions given above and also assuming that no expansion or compression of the liquid occurs, the equation reduces to the following.

$$\frac{1}{r}\frac{\partial(rV_r)}{\partial r} + \frac{\partial V_z}{\partial z} = 0 \qquad (4.4)$$

(iii) The Constitutive Equation

This is also known as the rheological equation of state and is given by equation (4.5). It shows the relation between the stress as τ_{ik} and the deformation rate for a purely viscous generalised Newtonian fluid.

$$\tau_{ik} = 2\eta(q)e_{ik} \qquad (4.5)$$

where e_{ik} is the first rate of strain tensor [7, 95] and represents velocity gradients with distance. Due to symmetry there are essentially six components of the rate of strain and consequently stress tensor and they are given by

$$e_{rr} = \frac{\partial V_r}{\partial r}, \qquad e_{\theta\theta} = \frac{V_r}{r}, \qquad e_{zz} = \frac{\partial V_z}{\partial z}$$

$$e_{r\theta} = \frac{r}{2}\frac{\partial \omega}{\partial r}, \qquad e_{rz} = \frac{1}{2}\left[\frac{\partial V_r}{\partial z} + \frac{\partial V_z}{\partial r}\right], \qquad e_{z\theta} = \frac{r}{2}\frac{\partial \omega}{\partial z} \tag{4.6}$$

$$\omega = \frac{V_\theta}{r} \tag{4.7}$$

where ω is the rotational angular speed of the fluid

q is a representative deformation rate for the flow and is given by

$$q = \left[2 \{ e_{rr}^2 + e_{\theta\theta}^2 + e_{zz}^2 + 2(e_{r\theta}^2 + e_{rz}^2 + e_{\theta z}^2) \} \right]^{1/2} \tag{4.8}$$

Depending on the precise form of the variable viscosity, $\eta(q)$ in equation (4.5) we may use the Cross and Carreau fluid models (see section 3.4.2) which represent shear-thinning behaviour and are given by

Cross $$\eta(q) = \eta_\infty + (\eta_0 - \eta_\infty) / (1 + (\lambda q)^{1-n}) \tag{4.9}$$

Carreau $$\eta(q) = \eta_\infty + (\eta_0 - \eta_\infty)(1 + \lambda^2 q^2)^{(n-1)/2} \tag{4.10}$$

where η_0 is the zero shear viscosity

η_∞ is the infinite shear viscosity

$\lambda>0$, $n<1$ are constants

$\eta(q)$ is a constant η_0 for Newtonian fluids with $n=1$

4.2 Primary Flow Simulation

4.2.1 Cylindrical Stirrer

Due to symmetry about the axis of rotation a section through the axis gives a two-dimensional geometry (Fig. 4.2). The base of the container (radius r_c) is at $z=0$ and the base of the rotor (radius r_b)

is at $z=z_b$ with the fluid surface at $z=z_c$ assumed flat (Fig. 3.1).

Primary flow occurs as the Reynolds number approaches zero i.e. very slow flows with negligible contribution from inertial forces ($\rho \approx 0$). The fluid moves in closed loops or shells around the stirrer and there is negligible motion in the vertical and radial directions. Therefore, $v_r=v_z=0$ in these directions and consequently $e_{rr}=0$, $e_{\theta\theta}=0$, $e_{zz}=0$ and $e_{rz}=0$. Also, the r and z equations of motion disappear and only the θ equation of motion remains.

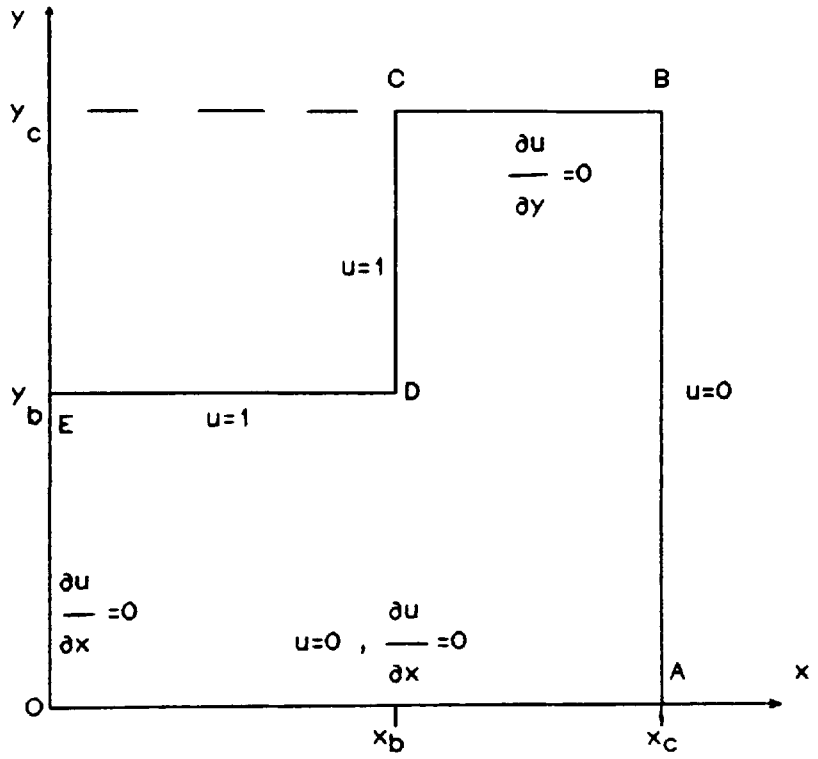

Figure 4.2 Boundary conditions for the cylindrical stirrer rotating at $Re \rightarrow 0$ (primary flow).

For convenience all distances, such as r and z are non-dimensionalised with respect to the rotor radius r_b and velocities with respect to the rotational speed Ω for eventual scale-up and comparative purposes. We, therefore, write

$$z = r_b y, \qquad r = r_b x \tag{4.11}$$

In these x, y co-ordinates the velocity distribution is taken as

$$V_x = 0, \qquad V_\theta = r_b x \Omega u\ (x,y), \qquad V_y = 0 \tag{4.12}$$

In the non-dimensional form the stirrer rotates at an angular speed of 1. Furthermore, for primary flow equation (4.8) reduces to

$$q = \Omega\dot{\gamma} = \Omega x \left[\left[\frac{\partial u}{\partial x} \right]^2 + \left[\frac{\partial u}{\partial y} \right]^2 \right]^{1/2} \tag{4.13}$$

where q is the deformation rate.

$\dot{\gamma}$ is the non-dimensional strain rate.

Incidentally, equation (4.13) in its relevant form reduces to give the usual strain rate in flows due to concentric cylinders of infinite length [92] and flows between parallel plates [95].

The boundary conditions used are given in Figure 4.2 and are as follows.

On	OA, AB	$u = 0$	stationary walls with no slip
On	DE, CD	$u = 1$	no slip at rotor
On	BC	$\partial u/\partial y = 0$	from no normal stress on the free surface $\tau_{z\theta} = 0$
On	OE	$\partial u/\partial x = 0$	usual symmetry across y-axis

(4.14)

where $x_c = r_c/r_b, \quad y_b = z_c/r_b, \quad y_c = z_c/y_b$ (4.15)

Thus, taking all the assumptions made into consideration and substituting equation (4.12) into equation (4.2), the following equation was obtained from equation (4.2)

$$\frac{\partial}{\partial x}\left[P(x,y)\frac{\partial u}{\partial x}\right]+\frac{\partial}{\partial y}\left[P(x,y)\frac{\partial u}{\partial y}\right]=0 \qquad (4.16)$$

where $$P(x,y)=x^3\mu(\dot{\gamma}) \qquad (4.17)$$

$$\mu(\dot{\gamma})=\frac{\eta(\Omega\dot{\gamma})}{\eta_0} \qquad (4.18)$$

The self-adjoint non-linear elliptic partial differential equation (4.16) was solved assuming P to be known and subject to the boundary conditions given in (4.14) using the finite difference approximation and a method from Varga [93] used by Paddon [66] (see section 4.2.5) to study a problem similar to that investigated here.

The finite element method has been used to study the Newtonian flow around a rotating cylinder [31] the results of which are briefly presented in Chapter 5. However, the finite difference method proved to be far simpler with computation time considerably less than for the finite element method. Therefore, on the basis of this limited comparison since the results obtained from the two techniques are virtually the same and together with the fact that it is a cheaper method the finite difference approximation technique was used for this study.

It should be noted here that Paddon's method [66] together with finite difference approximation was used for preliminary work on primary flows only for the cylindrical stirrer [8]. It was used unsuccessfully for solving the equations due to secondary flows (see section 4.3.1) and therefore a different method by Pao [67] was utilised for secondary flows and subsequent primary flows, for both the cylindrical and disc rotors.

4.2.2 Couple on the Cylindrical Stirrer

The couple M on the cylindrical stirrer is given by

$$M = 2\pi\Omega\eta_0 r_b^3 \left[\int_0^1 x^3 \mu(\gamma) \left| \frac{\partial u}{\partial y} \right| dx + \int_{y_b}^{y_c} \mu(\gamma) \left| \frac{\partial u}{\partial x} \right| dy \right] \qquad (4.19)$$

contribution from base DE; contribution from side CD

Since each derivative of u has a singularity at the sharp corner D (i.e. rim of rotor) there is some difficulty in using (4.19) as it stands. Following the standard technique (55) for removing such singularities M may be calculated as

$$M = 2\pi\Omega\eta_0 r_b^3 \left[I_1 + I_2 + K_1 \right] \qquad (4.20)$$

where

$$I_1 = \int_0^1 x^3 \left[\mu(\gamma) \left| \frac{\partial u}{\partial y} \right| - \frac{2}{3} \mu_\infty |G_D| (1-x)^{-1/3} \right] dx \qquad (4.21)$$

$$I_2 = \int_{y_b}^{y_c} \left[\mu(\gamma) \left| \frac{\partial u}{\partial x} \right| - \frac{2}{3} \mu_\infty |G_D| (y-y_b)^{-1/3} \right] dy \qquad (4.22)$$

$$K_1 = \mu_\infty |G_D| \left[\frac{81}{220} + (y_c - y_b)^{2/3} \right] \qquad (4.23)$$

Both integrals of I_1 and I_2 are taken to be zero at the corner D and G_D is a constant determined from the knowledge of u near the corner.

4.2.3 Disc Stirrer

A diagram of the disc stirrer is shown in Figure 3.2. It has very similar dimensions to that of the cylindrical stirrer with the radius r_b the same. The boundary conditions are also very similar (Fig. 4.3) and are given below.

On	OA, AB	$u = 0$	stationary walls with no slip	
On	ED, DH, HG, GC	$u = 1$	no slip at rotor	(4.24)
On	BC	$\partial u/\partial y = 0$	no normal stress at free surface	
On	OE	$\partial u/\partial x = 0$	usual symmetry across y-axis	

where $x_c = r_c/r_b$, $x_g = r_g/r_b$, $y_b = z_b/r_b$,

$y_g = z_g/r_b$, $y_c = z_c/r_b$ (4.25)

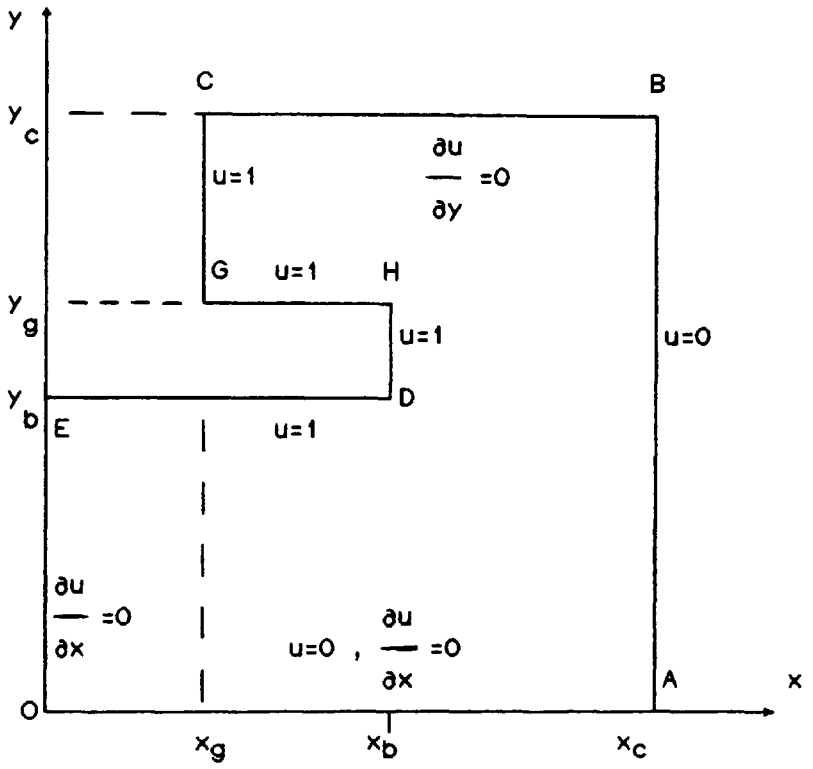

Figure 4.3 Boundary conditions for the disc stirrer rotating at $Re \rightarrow 0$ (primary flow).

For Reynolds numbers approaching zero, the fluid flows in closed shells around the disc stirrer and, therefore, the same equations apply as for the cylindrical stirrer. Equation (4.16) was solved for the disc geometry, using Pao's method (see section 4.2.6) and the above boundary conditions.

4.2.4 Couple on the Disc Stirrer

The expression for the couple M on the disc stirrer is more complicated than that on the cylindrical one. In this case, there is a contribution from four sides CG, GH, HD and DE and the extra corner at H has to be considered as well as that at D.

The couple is given by the following

$$M = 2\pi\Omega\eta_0 r_b^3 \left[\int_0^1 x^3 \mu(\gamma) \left| \frac{\partial u}{\partial y} \right| dx + \int_{y_b}^{y_g} \mu(\gamma) \left| \frac{\partial u}{\partial x} \right| dy + \int_{x_g}^1 x^3 \mu(\gamma) \left| \frac{\partial u}{\partial y} \right| dx + \frac{r_g^3}{r_b^3} \int_{y_g}^{y_c} \mu(\gamma) \left| \frac{\partial u}{\partial x} \right| dy \right] \quad (4.26)$$

where r_g is the radius of the shaft.

The singularities at the corners D and H may be removed using the same standard technique [55] as that used for the cylindrical rotor and the couple M may be evaluated as

$$M = 2\pi\Omega\eta_0 r_b^3 \left[I_1 + I_3 + I_4 + I_5 + K_2 \right] \quad (4.27)$$

where

$$I_1 = \int_0^1 x^3 \left[\mu(\gamma) \left| \frac{\partial u}{\partial y} \right| - \frac{2}{3} \mu_\infty |G_D| (1-x)^{-1/3} \right] dx \quad (4.28)$$

$$I_3 = \int_{y_b}^{y_g} \left[\mu(\gamma) \left| \frac{\partial u}{\partial x} \right| - \frac{2}{3} \mu_\infty |G_D| (y-y_b)^{-1/3} - \frac{2}{3} \mu_\infty |G_H| (y_g - y)^{-1/3} \right] dy \quad (4.29)$$

$$I_4 = \int_{x_g}^1 x^3 \left[\mu(\gamma) \left| \frac{\partial u}{\partial y} \right| - \frac{2}{3} \mu_\infty |G_H| (1-x)^{-1/3} \right] dx \quad (4.30)$$

$$I_5 = \frac{r_g^3}{r_b^3} \int_{y_g}^{y_c} \mu(\gamma) \frac{\partial u}{\partial x} dy \quad (4.31)$$

$$K_2 = \left[\frac{81}{220} \right] \mu_\infty |G_D| + \mu_\infty (y_g - y_b)^{2/3} \left[|G_D| + |G_H| \right] - \left[\left[\frac{81}{220} \right] (1-x_g)^{1/3} + \left[\frac{27}{20} \right] x_g (1-x_g)^{8/3} + 3x_g^2 (1-x_g)^{5/3} + x_g^3 (1-x_g)^{2/3} \right] \quad (4.32)$$

The integrands I_1, I_3, I_4 and I_5 are taken to be zero at the corners. G_D and G_H are constants determined from the knowledge of u near the corners D and H respectively.

4.2.5 Power Number

The dimensionless Power number N_p on either the cylindrical or disc stirrer is given by

$$N_p = \frac{M}{\rho \Omega^2 r_b^5} \tag{4.33}$$

4.2.6 Finite Difference Approximation and Paddon's Method

A finite difference grid of width h and height k defined by the following and shown in Figure 4.4 was used.

$$x_i = ih \quad (i=0,\ 1..n,\ n+1..N) \qquad y_j = jk \quad (j=0,\ 1..m,\ m+1..M) \tag{4.34}$$

$$\text{where} \quad nh = 1, \quad Nh = x_c, \quad mk = y_b, \quad Mk = y_c \tag{4.35}$$

For interior grid points in regions 1, 2 and 3, equation (4.16) was discretised [1,66] using the five-point molecule shown in Figure 4.5 and given by

$$-a_{ij}\, u_{i,j-1} - b_{ij}\, u_{i-1,j} + c_{ij}\, u_{ij} - d_{ij}\, u_{i+1,j} - e_{ij}\, u_{i,j+1} = O(h^4) \tag{4.36}$$

where

$$a_{ij} = \frac{1}{\alpha_1} P_{i,j-1/2}; \quad b_{ij} = \alpha_1 P_{i-1/2,j}; \quad d_{ij} = \alpha_1 P_{i+1/2,j}; \quad e_{ij} = \frac{1}{\alpha} P_{i,j+1/2} \tag{4.37}$$

$$\alpha_1 = k/h; \quad c_{ij} = a_{ij} + b_{ij} + d_{ij} + e_{ij} \tag{4.38}$$

Values of points in region 4 are taken to be zero for convenience since we are only concerned with points in the fluid and not in the rotor.

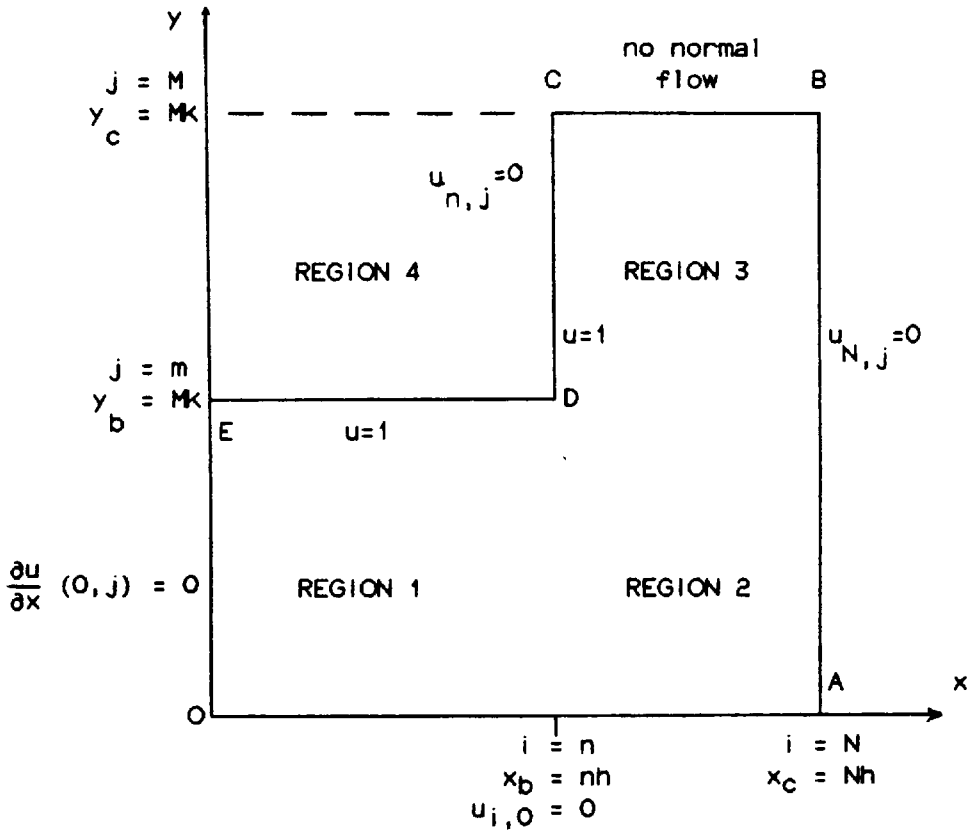

Figure 4.4 The cylindrical geometry showing a finite difference approximation grid of width h and height K.

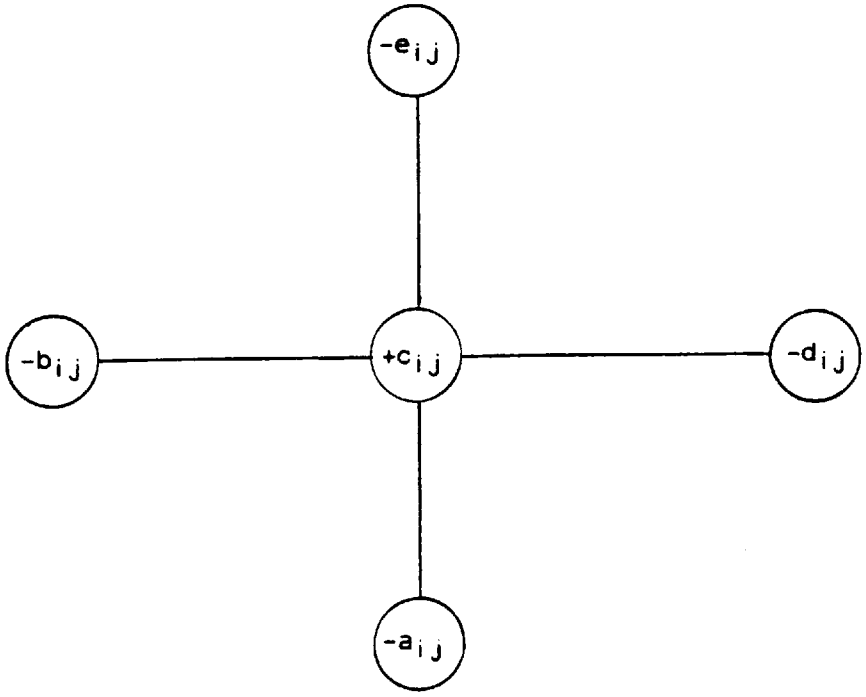

Figure 4.5 The five-point molecule used for discretisation.

For points on boundary OE, (to $O(h^3)$), $\frac{\partial u}{\partial x}(0,j) = 0$ gives

$$u_{0,j} = \left[\frac{4}{3}\right] u_{1,j} - \left[\frac{1}{3}\right] u_{2,j} + O(h^3) \qquad (4.39)$$

For points on boundary BC, (to $O(h^3)$), $\frac{\partial u}{\partial y}(i,M) = 0$

gives, $$u_{i,M} = \left[\frac{4}{3}\right] u_{i,M-1} - \left[\frac{1}{3}\right] u_{i,M-2} + O(h^3) \qquad (4.40)$$

Therefore, u_{ij} is unknown in regions 1,2,3 and on the boundaries OE and BC. If the values of P are known, equations (4.36), (4.39) and (4.40) give a set of simultaneous equations of the form

$$AU = B \qquad (4.41)$$

in which A is a block tridiagonal (N-1)(M-1) by (N-1)(M-1) matrix, U is the unknown and B is a known vector of length (N-1)(M-1). More details may be found in reference [66].

A computer program was developed in which equation (4.41) was solved iteratively using Stone's Strongly Implicit method [84], which is considered arithmetically economical, and the NAG routine D03EBF [57]. A flow diagram showing the main features of the program is shown in Figure 4.6.

Due to non-linearity through P, provision is made within the computer program to obtain angular velocity u(x,y) for a particular non-Newtonian fluid by starting from a Newtonian solution. The required non-Newtonian solution could be reached via a sequence of steps in which the non-Newtonian parameters η_0, η_∞, n and λ were incremented from Newtonian towards those of the required fluid. However, it was found that the same non-Newtonian solution could often be obtained in one direct step from the initial approximation.

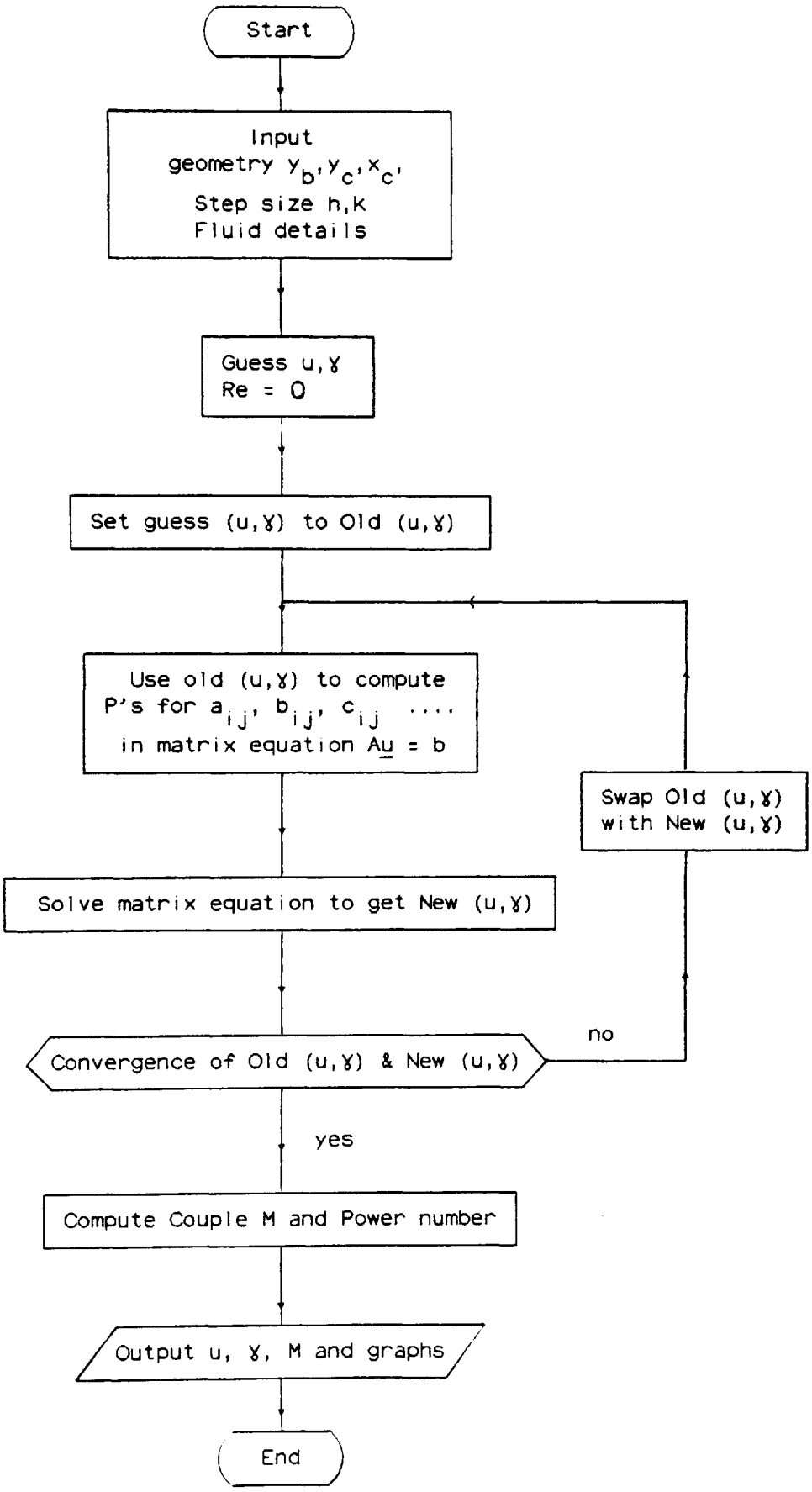

Figure:4.6 Flow Diagram for Primary Flow Simulation for the Cylindrical Stirrer using Paddon's Method.

The strain rate $\gamma(x,y)$ was also iteratively calculated to $O(h^2)$ from $u(x,y)$ until converged values were obtained and Richardson Extrapolation was used to improve the accuracy of u and γ. Convergence was typically obtained within 150 iterations (80 seconds program run-time on the DEC-20 mainframe computer) for a suitable choice of the iteration acceleration factor [84].

The couple M was calculated from u and γ using the trapezium rule and equation (4.20) where G_D is given by

$$G_D = \left[\frac{2}{\sqrt{3}}\right] K^{-2/3} \left[\alpha_1^{4/3}(u_{n+1,m} - 1) + (u_{n,m-1} - 1)\right] / (\alpha_1^{+2/3} + 1) + O(h^2) \quad (4.42)$$

involving various points in the fluid around $D = (x_n, y_n)$ are taken. The Power number N_p was calculated using equation (4.33)

Using the NAG graphics package together with the above computer program, contours of the angular velocity u and strain rate γ were obtained. As mentioned before, Paddon's method described above was used for preliminary work on primary flows around the cylindrical stirrer only. The results obtained from this method may be found in reference [8]. Pao's approach replaced Paddon's method for further work and is outlined in the following section.

4.2.7 Pao's Method

This method proved successful for solving the equations due to both the primary flows and the more complicated secondary flows. Pao represented the angular velocity in terms of a quantity Γ (Eqn. 4.44). The primary flow equation of motion in the θ direction with zero Reynolds number may now be written as follows,

$$\mu \left[\frac{\partial^2 \Gamma}{\partial x^2} + \frac{\partial^2 \Gamma}{\partial y^2} - \frac{1}{x} \frac{\partial \Gamma}{\partial x} \right] + \frac{\partial \mu}{\partial x} \left[\frac{\partial \Gamma}{\partial x} - \frac{\Gamma}{x} \right] + \frac{\partial \mu}{\partial y} \left[\frac{\partial \Gamma}{\partial y} \right] = 0 \qquad (4.43)$$

where $\Gamma = x^2 u$ (4.44)

The above partial differential equation may be differenced using central differences with h=k to give the following,

$$\Gamma_{ij} = \frac{1}{4 \left[\mu_{ij} + \frac{h^2}{2x_i} \frac{\partial \mu}{\partial x}_{ij} \right]} \left[\mu_{ij} (\Gamma_{i+1,j} + \Gamma_{i-1,j} + \Gamma_{i,j+1} + \Gamma_{i,j-1}) + \frac{h}{2} \left[\left[\frac{\partial \mu}{\partial x}_{ij} - \frac{\mu_{ij}}{x_i} \right] \left[\Gamma_{i+1,j} - \Gamma_{i-1,j} \right] + \left[\frac{\partial \mu}{\partial y}_{ij} \left[\Gamma_{i,j+1} - \Gamma_{i,j-1} \right] \right] \right] \qquad (4.45)$$

where

$$\frac{\partial u}{\partial x}_{ij} = \frac{\mu_{i+1,j} - \mu_{i-1,j}}{2h} + O(h^2)$$

$$\frac{\partial u}{\partial y}_{ij} = \frac{\mu_{i,j+1} - \mu_{i,j-1}}{2h} + O(h^2) \qquad (4.46)$$

Essentially the same boundary conditions as those given by equation (4.14) were used except that this time Γ replaced u and was determined by equation (4.44). Once the values of Γ were determined everywhere in the fluid, the corresponding values of u were calculated using this equation. Incidentally, $\Gamma = 0$ on OE. The strain rates and Power numbers were calculated using equation (4.13), (4.20), and (4.33) respectively.

The computer program developed using Paddon's method was replaced by another program utilizing Pao's technique. The latter method proved to be far simpler than that of Paddon's, since no matrix equations were used. No apparent difference in the computed values of angular velocity u and strain rate $\dot{\gamma}$ in the two methods were encountered when compared where appropriate. In other words, the two methods agree in the final values and, therefore, it seemed only sensible to proceed with the simpler method.

The new version of the computer program is shown by the flow diagram in Figure 4.7. This is, in fact, the first part of a more complex computer program (not presented) which determines the parameters for both secondary and primary flows (Fig. 4.10). The program made use of the simple non-linear Jacobi iteration method [84] to obtain the required values. Initial guess values for Γ were used from which new Γ values were obtained using equation (4.45). These new values then replaced the guessed values and the process was repeated for subsequent iterates until the final two iterates were found to be within a certain tolerance; 0.002 was used for our purpose.

Once the value of Γ was obtained at various points in the geometry, equation (4.44) was used to obtain the corresponding u values. The values for strain rates were obtained in a similar way using equation (4.13) and couple values together with Power numbers were also determined. The relevant contours of Γ, u and γ were obtained after making the necessary changes in the NAG graphics subroutine to give clearer diagrams (see section 4.3.2).

The computer program developed for the cylindrical stirrer using Pao's technique was changed as necessary to give a program to solve the equations for the disc stirrer. The changes are outlined in section 4.3.2 and a flow diagram is shown in figure 4.7. In practice, the primary flow calculation was carried out by the first part of a more complex program which could also deal with secondary flows. This new program was used in a similar way to the one above to give the values of Γ, u, strain rates γ and the couple. Couple values were determined using equation (4.27) with G_D (from equation 4.42) and G_H (from equation 4.47 below) calculated by taking points in the fluid around the corners D and H. The relevant contours of Γ, u and γ were also obtained.

$$G_H = \left[\frac{2}{\sqrt{3}}\right] k^{-2/3} \left[\alpha^{4/3} \left[u_{n+1,m2} - 1\right] + \left[u_{n,m2+1} - 1\right]\right] / \left[\alpha_1^{2/3} + 1 \right] \qquad (4.47)$$

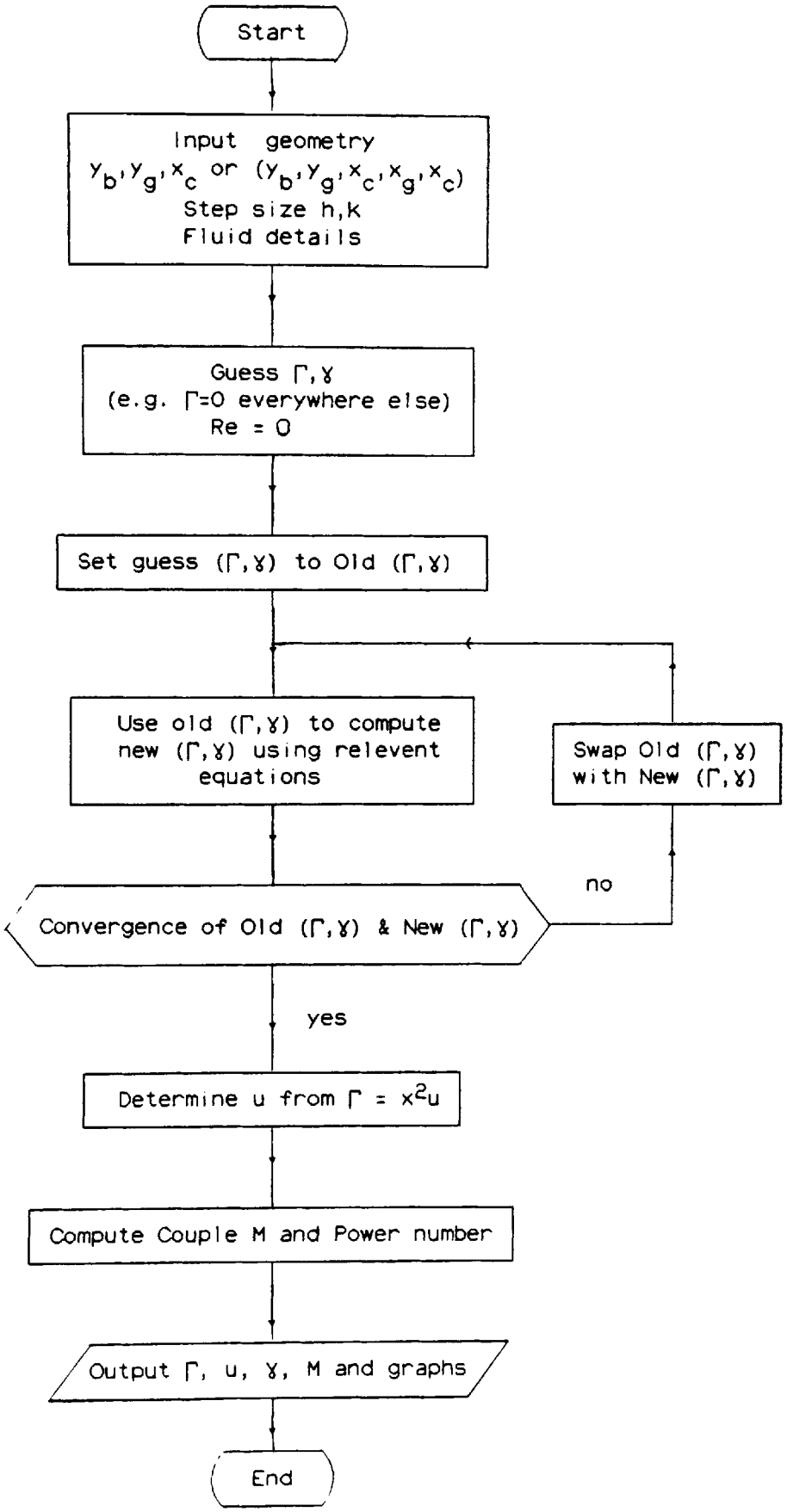

Figure: 4.7 Flow Diagram for Primary Flow Simulation for the Cylindrical (or Disc) Stirrer using Paddon's Method.

4.3 Secondary Flow Simulation

4.3.1 Cylindrical Stirrer

Streamline or secondary flows occur at higher Reynolds numbers than those required for primary flows where Re is essentially zero. In the secondary flow situation the fluid particles do not merely travel around with the rotor in closed loops, but have motion in all r, θ and z directions. Therefore, secondary flows are substantially more difficult to model than primary flows.

The velocity distribution is given by the following

$$V_r = \frac{r_b \Omega}{x} \frac{\partial \alpha}{\partial y}, \qquad V_\theta = r_b \Omega u x, \qquad V_z = \frac{-r_b \Omega}{x} \frac{\partial \alpha}{\partial x} \tag{4.48}$$

where α is a non-dimensional stream function.

With this velocity distribution, the continuity equation (4.4) is automatically satisfied. Again, in the non-dimensionalised form the stirrer rotates at an angular speed of 1.

Thus noting all the assumptions made and substituting equations (4.5) and (4.47) into the equations of motion (4.1), (4.2) and (4.3) gives from the θ equation

$$\frac{\partial}{\partial x}\left[x^3 \mu(\gamma) \frac{\partial u}{\partial x} \right] + \frac{\partial}{\partial y}\left[x^3 \mu(\gamma) \frac{\partial u}{\partial y} \right] = F_p \tag{4.49}$$

where F_p is given below in equation (4.52)

The isotropic pressure p is eliminated from the r and z equations by differentiation and subtraction. A fourth order equation in α is obtained which is split into two second order elliptic type equations similar to that obtained for the θ equation. These are given by the following,

$$\frac{\partial}{\partial x}\left[x^3\,\frac{\partial \beta}{\partial x}\right] + \frac{\partial}{\partial y}\left[x^3\,\frac{\partial \beta}{\partial y}\right] = F_s \qquad (4.50)$$

$$\frac{\partial}{\partial x}\left[x^3\,\frac{\partial \psi}{\partial x}\right] + \frac{\partial}{\partial y}\left[x^3\,\frac{\partial \psi}{\partial y}\right] = x^3\beta \qquad (4.51)$$

where $$F_p = Re \times \left[\, 2u\alpha_y + x\,(\alpha_y u_x - \alpha_x u_y)\,\right] \qquad (4.52)$$

$$F_s = \frac{1}{\mu}\Big[\, Re\,\Big[\,\alpha_y\,(\alpha_{xxx} + \alpha_{xyy}) - \alpha_x\,(\alpha_{yyy} + \alpha_{xxy}) + \frac{1}{x}(\alpha_x\alpha_{xy} - \alpha_y\,(2\alpha_{yy} + 3\alpha_{xx})) + \frac{3}{x^2}\,\alpha_x\alpha_y - 2x^3 u u_y\,\Big] - \frac{1}{x^2}\left[\, A^x\mu_x + A^y\mu_y + A^{xy}\mu_{xy} + A^{xx}\mu_{xx} + A^{yy}\mu_{yy}\,\right]\Big] \qquad (4.53)$$

$$\gamma = \frac{1}{x^2}\Big[\, x^6\left[\, u_x^2 + u_y^2\,\right] + 4\alpha_y^2 + \alpha_x^2 + 2x\left[\,\alpha_x\,(\alpha_{yy} - \alpha_{xx}) - 2\alpha_y\,\alpha_{xy}\,\right] + x^2\left[\, 4\alpha_{xy}^2 + \left[\,\alpha_{yy} - \alpha_{xx}\,\right]^2\,\right]\Big]^{1/2} \qquad (4.54)$$

$$\alpha = x^2\,\psi \qquad (4.55)$$

$$\beta = \frac{\chi}{x}, \quad \chi = \frac{\partial V_x}{\partial y} - \frac{\partial V_y}{\partial x} \qquad (4.56)$$

$$Re = \frac{\rho\, r_b^2\, \Omega}{\eta_o} \qquad (4.57)$$

and for convenience of notation

$$\left.\begin{aligned}
u_x &= \frac{\partial u}{\partial x}\,, \quad \alpha_x = \frac{\partial \alpha}{\partial x}\,, \quad \alpha_{xx} = \frac{\partial^2 \alpha}{\partial x^2}\,, \quad \alpha_{xy} = \frac{\partial^2 \alpha}{\partial x \partial y} \\
u_y &= \frac{\partial u}{\partial y}\,, \quad \alpha_y = \frac{\partial \alpha}{\partial y} \qquad \text{etc} \\
A^x &= x^3\left[\, 2\alpha_{xxx} + 2\alpha_{xyy}\,\right] \\
A^y &= x^3\left[\, 2\alpha_{yyy} + 2\alpha_{xxy}\,\right] + x^2\left[\, -2\alpha_{xy}\,\right] \\
A^{xy} &= x^3\left[\, 4\alpha_{xy}\,\right] + x^2\left[\, -2\alpha_y\,\right] \\
A^{xx} &= x^3\left[\,\alpha_{xx} - \alpha_{yy}\,\right] - x^2\alpha_x \\
A^{yy} &= x^3\left[\, -\alpha_{xx} + \alpha_{yy}\,\right] + x^2\,\alpha_x
\end{aligned}\right\} \qquad (4.58)$$

The boundary conditions for secondary flow are given by Figure 4.8.

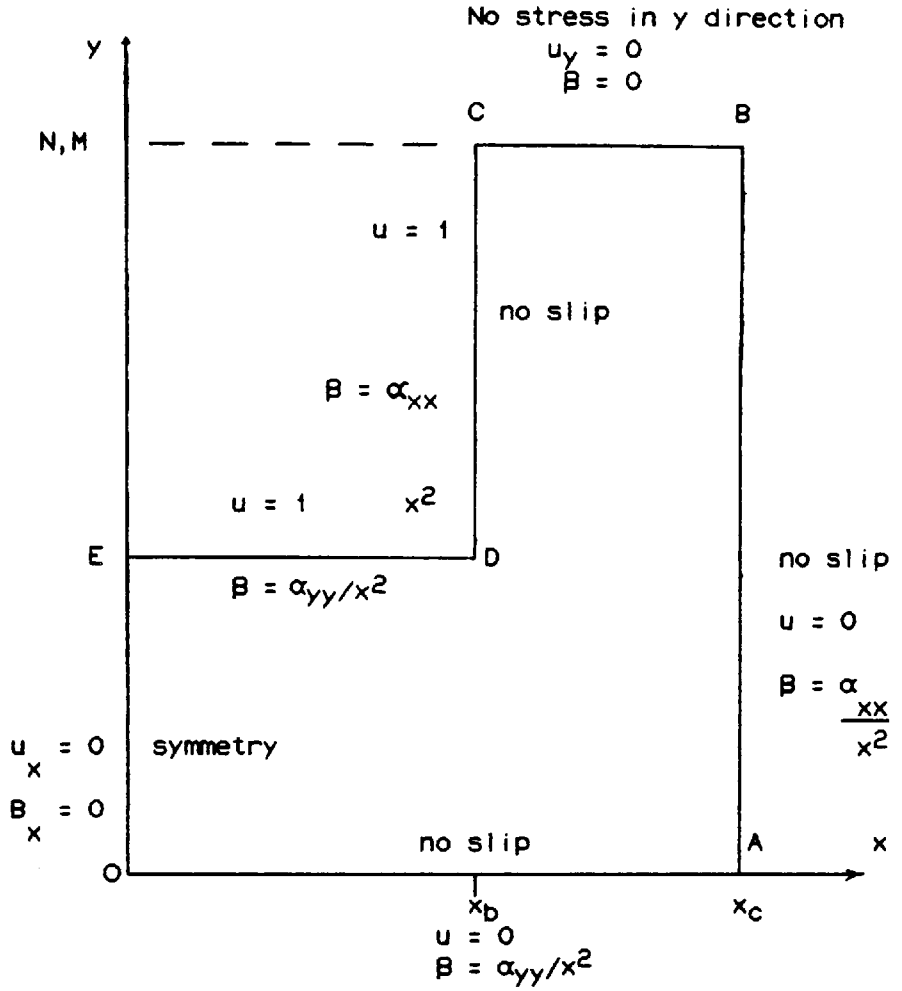

Figure 4.8 Boundary conditions for the cylindrical stirrer rotating under secondary flow regime (Paddon's method).

It can be seen that the partial differential equations (4.49), (4.50) and (4.51) are much more complex than those for primary flows. Using Paddon's method, an attempt was made to solve the three equations for u, β and ψ respectively, from which α could be determined.

Difficulty was encountered in obtaining the secondary flow solution for a Newtonian fluid flowing at Reynolds number greater than 5. Furthermore, iteration to determine the values of u, β and ψ within a certain tolerance limit had to be carried out separately and convergence could not generally be achieved. Also the values of β that were obtained were nearly all positive and therefore did not average out to

be zero over the grid i.e. $\iiint_{fluid} \chi\beta = 0$ [23]. Further inspection showed that the boundary values for β being calculated from the stream function α were almost always positive when negative boundary values for β were expected. A different approach [29, 67] for calculating the boundary conditions was then used but divergence took place with β oscillating increasingly wildly between mainly negative values and mainly positive values. Further progress with this method seemed unlikely and it was not certain which terms were causing the difficulty. A number of different methods of attempting to obtain convergence were tried out, but failed.

Therefore, it was decided to adopt a non-separated iterative method by Pao [67] to solve the equations. The angular velocity u may be expressed in terms of Γ as with primary flows and the equations written in terms of Γ, α and χ rather than u, α and β. The following partial differential equations are then obtained.

$$Re\left[V_x \frac{\partial\Gamma}{\partial x} + V_y \frac{\partial\Gamma}{\partial y}\right] = \mu\left[\frac{\partial^2\Gamma}{\partial x^2} + \frac{\partial^2\Gamma}{\partial y^2} - \frac{1}{x}\frac{\partial\Gamma}{\partial x}\right] + \frac{\partial\mu}{\partial x}\left[\frac{\partial\Gamma}{\partial x} - \frac{2\Gamma}{x}\right] + \frac{\partial\mu}{\partial y}\frac{\partial\Gamma}{\partial y} \tag{4.59}$$

$$x\chi = \alpha_{xx} + \alpha_{yy} - \frac{1}{x}\alpha_x \tag{4.60}$$

$$Re\left[V_x \frac{\partial\chi}{\partial x} + V_y \frac{\partial\chi}{\partial y} - V_x \frac{\chi}{x} - \frac{2\Gamma}{x^3}\frac{\partial\Gamma}{\partial y}\right] = \mu\left[\frac{\partial^2\chi}{\partial x^2} + \frac{\partial^2\chi}{\partial y^2} + \frac{1}{x}\frac{\partial\chi}{\partial x} - \frac{\chi}{x^2}\right]$$

$$+ \frac{\partial u}{\partial x}\left[2\frac{\partial\chi}{\partial x} + \frac{\chi}{x}\right] + \frac{\partial\mu}{\partial y}\left[2\frac{\partial\chi}{\partial y}\right] + \frac{\partial^2\mu}{\partial x\partial y}\left[\frac{4}{x}\alpha_{xy} - \frac{2}{x^2}\alpha_y\right] + \left[\frac{\partial^2\mu}{\partial x^2} - \frac{\partial^2\mu}{\partial y^2}\right]\left[\chi - \frac{2}{x}\alpha_{yy}\right] \tag{4.61}$$

The strain rate γ is given by the following equation

$$\gamma = \frac{1}{x}\left[x^2\left[\left[\frac{\partial\Gamma}{\partial x}\right]^2 + \left[\frac{\partial\Gamma}{\partial y}\right]^2\right] + 4\Gamma\left[1 - x\frac{\partial\Gamma}{\partial x}\right] + x^4\chi^2 + 4x^2\left[\alpha_{xy}^2 - (\alpha_{xy})(\alpha_{yy})\right] + 4x\left[\alpha_x\alpha_{yy} - \alpha_y\alpha_{xy}\right] + 4\alpha_y^2\right]^{1/2} \tag{4.62}$$

The equations (4.59), (4.60) and (4.61) were differenced using central differences and letting h=k which are step lengths as given by equation (4.35) to give the following

$$\Gamma_{ij} = \frac{1}{W}\left[\mu\left[\Gamma_{i+1,j} + \Gamma_{i-1,j} + \Gamma_{i,j+1} + \Gamma_{i,j-1}\right] + \frac{h}{2}\left[\left[\frac{\partial\mu}{\partial x} - \frac{\mu}{x_i}\right]\left[\Gamma_{i+1,j} - \Gamma_{i-1,j}\right] + \frac{\partial\mu}{\partial y}\left[\Gamma_{i,j+1} - \Gamma_{i,j-1}\right]\right] - \frac{Re}{4x_i}\left[\left[\alpha_{i,j+1} - \alpha_{i,j-1}\right]\left[\Gamma_{i+1,j} - \Gamma_{i-1,j}\right] - \left[\alpha_{i+1,j} - \alpha_{i-1,j}\right]\left[\Gamma_{i,j+1} - \Gamma_{i,j-1}\right]\right]\right] \quad (4.63)$$

$$\alpha_{ij} = \frac{1}{4}\left[\alpha_{i+1,j} + \alpha_{i-1,j} + \alpha_{i,j+1}\,\alpha_{i,j-1} - \frac{h}{2x_i}\left[\alpha_{i+1,j} - \alpha_{i-1,j}\right] - h^2 x_i\,\chi_{ij}\right] \quad (4.64)$$

$$\chi_{ij} = \frac{1}{W1}\left[\frac{\mu}{4}\left[\chi_{i+1,j} + \chi_{i-1,j} + \chi_{i,j+1} + \chi_{i,j-1} + \frac{h}{2x_i}\left[\chi_{i+1,j} - \chi_{i-1,j}\right]\right] + \frac{h}{4}\left[\frac{\partial\mu}{\partial y}\left[\chi_{i,j+1} - \chi_{i,j-1}\right] + \frac{\partial\mu}{\partial x}\left[\chi_{i+1,j} - \chi_{i-1,j}\right]\right] + \frac{1}{4x_i}\frac{\partial^2\mu}{\partial x\partial y}\left[\alpha_{i+1,j+1} + \alpha_{i-1,j-1} - \alpha_{i-1,j+1} - \alpha_{i+1,j-1} - \frac{h}{x_i}\left[\alpha_{i,j+1} - \alpha_{i,j-1}\right]\right] + \frac{1}{2x_i}\left[\frac{\partial^2\mu}{\partial y^2} - \frac{\partial^2\mu}{\partial x^2}\right]\left[\alpha_{i,j+1} - 2\alpha_{ij} + \alpha_{i,j+1}\right] - \frac{Re}{16x_i}\left[\left[\alpha_{i,j+1} - \alpha_{i,j-1}\right] * \left[\chi_{i+1,j} - \chi_{i-1,j}\right] - \left[\alpha_{i+1,j} - \alpha_{i-1,j}\right] * \left[\chi_{i,j+1} - \chi_{i,j-1}\right] - \frac{4h\Gamma_{ij}}{x_i^2}\left[\Gamma_{i,j+1} - \Gamma_{i,j-1}\right]\right]\right] \quad (4.65)$$

where

$$W = \frac{1}{4\left[\mu + \frac{h^2}{2x_i}\frac{\partial \mu}{\partial x}\right]} \quad , \quad \mu = \mu_{ij}$$

$$W1 = \frac{1}{4}\left[\mu_{ij}\left[4 + \frac{h^2}{x_i^2}\right] - \frac{h}{x_i}\mu_x - h^2\mu_{xx} + h^2\mu_{yy} - Re\frac{h}{2x_i}\left[\alpha_{i,j+1} - \alpha_{i,j-1}\right]\right.$$

$$\frac{\partial \mu}{\partial x} = \frac{\mu_{i+1,j} - \mu_{i-1,j}}{2h} \quad , \quad \frac{\partial \mu}{\partial y} = \frac{\mu_{i,j+1} - \mu_{i,j-1}}{2h} \qquad (4.66)$$

$$\frac{\partial^2 \mu}{\partial x^2} = \frac{\mu_{i+1,j} - 2\mu_{ij} + \mu_{i-1,j}}{h^2} \quad , \quad \frac{\partial^2 \mu}{\partial y^2} = \frac{\mu_{i,j+1} - 2\mu_{ij} + \mu_{i,j-1}}{h^2}$$

$$\frac{\partial^2 \mu}{\partial x \partial y} = \frac{1}{4h^2}\left[\mu_{i+1,j+1} + \mu_{i-1,j-1} - \mu_{i-1,j+1} - \mu_{i+1,j-1}\right]$$

The boundary conditions used here are given below and shown in Figure 4.9 and obtained in conjuction with the boundary conditions of Figure 4.8.

On	OA	$\Gamma = 0$	no slip at stationary walls
		$\chi = \alpha_{yy}/x$	from equation (4.60)
On	AB	$\Gamma = 0$	no slip at stationary walls
		$\chi = \alpha_{xx}/x$	from equation (4.60)
On	BC	$\partial\Gamma/\partial y = 0$	no normal stress on the free surface
		$\chi = 0$	from equation (4.56)
On	CD	$\Gamma = 1$	no slip at rotor
		$\chi = \alpha_{xx}/x$	from equation (4.60)
On	DE	$\Gamma = x^2$	no slip at rotor
		$\chi = \alpha_{yy}/x$	from equation (4.60)
On	OE	$\Gamma = 0$	from equation (4.44)
		$\chi = 0$	from equation (4.56)
		$\alpha = 0$	on all boundaries

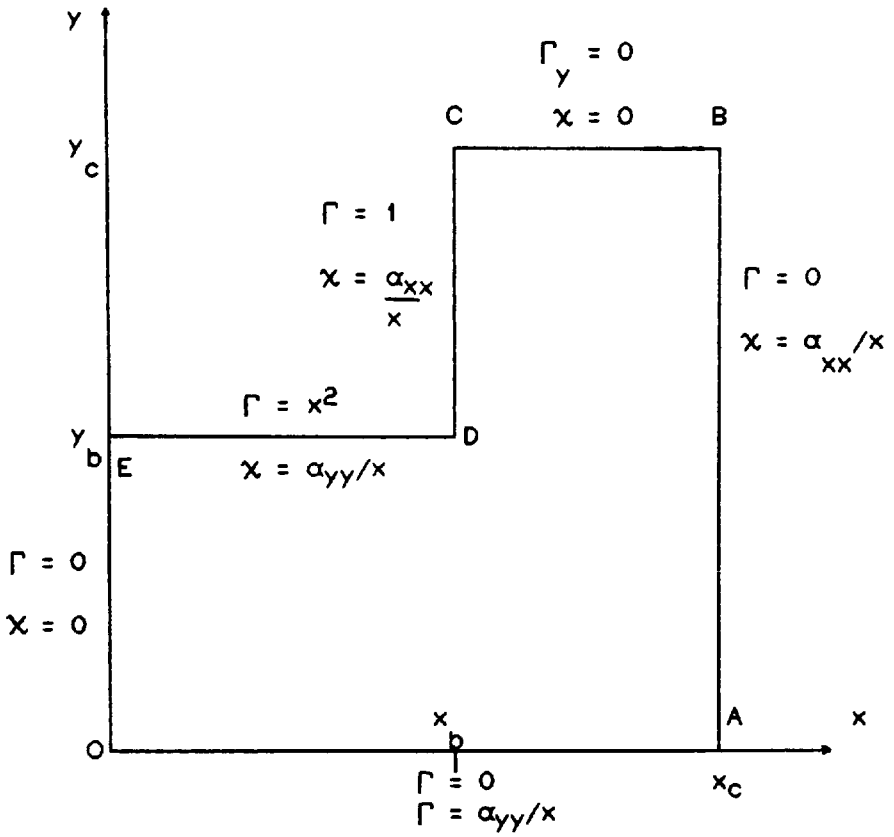

Figure 4.9 Boundary conditions for the cylindrical stirrer rotating under secondary flow regime (Pao's method).

The computer program which utilized Pao's method for secondary flows for the cylindrical stirrer also include the equations for primary flows. A flow diagram of the essential steps in this program is given in Figure 4.10. The Jacobi iteration method was used to obtain the values of Γ, α and χ. An advantage of this method was that no complicated matrix was necessary and unlike Paddon's method co-iteration could be used. In other words, there was no preference as to which of Γ, α and χ values should be calculated first and all of these parameters could be determined simultaneously.

The primary flow solution was used as the initial guess for Γ_{ij} and zero values used for α_{ij} and χ_{ij} in equations (4.63), (4.64) and (4.65) respectively from which new values were obtained. These values

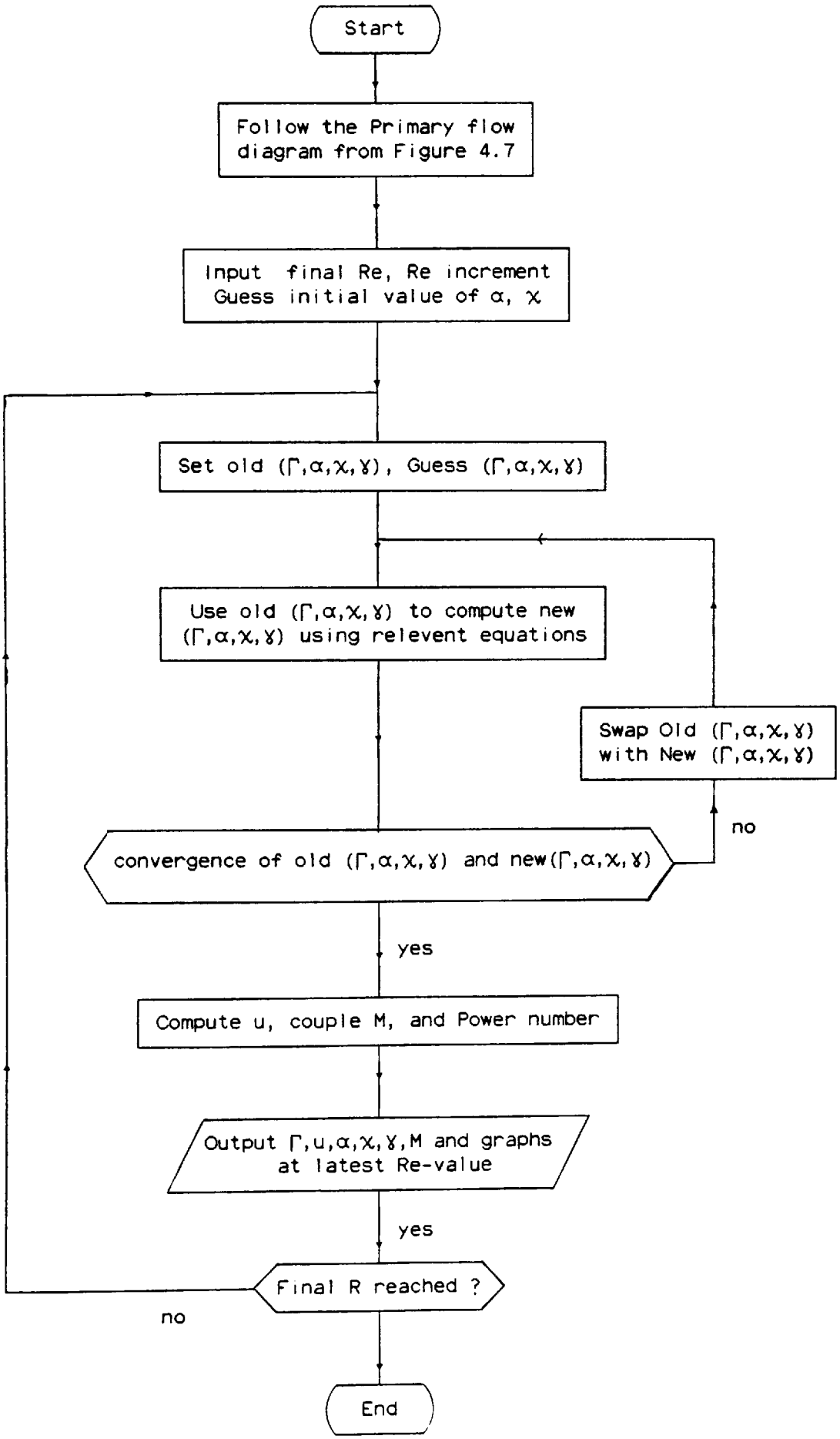

Figure:4.10 Flow Diagram for Primary and Secondary Flow Simulation for the Cylindrical (or Disc) Stirrer using Pao's Method.

then replaced the guessed or old values and the process repeated for subsequent iterates until the final two values were found to be within a tolerance of 0.002 or in some cases 0.005. Convergence could be achieved with this method and the values of β averaged out to be near zero over the fluid i.e. $\iiint_{fluid} \chi \approx 0$.

Using equation (4.44) and knowing Γ_{ij} at various points, the values of angular velocity u could be determined. Strain rates $\dot{\gamma}$, couple values and Power numbers were also calculated.

An option existed in the computer program enabling contours to be drawn for Γ, u, α, χ and $\dot{\gamma}$. The NAG graphics routine was utilised for this purpose. It should be noted here that part of the NAG graphics routine in the program was amended to eliminate all headings so that only the contouring part existed. This was because the titles obtained using the NAG graphics were not very clear. Plot 10 routines [74] were added instead which gave far clearer titles as shown by the contour diagrams in subsequent chapters.

4.3.2 Discharge Efficiency

The Pumping number N_q [85] is given by

$$N_q = 2\pi\Delta\alpha \tag{4.67}$$

and the discharge efficiency DE [58] is given by the ratio of the Power number to the Pumping number as follows

$$DE = \frac{N_p}{N_q} \tag{4.68}$$

4.3.3 Disc Stirrer

As mentioned earlier, the disc stirrer is only a slightly more complicated version of the cylindrical stirrer. The same equations of motions applied and the same assumptions were made. Obviously, the boundary conditions were different and are given in Figure 4.11.

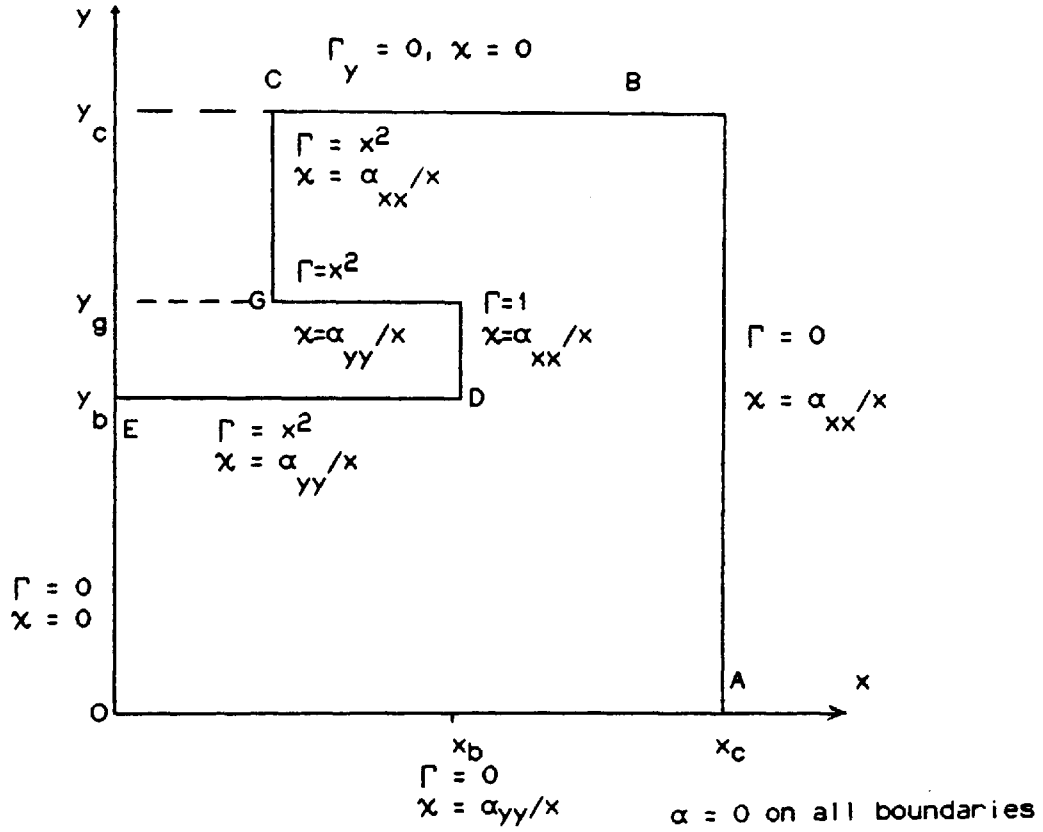

Figure 4.11 Boundary conditions for the disc stirrer rotating under secondary flow regime (Pao's method).

In order to gain a better understanding of the numerical and computing processes involved in solving the relevant equations it was decided that I should develop the computer program to determine the various parameters for the finite disc stirrer. The program for the cylindrical rotor was used as the basis for the disc stirrer since the same equations applied. A number of changes were made and are outlined below. A listing of this program is given in Appendix 4.

(i) The diagram at the beginning of the program was amended to give the finite disc with boundary conditions as shown.

(ii) Two more dimensions x_g and y_g were added to the input section

(iii) The boundary conditions were changed where necessary to incorporate the new ones required for the disc.

(iv) The "new" corner at H was incorporated where required in the various calculations.

(v) The couple calculation was amended to include contributions from the extra sides CG and GH and also from the new corner at H. In fact, equation (4.27) was used to determine the couple for the disc.

(vi) The print subroutine for the output of various parameters was changed as necessary to give the correct values at the correct i,j points in the geometry.

(vii) It was found that the NAG graphics subroutine gave unclear headings and labelling of the axes. Therefore, this subroutine was amended to eliminate the part giving headings and only that giving the contouring remained. The Plot 10 routines were then incorporated so that better titles were printed out together with the contours.

After all amendments had been made the program was tested to ensure that it was working correctly and the necessary corrections made if required.The flow diagram of this program is given in Figure 4.10.

As a final check to ensure that the program was running properly, it was tested out for a geometry which resembled almost a cylindrical rotor rotating in a Newtonian fluid. The results were then compared with those obtained when using the computer program for the cylindrical stirrer for similar dimensions and fluid. As expected, virtually the

same results for the various parameters were obtained. The only differences encountered were those at the corner H. The results are given in Chapter 5.

4.4 Conclusion

A mathematical technique using finite difference methods has been developed to model the flows induced by the slow rotation of a finite cylindrical or disc stirrer in Newtonian and shear-thinning non-Newtonian fluids contained in a flat bottomed outer cylinder. The results obtained by other workers have been compared with those obtained using our method for similar geometries and are disscussed in Chapter 5.

For the two stirrers investigated in this study, the mathematical results have been compared with the corresponding experimental values and these are presented in later chapters.

From the above comparisons which are given in subsequent chapters, we shall see that our method shows promising results and we feel confident that it may be extended for the theoretical study of the more complex flows generated by more complicated systems.

CHAPTER 5

JUSTIFICATION OF THE MATHEMATICAL METHOD AND THE COMPUTER PROGRAMS

5.0 Introduction

In order to justify the mathematical method used for this study to investigate the flows induced by rotating stirrers, we have compared the results obtained using our method with those of other workers for similar geometries.

The results from our mathematical technique which utilizes the finite difference method to study the flows between concentric cylinders have been compared with those of Havard [31] who used the finite element method to study an identical arrangement of concentric cylinders.

The justification of changing to a method by Pao from that of Paddon, which was used in our preliminary experiments, is also given by comparison of primary flow results in similar geometries.

The results for the cylindrical stirrer and a disc rotor resembling an almost cylindrical rotor are also discussed. This is to ensure that the computer program developed for the disc stirrer could be compared with that for the cylindrical stirrer and to determine whether the program for the disc was functioning correctly.

Our finite difference technique and Pao's method have been tested for the disc geometries studied by Pao [67] and Spragg [85] and a comparison of the results is given. The general nature of the flow patterns for a rotating disc are compared with the results of Griffiths et al [29] and Waters and King [101].

5.1 Results From The Finite Difference and Finite Element Methods

Havard used the finite element method to study the primary flows due to a cylindrical stirrer rotating in a Newtonian fluid contained in a cylindrical outer vessel. The contours for the angular velocity u are shown in Figure 5.1. The results from our finite difference method (see section 4.2.5) are shown by crosses on the same diagram.

The finite element method proved to be more complex, with computation time considerably greater than for the finite difference method. Therefore, it seemed appropriate, in view of the close agreement between the results obtained by both methods, to continue using the finite difference technique in our study.

5.2 Results From Pao's and Paddon's Methods

In our initial investigation, we used a method by Paddon to study the flows in concentric cylinders. As mentioned earlier, this method only gave satisfactory results for primary flows ($Re \rightarrow 0$) and failed when used for secondary flows. Therefore, a method used by Pao was utilised for solving the equations for both primary and secondary flows for similar arrangements. Sample primary flow velocities (u) from the two methods are presented in Figures 5.2 and 5.3.

It can be seen from these data for a Newtonian fluid, that most of the u values agree very well within two decimal places. In fact, the contours of the angular velocities (not presented) from the two methods were found to be almost identical for both Newtonian and non-Newtonian fluids. Although, the strain rate (g) results are not presented, the values were also found to agree very well within two decimal places and the contours found to be almost identical.

In our preliminary studies of concentric cylinders, the experimental results compared very well with the theoretical results obtained using Paddon's method (see [8]). From the above, we can see that comparison of this method with results from Pao's technique for a similar geometry under similar conditions is also very good. We, therefore, conclude that Pao's method may be used for the study of further work.

5.3 Comparison of Our Results With Those of Pao

A numerical computation for a viscous incompressible Newtonian fluid confined in a circular cylindrical chamber was carried out by Pao [67], where the disc on top was rotating with a constant angular velocity (u) (Fig. 5.4a). Pao solved the Navier Stokes equations for various Reynolds numbers and presented the results for Re = 1, 100 and 400. In order to compare the theoretical results obtained from our program with those of Pao, a similar geometry was considered as shown in Figure 5.4b. The disc is represented by the bottom of a cylindrical stirrer and does not cover the horizontal cross-section of the container completely as in Pao's geometry. Since our calculation required a minimum of two grid points about D we were unable to make the rotor radius exactly the same as the outer cylindrical stirrer.

Figures 5.4 and 5.5 show the lines of constant circulation or velocity represented by Γ or T (= x^2u) for Re = 1 and 100. The general shape of the contours is seen to be the same with differences occurring when z = y > 1 and r = x > 1, due to the extra side CD of the cylinder in Figures 5.4b and 5.5b. Inspection of the actual values shows Γ or T that decreases away from the rotor in a similar way in both figures as expected.

Figures 5.6a and 5.6b show flow patterns or streamlines which Pao denotes by ψ and which are essentially the same as alfa (α) in our diagram. With the cylindrical rotor, the results are slightly affected by the side CD and the streamlines are more towards the corner D, but again the general shape is the same. The magnitude of the streamline values decrease from the centre outwards and for both geometries the values are similar.

At Re = 400, Pao does not present lines of circulations but the streamlines are shown in Figure 5.7a These are very similar to those in Figure 5.7b for the cylindrical rotor with slight differences occurring at the corner D. The streamlines in both cases are elongated compared with those at Re = 100. The same general trend of the values decreasing from middle outwards is obtained and again the direction of the flow is the same for both geometries and both Reynolds number.

5.4 Results for the Cylindrical and Near-Cylindrical Disc Stirrers.

Sample data obtained from the computer program for the disc stirrer for an almost cylindrical stirrer geometry are shown in Figures 5.8 - 5.10. The corresponding results obtained when the program for the cylindrical rotor is run for a similar geometry are also given. It should be noted that since shear forces dominate the flow [77], for convenience the strain rate $\dot{\gamma}$ will be referred to as the shear rate g for subsequent discussions.

It may be seen from the two sets of results that below the height y_b = 1.8 the contours are exactly the same for all the velocities (u), shear rates (g) and streamlines (alfa) and as expected differences begin to occur above y_g for the disc rotor.

The couple values for the cylindrical rotor and the near disc rotor were found to be 0.0003191 Nm and 0.0003048 Nm respectively.

The upper part of the near cylindrical rotor is at a smaller radius than the cylindrical stirrer and, therefore, the contribution to the couple is smaller as expected.

From the above comparisons, we may conclude that the computer program for the disc stirrer was working correctly. However, as a final check the results from this program are compared with those of Spragg which follow.

5.5 Comparison of Our Results With Those of Spragg

Spragg [85] carried out a theoretical investigation of the steady laminar Newtonian and non-Newtonian flow induced by a rotating disc, mounted coaxially on a shaft in a cylindrical vessel. This arrangement is very similar to that investigated in this study. Before making any comparison with Spragg's results it should be noted here that the boundary condition $\partial V_\theta/\partial r = 0$ used by Spragg on the axis of symmetry for the equivalent of xu should, in fact, be $\{\partial(V_\theta/r)\}/\partial r = 0$ as in this and other work [29]. Therefore, the results obtained by Spragg for the rotating disc stirrer are not strictly correct, although the results do not appear to be greatly affected even near the axis of symmetry.

Our computer program was tested for a disc geometry similar to that used by Spragg and the results are discussed below. Spragg used a slightly different formula to determine the Reynolds number for his equations. Therefore, to ensure that the same effective Reynolds number was used in our program, a new value was determined by comparison; hence the difference in the value of Re shown on the diagrams.

In Figures 5.11a and 5.11b, the constant contours of the stream function (α streamlines) are presented for a Newtonian fluid. It can be seen that the general pattern is the same in both figures. However, in Spragg's results the values of α are negative above the disc and positive below, whereas in our results the negative values occur below the disc and positive values above. This is explained by the way the velocities in the x and y directions are defined by Spragg in terms of α.

The values above the disc are of the same order of magnitude in both diagrams. Although, not all the streamlines are shown below the disc in Figure 5.11a, it is apparent from the diagram that the values of α decrease by a factor of approximately 100 towards the outer walls of the vessel which is not so in Spragg's results. Half way along the disc, however, the magnitude of α is about 0.01 in both diagrams.

The vorticity and swirl velocity (xu) contours for a non-Newtonian fluid are presented in Figures 5.12 - 5.13. A shear-thinning Carreau fluid model was used and from Figures 5.12a and 5.12b, it can be seen that the general trend of the vorticity contours is the same with most of the negative values occurring above the disc in the bulk of the fluid, near the base and the lower wall of the vessel. Positive vorticity values occur below the disc in the bulk of the fluid, along the shaft and near the upper wall of the vessel.

Comparison of the swirl velocity (xu) contours (Figs. 5.13a and 5.13b) for the Carreau fluid also shows a similar trend between the two figures. The contours form loops around the disc section, and away from the stirrers towards the outer walls the values become smaller as expected. It is not easy to compare the exact values of the various contours as we do not know the contribution from the error in Spragg's geometry.

The comparison of results obtained from our method with those of Spragg for the Pumping number versus either Reynolds number, the ratio x_b/x_c or the ratio y_b/y_c (in our notation) are given in Figures 5.14, 5.15 and 5.16 respectively. It can be seen that our results compare favourably with those of Spragg.

Hence, we may conclude that generally the results obtained using our method for Spragg's geometry all compare very well with those of Spragg. We, therefore, feel confident that we may use the computer program for the disc stirrer to determine various parameters in our geometry.

5.6 Comparison With Other Work

The results of Griffiths et al [29] who studied the flows due to a rotating plate or thin disc in a Newtonian fluid are presented in Figure 5.17. The general shape and direction of the streamlines are very similar to those obtained using our method (e.g. Fig. 5.18). The streamlines are travelling in a clockwise direction below the disc and anticlockwise above as expected and in agreement with all our results. Furthermore, Griffiths et al claim that their theoretical results compared very well with experimental values.

Waters and King [101] used analytical methods to solve the equations due to the rotation of a finite disc and various stirrers of ellipsoidal shape. The results for the finite disc are presented in Figure 5.18. Although, the streamlines are of a similar general shape the direction of them are different, again due to the way the equations are defined i.e. in an opposite sense to ours.

5.7 Conclusion

From all the comparisons given here, we can see that the results from our mathematical technique compare very well with the results of other workers. The comparison of our work with that of Havard and Pao provided us with a very good check to ensure that our numerical method and the computer program for the cylindrical stirrer were working correctly. Knowing that our program for the disc stirrer was working correctly (see section 5.4), as a final check it was tested for Spragg's geometry, which gave us satisfying results. Furthermore, general comparison with the work of Griffiths et al and Waters and King also gave very good agreement with our results.

We may conclude, therefore, that since comparison with the work of others give encouraging results, we may proceed with using our method to investigate the flows due to a rotating cylindrical stirrer and a disc stirrer.

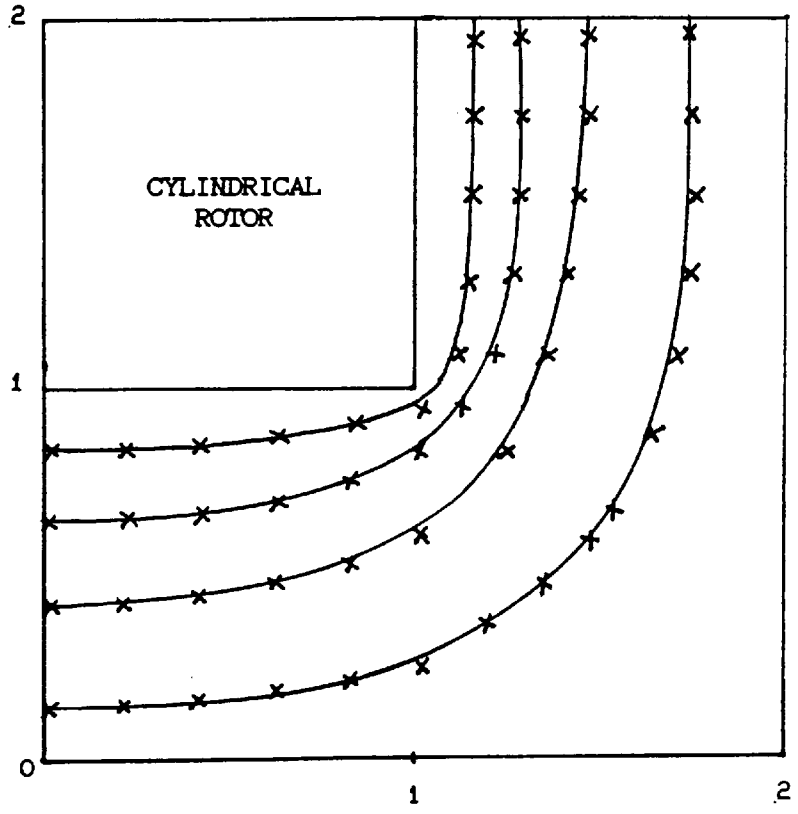

Figure 5.1 Typical angular velocity results from the finite element method — and the finite difference method × .

```
u(i,j),starting row j=M(i=0,1..N)

j=10
 1.000 1.000 1.000 1.000 1.000 1.000 0.589 0.342 0.183 0.076 0.000
j=9
 1.000 1.000 1.000 1.000 1.000 1.000 0.588 0.341 0.182 0.076 0.000
j=8
 1.000 1.000 1.000 1.000 1.000 1.000 0.584 0.336 0.179 0.074 0.000
j=7
 1.000 1.000 1.000 1.000 1.000 1.000 0.574 0.325 0.172 0.070 0.000
j=6
 1.000 1.000 1.000 1.000 1.000 1.000 0.552 0.305 0.159 0.065 0.000
j=5
 1.000 1.000 1.000 1.000 1.000 1.000 0.498 0.268 0.138 0.056 0.000
j=4
 0.734 0.731 0.721 0.698 0.653 0.561 0.351 0.205 0.109 0.045 0.000
j=3
 0.499 0.494 0.482 0.455 0.408 0.333 0.229 0.142 0.078 0.033 0.000
j=2
 0.304 0.301 0.290 0.270 0.237 0.191 0.136 0.088 0.050 0.021 0.000
j=1
 0.143 0.141 0.139 0.125 0.109 0.087 0.063 0.042 0.024 0.010 0.000
j=0
 0.000 0.000 0.000 0.000 0.000 0.000 0.000 0.000 0.000 0.000 0.000
```

Figure 5.2 Typical primary flow velocities for a Newtonian fluid using Paddon's method.

```
u(i,j),starting row j=M(i=1..N)

j=11
 1.000 1.000 1.000 1.000 1.000 1.000 0.587 0.340 0.182 0.075 0.000
j=10
 1.000 1.000 1.000 1.000 1.000 1.000 0.586 0.338 0.180 0.075 0.000
j=9
 1.000 1.000 1.000 1.000 1.000 1.000 0.581 0.333 0.177 0.073 0.000
j=8
 1.000 1.000 1.000 1.000 1.000 1.000 0.571 0.323 0.170 0.070 0.000
j=7
 1.000 1.000 1.000 1.000 1.000 1.000 0.549 0.303 0.157 0.064 0.000
j=6
 1.000 1.000 1.000 1.000 1.000 1.000 0.496 0.265 0.137 0.056 0.000
j=5
 0.740 0.740 0.726 0.702 0.656 0.563 0.350 0.203 0.108 0.045 0.000
j=4
 0.507 0.507 0.489 0.459 0.411 0.335 0.228 0.141 0.078 0.033 0.000
j=3
 0.312 0.312 0.297 0.273 0.239 0.192 0.136 0.087 0.049 0.021 0.000
j=2
 0.148 0.148 0.139 0.127 0.110 0.088 0.063 0.042 0.024 0.010 0.000
j=1
 0.000 0.000 0.000 0.000 0.000 0.000 0.000 0.000 0.000 0.000 0.000
```

Figure 5.3 Typical primary flow velocities for a Newtonian fluid using Pao's method.

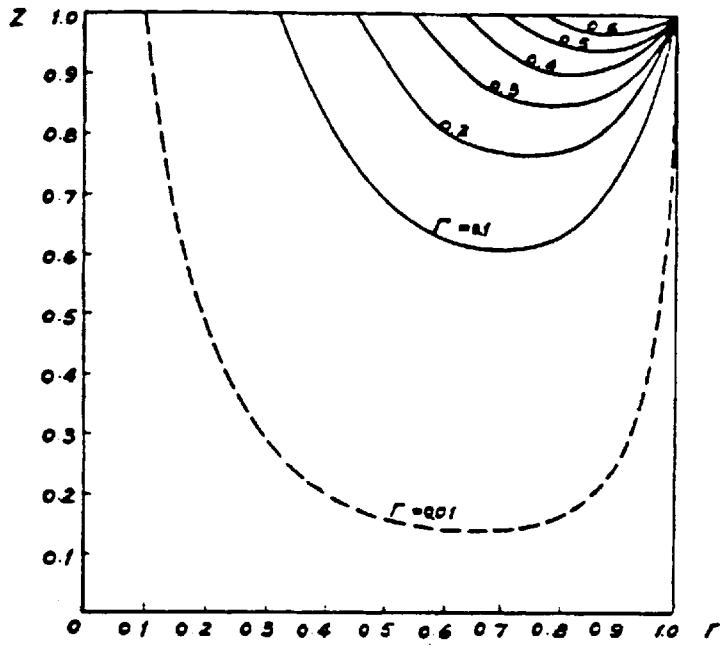

(a)

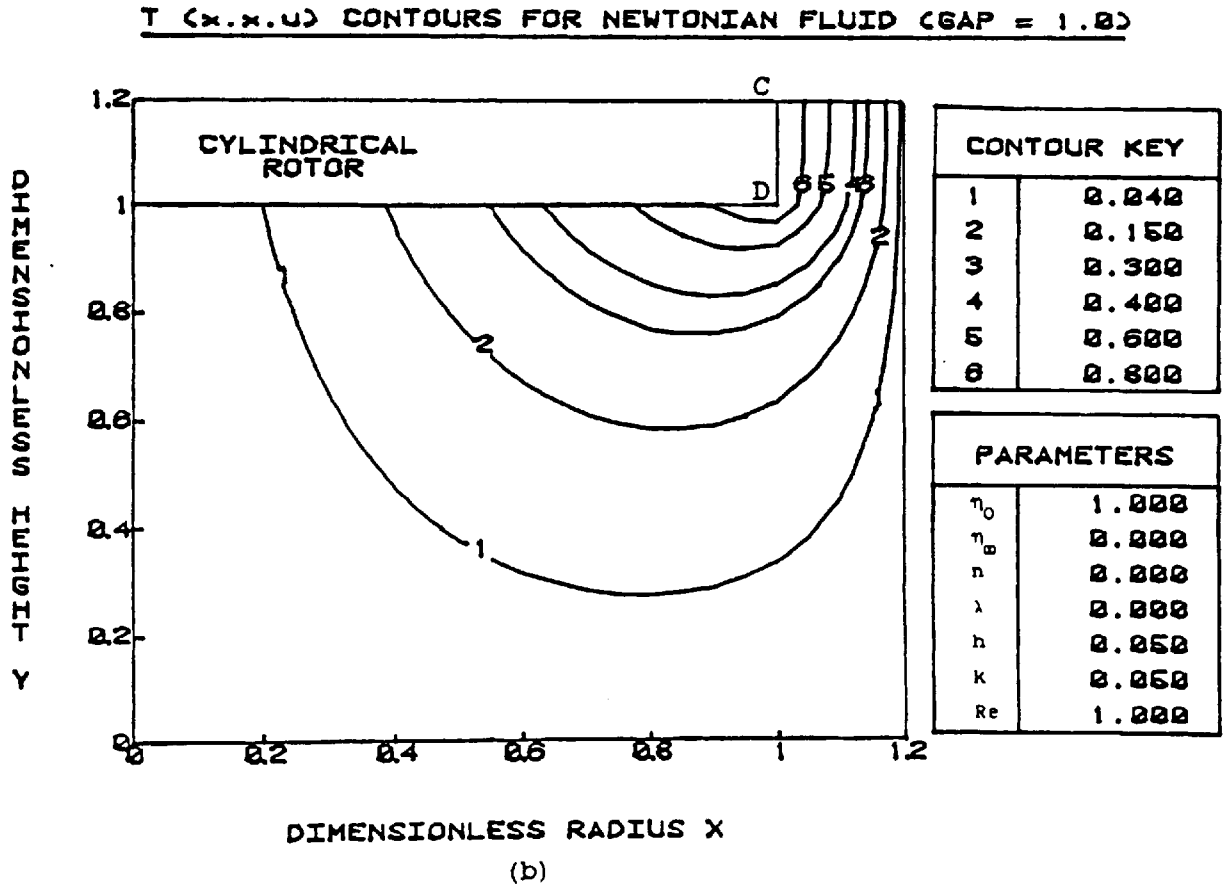

(b)

Figure 5.4 Lines of constant circulation at Re = 1 obtained by Pao (a) for a disc geometry and Newtonian fluid and that obtained using our computer program (b) for a similar geometry.

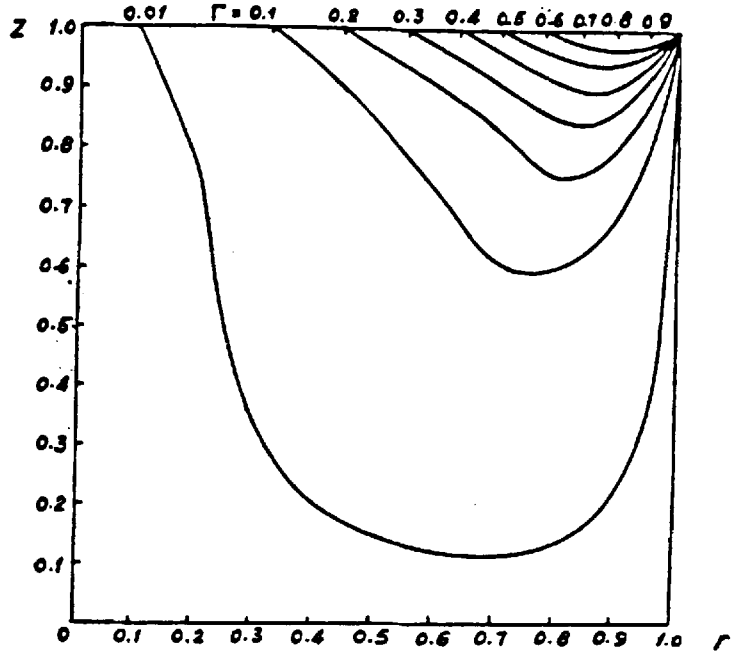

(a)

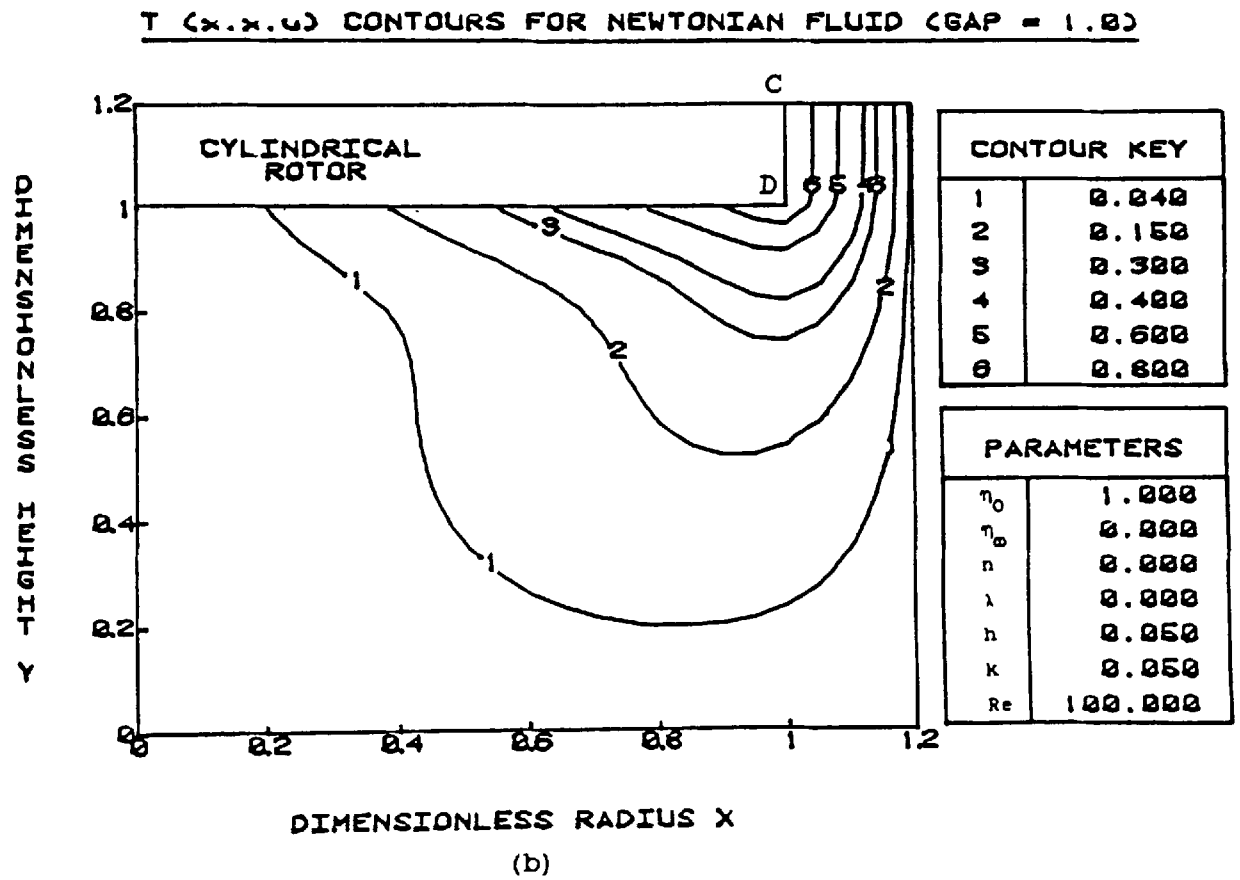

(b)

Figure 5.5 Lines of constant circulation at Re = 100 obtained by Pao (a) for a disc geometry and Newtonian fluid and that obtained using our computer program (b) for a similar geometry.

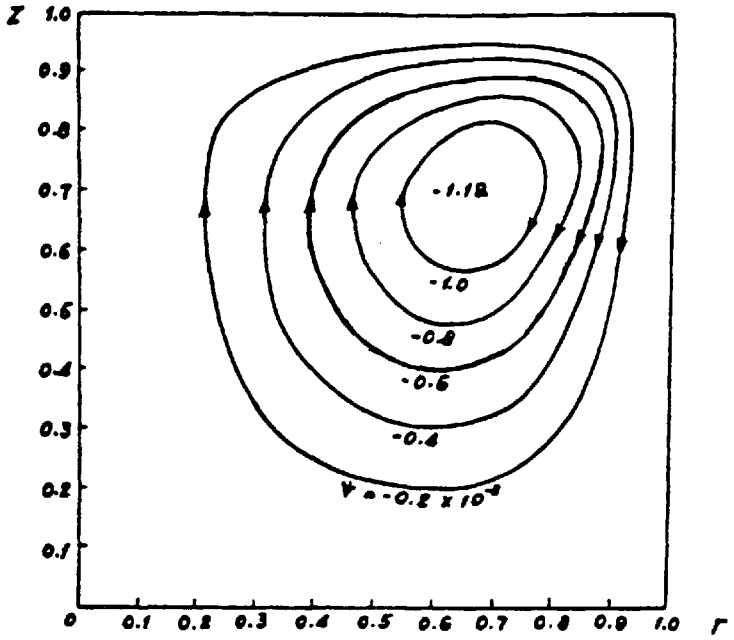

(a)

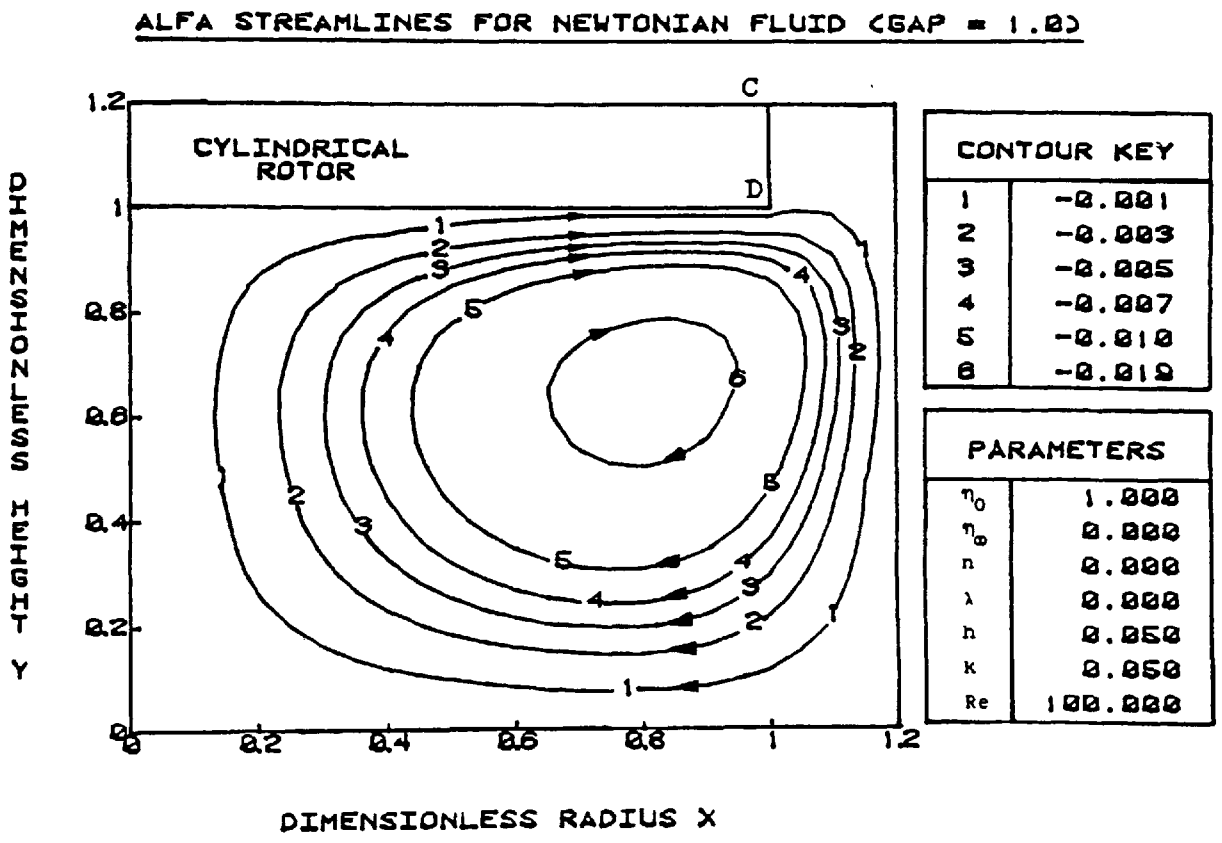

(b)

Figure 5.6 Streamlines at Re = 100 obtained by Pao (a) for a disc geometry and Newtonian fluid and that obtained using our computer program (b) for a similar geometry.

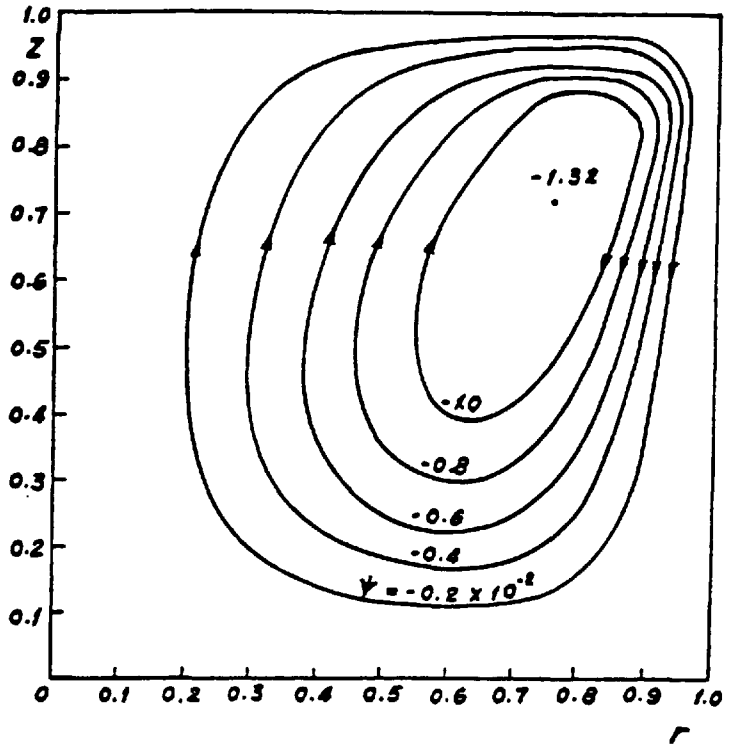

(a)

ALFA STREAMLINES FOR NEWTONIAN FLUID (GAP = 1.0)

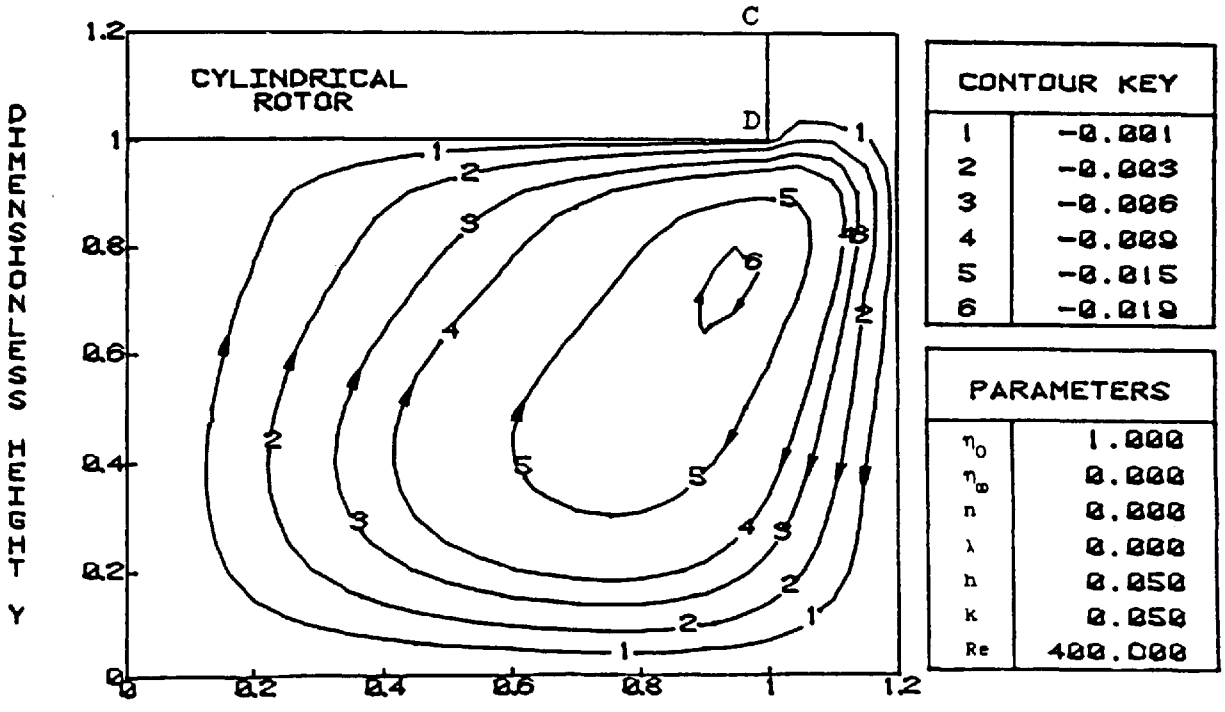

(b)

Figure 5.7 Streamlines at Re = 400 obtained by Pao (a) for a disc geometry and Newtonian fluid and that obtained using our computer program (b) for a similar geometry.

Figures 5.8-5.10 A comparison of the results for angular velocities (u), (5.8), vorticities (χ) (5.9) and stream functions (α) (5.10) for the cylindrical and near-cylindrical disc stirrers.

Figure 5.8(a)

U (VELOCITY) CONTOURS FOR NEWTONIAN FLUID (GAP = 1.0)

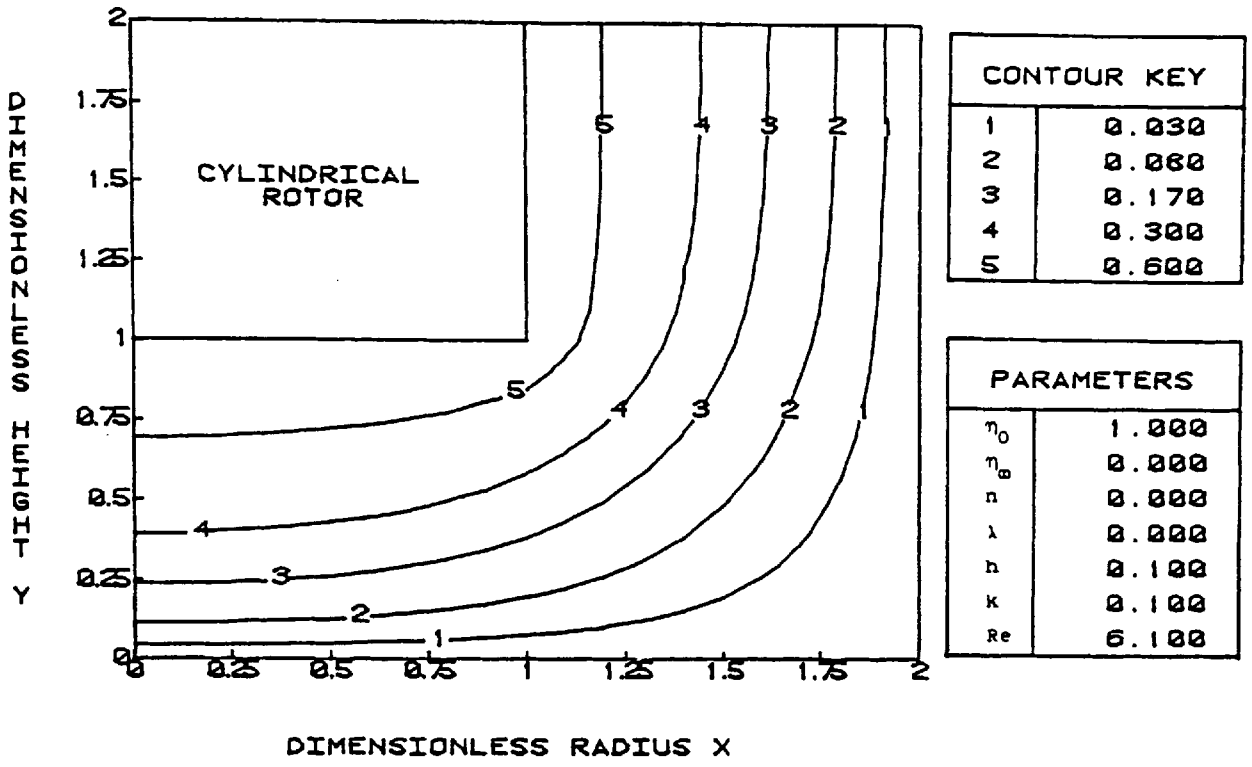

CONTOUR KEY	
1	0.030
2	0.060
3	0.170
4	0.300
5	0.600

PARAMETERS	
η_0	1.000
η_∞	0.000
n	0.000
λ	0.000
h	0.100
K	0.100
Re	6.100

Figure 5.8(b)

U (VELOCITY) CONTOURS FOR NEWTONIAN FLUID (GAP = 1.0)

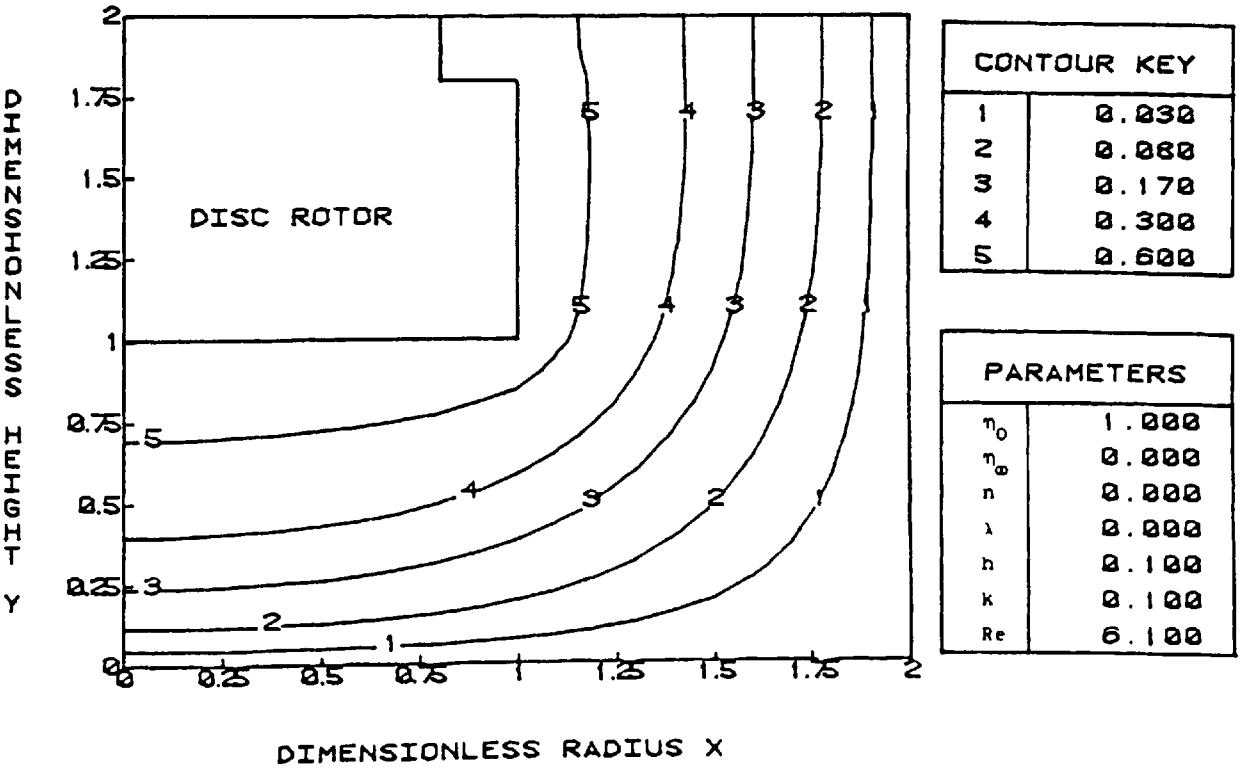

CONTOUR KEY	
1	0.030
2	0.060
3	0.170
4	0.300
5	0.600

PARAMETERS	
η_0	1.000
η_∞	0.000
n	0.000
λ	0.000
h	0.100
K	0.100
Re	6.100

Figure 5.9(a)

XI (VORTICITY) CONTOURS FOR NEWTONIAN FLUID (GAP = 1.0)

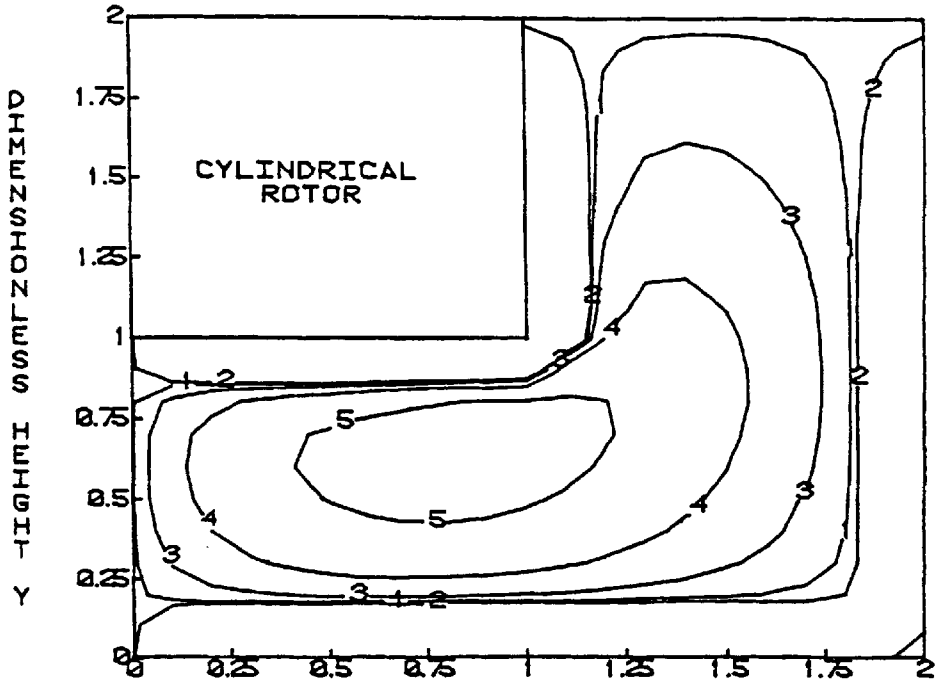

CONTOUR KEY	
1	0.001
2	-0.001
3	0.010
4	0.035
5	0.100

PARAMETERS	
η_0	1.000
η_∞	0.000
n	0.000
λ	0.000
h	0.100
K	0.100
Re	6.100

Figure 5.9(b)

XI (VORTICITY) CONTOURS FOR NEWTONIAN FLUID (GAP = 1.0)

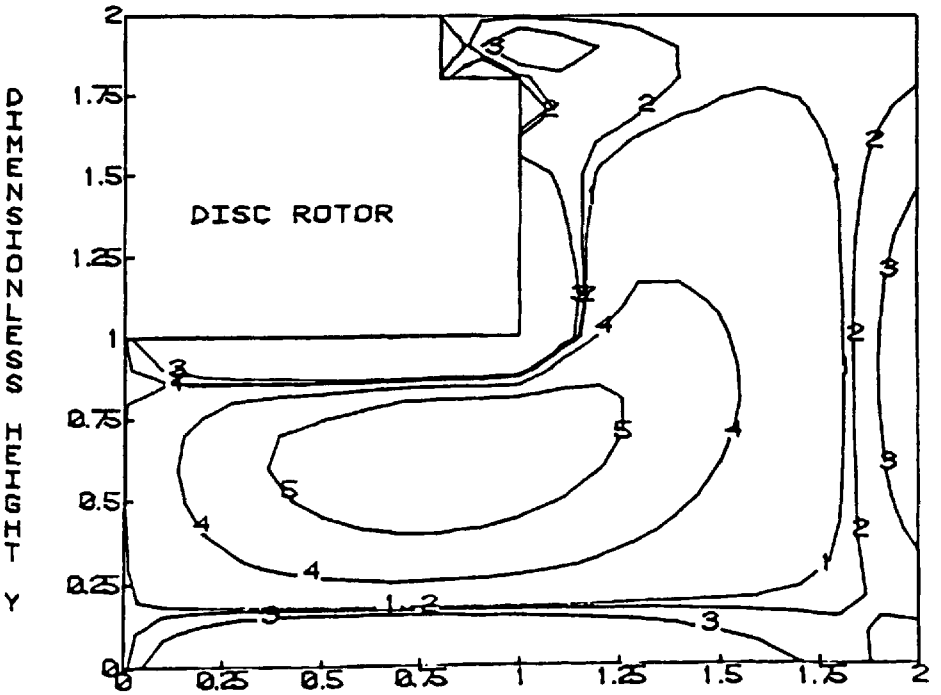

CONTOUR KEY	
1	0.001
2	-0.002
3	-0.010
4	0.035
5	0.090

PARAMETERS	
η_0	1.000
η_∞	0.000
n	0.000
λ	0.000
h	0.100
K	0.100
Re	6.100

Figure 5.10(a)

ALFA STREAMLINES FOR NEWTONIAN FLUID (GAP = 1.0)

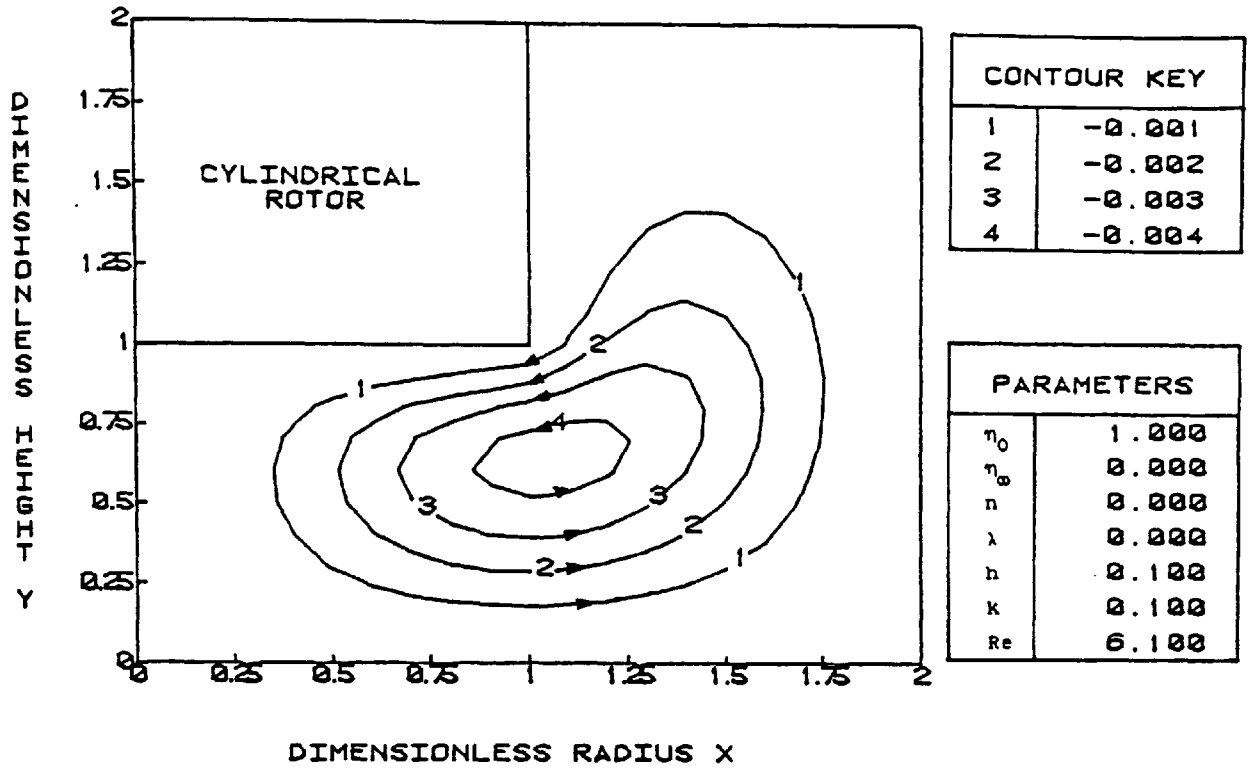

CONTOUR KEY	
1	-0.001
2	-0.002
3	-0.003
4	-0.004

PARAMETERS	
η_0	1.000
η_∞	0.000
n	0.000
λ	0.000
h	0.100
K	0.100
Re	6.100

Figure 5.10(b)

ALFA STREAMLINES FOR NEWTONIAN FLUID (GAP = 1.0)

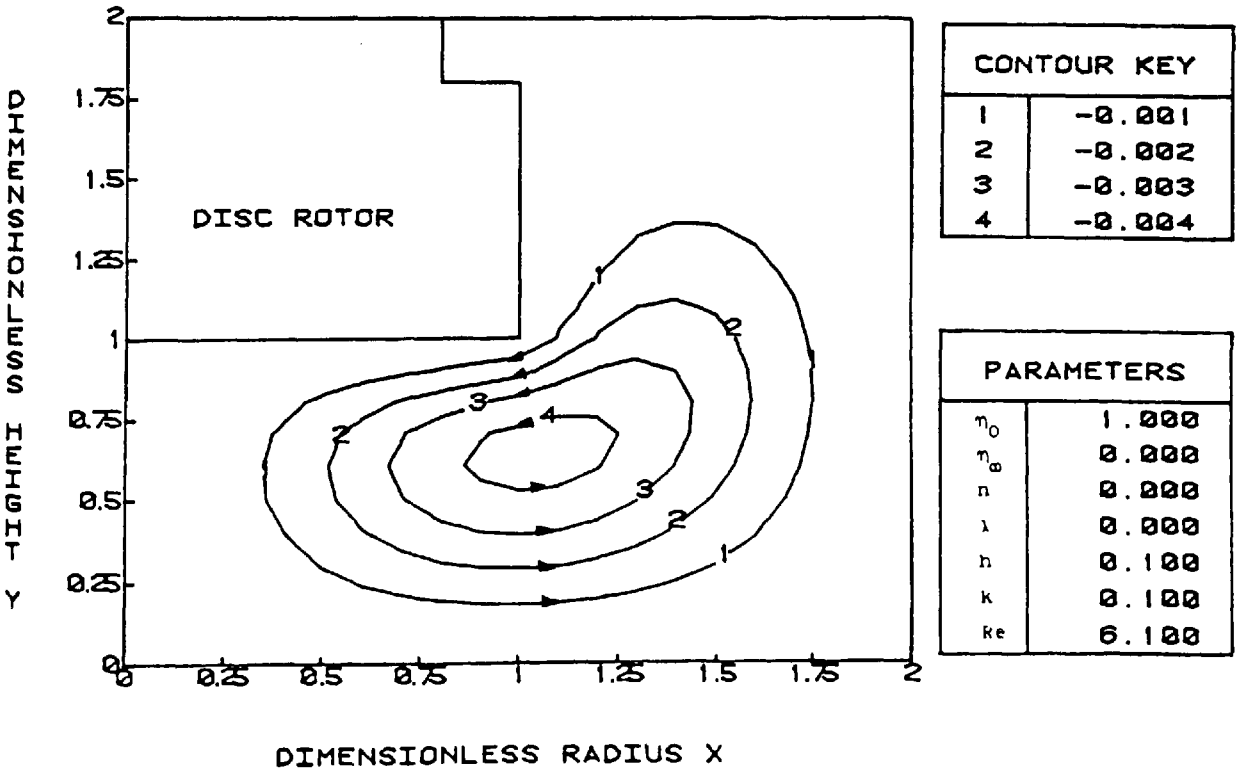

CONTOUR KEY	
1	-0.001
2	-0.002
3	-0.003
4	-0.004

PARAMETERS	
η_0	1.000
η_∞	0.000
n	0.000
λ	0.000
h	0.100
K	0.100
Re	6.100

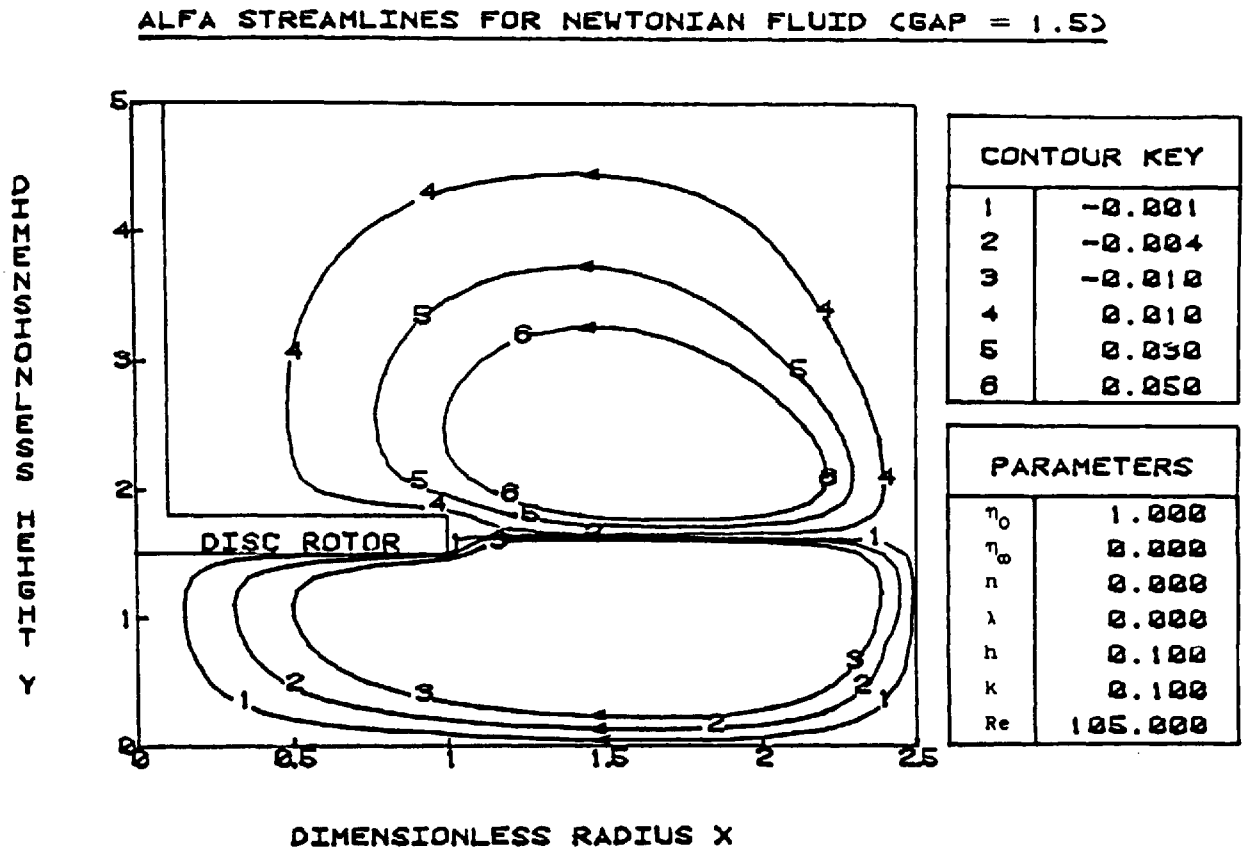

(a)

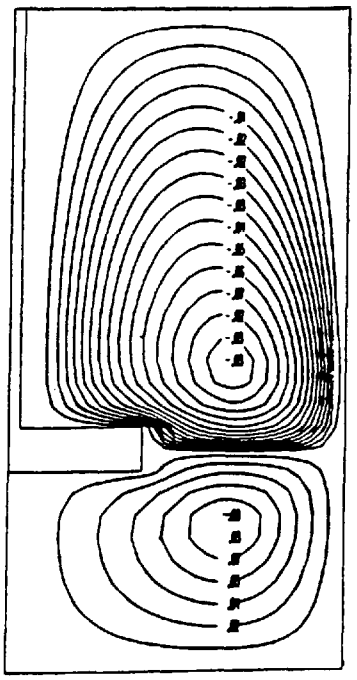

(b)

Figure 5.11 Streamlines at Re = 67 obtained by Spragg (a) for a disc geometry and Newtonian fluid and that obtained using our computer program (b) for a similar geometry (Re = 105).

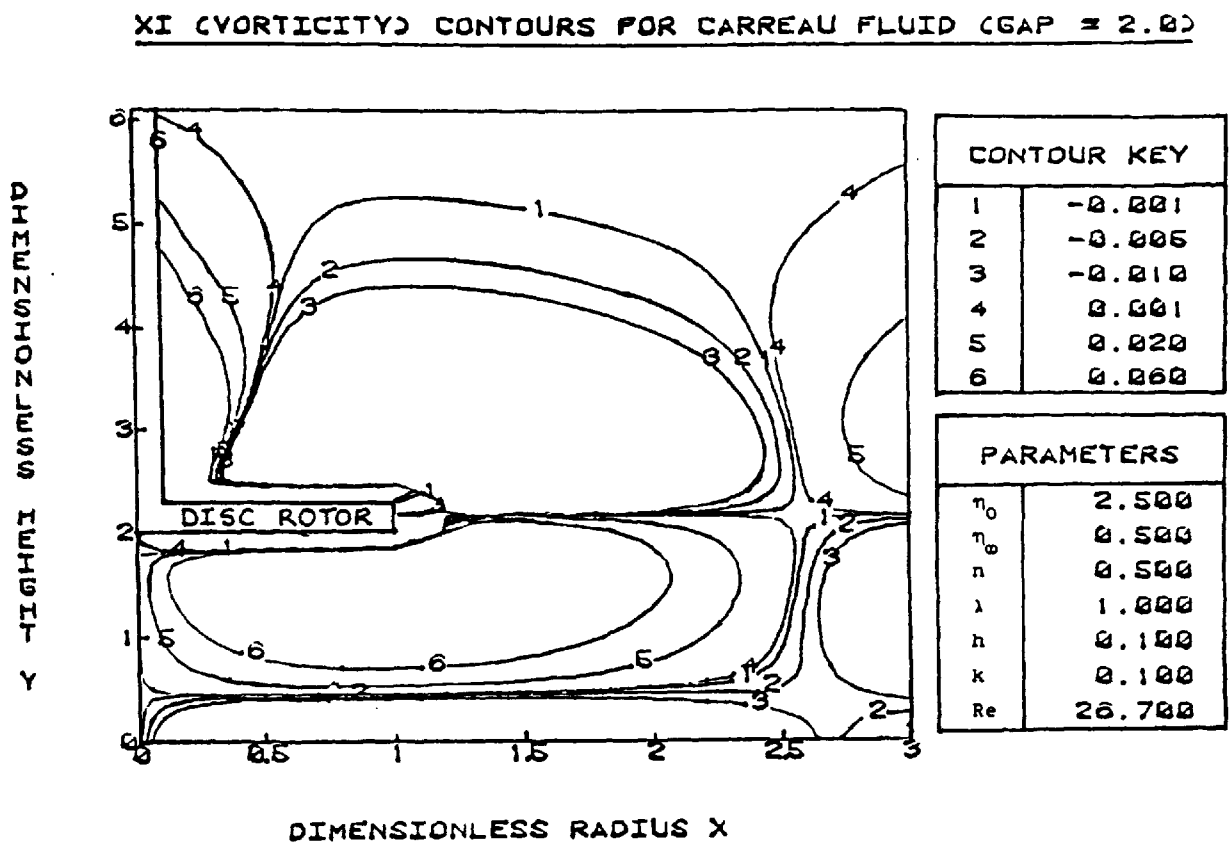

(a)

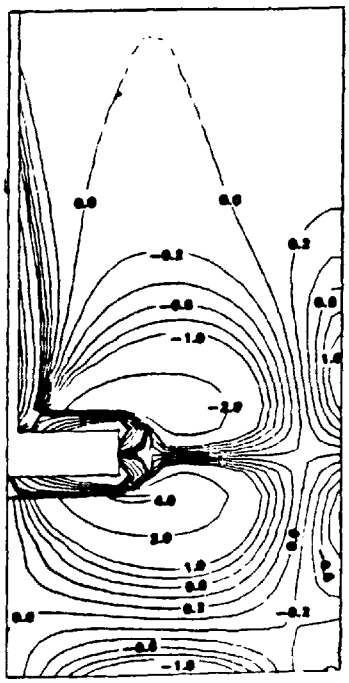

(b)

Figure 5.12 Vorticity contours at Re = 17 obtained by Spragg (a) for a disc geometry and Carreau fluid and that obtained using our computer program (b) for a similar geometry (Re = 26.7).

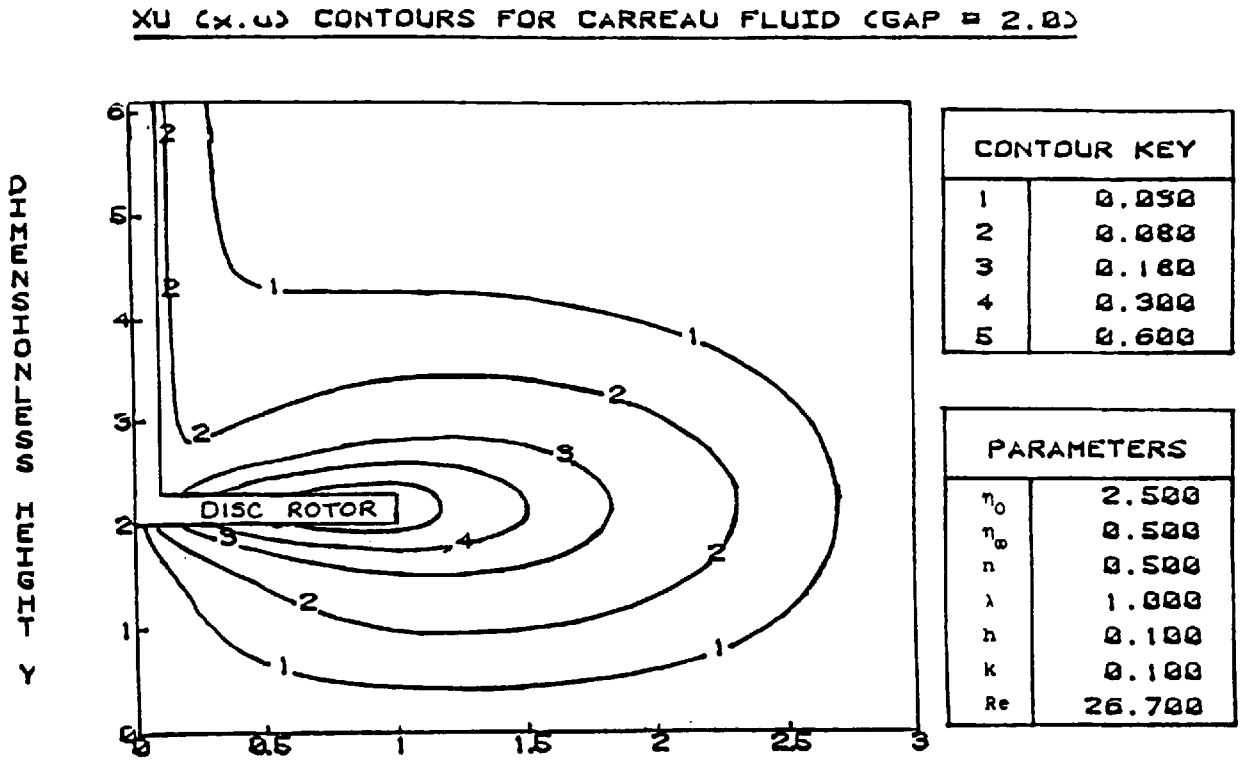

(a)

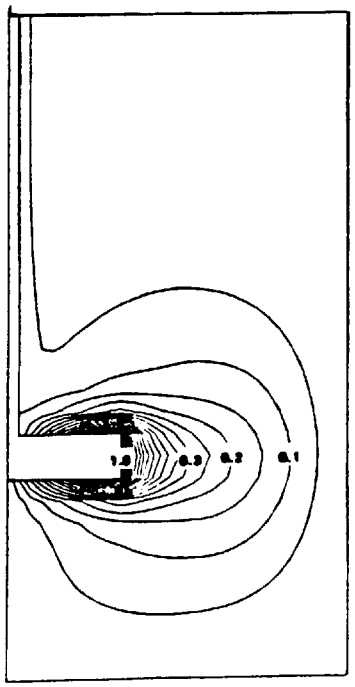

(b)

Figure 5.13 Swirl velocity contours at Re = 17 obtained by Spragg (a) for a disc geometry and Carreau fluid and that obtained using our computer program (b) for a similar geometry Re = 26.7).

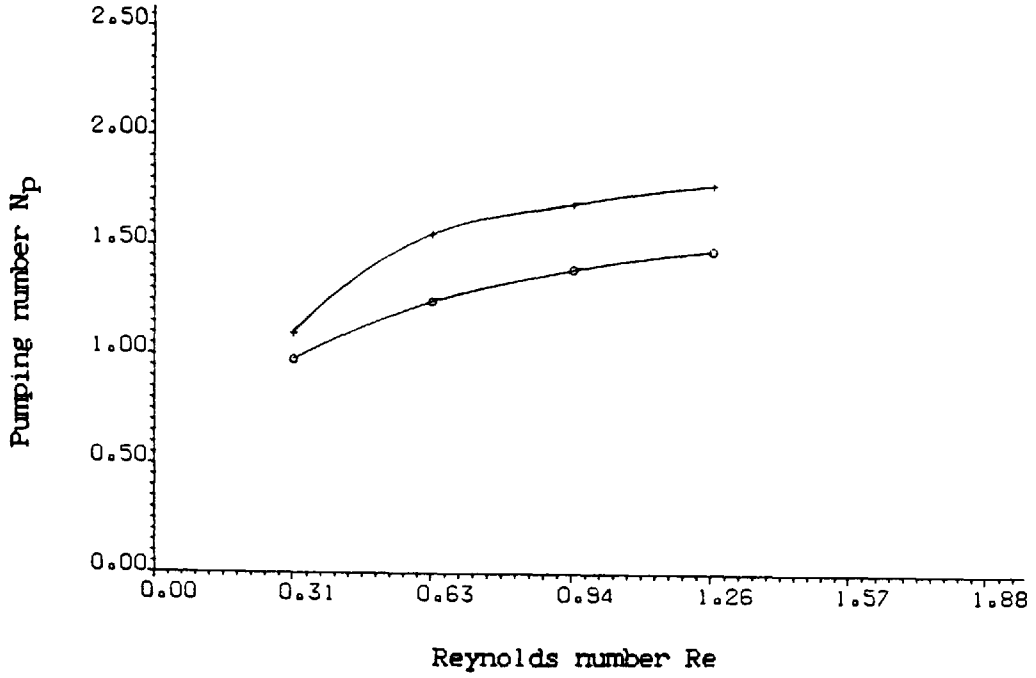

Figure 5.14 Pumping number versus the Reynolds number for a disc geometry and Newtonian fluid obtained by Spragg ∘ and that obtained using our method × .

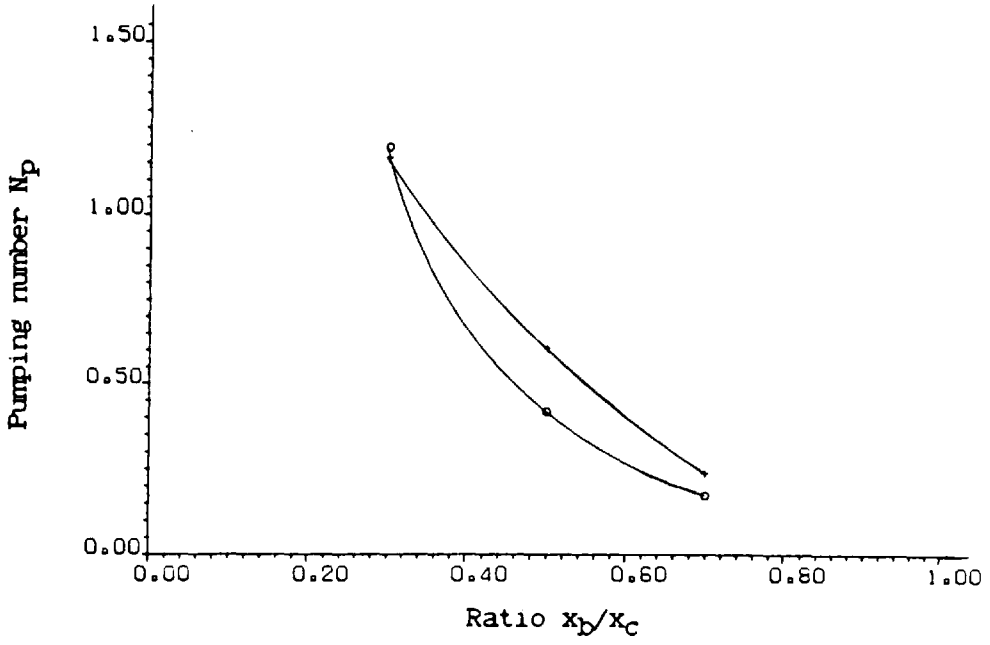

Figure 5.15 Pumping number versus the ratio x_b/x_c for a disc geometry and Newtonian fluid obtained by Spragg ∘ and that obtained using our method ×

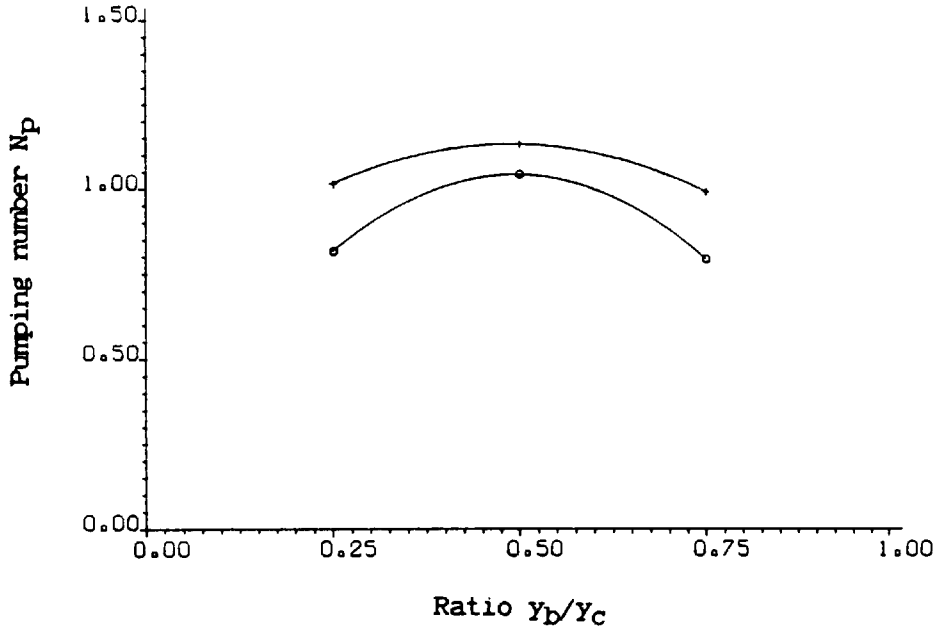

Figure 5.16 Pumping number versus the ratio y_b/y_c for a disc geometry and Newtonian fluid obtained by Spragg•and that obtained using our method × .

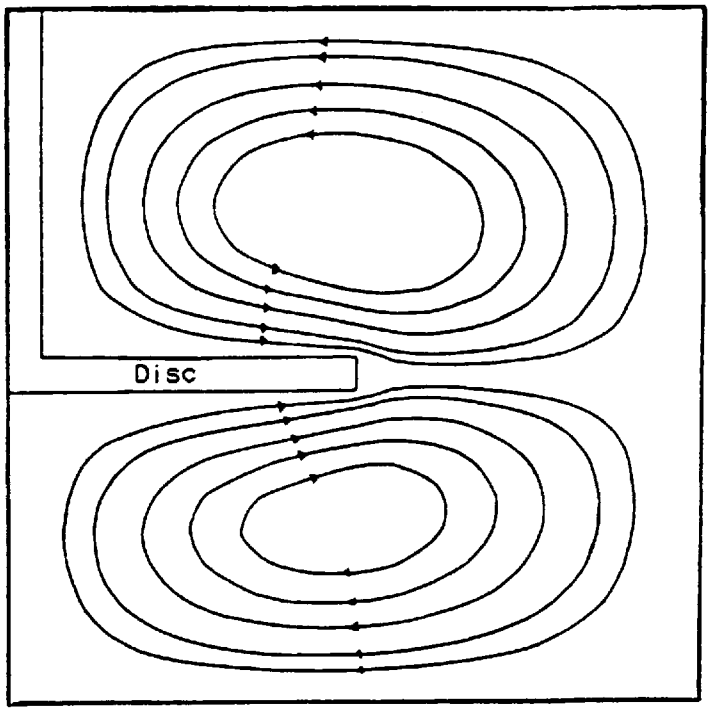

Figure 5.17 Streamlines from the work of Griffiths et al for a disc stirrer and a Newtonian fluid

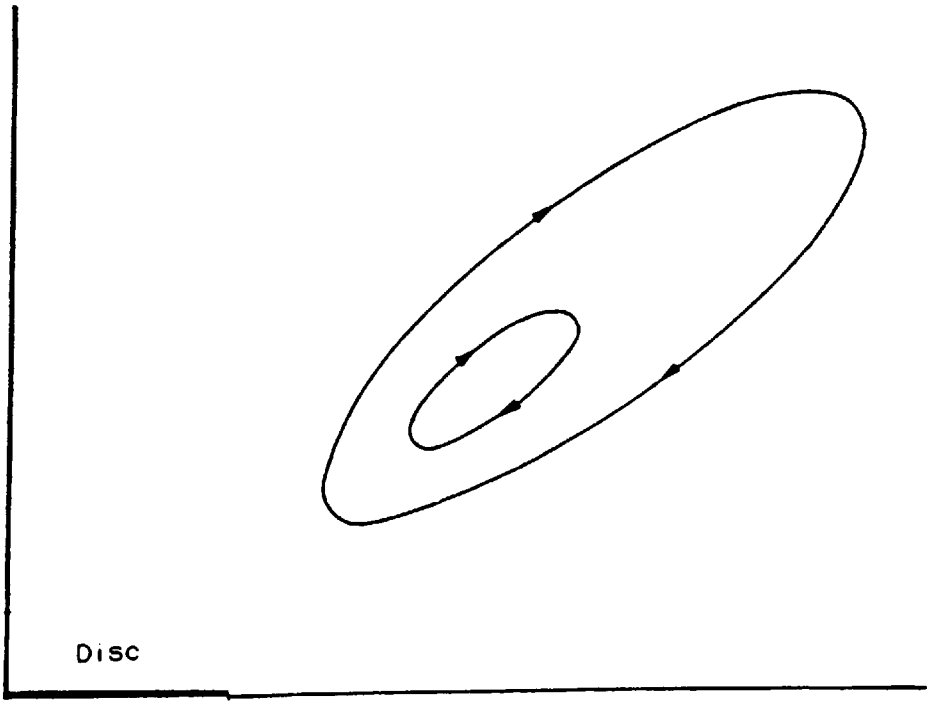

Figure 5.18 Streamlines predicted by the theory of Waters and King for a disc rotating in a Newtonian fluid

CHAPTER 6

RESULTS FOR PRIMARY FLOWS

6.0 Introduction

The results from the viscometric experiments for glycerol and Carbopol 910 are given in this chapter. The flow patterns obtained when the cylindrical or disc stirrer is rotating in the fluid, either glycerol or Carbopol 910, under primary flow conditions are described. The experimental and theoretical results obtained for angular velocities u and shear rate $\dot{\gamma}$ (denoted by g) are also given and compared. A table of the standard deviation values from the mean values of UDIFF and GDIFF is also presented.

6.1 Results From Viscometric Experiments

The viscometric curves for glycerol at 296 K and Carbopol 910 at 294 K are presented in Figure 6.1 and 6.2 respectively. The curves are a plot of the scale reading from the Haake Rotovisco viscometer (see section 3.4.2) against the rotor speed. Since glycerol is a Newtonian fluid, the viscosity is constant at all temperatures and is derived from the gradient of the line once the scale readings and speeds are multiplied by the instruments constants. The viscosity was found to be 1.06 Pas, which is in close agreement with the value obtained from the Physical Properties Data Service (PPDS) package [73].

In Figure 6.2, the gradient of the curve is seen to increase initially and then taper off. This behaviour shows the shear-thinning nature of Carbopol 910 in which the viscosity decreases with increase in speed of rotor. When the non-linear minimization technique was

used (see section 3.4.2), the Cross model was found to be the best fit for the data with the zero shear viscosity η_0 = 60.15, the infinite shear viscosity η_∞ = 0.34, and the constants n and λ equal to 0.35 and 1.24 respectively. The value of the constant λ used for numerical calculations was, in fact, a product of the model λ (1.24) and the speed of the rotor (Ω) as required in equation (4.18) and it is the latter value that is used for comparison purposes.

6.2 Flow Patterns

Typical primary flow patterns obtained from a recording of the bottom view of the apparatus are shown in Figure 6.3. Primary flow was obtained at very low Reynolds number i.e. Re ≈ 0.8 for glycerol and Re ≈ 0.16 for Carbopol 910. Although, a speed of 16 rpm (1.68 radians/second) was used for both fluids and also the same equation to determine the Reynolds number, the reason for the difference is due to the difference in densities and viscosities of the two fluids. Under the correct alignment of cameras and centering of the apparatus, close circular orbits around the stirrer were obtained as expected. The same flow pattern was obtained for both the cylindrical and disc stirrers. Each tracer particle was seen to follow the same circular path at the same height from the bottom of the vessel for approximately five minutes. The particles themselves were also seen to be spinning slightly as they travelled around the rotor.

It could be seen that as the speed of the stirrer was increased, hence increasing the Reynolds number, the flow patterns changed and the particles no longer followed circular paths due to secondary flow occurring. This type of flow is discussed in Chapter 7.

6.3 Angular Velocity Distributions

Contours of Γ are not presented for the geometries studied in this section since we are only concerned here with u values. Γ contours were useful when comparison with Pao's work [67] was carried out and were presented in Chapter 5.

Contours of constant fluid velocities u obtained by numerical simulation for both the cylindrical and disc stirrers rotating at height y_b = 0.8 (small gap) in glycerol (Newtonian) are shown in Figure 6.4 and 6.5 respectively. The values shown next to the black dots on the diagram are experimentally determined values of u. Not all the values are shown since congested diagrams would have been obtained. As expected the u values become smaller away from the stirrer towards the outer wall of the vessel. When comparing the u values for the two stirrers we can see that at a fixed position underneath the stirrers the fluid speed is the same. Differences begin to occur above y_b where the geometry differs.

Inspection of the velocity profiles for the two stirrers shows that for any height between D and H (defined in Fig.4.3) of the disc stirrer and the corresponding height for the cylindrical stirrer, the profile (i.e. velocity versus distance x away from the axis of symmetry) is very similar. However, above H the velocity profile for the disc is flatter because there is a greater distance x over which the velocity is distributed since u is always unity at the stirrer and zero at the outer walls of the vessel. The velocity profiles are shown in Figures 6.6 and 6.7.

Figures 6.8 and 6.9 show a direct comparison between the experimental and computational Newtonian u values for the geometry considered in

Figures 6.4 and 6.5. The data points lie reasonably near the bold line signifying the expected values. Any scatter may partly be assumed due to inherent experimental error and partly due to the fact that the tracer particles themselves were observed to be slightly spinning. The rotation of the stirrer results in transfer of kinetic energy to the fluid which in turn transfers it to the particles enabling them to move with the fluid. The spinning action uses up some of this kinetic energy, hence slowing down the tracer particles and giving lower experimental u values than the corresponding theoretical u values. It may be seen that a maximum of approximately 15% difference occurred between the experimental and theoretical values. The standard deviation values of UDIFF (i.e. percentage difference between experimental and corresponding theoretical u values) from the mean UDIFF values are given in Table 6.1 for all the geometries studied.

The results obtained for Carbopol 910 (a Cross fluid model) are very similar to those obtained for glycerol and are shown in Figures 6.10 to 6.13. This time, however, the experimental values agree within 25% of the theoretical values which may be seen by the slight scatter on either side of the bold line in Figures 6.12 and 6.13.

Comparison of corresponding geometies e.g. Figures 6.4 and 6.10 show that the fluid speed of Carbopol 910 at a fixed position near the stirrer is faster than for glycerol. This is as expected since Carbopol 910 is shear-thinning i.e. the viscosity decreases with an increase in shear rate. The shear rate is greatest near the stirrer since the speed changes most rapidly there.

Figures 6.14 to 6.21 show the comparison of the u values obtained experimentally and numerically with y_b = 1.3 (large gap). Again it can be seen that the experimental u values are in better agreement with theoretical values for glycerol (within ≈ 15%) than for Carbopol 910 (within ≈ 25%). Comparison of the two stirrers shows that at corresponding points in the fluid underneath the stirrers the fluid speed is the same with differences occurring above y_b.

When the large gap geometry is compared with its corresponding small gap geometry (e.g. Figures 6.4 and 6.14,6.5 and 6.15 etc.) we can see that the fluid speed at a fixed position above y_b is the same in both geometries. Differences start to occur below y_b = 1.3 due to the difference in heights y_b. Also, as expected and in agreement with the small gap results, the u values become smaller away from the stirrer.

6.4 Shear Rate Distributions

Figures 6.22 and 6.23 show contours of constant shear rates $\dot{\gamma}$ (represented by g) obtained by numerical simulation using equation 4.13 for the two stirrers under investigation rotating at a height y_b = 0.8 (small gap) in glycerol. For the cylindrical stirrer the contours simply curve upwards into the rotor as expected. For the disc stirrer, similar contours are obtained except near to the side HD where the contours form loops. It can also be seen for both stirrers that the shear rate is the highest at the stirrer and decreases towards the outer vessel wall. This is as expected since the highest shear occurs where the velocity change of the fluid is the greatest. Inspection of the actual numerical values from the computer printout show that the highest shear rate values occur at the corners. A sample printout is given in Appendix 3.

The values next to the black dots are representative of the experimentally determined values of g. Figures 6.24 and 6.25 show a direct comparison between the experimental and computational shear rate values for the cylindrical and disc rotors respectively. The data points are seen to be greatly scattered snd more points lie beneath the solid line than above. This shows that generally the experimental shear rate values are greater than their corresponding theoretical values. In fact, the experimental and theoretical values agree on average within 60% and 90% for the cylindrical and disc stirrers respectively. This high difference in g values may be due to several reasons. The experimental g values were determined using experimentally determined u values and sample zones as explained in section 3.6. Any error in the u values contributes to error in the g values. For example, since a sample zone of width 8 mm, i.e. 0.4 in dimensionless terms with $\Delta x = \Delta y = 0.25$ was used, the expected error in g is roughly four times that in u. Therefore, a maximum difference of 60% and 90% seems acceptable. Furthermore, the major contribution to this high error is probably given by the fact that g values were obtained by numerical differentiation of the experimental data; a method well known to be error prone. The standard deviations of GDIFF from the corresponding mean values of GDIFF for all the geometries studied are given in Table 6.1.

The results obtained for Carbopol 910 are generally similar to those for glycerol and are shown in Figures 6.26 and 6.27. The agreement between experimental and theoretical g values was found to be within approximately 90% and may be seen by the great scatter in Figures 6.28 and 6.29. This is as expected since the difference in the corresponding u values was found to be about 25%. Also, the high error in g values for Carbopol 910 may be due to the Cross model fit not being totally

representative for Carbopol 910.

Figures 6.30 to 6.37 show the comparison of experimental and theoretical shear rate values for the gap size y_b = 1.3. Again there is better agreement for glycerol (within ± 60%) than for Carbopol 910 (within ± 90%). Generally, more data points lie beneath the bold line than above, indicating that the experimental values are higher than the corresponding theoretical values. Comparison of the two stirrers shows that at corresponding points in the fluid underneath the rotors the theoretical shear rate values are virtually the same with differences occurring above y_b.

When comparison of the large gap geometry is made with its corresponding small gap geometry (Figures 6.30 and 6.22 etc.) we can see that the value of the shear rate at a fixed position above y_b is virtually the same in both geometries with differences occurring below the rotor height (i.e. gap size) y_b.

6.5 Conclusions

From the above comparisons of the results it can generally be seen that the experimental and theoretical u values agree relatively well quantitatively (within 15%) for the cylindrical and disc stirrers rotating in either the Newtonian or non-Newtonian fluid. In fact, the results for the cylindrical stirrer are in agreement with the results obtained from our preliminary work as presented in [8] and given in Appendix 1. The agreement between experimental and theoretical g values is not so good for the reasons given previously but is within an order of magnitude.

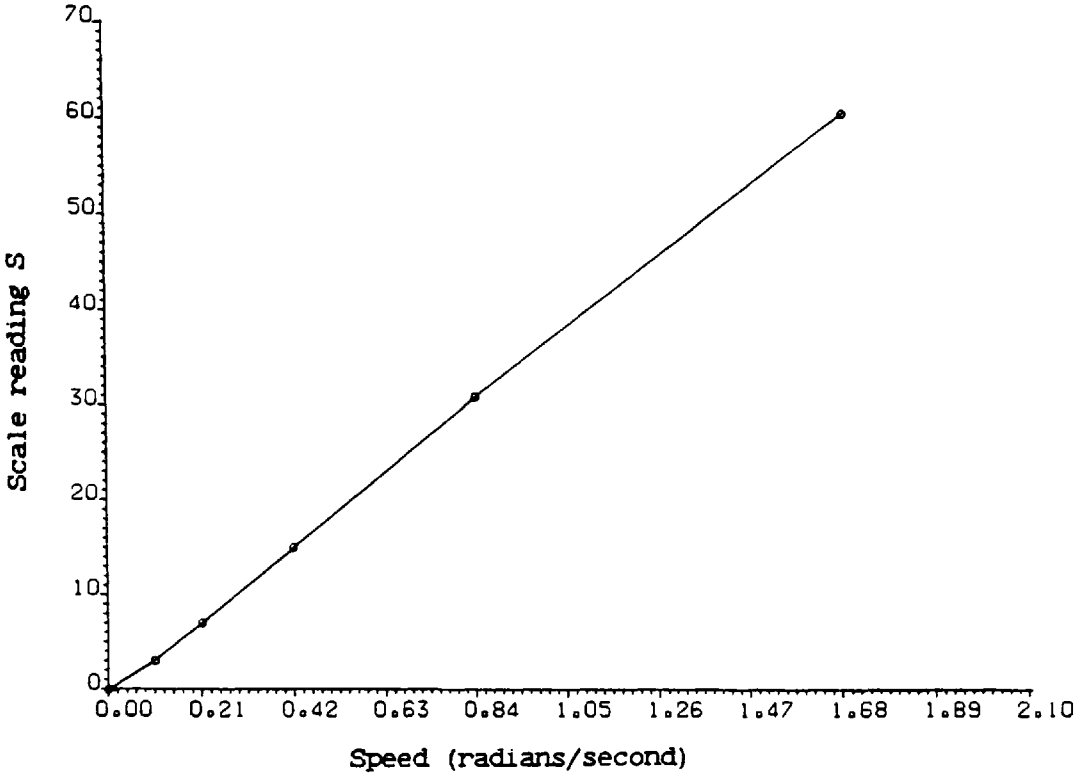

Figure 6.1 Viscometric curve for glycerol at 23°C

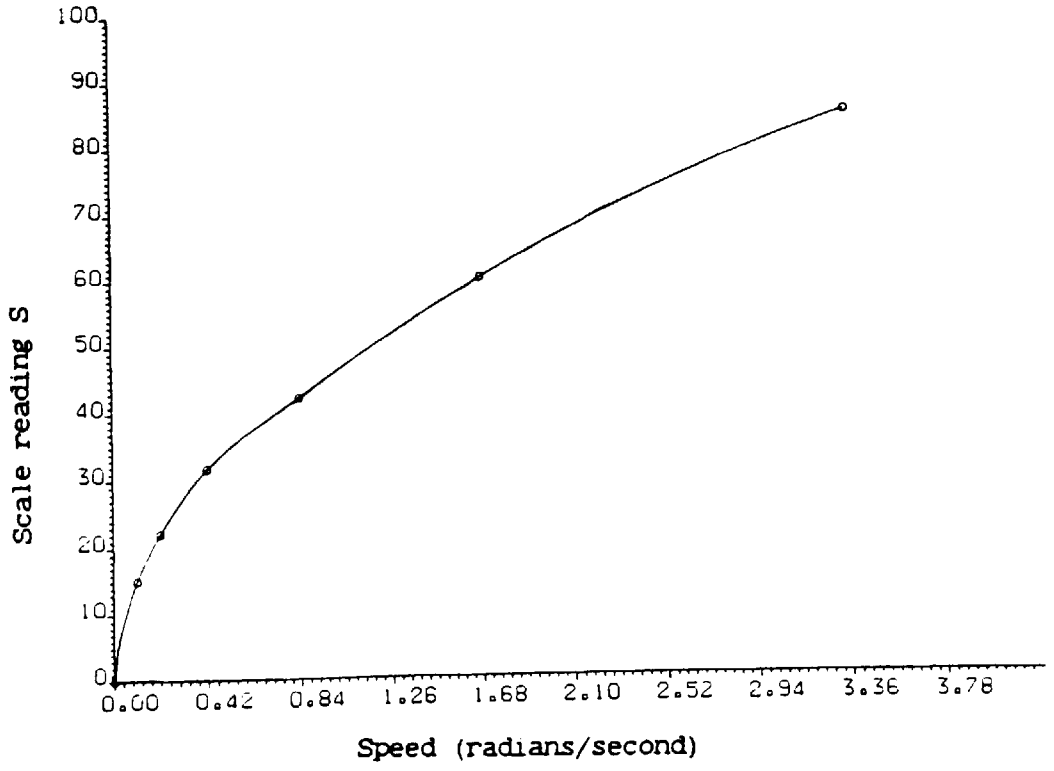

Figure 6.2 Viscometric curve for Carbopol 910 at 21°C

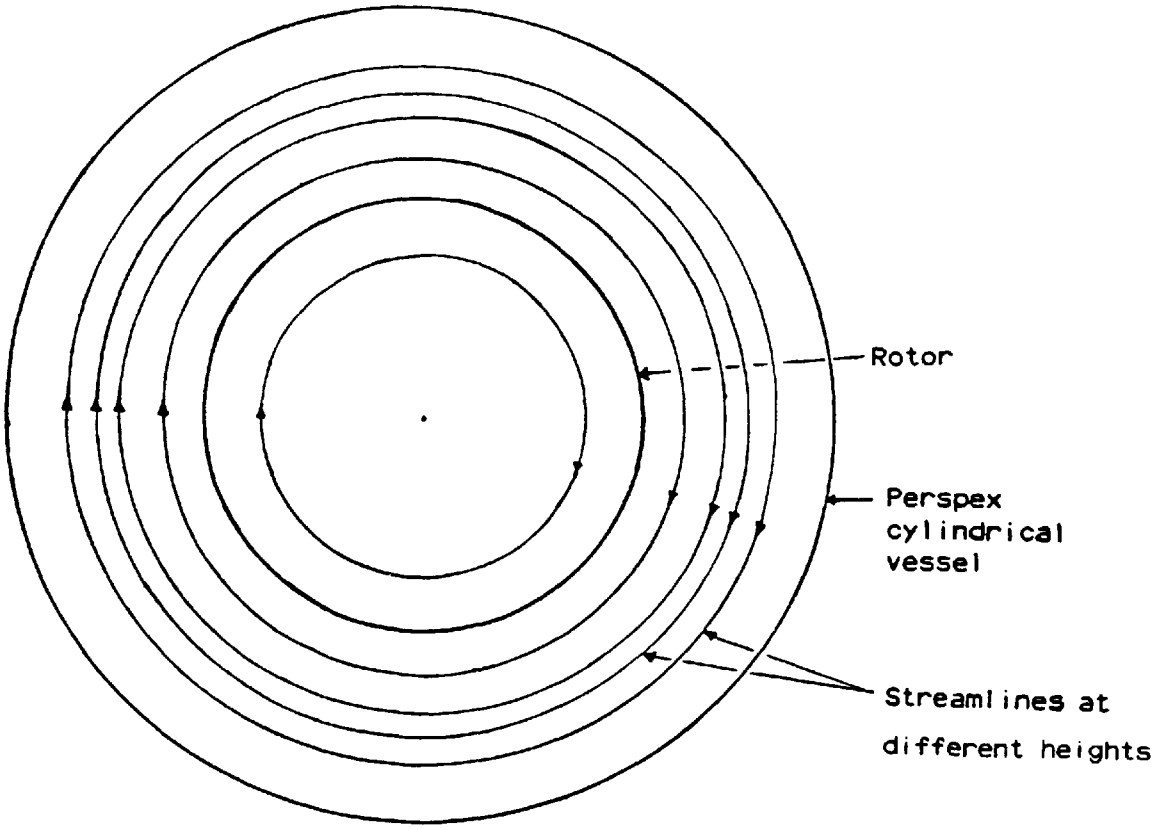

Figure 6.3 Typical primary flow patterns as seen from the bottom view of the apparatus.

Figure 6.4

U (VELOCITY) CONTOURS FOR NEWTONIAN FLUID (GAP = 0.8)

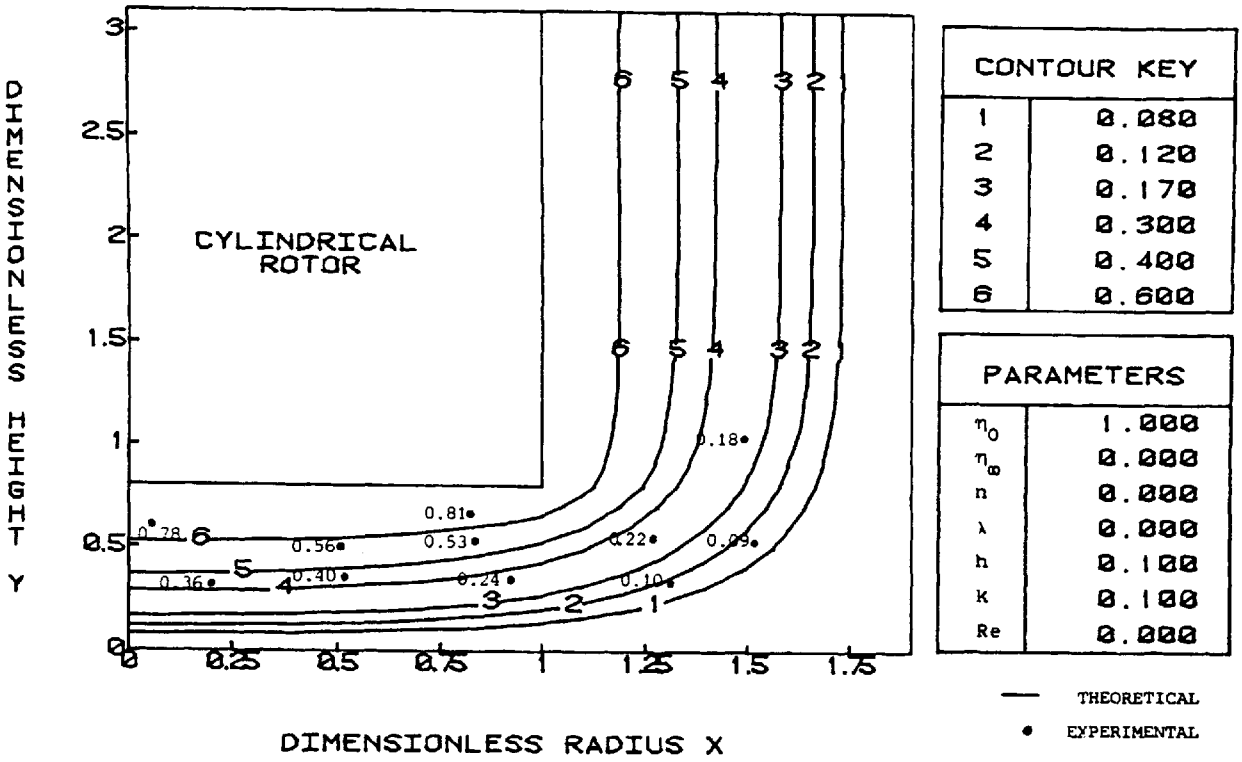

Figure 6.5

U (VELOCITY) CONTOURS FOR NEWTONIAN FLUID (GAP = 0.8)

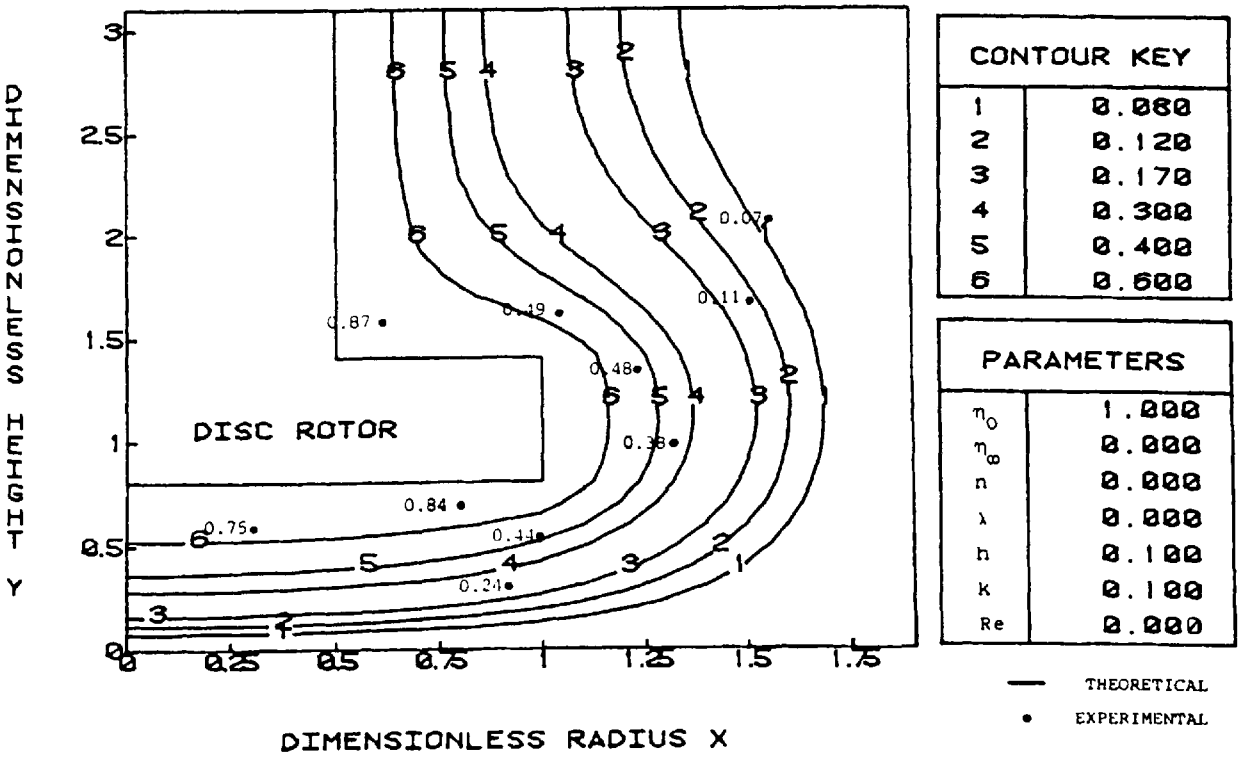

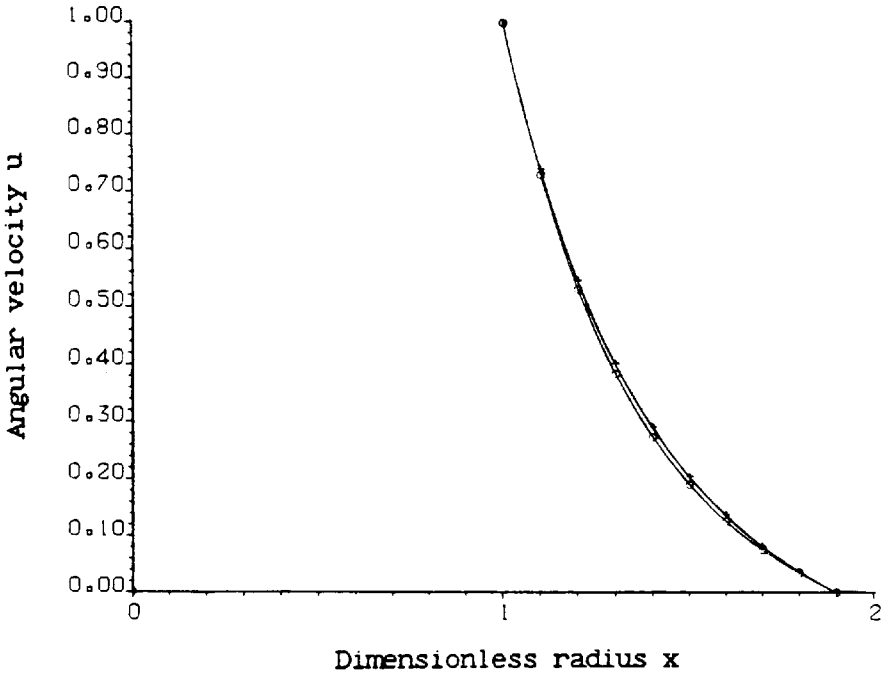

Figure 6.6 Velocity profile for the cylindrical × and disc ∘ stirrers at a fixed height below H.

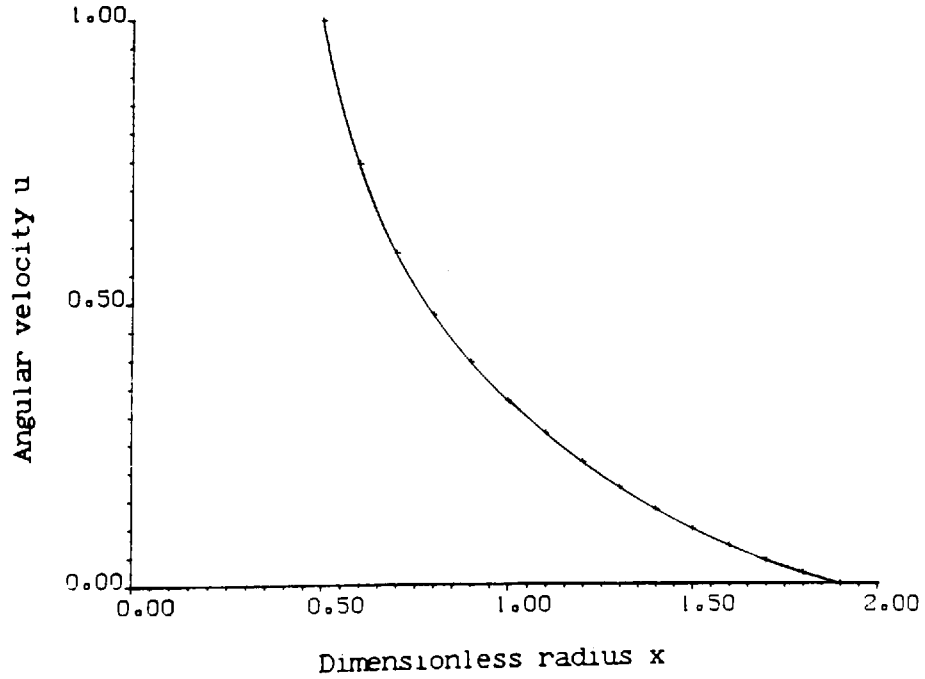

Figure 6.7 Velocity profile for the disc stirrer at a fixed height above H.

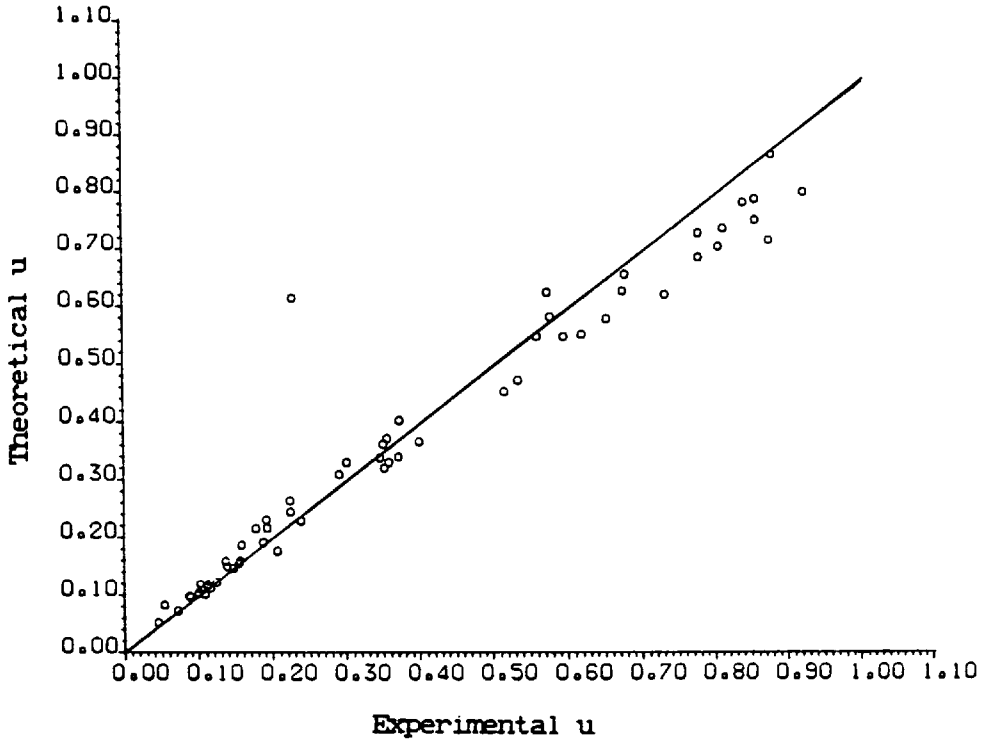

Figure 6.8 A comparison of theoretical and experimental u values for the cylindrical rotor in glycerol, gap = 0.8, Re → 0.

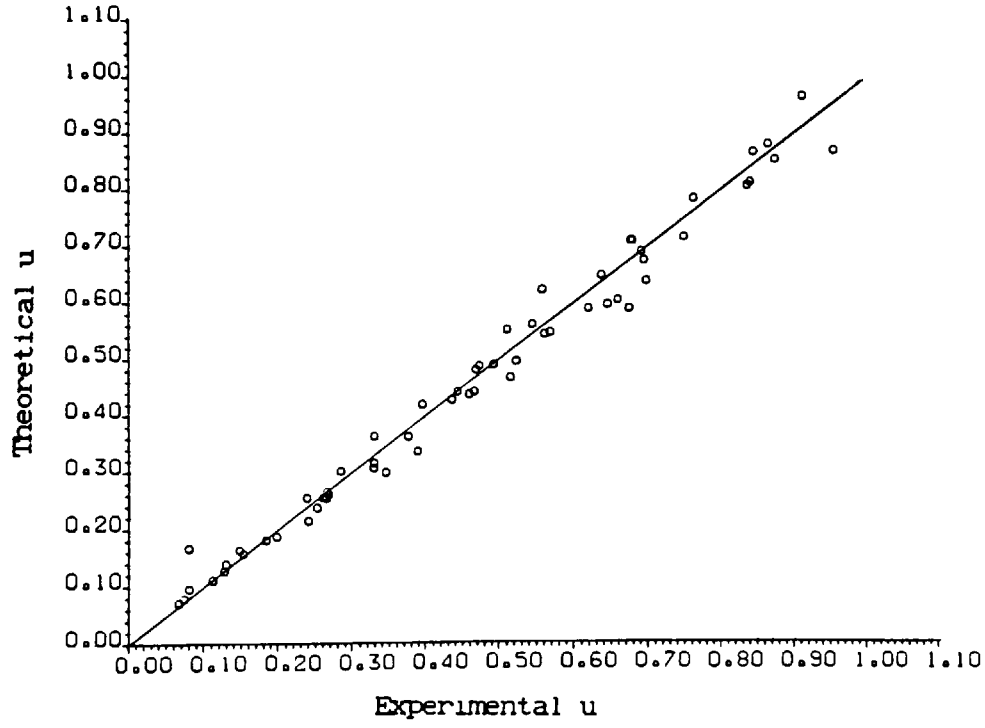

Figure 6.9 A comparison of theoretical and experimental u values for the disc rotor in glycerol, gap = 0.8, Re → 0.

	Mean Value of udiff	Standard Deviation of udiff	Mean Value of gdiff	Standard Deviation of gdiff
Cylindrical Stirrer				
Glycerol				
-Small Gap (0.8)	0.74	13.6	-61.0	59.2
-Large Gap (1.3)	3.30	14.5	-49.0	54.4
Carbopol 910				
-Small Gap (0.8	10.7	17.7	-21.5	82.0
-Large Gap (1.3)	12.5	14.0	-12.7	73.5
Disc Stirrer				
Glycerol				
-Small Gap (0.8)	-0.1	9.4	-43.0	92.4
-Large Gap (1.3)	0.1	7.8	-45.6	60.0
Carbopol 910				
-Small Gap (0.8)	7.3	13.3	-5.4	92.0
-Large Gap (1.3)	11.0	13.3	-44.7	96.5

Table: 6.1 The Mean and Standard Deviation Values for Primary Flow Parameters.

Figure 6.10

U (VELOCITY) CONTOURS FOR CROSS FLUID (GAP = 0.8)

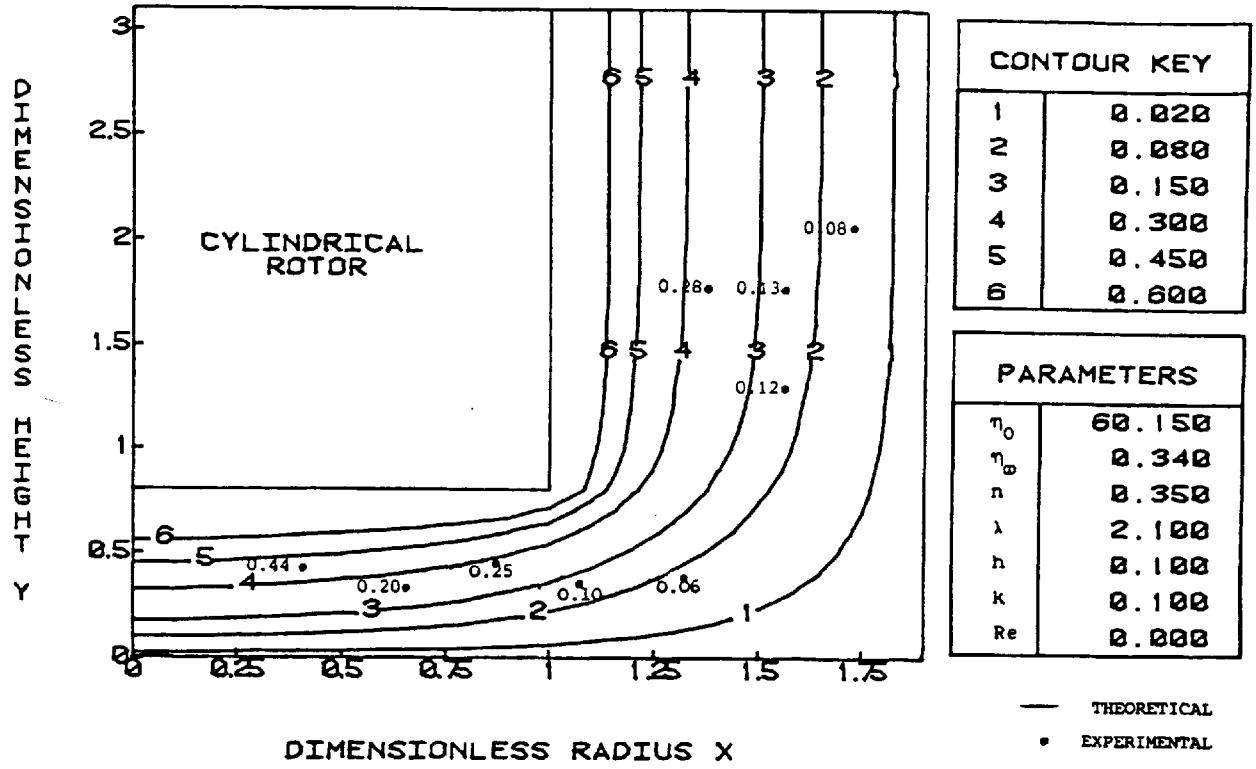

Figure 6.11

U (VELOCITY) CONTOURS FOR CROSS FLUID (GAP = 0.8)

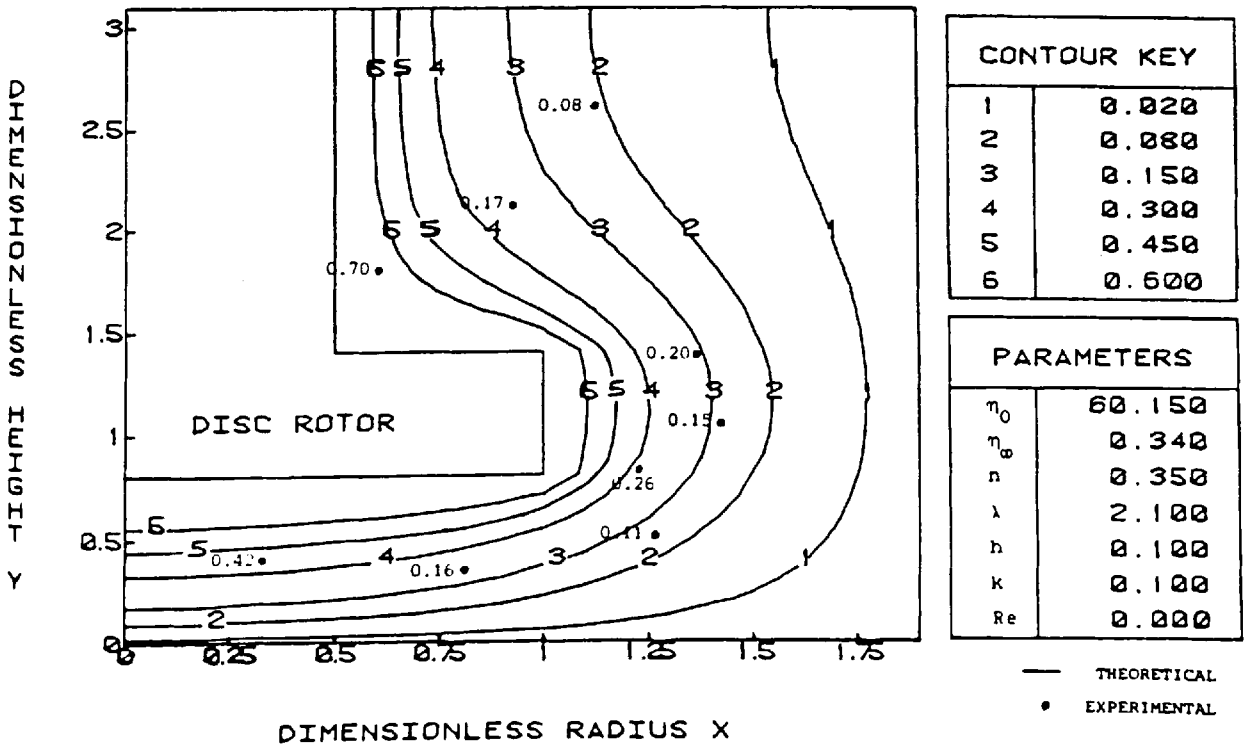

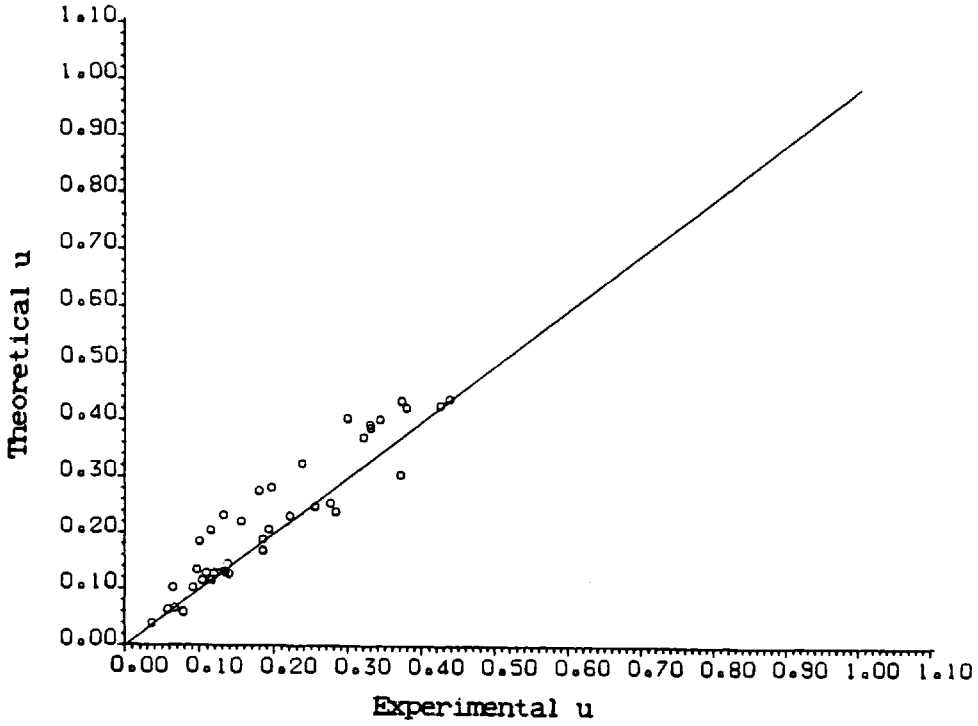

Figure 6.12 A comparison of theoretical and experimental u values for the cylindrical rotor in Carbopol 910, gap = 0.8, Re → 0.

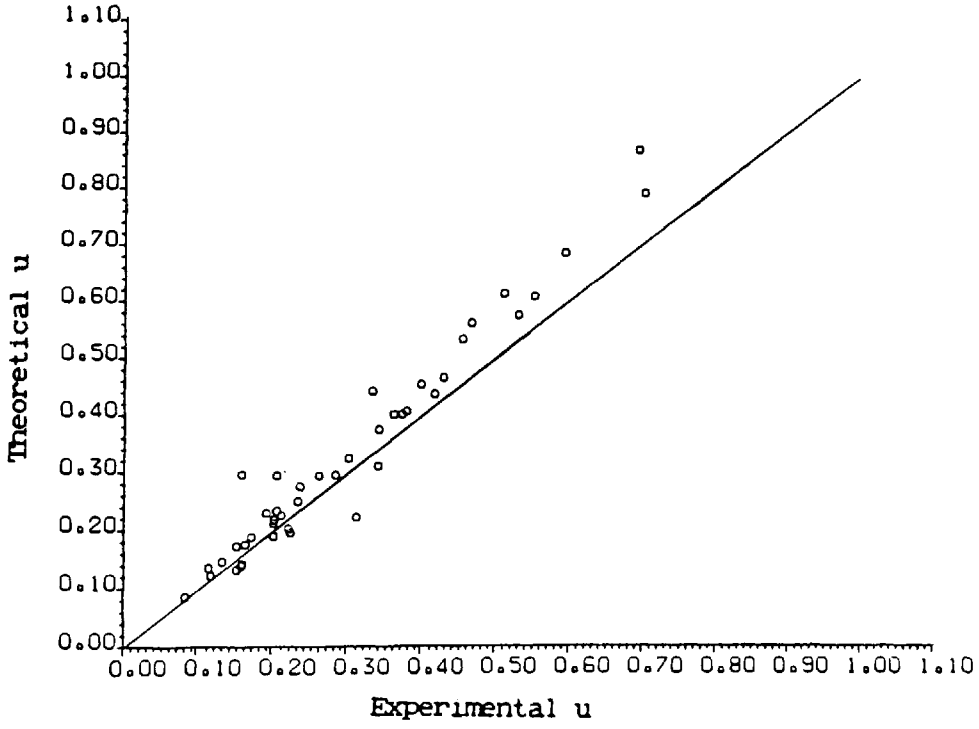

Figure 6.13 A comparison of theoretical and experimental u values for the disc rotor in Carbopol 910, gap = 0.8, Re → 0.

Figure 6.14

U (VELOCITY) CONTOURS FOR NEWTONIAN FLUID (GAP = 1.3)

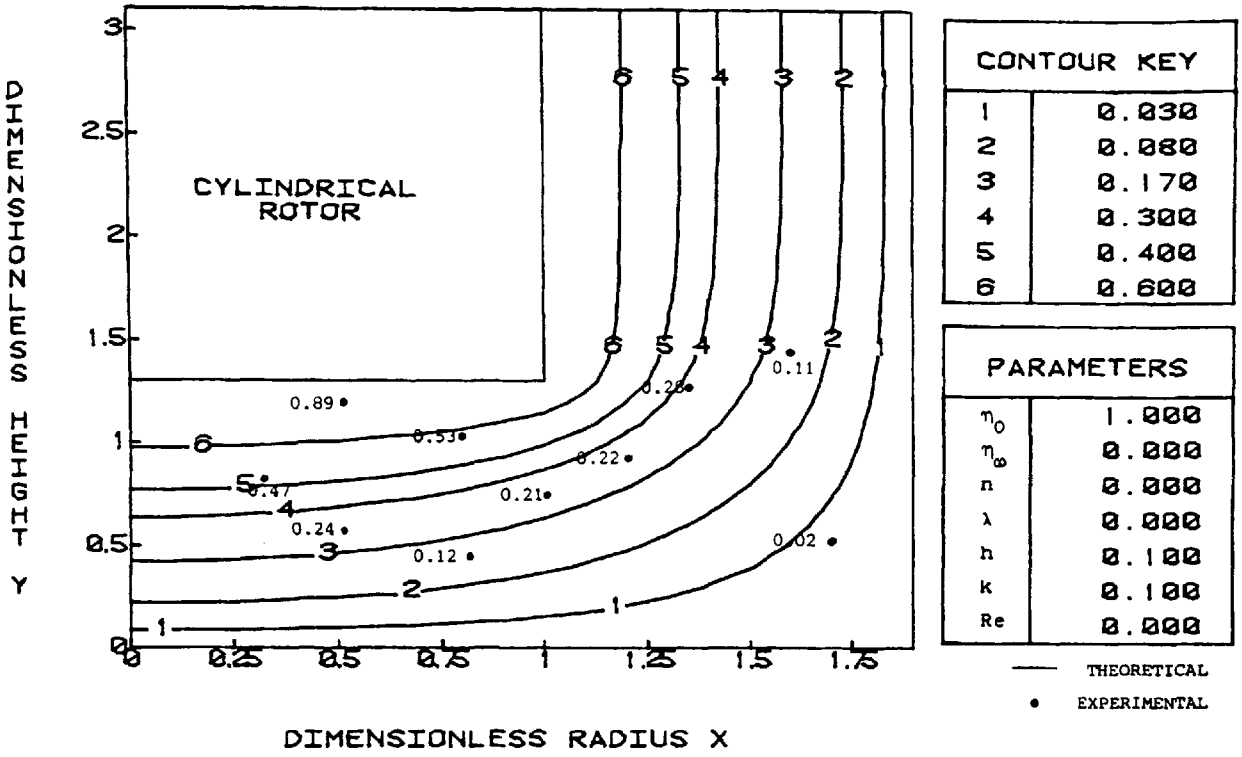

Figure 6.15

U (VELOCITY) CONTOURS FOR NEWTONIAN FLUID (GAP = 1.3)

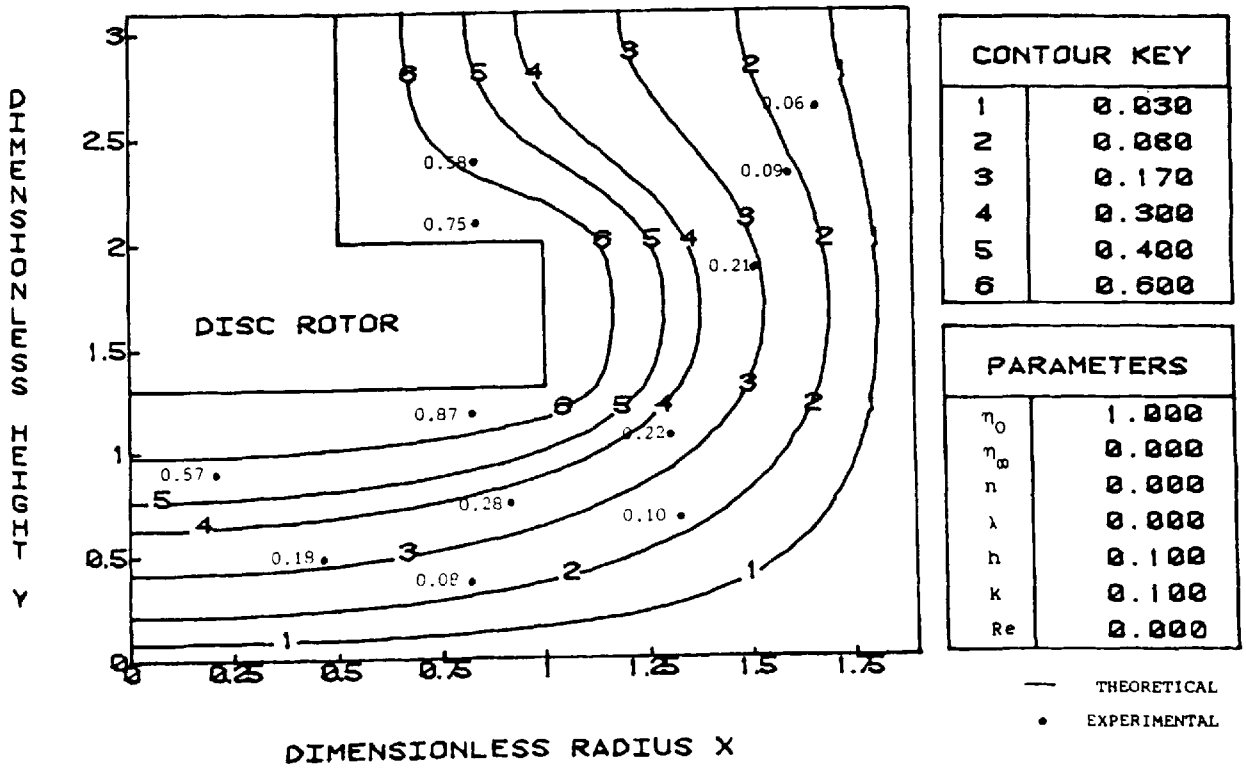

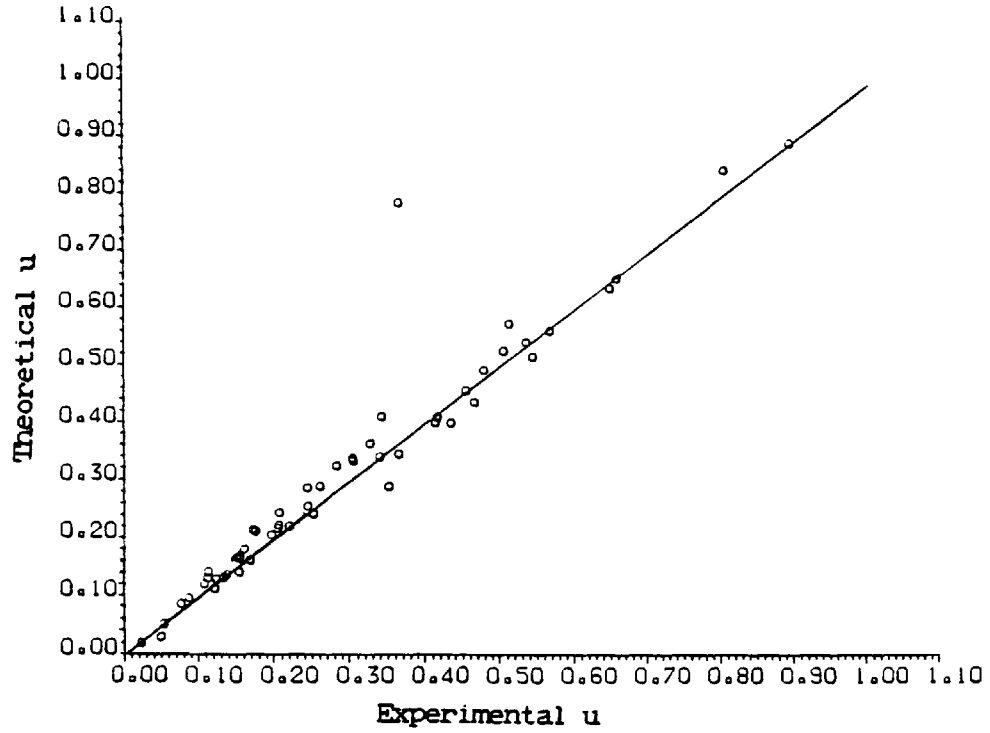

Figure 6.16 A comparison of theoretical and experimental u values for the cylindrical rotor in glycerol, gap = 1.3, Re → 0.

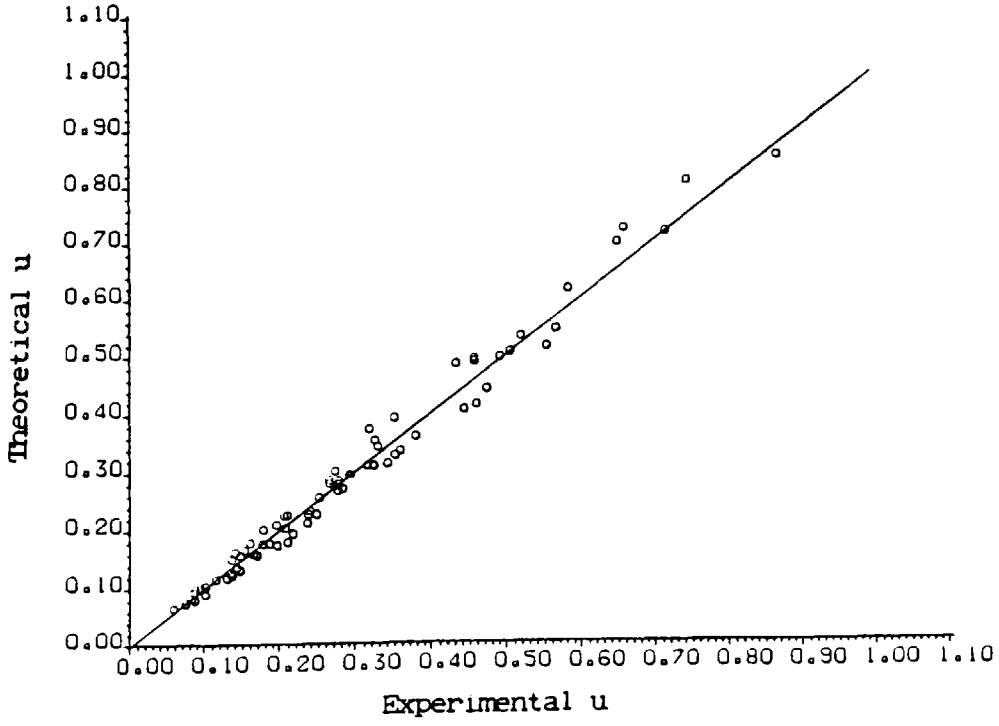

Figure 6.17 A comparison of theoretical and experimental u values for the disc rotor in glycerol, gap = 1.3, Re → 0.

Figure 6.18

U (VELOCITY) CONTOURS FOR CROSS FLUID (GAP = 1.3)

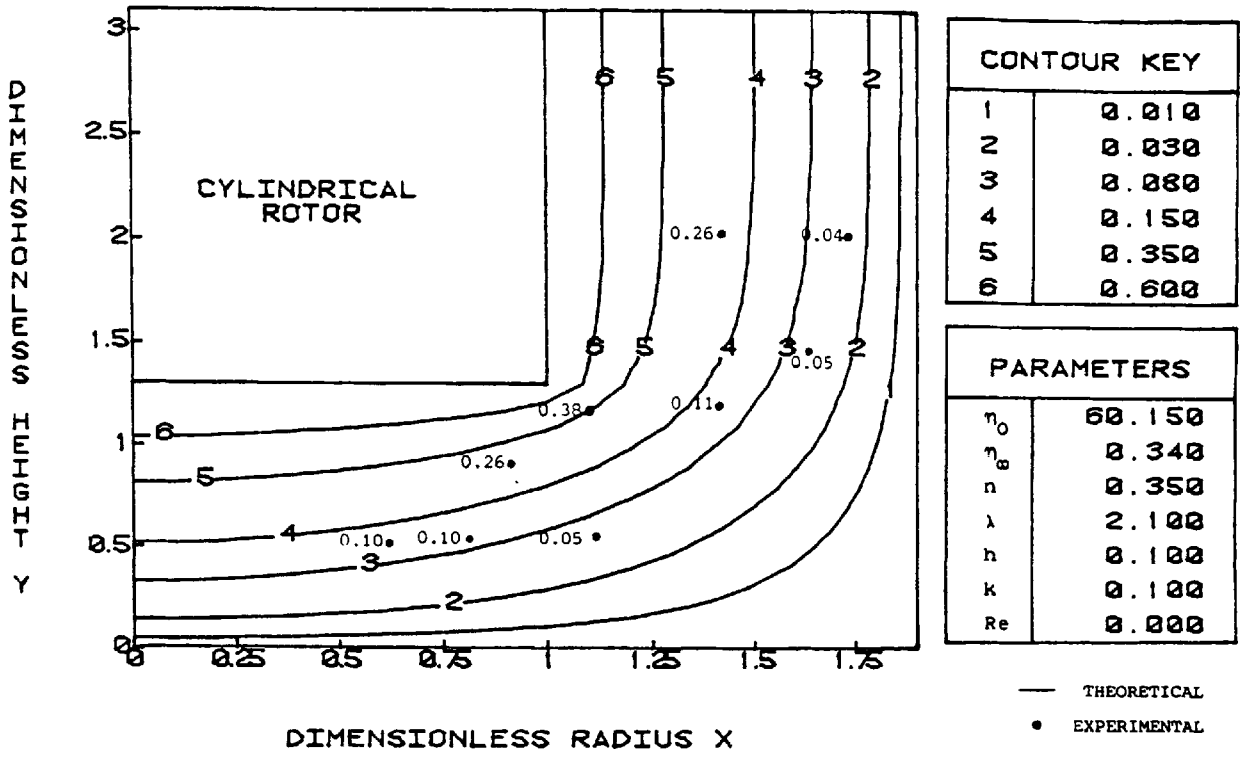

CONTOUR KEY	
1	0.010
2	0.030
3	0.080
4	0.150
5	0.350
6	0.600

PARAMETERS	
η_0	60.150
η_∞	0.340
n	0.350
λ	2.100
h	0.100
k	0.100
Re	0.000

— THEORETICAL
• EXPERIMENTAL

Figure 6.19

U (VELOCITY) CONTOURS FOR CROSS FLUID (GAP = 1.3)

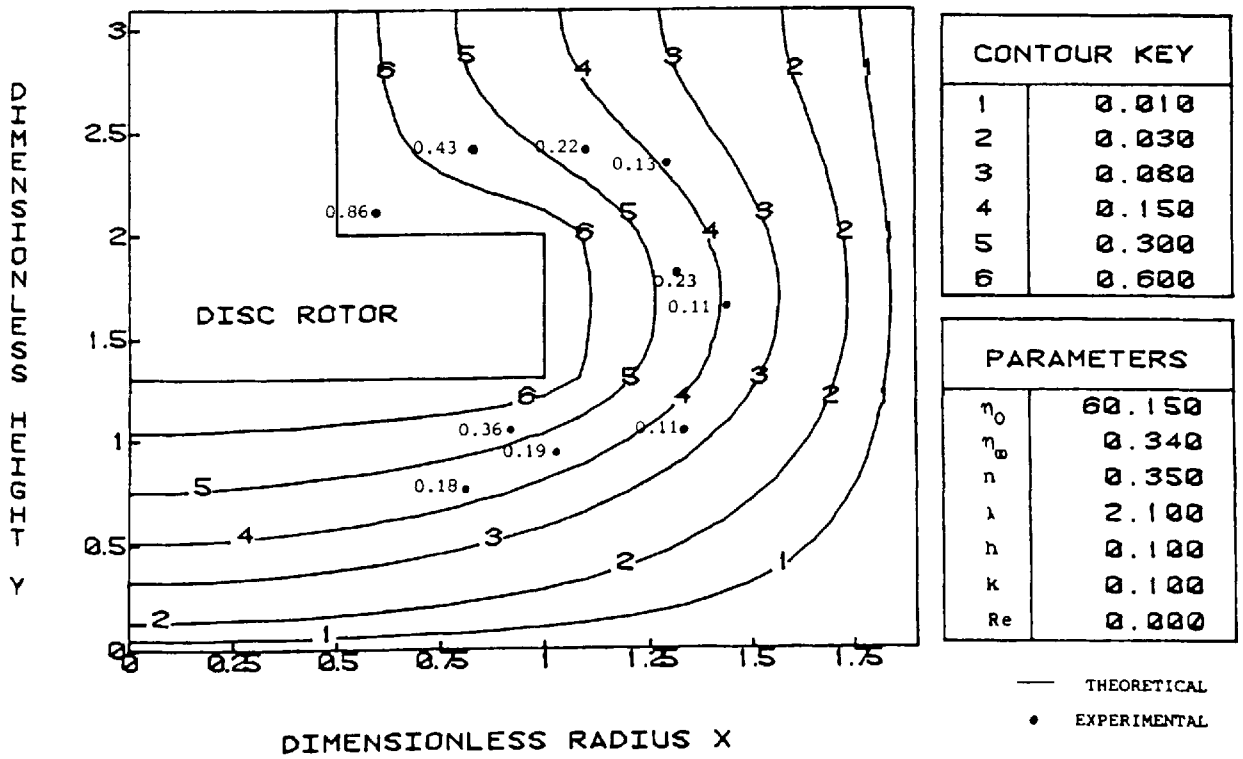

CONTOUR KEY	
1	0.010
2	0.030
3	0.080
4	0.150
5	0.300
6	0.600

PARAMETERS	
η_0	60.150
η_∞	0.340
n	0.350
λ	2.100
h	0.100
k	0.100
Re	0.000

— THEORETICAL
• EXPERIMENTAL

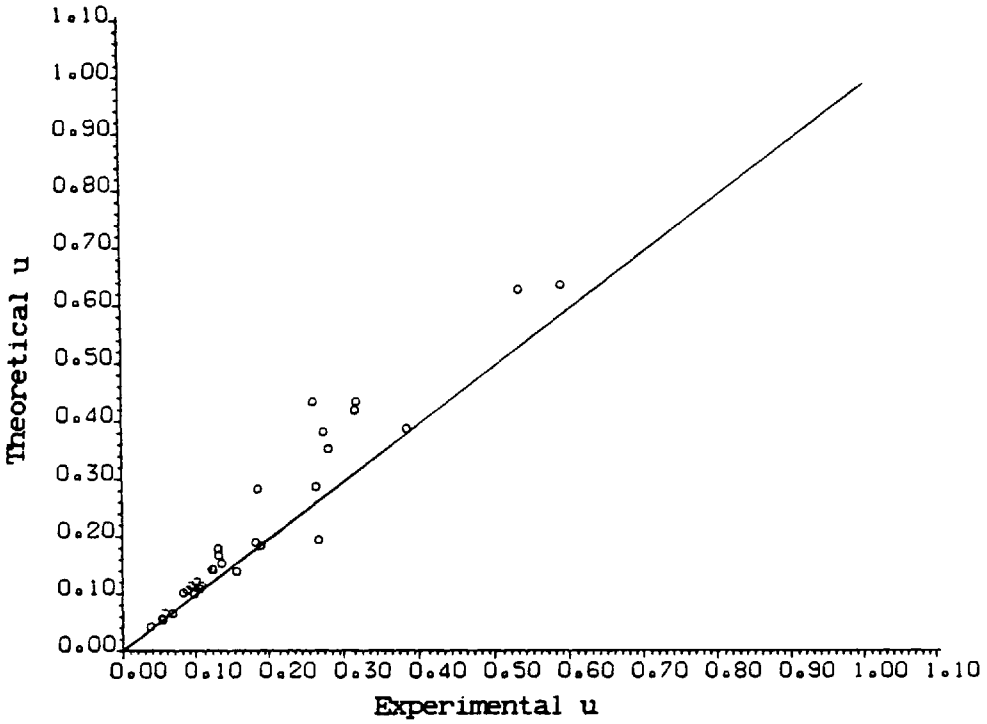

Figure 6.20 A comparison of theoretical and experimental u values for the cylindrical rotor in Carbopol 910, gap = 1.3, Re → 0.

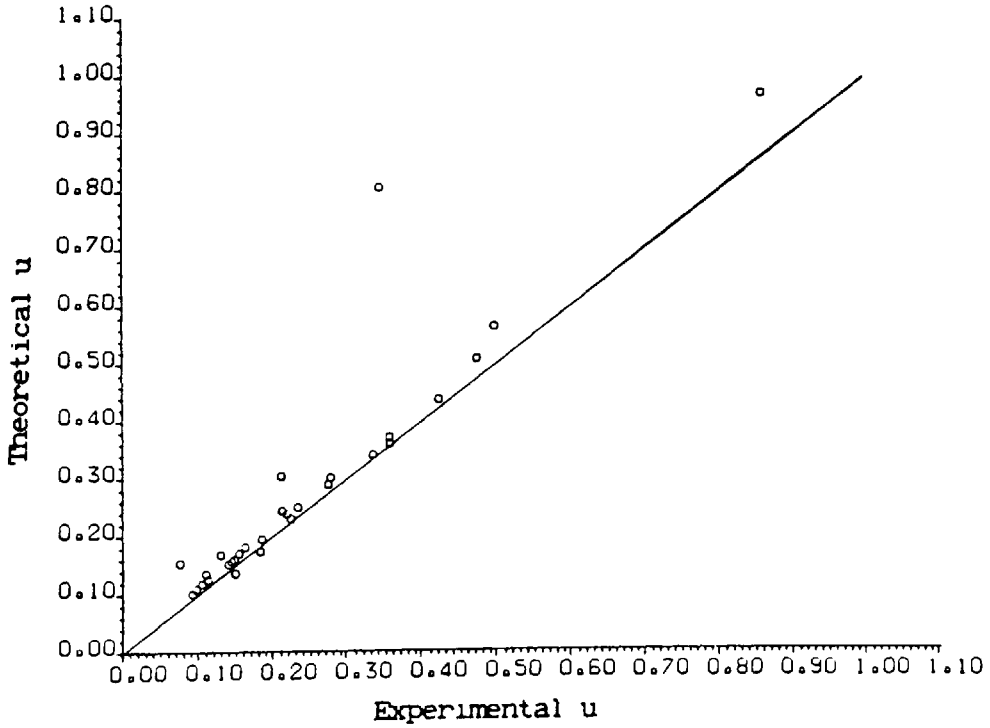

Figure 6.21 A comparison of theoretical and experimental u values for the disc rotor in Carbopol 910, gap = 1.3, Re → 0.

Figure 6.22

G (SHEAR-RATE) CONTOURS FOR NEWTONIAN FLUID (GAP = 0.8)

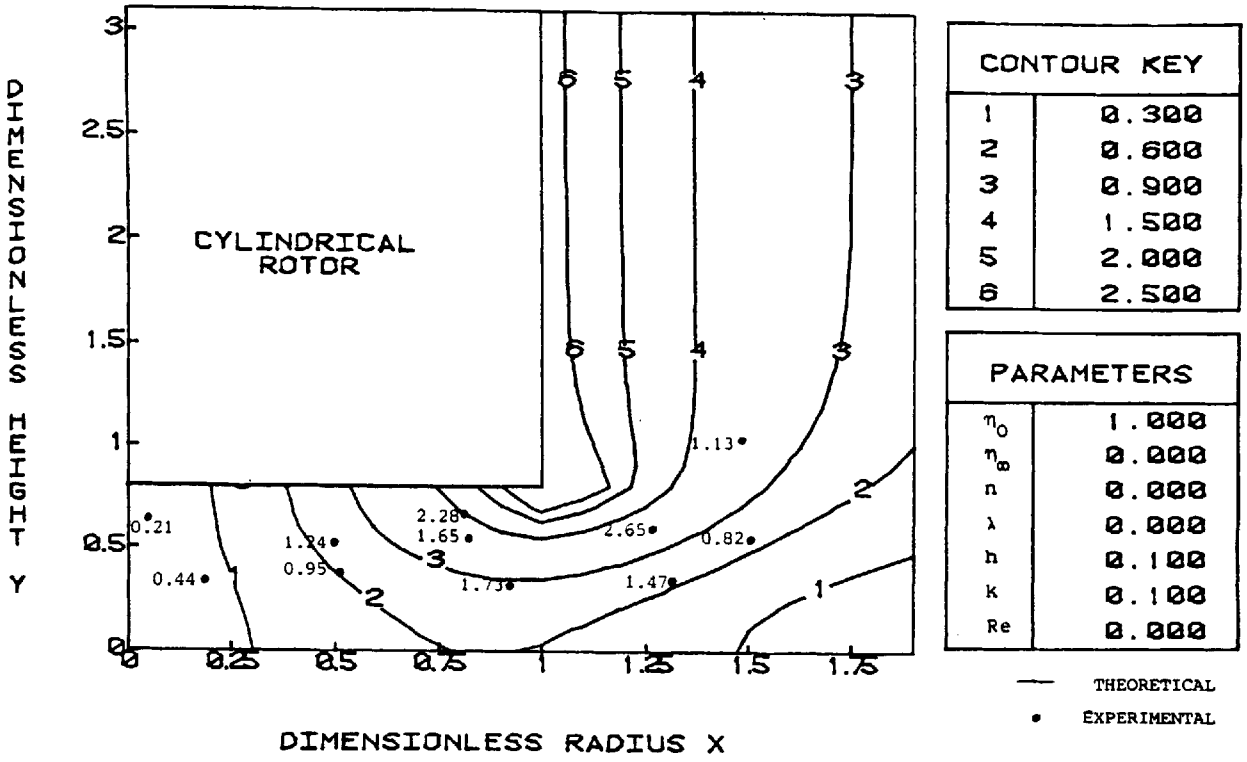

Figure 6.23

G (SHEAR-RATE) CONTOURS FOR NEWTONIAN FLUID (GAP = 0.8)

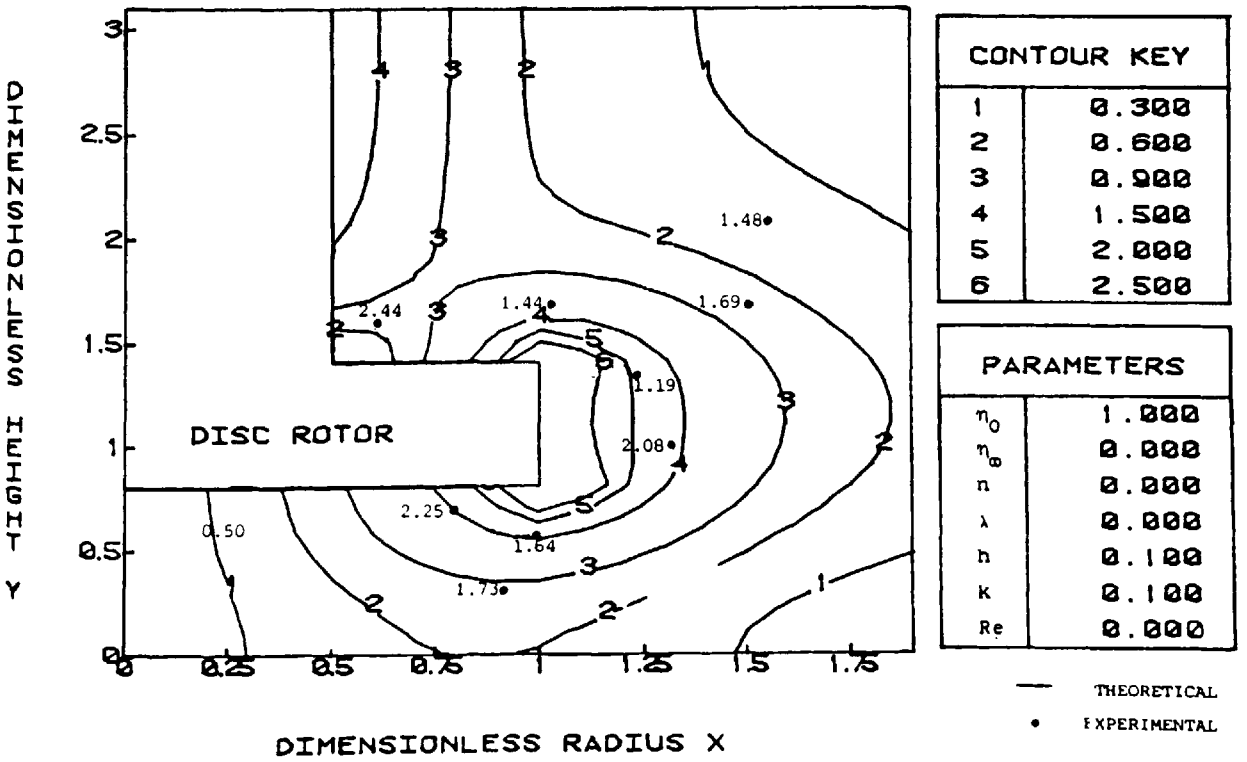

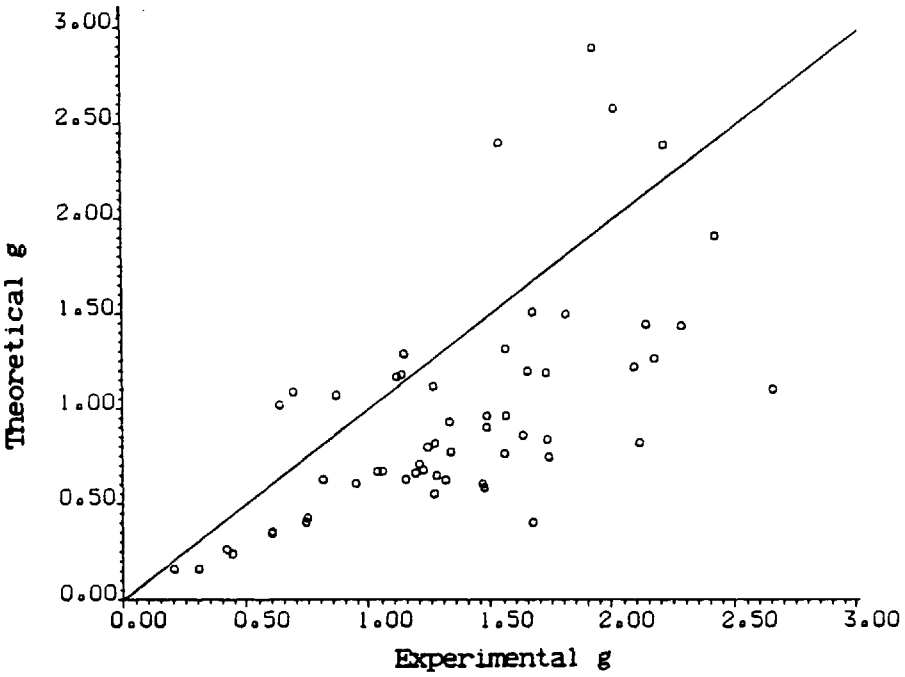

Figure 6.24 A comparison of theoretical and experimental g values for the cylindrical rotor in glycerol, gap = 0.8, Re → 0.

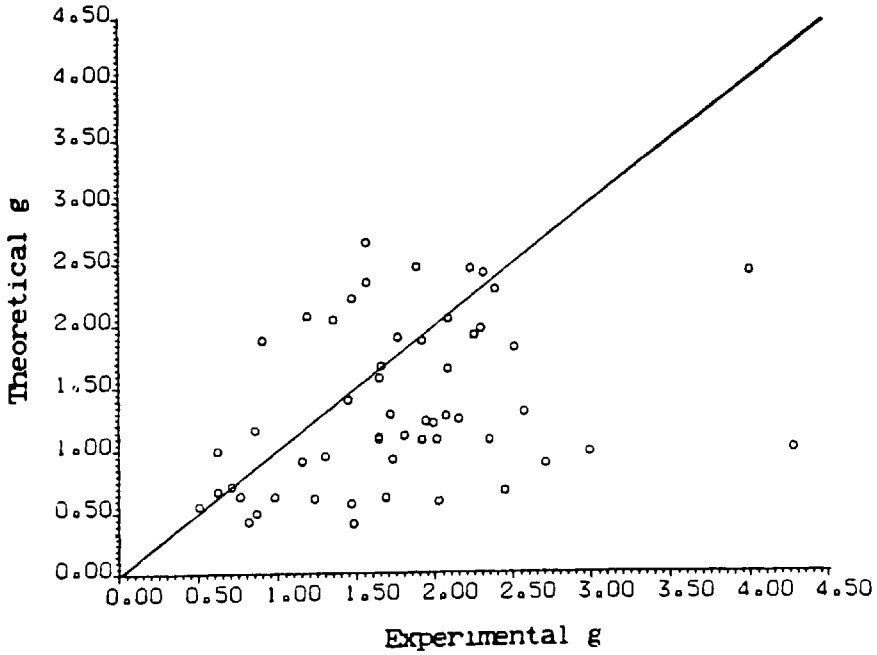

Figure 6.25 A comparison of theoretical and experimental g values for the disc rotor in glycerol, gap = 0.8, Re → 0.

Figure 6.26

G (SHEAR-RATE) CONTOURS FOR CROSS FLUID (GAP = 0.8)

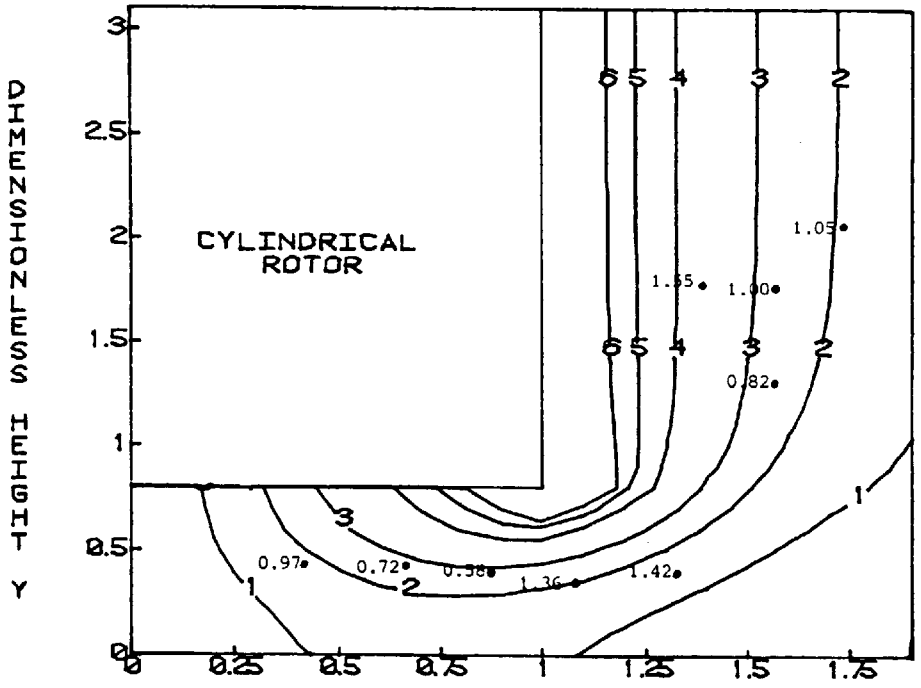

CONTOUR KEY	
1	0.300
2	0.600
3	0.900
4	1.500
5	2.000
6	2.500

PARAMETERS	
η_0	60.150
η_∞	0.340
n	0.350
λ	2.100
h	0.100
k	0.100
Re	0.000

— THEORETICAL
• EXPERIMENTAL

Figure 6.27

G (SHEAR-RATE) CONTOURS FOR CROSS FLUID (GAP = 0.8)

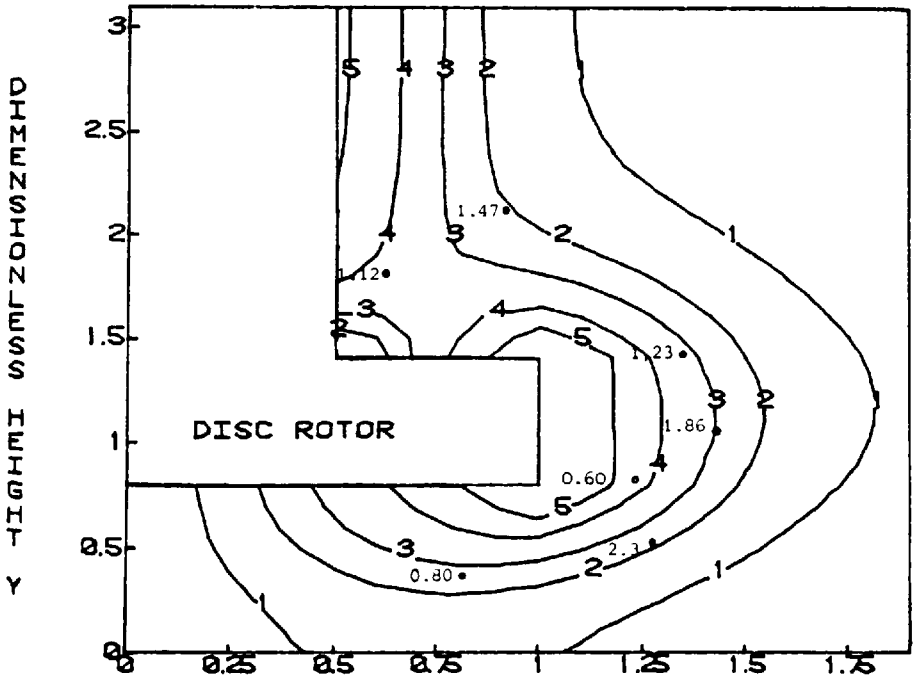

CONTOUR KEY	
1	0.300
2	0.600
3	0.900
4	1.500
5	2.500

PARAMETERS	
η_0	60.150
η_∞	0.340
n	0.350
λ	2.100
h	0.100
k	0.100
Re	0.000

— THEORETICAL
• EXPERIMENTAL

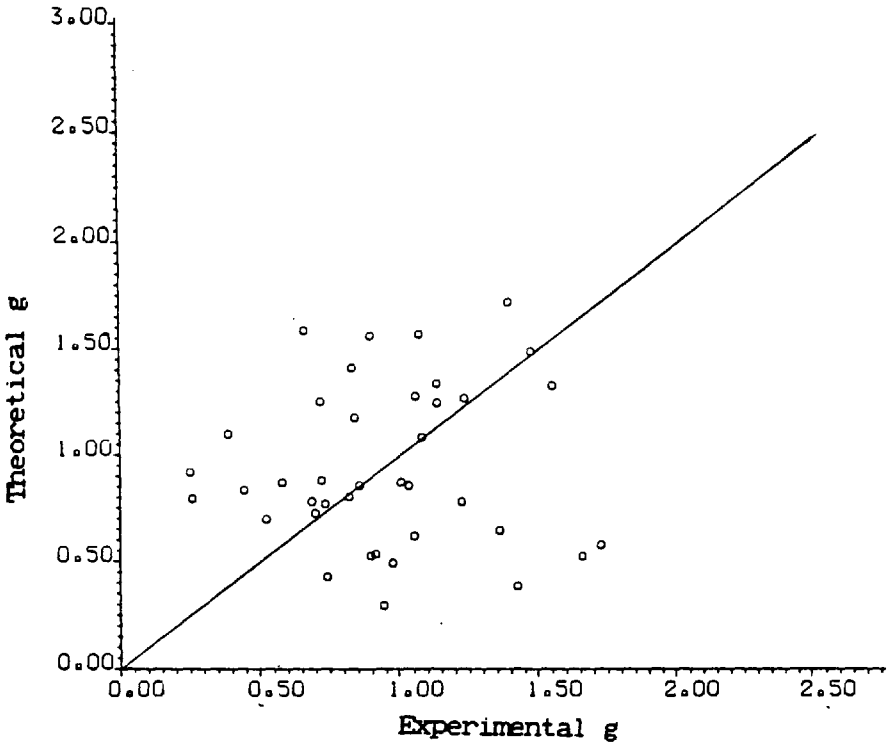

Figure 6.28 A comparison of theoretical and experimental g values for the cylindrical rotor in Carbopol 910, gap = 0.8, Re → 0.

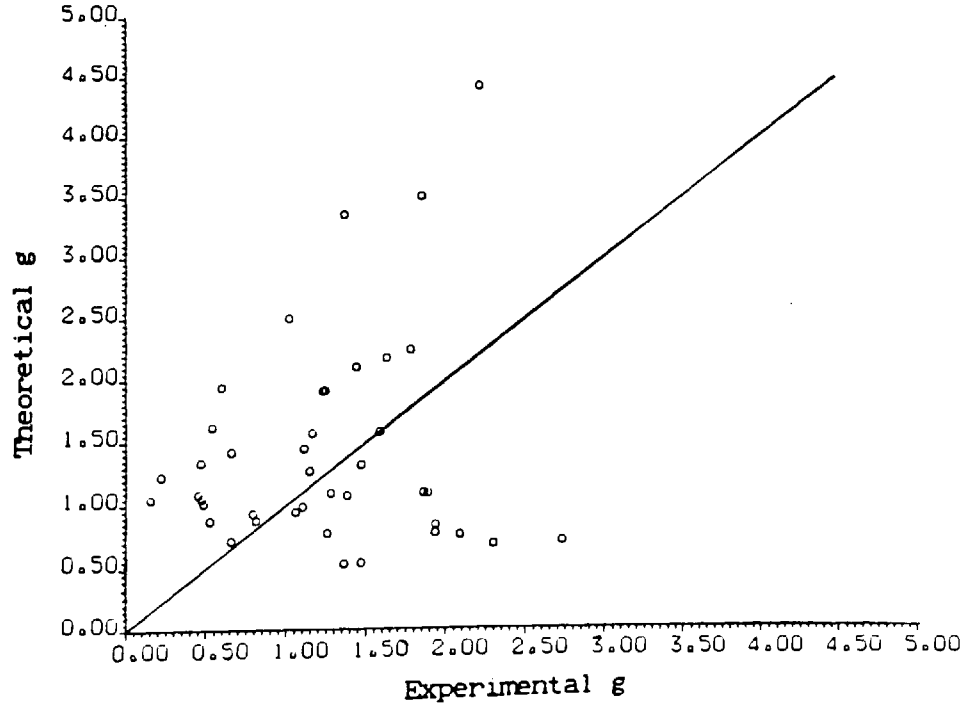

Figure 6.29 A comparison of theoretical and experimental g values for the disc rotor in Carbopol 910, gap = 0.8, Re → 0.

Figure 6.30

G (SHEAR-RATE) CONTOURS FOR NEWTONIAN FLUID (GAP = 1.3)

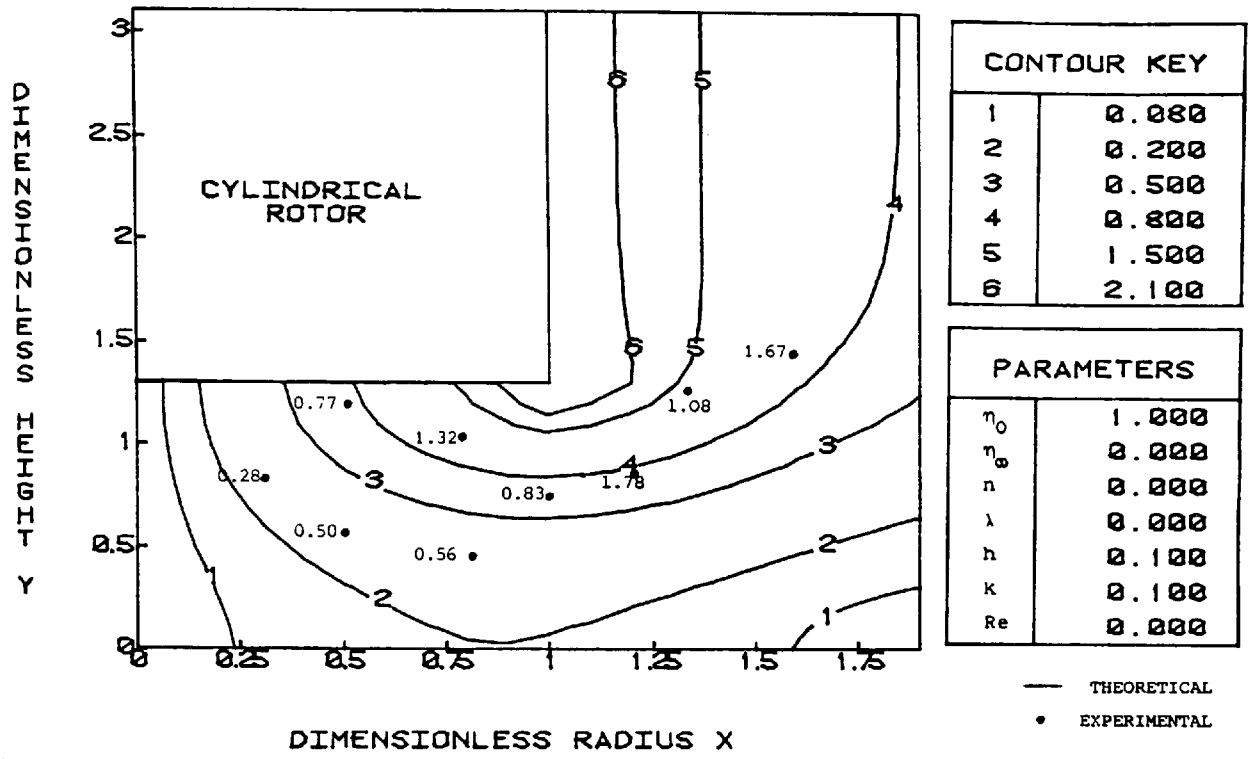

Figure 6.31

G (SHEAR-RATE) CONTOURS FOR NEWTONIAN FLUID (GAP = 1.3)

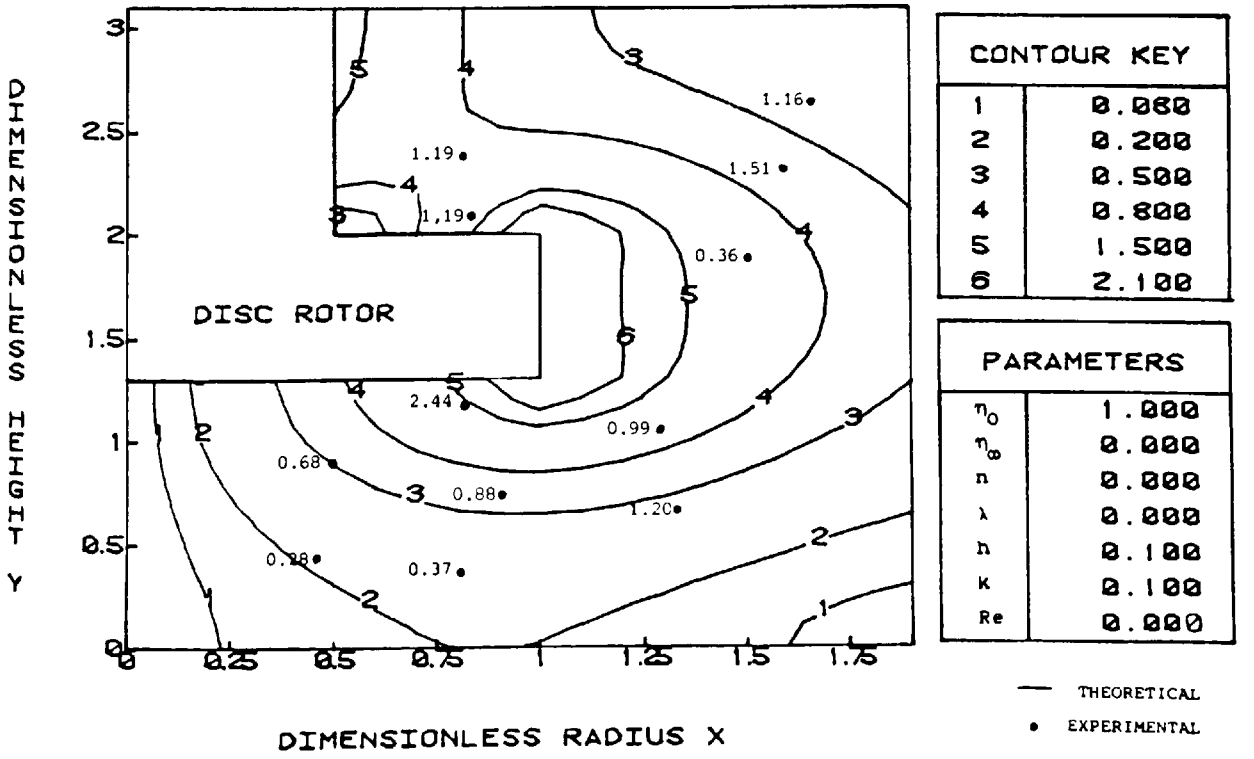

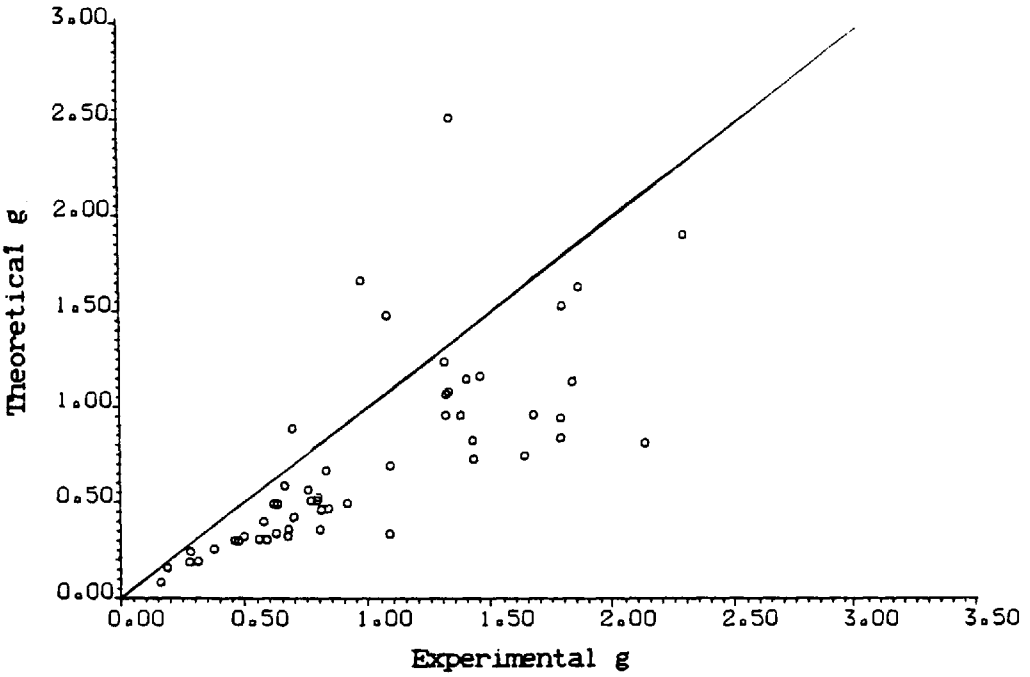

Figure 6.32 A comparison of theoretical and experimental g values for the cylindrical rotor in glycerol, gap = 1.3, Re → 0.

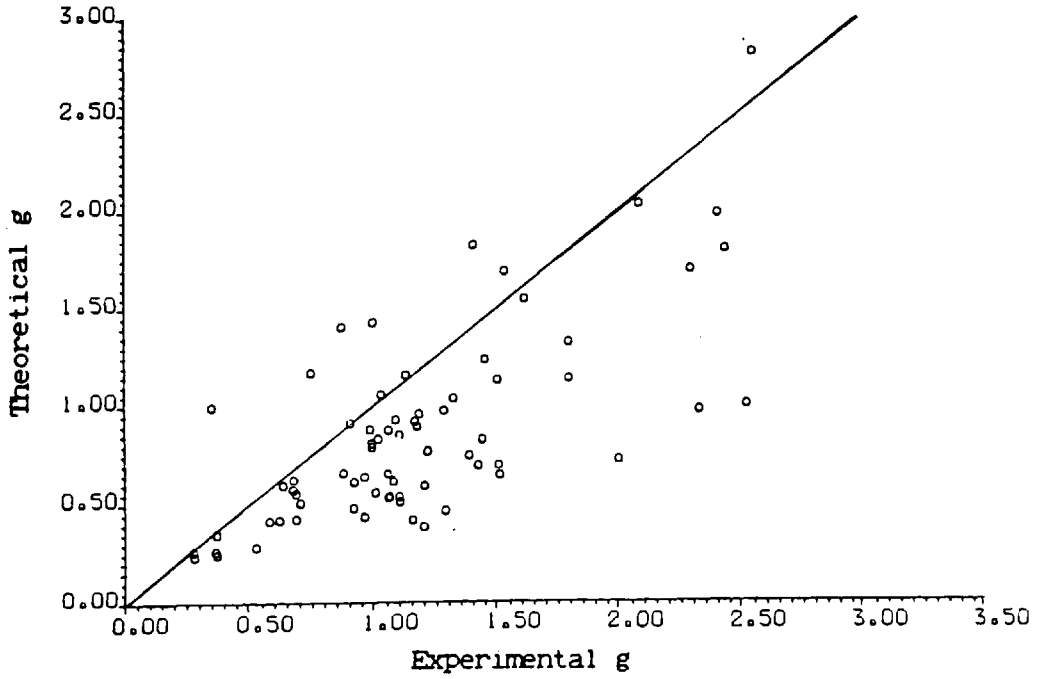

Figure 6.33 A comparison of theoretical and experimental g values for the disc rotor in glycerol, gap = 1.3, Re → 0.

Figure 6.34

G (SHEAR-RATE) CONTOURS FOR CROSS FLUID (GAP = 1.3)

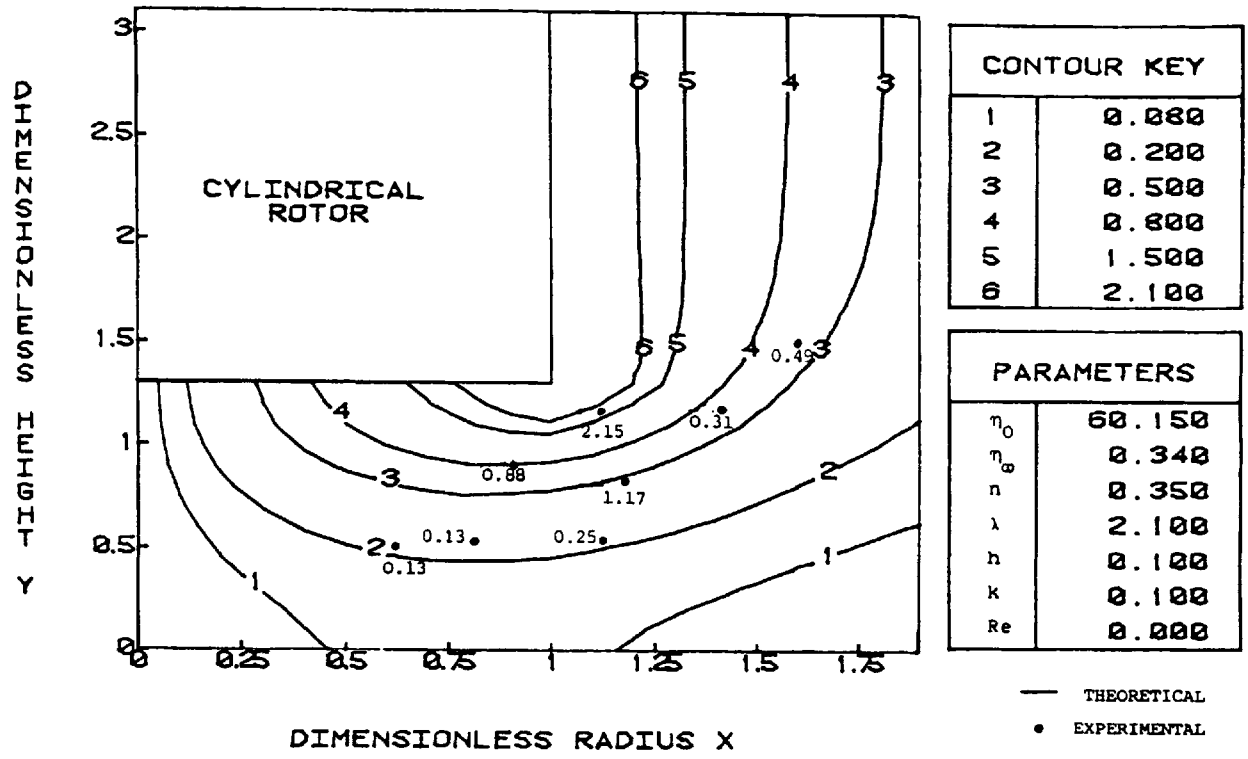

Figure 6.35

G (SHEAR-RATE) CONTOURS FOR CROSS FLUID (GAP = 1.3)

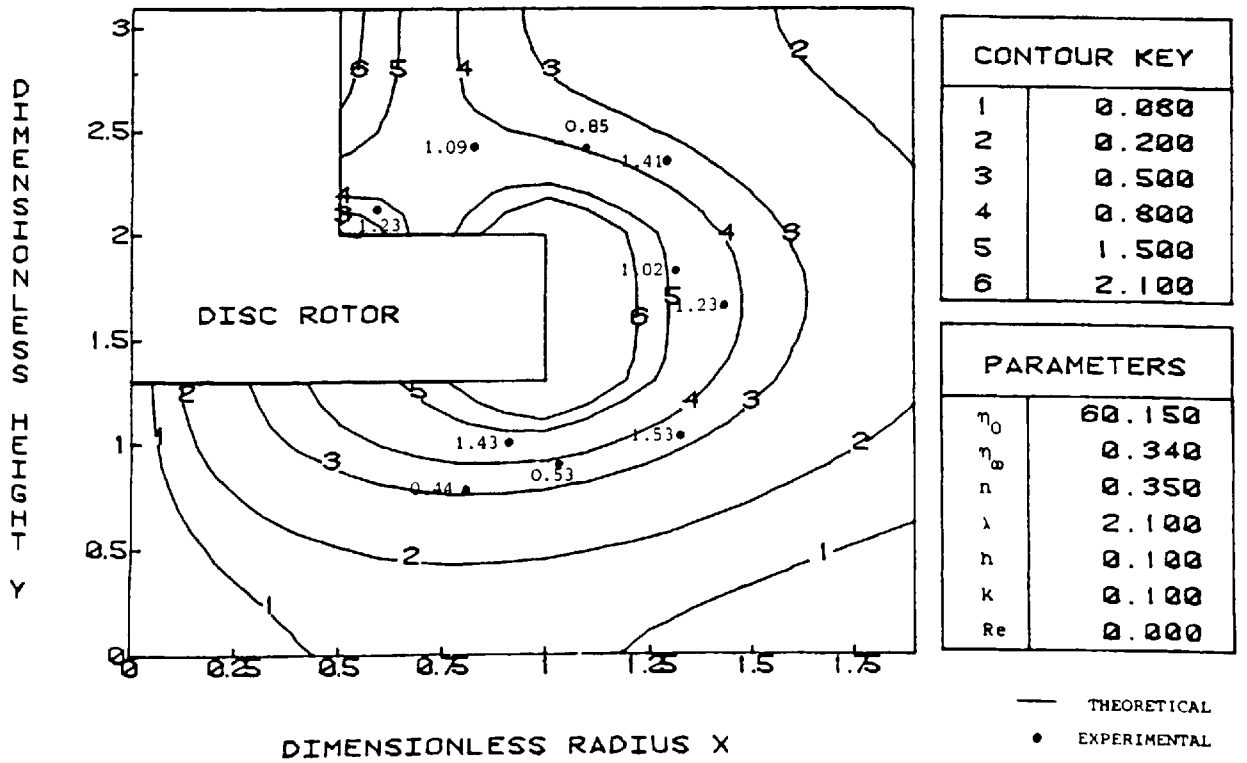

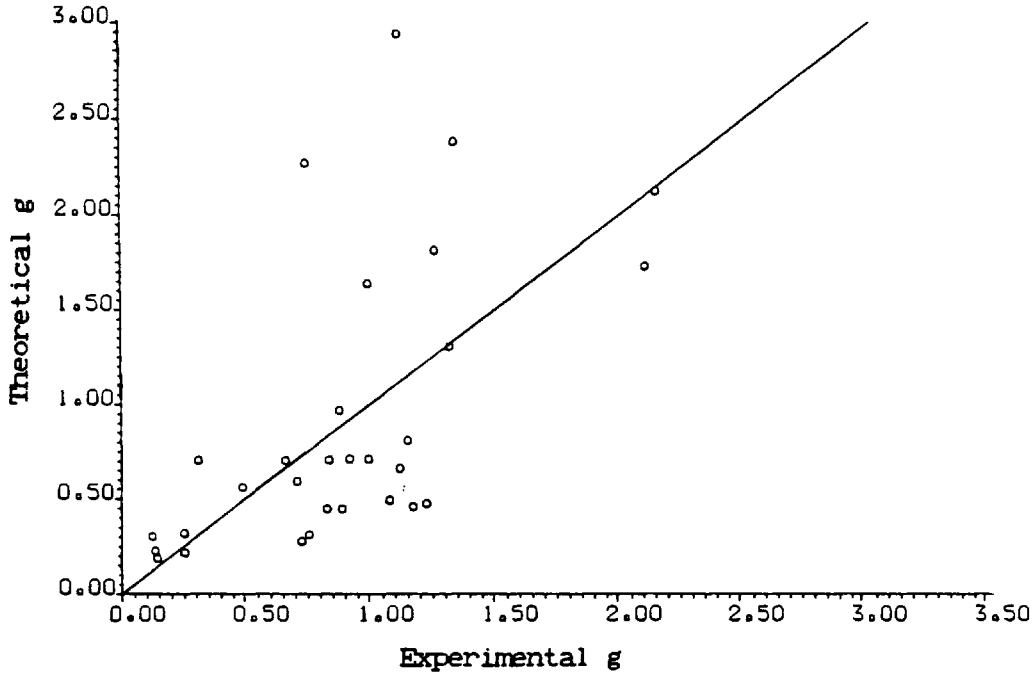

Figure 6.36 A comparison of theoretical and experimental g values for the cylindrical rotor in Carbopol 910, gap = 1.3, Re → 0.

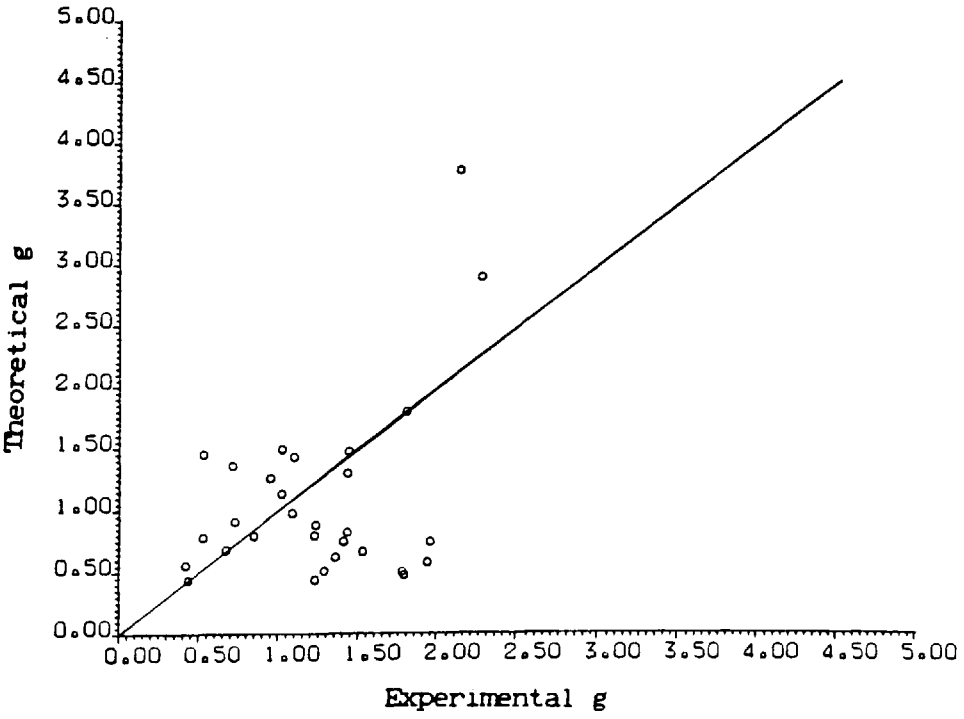

Figure 6.37 A comparison of theoretical and experimental g values for the disc rotor in Carbopol 910, gap = 1.3, Re → 0.

CHAPTER 7

RESULTS FOR SECONDARY FLOWS

7.0 Introduction

In this chapter, the flow patterns generated due to a cylindrical or disc stirrer rotating in the fluid under secondary flow conditions are described. The experimental and theoretical results obtained for the angular velocities u, shear rates γ (denoted by g), stream functions and vorticities χ are also given and compared. The standard deviation values from the mean values of u, g, α and χ as compared between the theoretical and experimental values are also presented. The incompressibility values shown give some indication as to the error involved in the method used for processing the experimental data.

7.1 Flow Patterns

Secondary flows were observed at a Reynolds number of approximately 6.1 for glycerol and 1.2 for Carbopol 910. This represented a speed of 128 rpm (13.4 radians per second). It was found that at this speed the secondary flows could be seen relatively clearly and the tracer particles could be tracked easily.

The secondary flow patterns were observed to be very different from those of primary flow. The fluid particles (represented by tracer particles) did not follow straightforward circular paths at a fixed height around the stirrers as in primary flows. Instead, each particle followed toroidal undulating paths which were off centre. In other words, there was motion in the vertical and radial directions as well as in the angular direction. Figure 7.1 shows a typical path of a particle as seen from the bottom view.

For the cylindrical stirrer it was seen that a particle which was initially travelling in small circular paths underneath the rotor subsequently followed larger circular paths with larger radii, the height also changing until it eventually travelled around the rotor. The particle was then seen to proceed in a similar fashion back to its original position before repeating its cycle.

For the disc stirrer, it was observed that the particles both above and below the disc behaved in a similar way to that described above. However, no particle above the disc was seen to travel to a position below it and no particle below the disc travelled to a position above it.

7.2 Angular Velocity Distributions

Figures 7.2 and 7.3 show theoretical contours of constant fluid angular velocities for the cylindrical and disc stirrer respectively, rotating with a speed of 13.4 radians per second (Re =6.1) at y_b = 1.3 in glycerol. From comparison of these contours with the corresponding primary flow geometries i.e. Figures 6.14 and 6.15, it can be seen that there is no apparent difference between them. The values next to the black dots are examples of experimentally determined values of u.

Direct comparisons between the experimental and computational u values are given in Figures 7.4 and 7.5. Points taken from three cycles below the cylindrical rotor are shown in Figure 7.4, while in Figure 7.5 two cycles, one taken from above and one from below the disc are shown. It can be seen that each cycle forms a distinct closed shape. The bold line represents the expected values of u and for the cylindrical stirrer, the agreement between the theoretical and experimental values is relatively good for points in the fluid away

from the rotor where lower fluid speeds occur and changes of speeds with distance are relatively small.

At points in the fluid nearer the rotor, the experimental values are lower than their corresponding theoretical values. This high deviation can be explained partly due to inherent experimental error and partly by the fact that at higher speeds of the fluid, the tracer particles are seen to be travelling in a 'jerky' movement resulting in some of the energy of the particles being used up. This 'jerky' movement may be due to the more pronounced shake in the rotor caused by its high speed. Therefore, less energy is available for the particle to travel along its flow path resulting in lower experimental flow velocities.

The agreement between the theoretical and experimental u values below the disc (Fig.7.5) is relatively good with most data points lying near the bold line. However, above the disc a greater deviation can be seen with many of the points lying below the line. Also for points above the disc nearer the shaft (where u = 1), the theoretical values are greater than the corresponding experimental values. This may again be explained by the reasons outlined above. The standard deviation values of UDIFF from the mean value of UDIFF are presented in Table 7.1.

The theoretical contours of angular velocities at height y_b = 0.8 in glycerol are not presented since the contours are virtually the same as those due to primary flow shown by Figures 6.4 and 6.5. Again, a strong pattern in the scatter between the experimental and theoretical values of the fluid velocities similar in nature to that described above was observed and can be explained by the reasons given above.

The results for Carbopol 910 are shown in Figures 7.6 and 7.7 for

the large gap (y_b = 1.3). Comparison of these with the corresponding geometry for primary flow (Figs. 6.18 and 6.19), it may be observed that for any point near the stirrer the speed is greater for the secondary flow than for the primary flow. This is expected, since Carbopol 910 is a shear-thinning fluid. This means that as the speed of the rotor is increased the rate of shear also increases especially near the stirrer. The fluid becomes thinner and subsequently moves at a higher speed than the rest of the fluid. Since very similar observations were made for the small gap (y_b = 0.8) geometry, the contours are not presented. In fact, differences between the large and small gap geometries for a particular rotor were observed only below the rotor as expected. At a fixed point in the fluid near the stirrer it was found that the velocities were generally greater for Carbopol 910 than for glycerol, again due to the shear-thinning nature of the fluid.

Figures 7.8 and 7.9 show the comparison of the theoretical u values with those obtained experimentally for the two stirrers rotating at y_b = 1.3 in Carbopol 910. Again, a distinct closed loop pattern is obtained for each cycle completed. For the cylindrical stirrer most of the data points are seen to lie beneath the bold line indicating that the experimental values are higher than the corresponding theoretical values. This high deviation from the expected values may be explained by experimental errors in measurement, errors in the smoothing method used for determining experimental u values and also errors incurred in fitting a fluid model to Carbopol 910. The slight 'wobble' of the rotor and 'jerkiness' of the tracer particles also contribute to the errors.

For points below the disc stirrer (Fig. 7.9), similar results to that described above were obtained. This is as expected since this part of the arrangement resembles that of the cylindrical rotor.

Above the disc, there is better agreement the theoretical and experimental values with many of the data points lying relatively near the bold line of expected values. This does not agree with the results of glycerol (Fig. 7.5) where the results show better agreement for points in the fluid below the disc. Similar results were obtained for the two stirrers rotating in Carbopol 910 at y_b = 0.8.

Comparison of the secondary flow standard deviation values of UDIFF (Table 7.1) show that these are generally higher than the corresponding primary flow standard deviations (Table 6.1).

7.3 Shear Rate Distributions.

Figures 7.10 and 7.11 show contours of constant shear rates obtained by numerical simulation for the cylindrical and disc stirrers rotating at a height y_b = 1.3 in glycerol. These contours are observed to be virtually the same as those for primary flow shown in Figures 6.30 and 6.31. Representative experimental g values are shown next to the black dots and a direct comparison between the experimental and numerical shear rates for the two stirrers are given in Figures 7.12 and 7.13.

The data points are seen to be greatly scattered with more points lying below the bold line than above. This shows that generally the experimental shear rates are greater than their corresponding theoretical values. This high scatter can again be explained by the great errors incurred in numerically differentiating the u values for the determination of g values. Also, the differences in the u values themselves contribute a great deal to the large scatter. The standard deviation values from the mean shear rate differences are given in Table 7.1. These are seen to be higher than the corresponding primary flow standard deviations (Table 7.1).

The theoretical contours of the shear rates for the stirrers rotating at y_b = 0.8 in glycerol are not presented since the contours are virtually the same as those for primary flows shown in Figures 6.22 and 6.23. Again a great deviation of the experimental shear rates from the theoretical values was observed which was very similar in nature to that described above and may be explained by the reasons outlined above.

The theoretical shear rate contours for Carbopol 910 are shown in Figures 7.14 and 7.15 for the large gap. When these results are compared with the results of the corresponding geometry for primary flow, it can be seen that for any point near the stirrer the shear rate is greater for secondary flow than for primary flow. These results agree with those for angular velocities (u) discussed in section 7.2 and can be explained by the fact that Carbopol 910 is shear-thinning with increasing speed and hence in shear rate. Comparison with experimental shear rates showed a wide scatter similar to that for glycerol (Figs.7.11 and 7.12) and are, therefore, not presented. It should be noted here that the theoretical and experimental shear rates only agreed generally within an order of magnitude.

7.4 Streamlines

Representative theoretical and experimental stream function values (denoted by alfa streamlines) are presented in Figures 7.16 - 7.23. From Figures 7.16 and 7.17, which give the results for a cylindrical stirrer rotating in glycerol at y_b = 1.3 and Re = 6.1, we can that the general shape of the streamlines is very similar. Incidentally, only three experimental streamlines are shown since measurements for the paths of only three tracer particles were taken. The streamlines are seen to be travelling in a clockwise direction.

Examination of the actual α values shows that the order of magnitude at corresponding points in the fluid is the same for both the experimental and theoretical results. The values of the inner streamlines are seen to be higher in magnitude indicating greater circulation than in the outer regions. However, there is no or very little flow near the stationary walls or in the upper part of the container. The amount of circulation may be given by the discharge efficiency or pumping number to be discussed in Chapter 8. Very similar results were obtained for the cylindrical stirrer rotating in glycerol at $y_b = 0.8$ and are, therefore, not presented.

Figure 7.18 shows the theoretical streamlines for the cylindrical stirrer rotating in Carbopol 910 at $y_b = 1.3$ and $Re = 2.1$. The general trend is seen to be the same as that for glycerol, although the streamlines in the case of Carbopol 910 are confined to the vicinity of the rotor. This is expected due to its shear-thinning nature. Comparison with the experimental results (Fig. 7.19) shows that although the magnitude of the α value and the general shape of the streamline is the same, the streamline is reversed, i.e. it is travelling in an anticlockwise direction. This behaviour is characteristic of elastic fluids [29,101]. The theoretical and experimental results of the streamlines only compare well by order of magnitude and not at all well in direction, because the elastic behaviour was not accounted for when developing the fluid model since Carbopol 910 was recommended as a simple 'inelastic' shear-thinning fluid [3, 11, 60].

At low speeds of the rotor (primary flow) the elastic behaviour was not noticeable. The presence of this property was not expected at the start of the research and, therefore, no initial tests which might have indicated the elastic behaviour of Carbopol 910, were carried out. It was only when secondary flows occurred and streamlines were

determined that we discovered the elastic property of the fluid. In fact, the direction of the streamlines was not immediately discernible during normal viewing of the particle motion due to the flows being fast and, therefore, it seemed reasonable at the time to fit a shear-thinning fluid model to Carbopol 910 which lacked elasticity. Furthermore, extra complication would have arisen with the inclusion of elasticity and would have been difficult to carry out in the time available.

Once the above flow reversal behaviour had been noticed during analysis of the results, it was necessary to carry out some simple tests to look for elasticity. Effects indicating elasticity were not immediately noticeable under normal conditions. However, when the bottle containing the Carbopol 910 was shaken small recoil was observed and when Carbopol 910 was touched with the finger negligible liquid stringiness could also be seen. Observation of a thin rotating rod placed in the fluid showed very slight Weissenberg effect. All these observations indicate the presence of a small amount of elasticity. Finally, Carbopol 910 was tested out for elastic effects using a Rank Shearometer by P.R. Williams, Chemical Engineering Department, University College, Swansea and the results are presented here.

The elasticity is represented by the oscillatory dynamic rigidity G' and the greater the value of G' the the greater is the elasticity of the fluid. An average value of G' for Carbopol 910 was found to be 222 Pas at 300 Hz. This result was compared with that of silicon fluid (of viscosity equivalent to 1.06 Pas), which is generally regarded as weakly elastic and for which G' was found to be 4400 Pas. This shows that Carbopol 910 is roughly ten times less elastic than the weakly elastic silicon fluid. In fact, this agrees with the findings of Nienow et al [59] for Carbopol 940 and of Chhabra and Uhlerr [15]

for Carbopol 961. In light of the above results which show very small elasticity of Carbopol 910, it is no wonder that Carbopol 910 is generally considered as relatively inelastic. Therefore, the fact that this property was not incorporated in the mathematical model for Carbopol 910 in our work can be justified. Obviously, for any future work this property will need to be included in the mathematical expressions for better comparison of results with experimental results.

In Figures 7.20 and 7.21, the results for disc stirrer ritating in glycerol at y_b = 0.8 are given. The general trend is seen to be the same in both figures with positive α values occurring above the disc and negative values occurring below as expected, since the direction of the fluid is reversed above the disc with respect to that below. However, the order of magnitude of the α values is seen to be the same. These streamline results are in agreement with those of Griffiths et al [29] for a Newtonian fluid and also comparable to those of a rotating cylindrical stirrer discussed above.

The theoretical and experimental α values for the disc stirrer rotating in Carbopol 910 at y_b = 0.8 and Re = 6.1 are presented in Figures 7.22 and 7.23. These are very much in agreement with the results given in 7.18 and 7.19 respectively, for the rotating cylinder with the streamlines being reversed at corresponding points in the fluid. The experimental results can again be explained by the presence of slight elasticity and inherent experimental errors and the theoretical results by the inaccuracy of the fluid model.

The results for the disc stirrer rotating in either glycerol or Carbopol 910 at y_b = 1.3 were found to be very similar to their corresponding results for y_b = 0.8 given above and are, therefore, not shown.

7.5 Vorticity Results

Typical vorticity contours obtained theoretically for the cylindrical stirrer rotating in glycerol or Carbopol 910 at y_b = 1.3 are given in Figures 7.24 and 7.25. For both fluids, the negative vorticity contours occur near the walls of the rotor and the container whereas the positive values occur in the bulk of the fluid. Due to the shear-thinning nature of Carbopol 910 model, the vorticity contours are confined to the vicinity of the stirrer as shown by Figure 7.25. This is expected since the speed of the fluid is higher here and the viscosity is lower. The values given by the black dots are representative vorticity values. It can be seen that for glycerol these experimental values are of the same order of magnitude and sign as the theoretical ones, but for Carbopol 910 the values are of opposite sign, although still of the same order of magnitude.

In Figures 7.26 and 7.27, a direct comparison of the theoretical and experimental vorticity values for the large gap (y_b = 1.3) is shown. Again there is a lot of scatter with the actual theoretical values being generally higher than the corresponding experimental values, with a better agreement at low vorticity values for glycerol. There are a few points where negative theoretical values occur which do not agree with the positive experimental values. These points occur near contours 1 and 2 (Fig. 7.24) near the rotor where fast flow is occurring and there is a quick change from positive to negative values over small distances. Errors in sign are, therefore, likely to occur at these points.

The agreement is not good for Carbopol 910 as can be seen from Figure 7.27. Negative vorticity values occur which do not agree with the corresponding theoretical positive at the same points in the

fluid, although the order of magnitude is virtually the same for most data points. The difference in signs indicates that the fluid model is not exactly correct for the fluid and the sign change occurs due to the presence of elasticity. The fact that Carbopol 910 was found to be slightly elastic may also contribute to the large differences between the experimental and theoreical values. Furthermore, computer rounding of the experimental values also contribute to the differences.

Since the vorticity values are very small, even slight differences between the experimental and theoretical values appear as very large percentage differences which have no real meaning and, therefore, percentage differences have not been given. However, standard deviation of these diffences from the mean difference in vorticity values have been listed in Table 7.1.

Similar results for the cylindrical stirrer rotating at $y_b = 0.8$ in the two fluids were obtained and are not presented although the standard deviation and mean values are given in Table 7.1.

Representative theoretical vorticity contours for the disc stirrer rotating at $y_b = 0.8$ in glycerol or Carbopol 910 are shown in Figures 7.28 and 7.29. Positive values are seen to occur in the bulk of the fluid below the disc and on the boundaries above the while negative values occur in the bulk of the fluid above the disc and near the boundaries below the disc. Typical experimental values are shown next to the black dots on the diagrams. Again for Carbopol 910 the experimental and theoretical values are of opposite signs at all observed points in the fluid which can be seen more clearly in Figure 7.31.

A direct comparison of experimental and theoretical values for glycerol and Carbopol 910 are given in Figures 7.30 and 7.31 respectively.

Again, it is observed that the results are comparable with those obtained for the cylindrical stirrer and again we may attribute the large scatter to inherent experimental error together with errors incurred by the method used for determining experimental vorticities.

7.5.1 Incompressibility Results

As mentioned in Chapter 3, incompressibility values were determined as a check on the method for treating the original experimental data and then calculating vorticities. Ideally, the incompressibility values should have been zero indicating no errors in our process for the determination of vorticities, since glycerol and Carbopol 910 were assumed to be incompressible. However, in practice this is not the case as shown in Table 7.1. The errors range from about -24% to 10% indicating a maximum error of ≈ 25% in the method for determining experimental values.

7.6 Conclusion

The experimental and numerical angular velocities for the cylindrical and disc stirrers rotating in glycerol is found to agree relatively well at points in the fluid away from the rotor. However, as expected, the agreement is not so good nearer the rotor the reasons for which are given in section 7.2. For the two sirrers rotating in Carbopol 910, the agreement is again better at lower speeds which occur away from the rotor than at higher speeds.

The results for shear rates for all the geometries and both glycerol and Carbopol 910 are greatly scattered as expected, since the differences in the u values themselves and the numerical differentiation

of the u values contribute to the errors incurred in determining the shear rates.

The agreement between the experimental and theoretical α streamlines for glycerol and Carbopol 910 are relatively good for both stirrers and gap size with the direction of the streamlines being the same. Although, the order of magnitude of the experimental and theoretical α values are found to be the same for Carbopol 910, the direction of the streamlines is reversed. This gives some indication of the presence of elasticity in the fluid. Various tests carried out on Carbopol 910 after determination of these α values confirmed the elastic nature of the fluid.

The agreement between the experimental and numerical values of vorticity for glycerol are as good as one would expect, since errors are incurred by the velocities in the x (V_x) and y (V_y) directions and also by the method used to determine vorticity values. As for Carbopol 910, the order of magnitude is the same, but the signs of the experimental and theoretical vorticities are different for the same points in the fluid again due to the elastic nature of Carbopol 910.

It should be noted here that elasticity in Carbopol 910 was not expected and, therefore, no provision in the model was made for this. If this property had been accounted for as well as the shear-thinning nature of Carbopol 910, we feel confident that the agreement between the experimental and theoretical values of the various parameters would have been better.

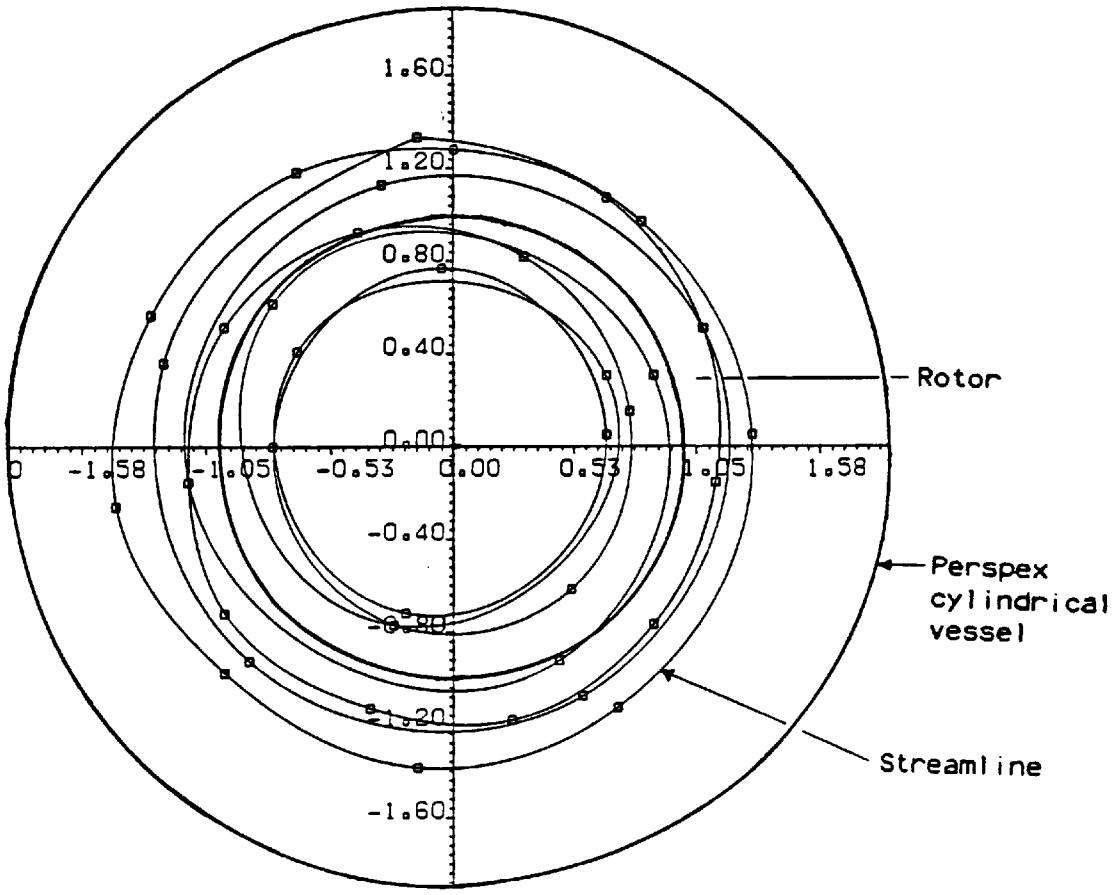

Figure 7.1 A typical secondary flow pattern as seen from the bottom view of the apparatus.

Figure 7.2

U (VELOCITY) CONTOURS FOR NEWTONIAN FLUID (GAP = 1.3)

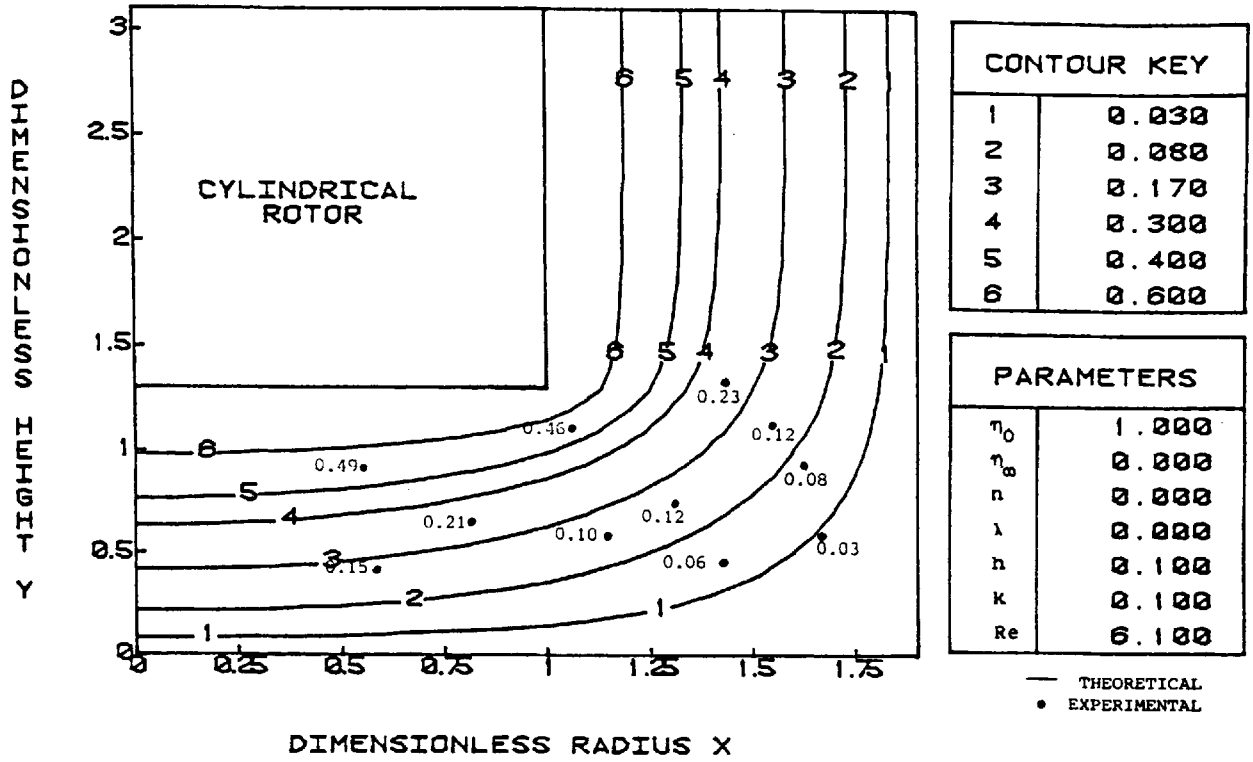

Figure 7.3

U (VELOCITY) CONTOURS FOR NEWTONIAN FLUID (GAP = 1.3)

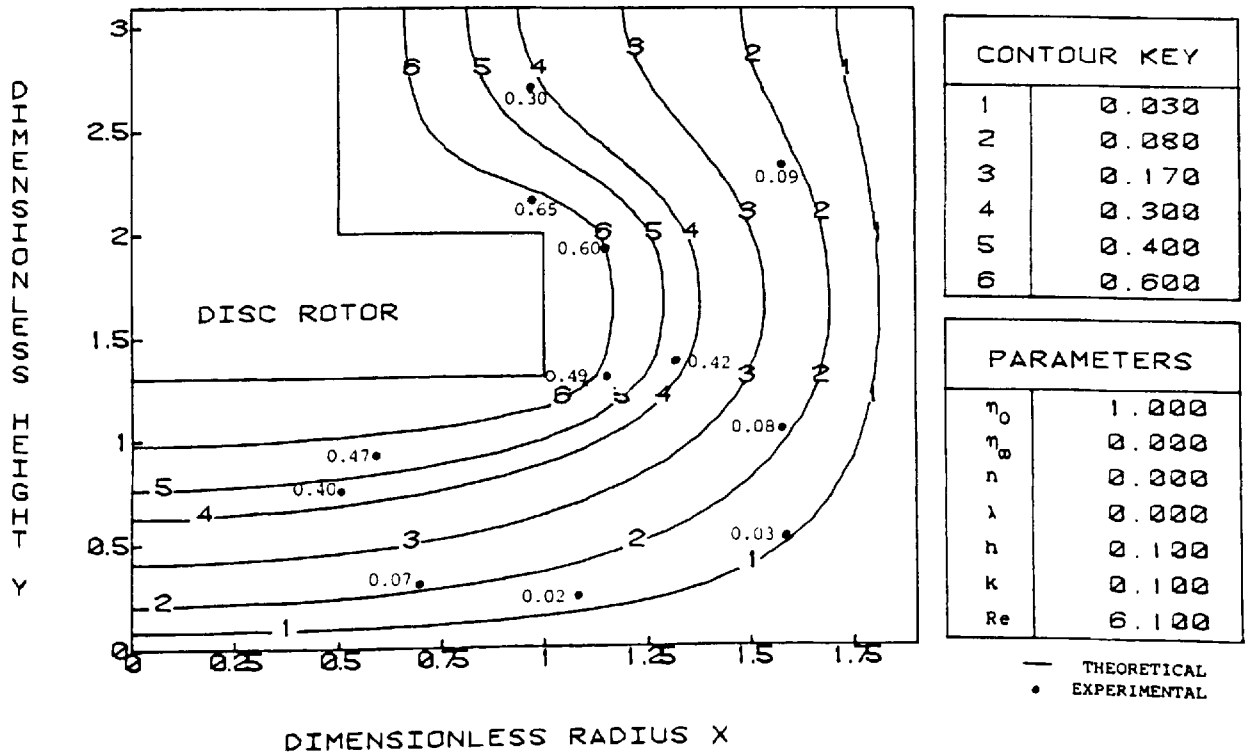

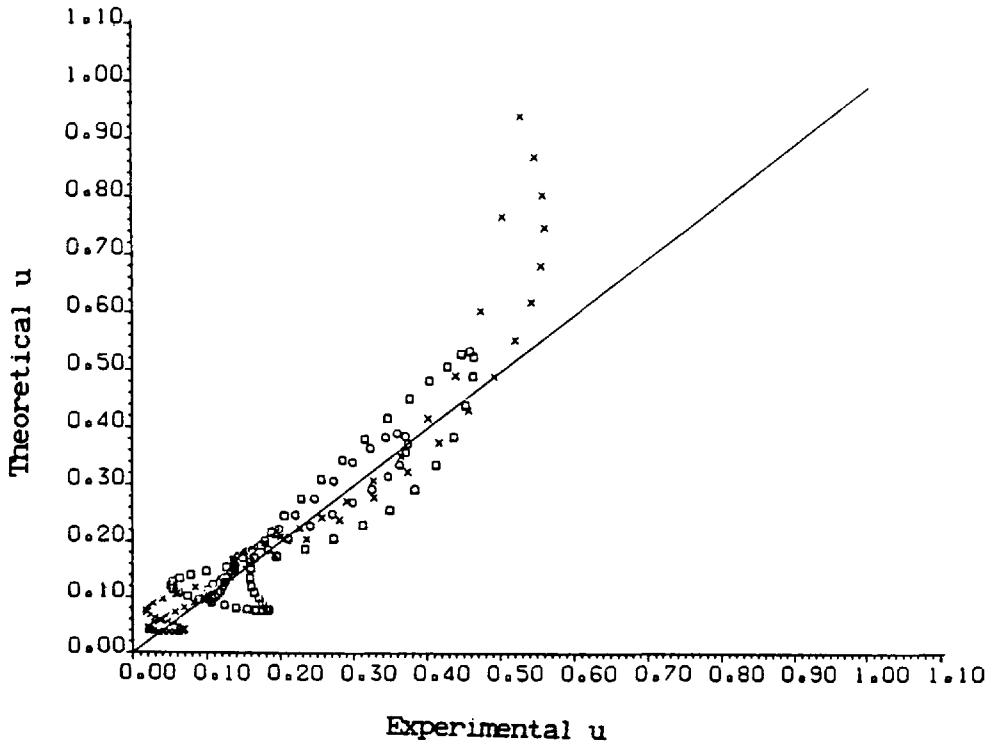

Figure 7.4 A comparison of theoretical and experimental u values for the cylindrical rotor in glycerol, gap = 1.3, Re = 6.1.

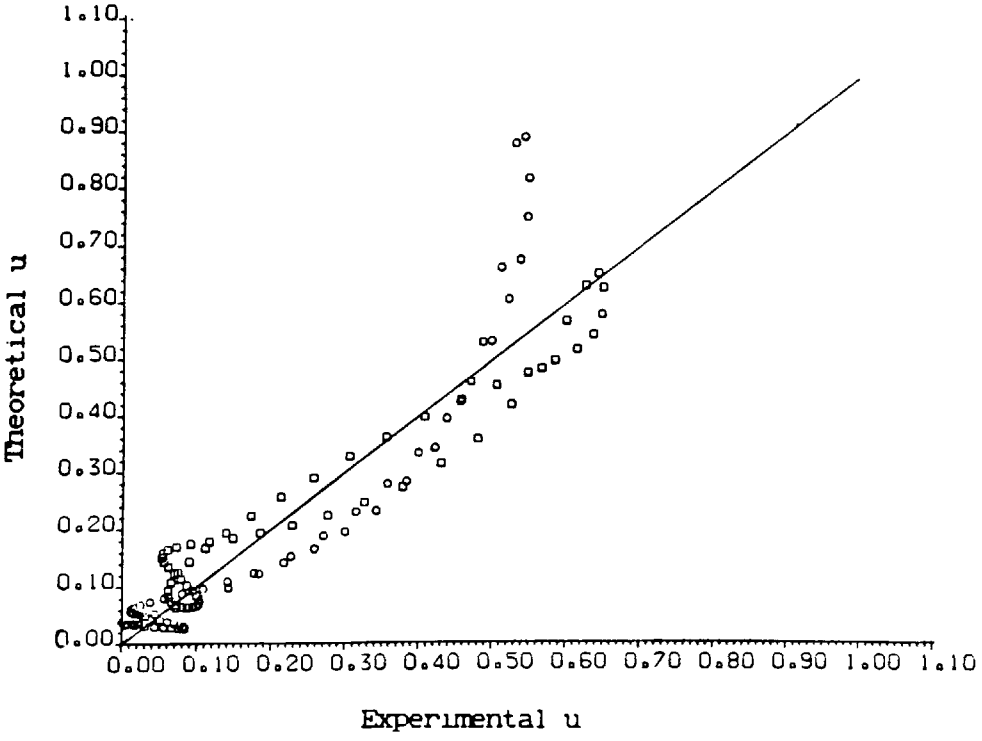

Figure 7.5 A comparison of theoretical and experimental u values for the disc rotor in glycerol, gap = 1.3, Re = 6.1.

	Mean Value of udiff	SD of udiff	Mean Value of gdiff	SD of gdiff	Mean Value of vdiff	SD of vdiff	%I
Cylindrical Stirrer							
Glycerol							
-Small Gap (0.8)	-2.9	42.6	-59.8	131.5	8.3	114.4	4.9
-Large Gap (1.3)	1.4	38.3	-68.2	73.6	39.2	101.6	-4.3
Carbopol 910							
-Small Gap (0.8)	-62.3	55.0	-79.5	119.0	242	122.3	-24.2
-Large Gap (1.3)	-20.1	71.7	-90.1	168.6	1874	2047	-5.4
Disc Stirrer							
Glycerol							
-Small Gap (0.8)	-16.4	43.7	-53.5	115.2	-13	171.8	9.9
-Large Gap (1.3)	-3.6	58.5	-128.5	176.6	-9	1690	-7.4
Carbopol 910							
-Small Gap (0.8)	-176.5	272.6	-36.2	130.8	∞	∞	-14.3
-Large Gap (1.3)	-6.8	56.4	-99.4	115.7	493.3	483	-1.5

Table:7.1 The Mean, Standard Deviation (SD) and Incompressibility Values (I) for Secondary Flow Parameters.

Figure 7.6

U (VELOCITY) CONTOURS FOR CROSS FLUID (GAP = 1.3)

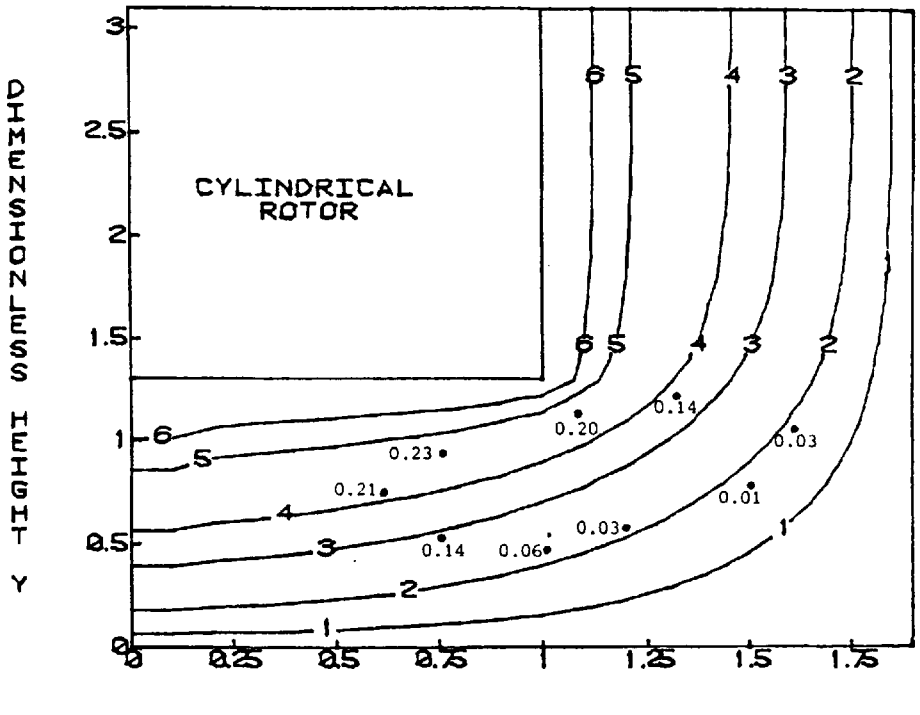

CONTOUR KEY	
1	0.010
2	0.030
3	0.080
4	0.150
5	0.400
6	0.600

PARAMETERS	
η_0	60.150
η_∞	0.340
n	0.350
λ	16.570
h	0.100
k	0.100
Re	1.200

— THEORETICAL
• EXPERIMENTAL

Figure 7.7

U (VELOCITY) CONTOURS FOR CROSS FLUID (GAP = 1.3)

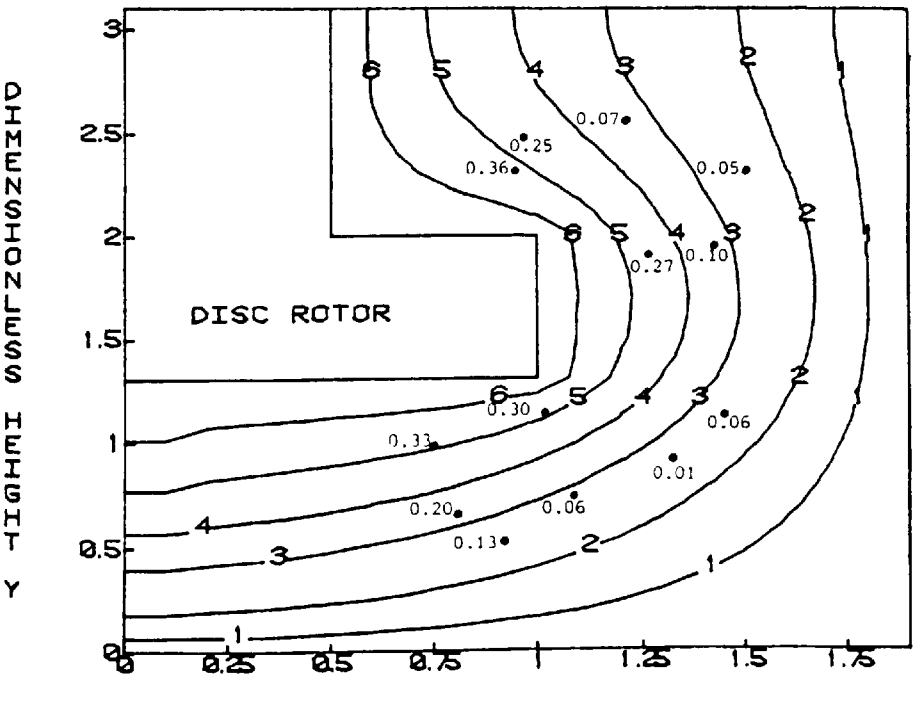

CONTOUR KEY	
1	0.010
2	0.030
3	0.080
4	0.150
5	0.300
6	0.600

PARAMETERS	
η_0	60.150
η_∞	0.340
n	0.350
λ	16.570
h	0.100
k	0.100
Re	1.200

— THEORETICAL
• EXPERIMENTAL

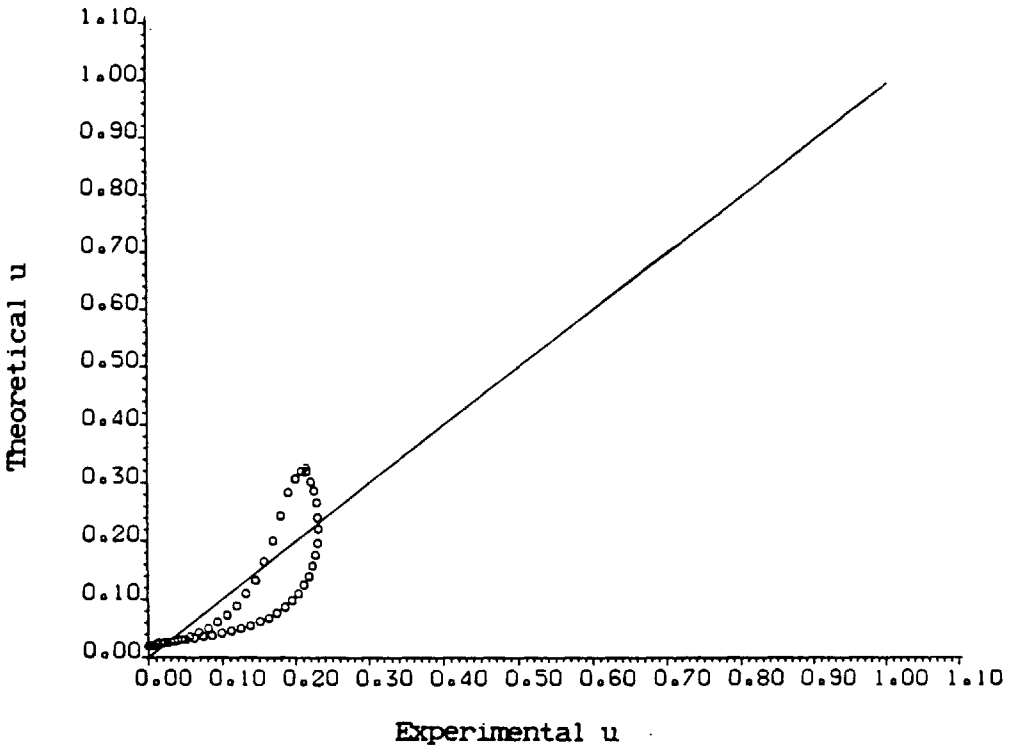

Figure 7.8 A comparison of theoretical and experimental u values for the cylindrical rotor in Carbopol 910, gap = 1.3, Re = 1.2.

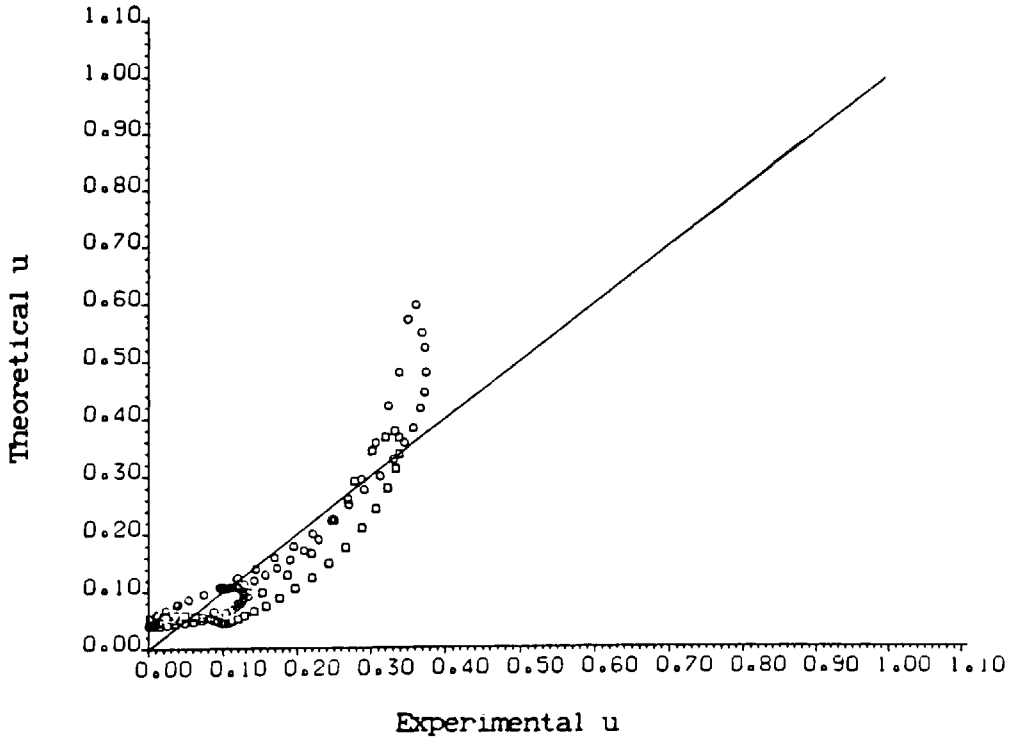

Figure 7.9 A comparison of theoretical and experimental u values for the disc rotor in glycerol, gap = 1.3, Re = 1.2.

Figure 7.10

G (SHEAR-RATE) CONTOURS FOR NEWTONIAN FLUID (GAP = 1.3)

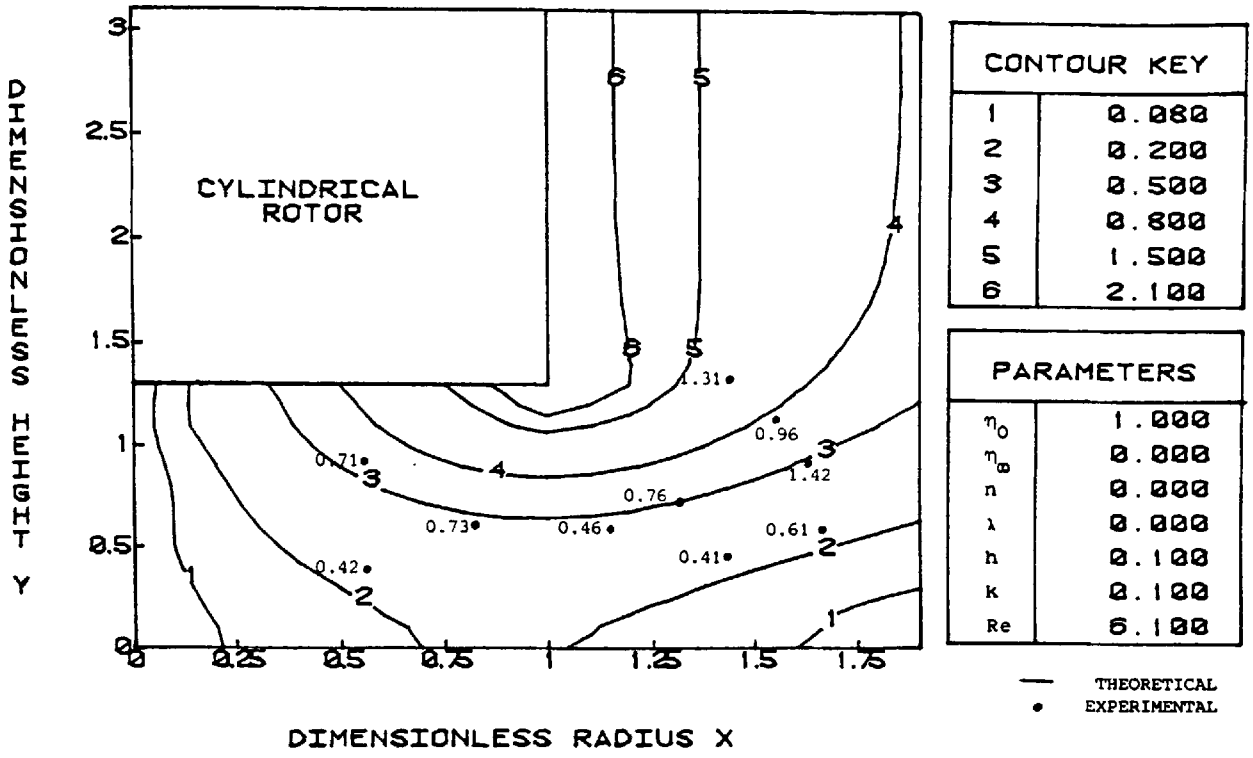

Figure 7.11

G (SHEAR-RATE) CONTOURS FOR NEWTONIAN FLUID (GAP = 1.3)

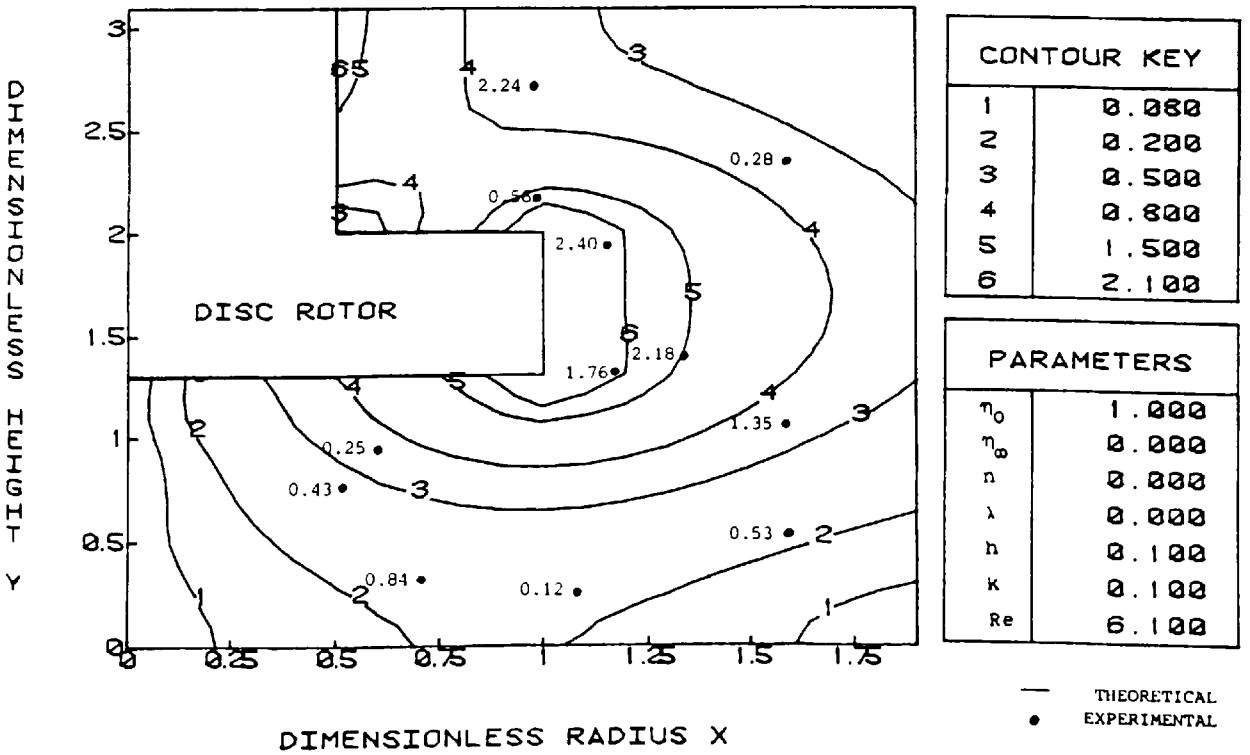

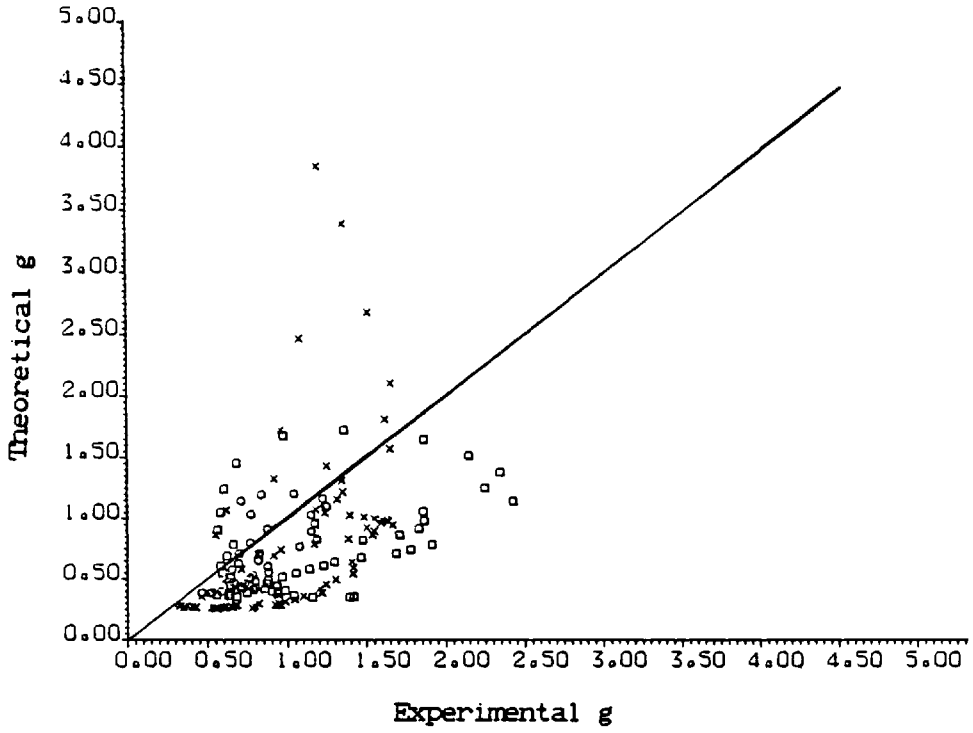

Figure 7.12 A comparison of theoretical and experimental g values for the cylindrical rotor in glycerol, gap = 1.3, Re = 6.1.

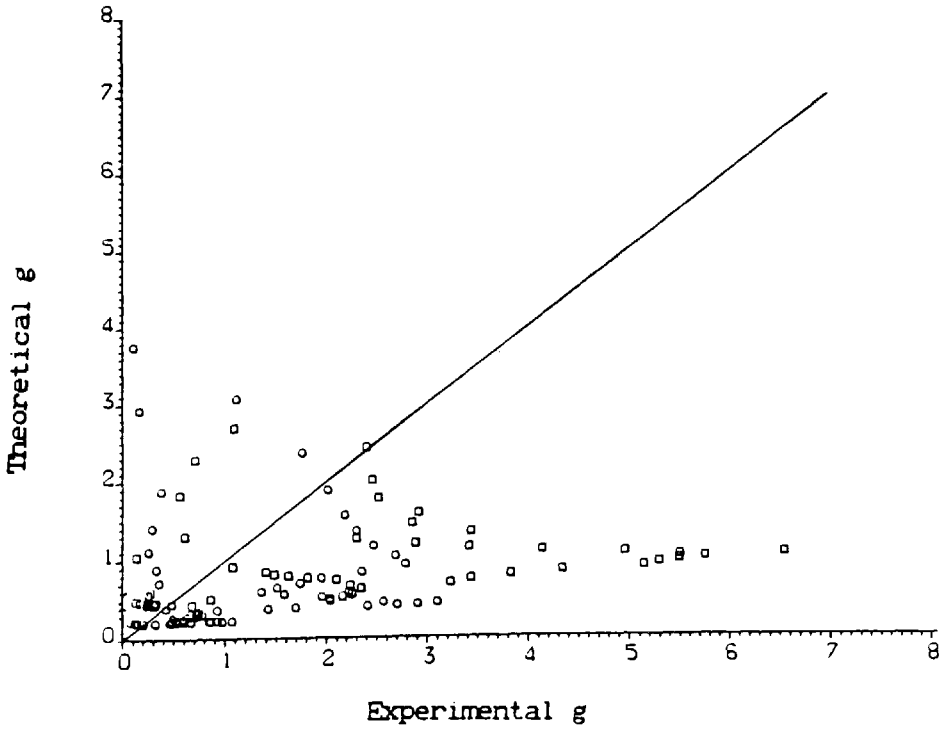

Figure 7.13 A comparison of theoretical and experimental g values for the disc rotor in glycerol, gap = 1.3, Re = 6.1.

Figure 7.14

G (SHEAR-RATE) CONTOURS FOR CROSS FLUID (GAP = 1.3)

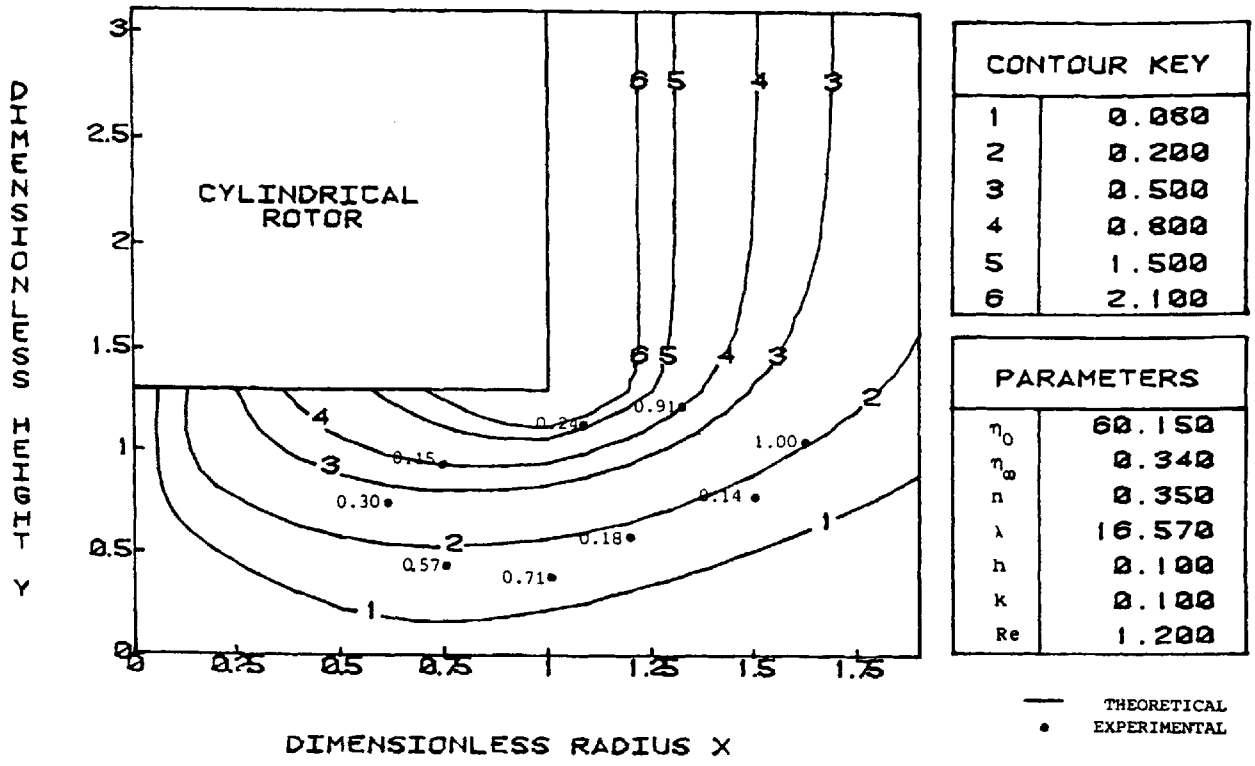

Figure 7.15

G (SHEAR-RATE) CONTOURS FOR CROSS FLUID (GAP = 1.3)

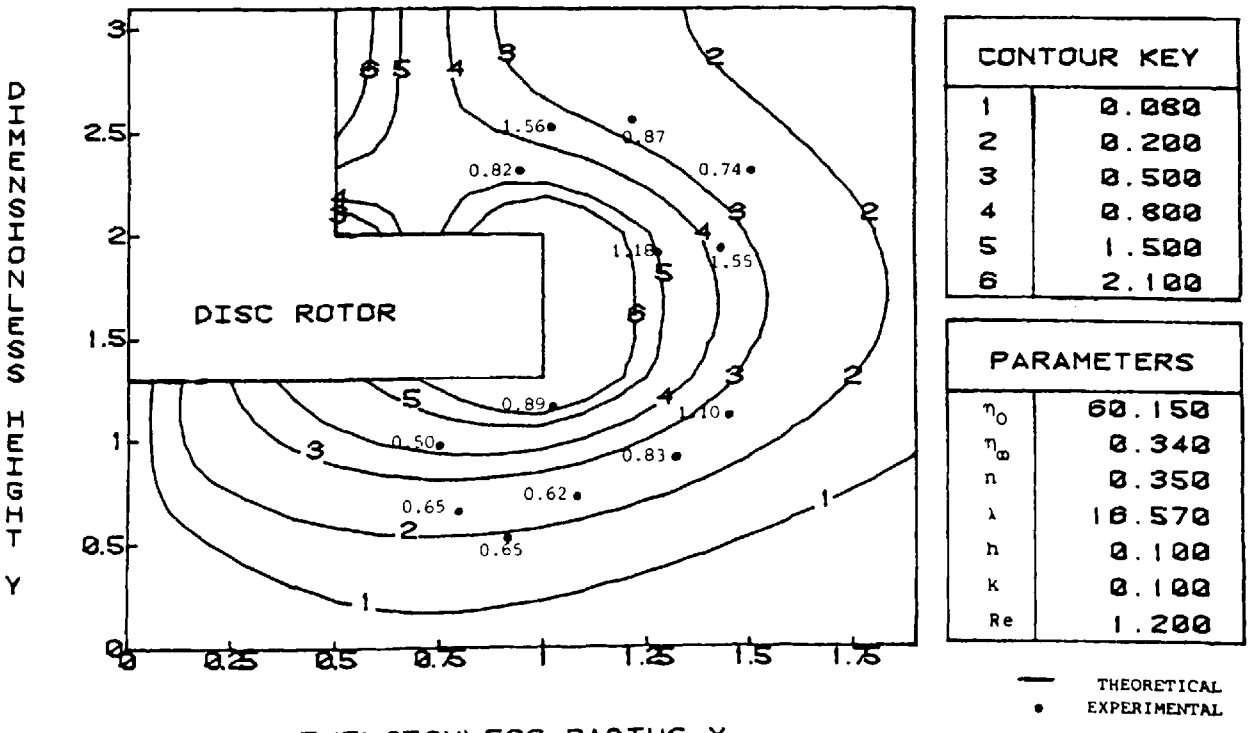

Figure 7.16

ALFA STREAMLINES FOR NEWTONIAN FLUID (GAP = 1.3)

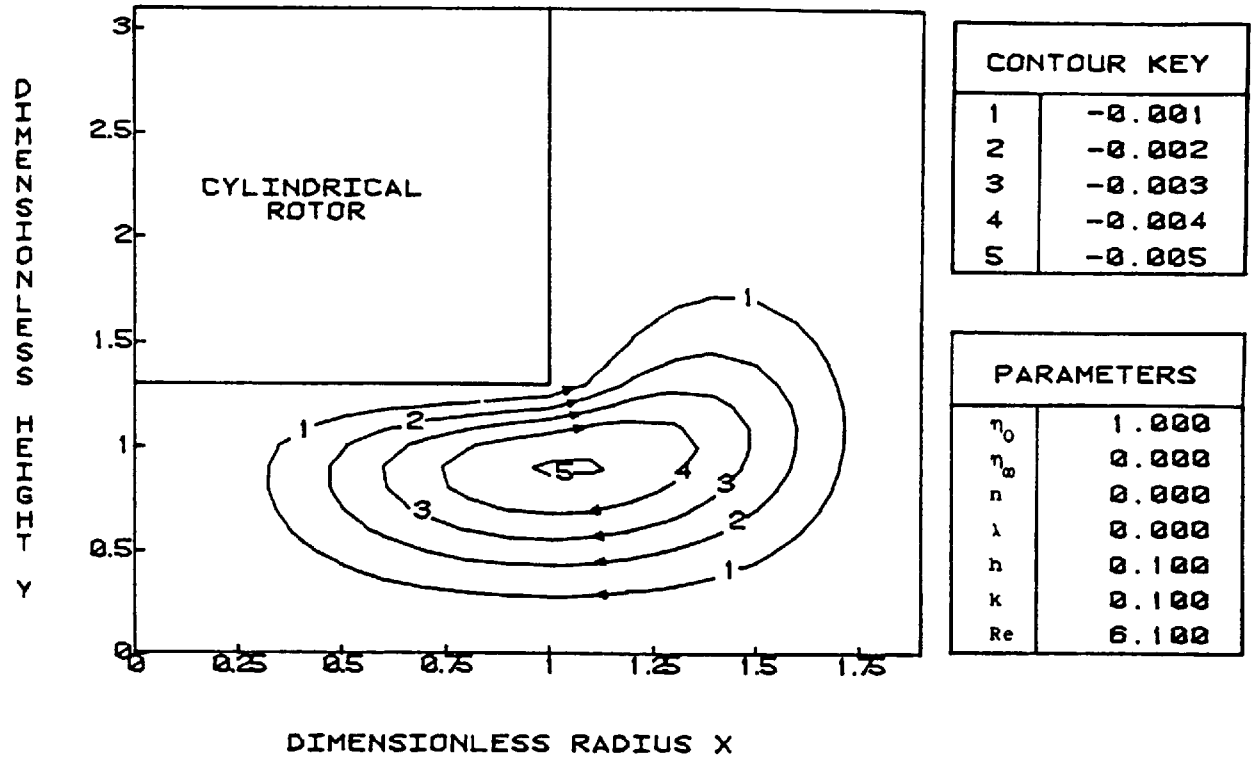

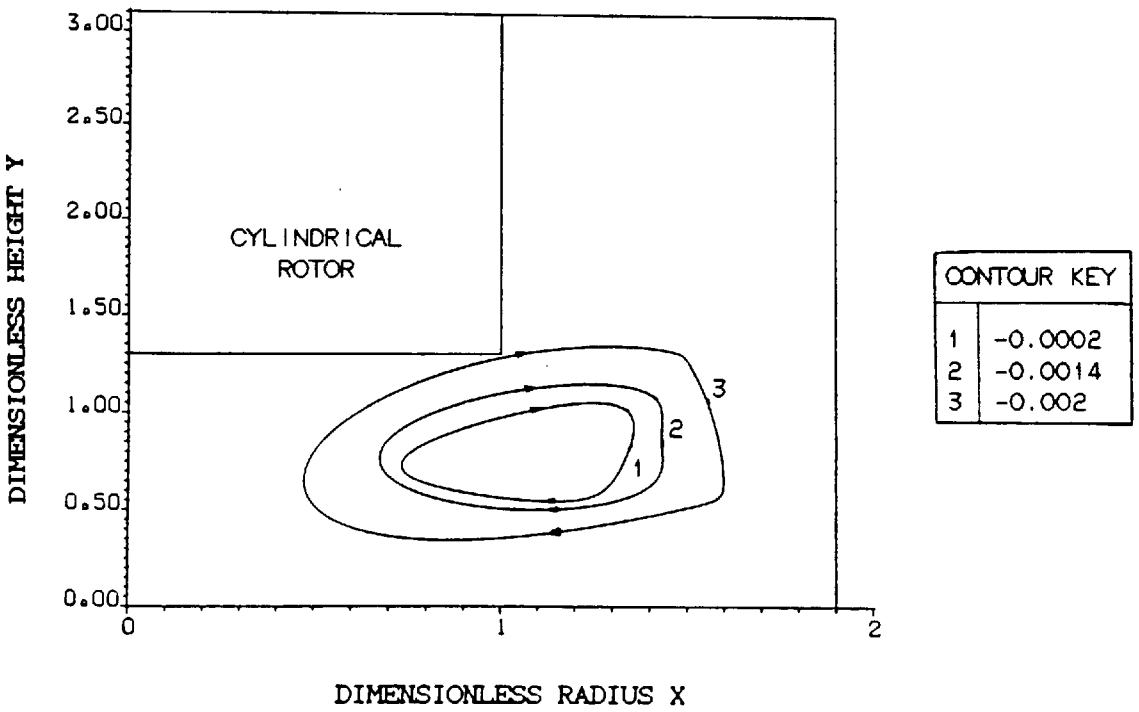

Figure 7.17 Experimental streamlines for the cylindrical stirrer rotating at gap = 1.3 and Re = 6.1 in glycerol.

Figure 7.18

ALFA STREAMLINES FOR CROSS FLUID (GAP = 1.3)

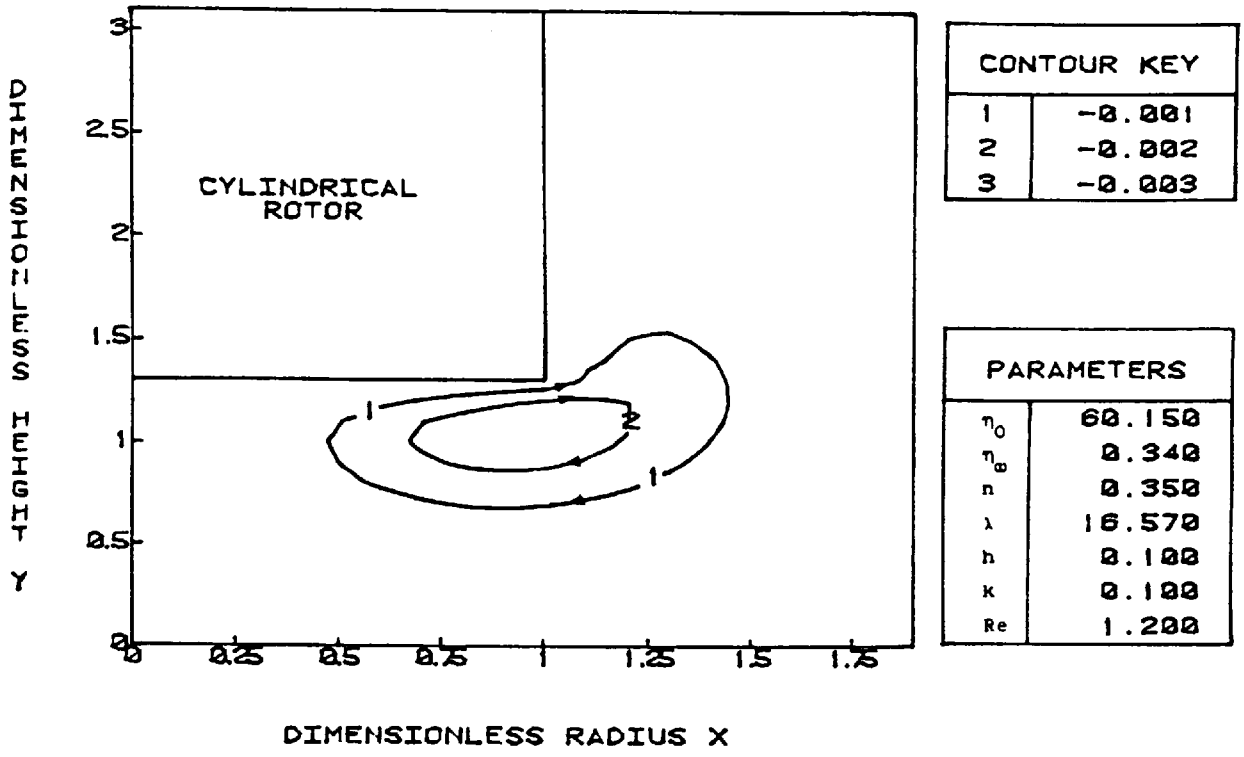

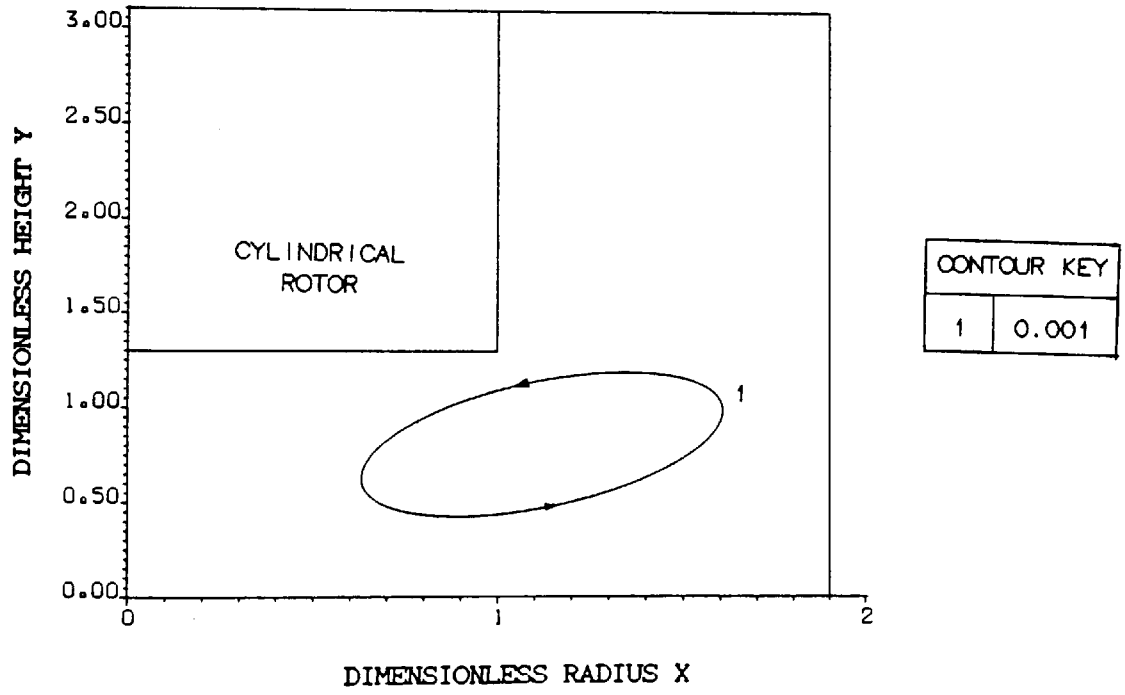

Figure 7.19 Experimental streamlines for the cylindrical stirrer rotating at gap = 1.3 and Re = 1.2 in Carbopool 910.

Figure 7.20

ALFA STREAMLINES FOR NEWTONIAN FLUID (GAP = 0.8)

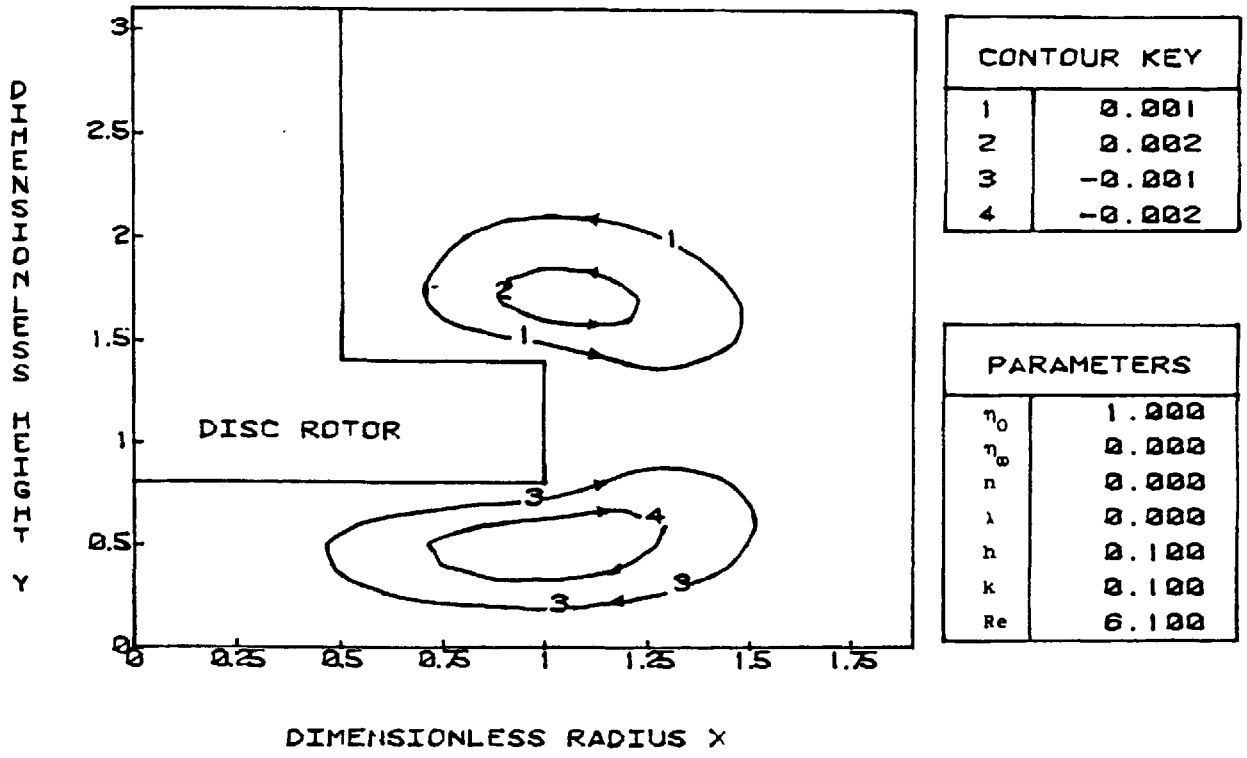

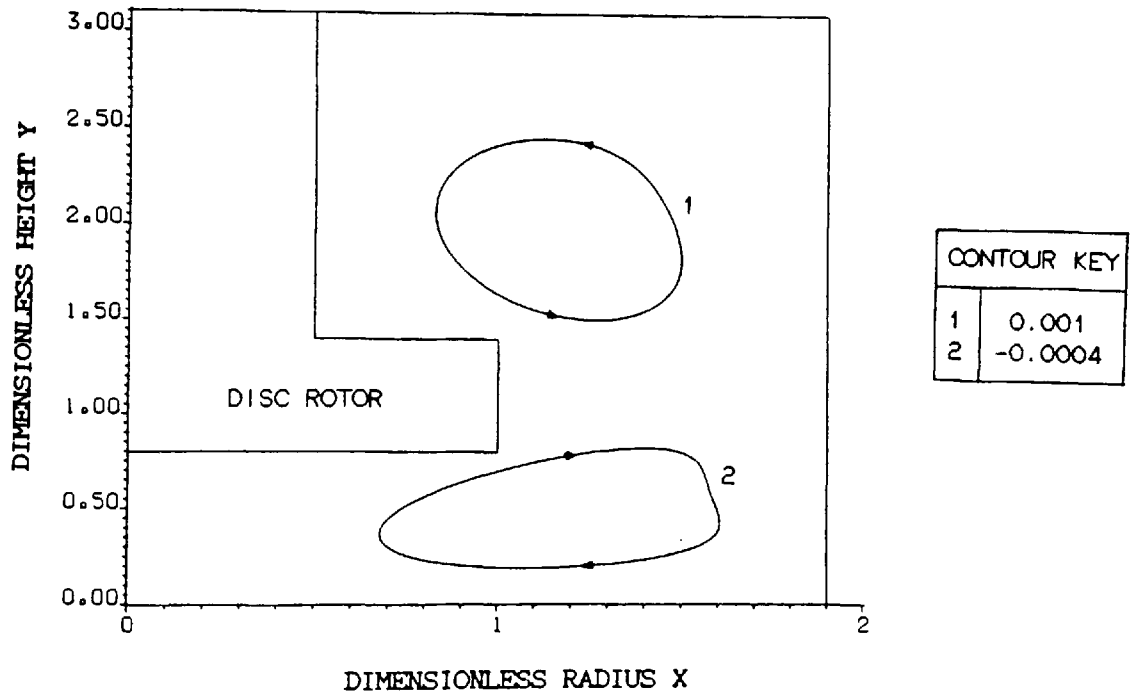

Figure 7.21 Experimental streamlines for the disc stirrer rotating at gap = 0.8 and Re = 6.1 in glycerol.

Figure 7.22

ALFA STREAMLINES FOR CROSS FLUID (GAP = 0.8)

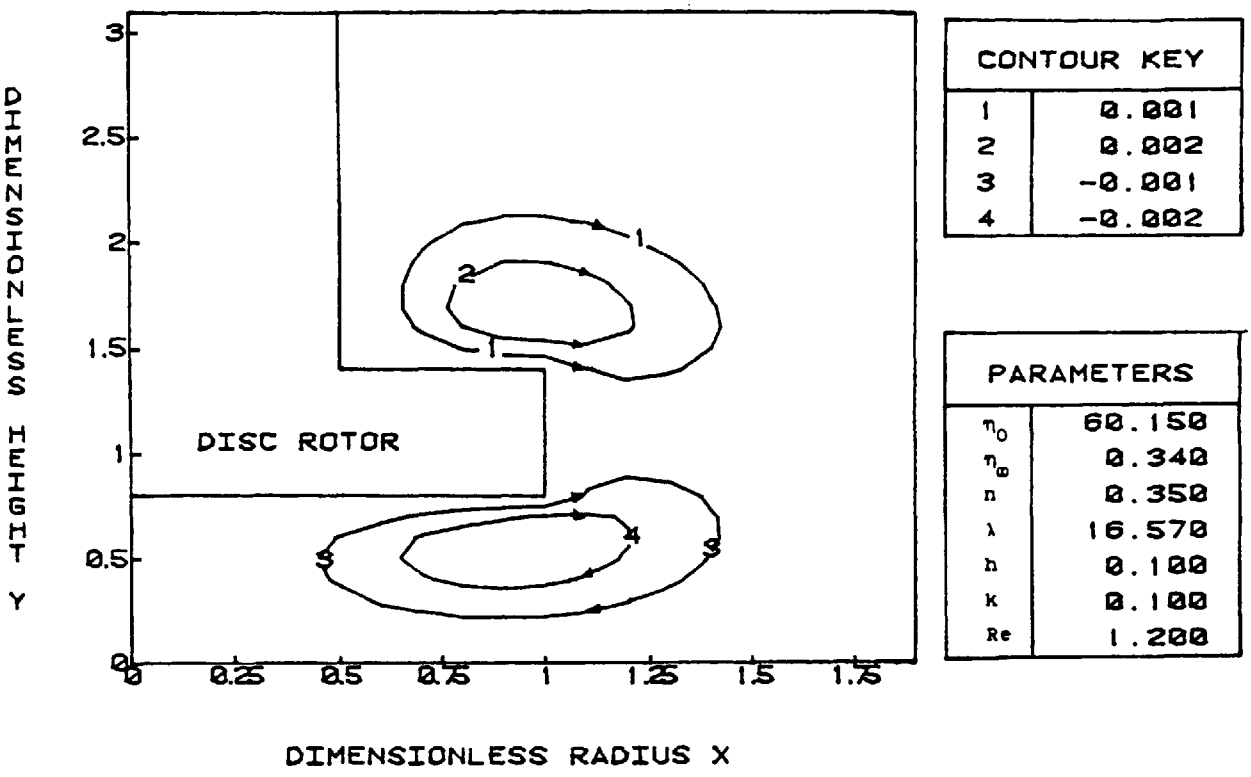

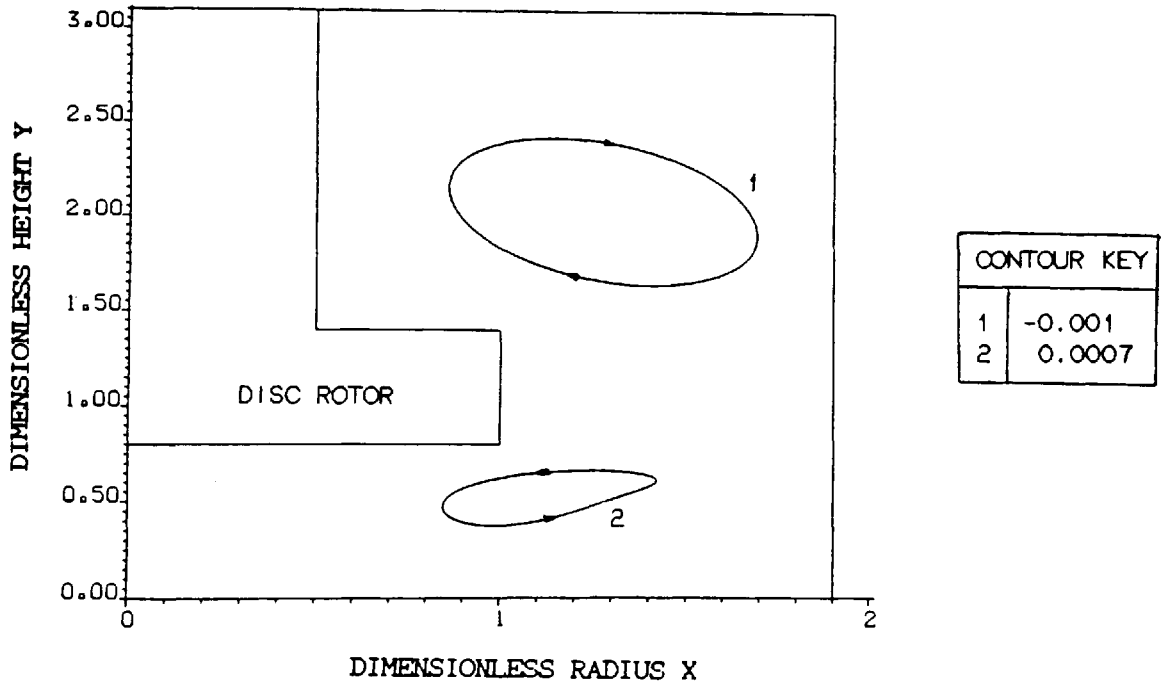

Figure 7.23 Experimental streamlines for the disc stirrer rotating at gap = 0.8 and Re = 1.2 in Carbopol 910.

Figure 7.24

XI (VORTICITY) CONTOURS FOR NEWTONIAN FLUID (GAP = 1.3)

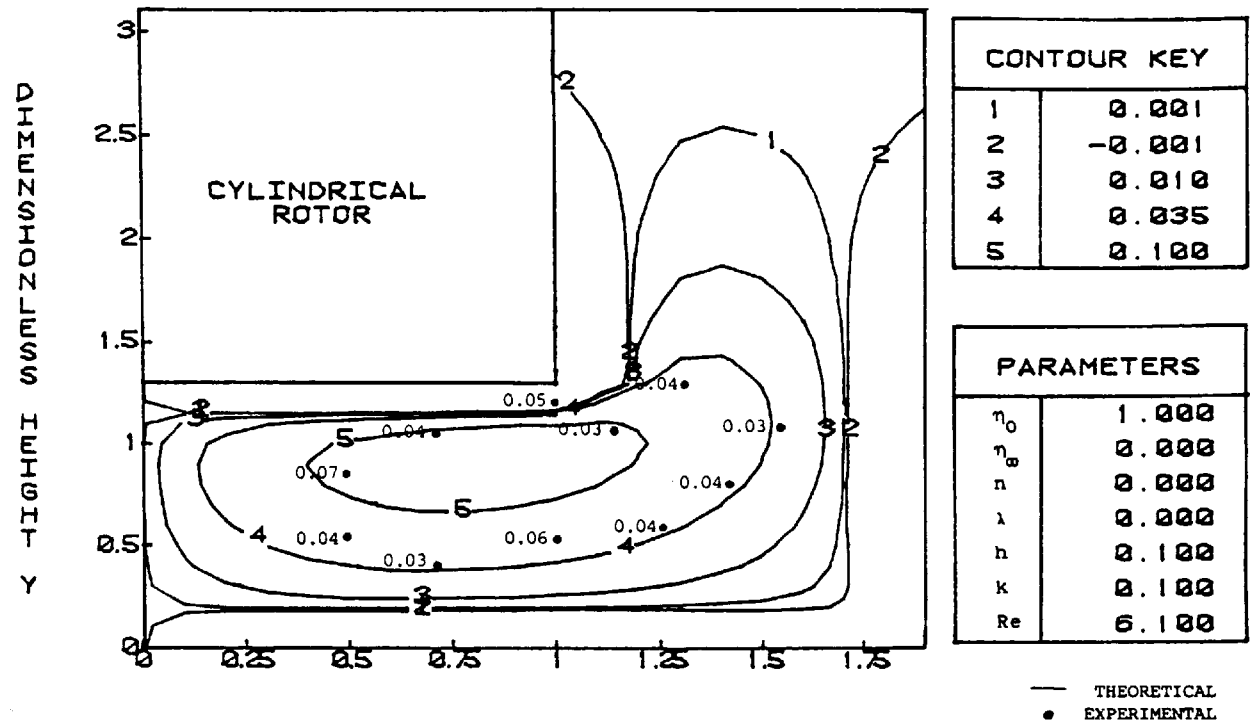

CONTOUR KEY	
1	0.001
2	-0.001
3	0.010
4	0.035
5	0.100

PARAMETERS	
η_0	1.000
η_∞	0.000
n	0.000
λ	0.000
h	0.100
k	0.100
Re	6.100

Figure 7.25

XI (VORTICITY) CONTOURS FOR CROSS FLUID (GAP = 1.3)

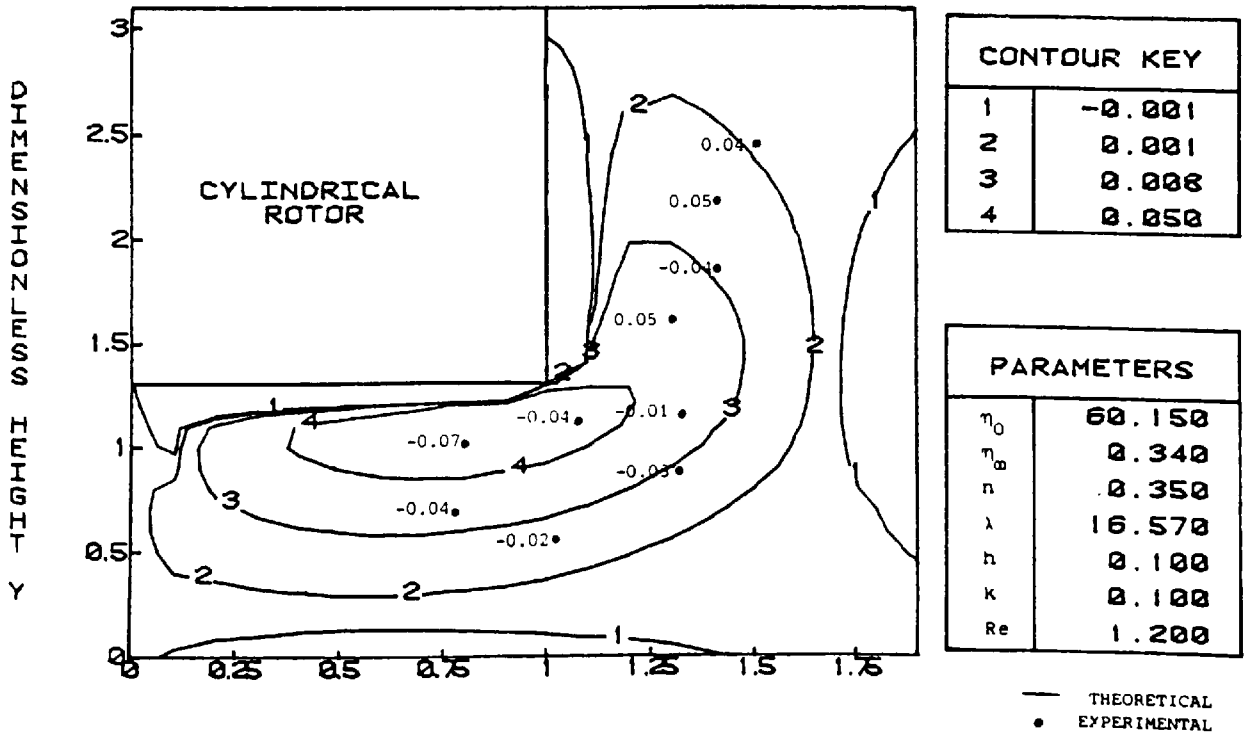

CONTOUR KEY	
1	-0.001
2	0.001
3	0.008
4	0.050

PARAMETERS	
η_0	60.150
η_∞	0.340
n	0.350
λ	16.570
h	0.100
k	0.100
Re	1.200

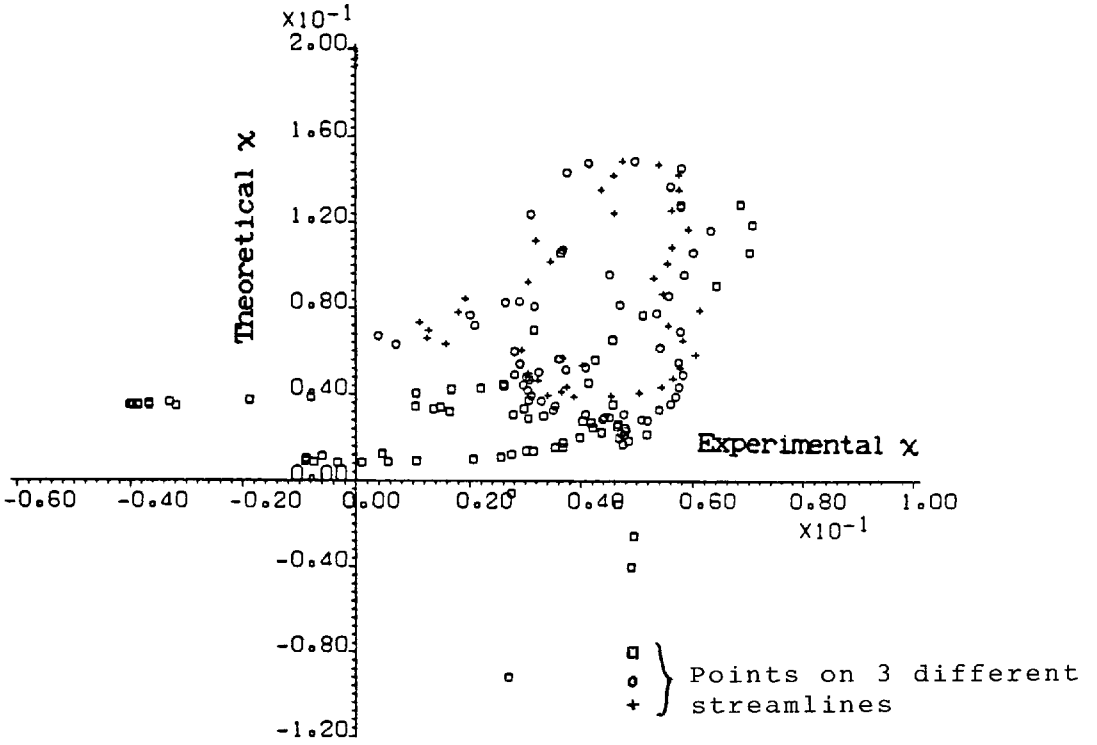

Figure 7.26 A comparison of theoretical and experimental vorticity values for the cylindrical rotor in glycerol, gap = 1.3, Re = 6.1.

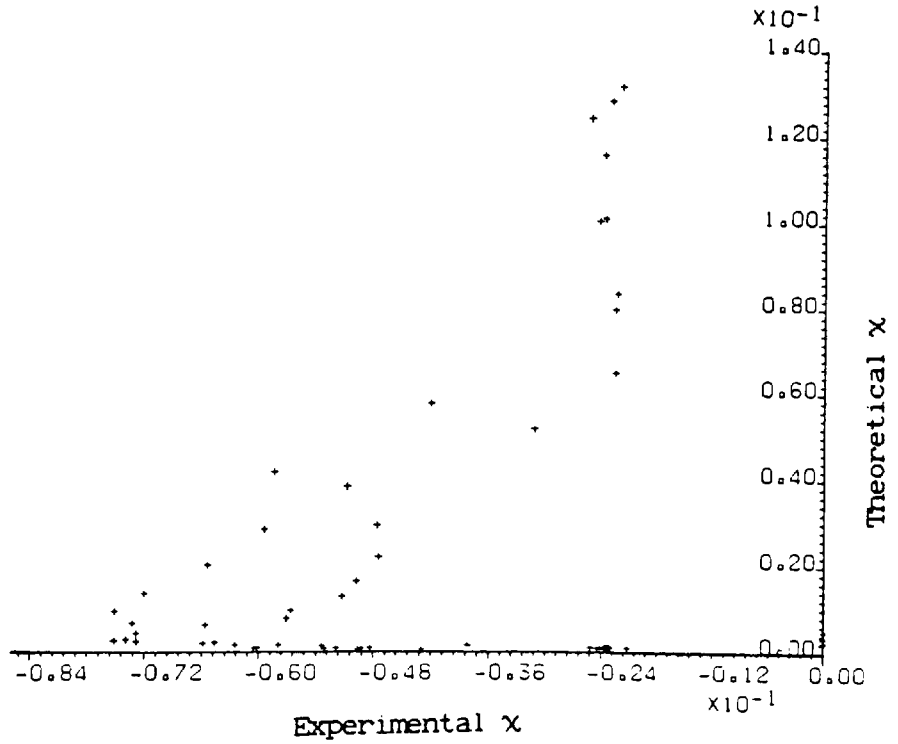

Figure 7.27 A comparison of theoretical and experimental vorticity values for the cylindrical rotor in Carbopol 910, gap = 1.3, Re = 1.2.

Figure 7.28

XI (VORTICITY) CONTOURS FOR NEWTONIAN FLUID (GAP = 0.8)

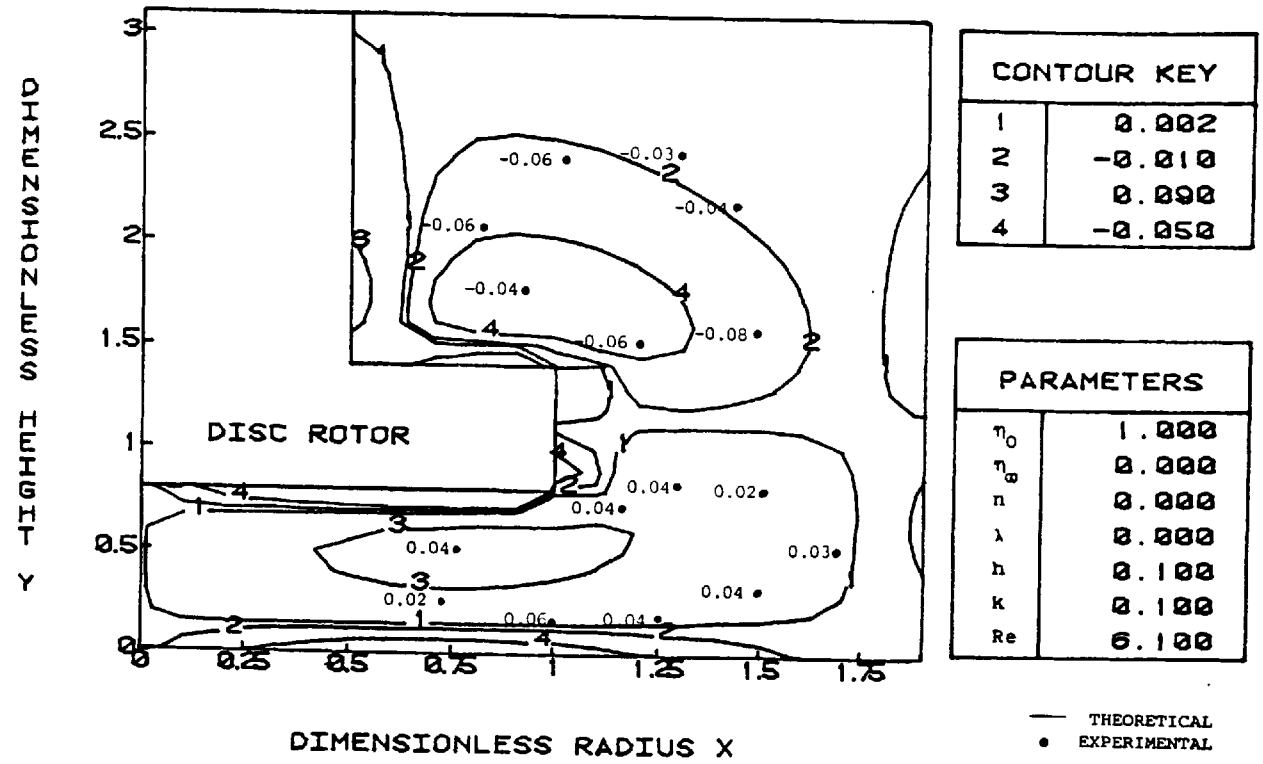

Figure 7.29

XI (VORTICITY) CONTOURS FOR CROSS FLUID (GAP = 0.8)

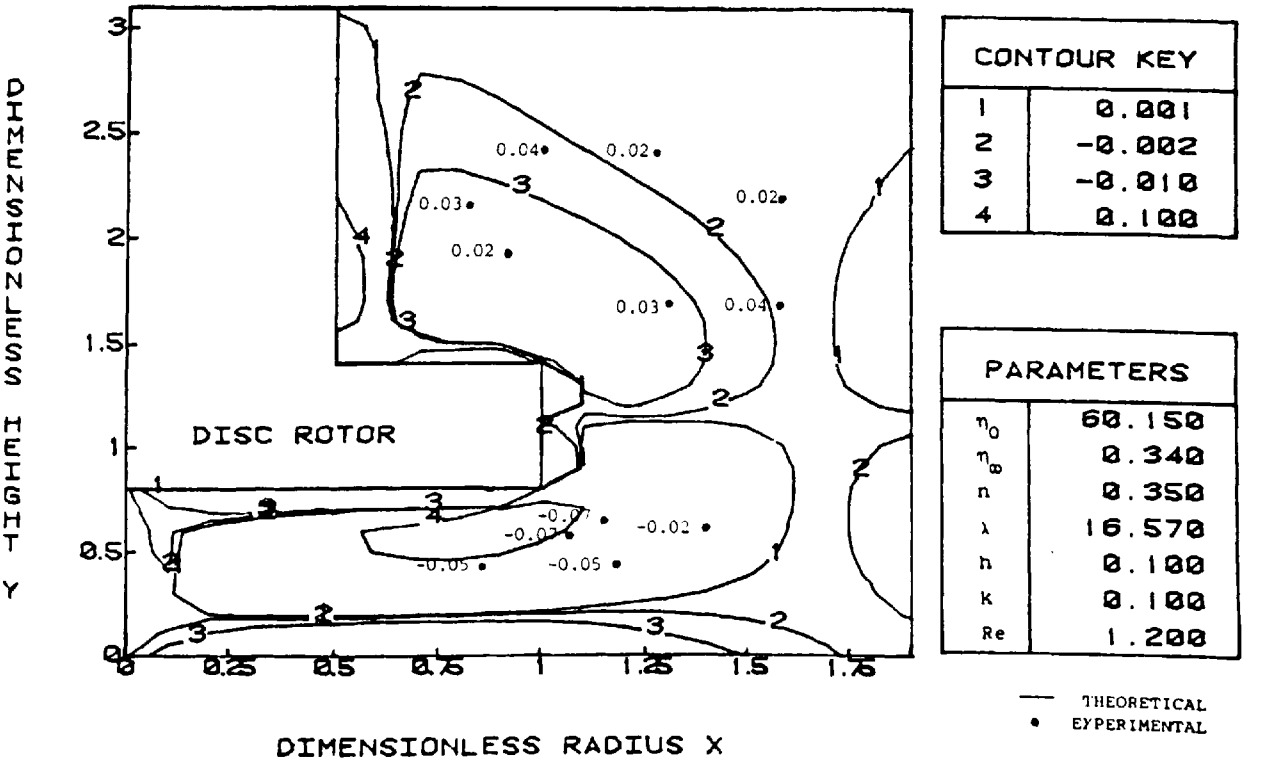

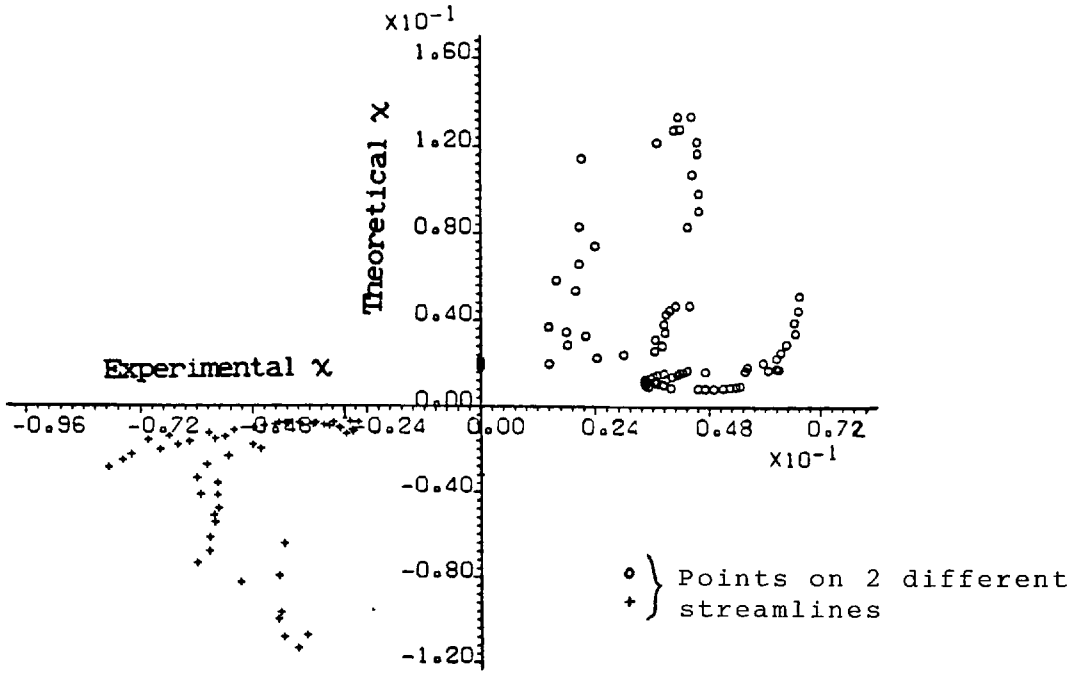

Figure 7.30 A comparison of theoretical and experimental vorticity values for the disc rotor in glycerol, gap = 0.8, Re = 6.1.

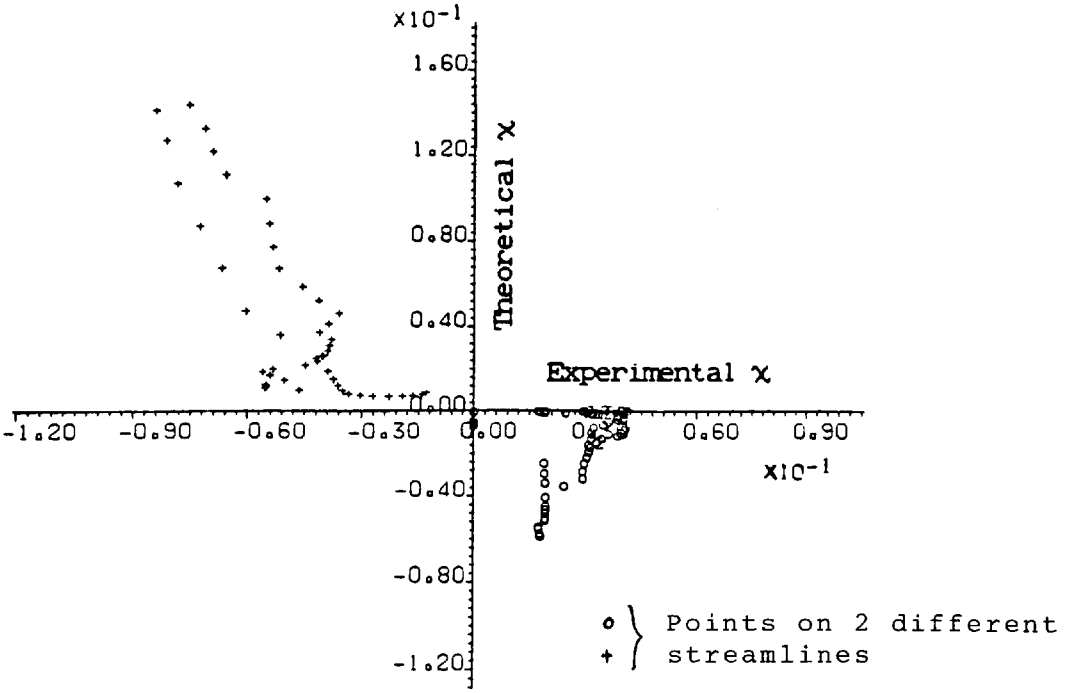

Figure 7.31 A comparison of theoretical and experimental vorticity values for the disc rotor in Carbopol 910, gap = 0.8, Re = 1.2.

CHAPTER 8

FURTHER RESULTS

8.0 Introduction

In this chapter, the variation of the theoretical couple, or torque values and Power numbers with the gap size y_b for the cylindrical and disc stirrers is examined. The way in which theoretical couple values change with the step size h for the cylindrical stirrer rotating in either glycerol or Carbopol 910 is also discussed. Numerical pumping numbers and discharge efficiencies for all the arrangements investigated are presented to give some indication of which geometry is the best at discharging fluid. A comparison of the experimental and theoretical couple values and Power numbers for these geometries is also carried out.

8.1 Variation of Numerical Couple and Power Number with the Gap Size y_b:

The way in which the numerical couple or torque values vary with the gap size y_b for the cylindrical or disc stirrer rotating as $Re \rightarrow 0$ in glycerol or Carbopol 910 is shown in Figure 8.1. The height of fluid y_c is kept constant for all arrangements. For both stirrers, the values of the couple decrease with an increase in gap size. This is as expected, since for a smaller gap more of the stirrer is immersed in the fluid for the same height of liquid y_c and, therefore, more energy is required to rotate the stirrer.

The couple values are seen to decrease more rapidly with an increase in gap size for the cylindrical rotor than for the disc rotor, and for corresponding gap size and fluid the couples are generally higher for

the cylindrical stirrer. This can be explained by the fact that there is a greater contribution to the couple from the upper side of the cylindrical rotor ,since it is further away from the axis of rotation than the upper side of the disc stirrer.

For a particular rotor, the values of the couple are generally higher for Carbopol 910 than for glycerol. This is partly due to the 'nominal' viscosities of the fluids being different and partly due to the zero shear viscosity η_0 being larger for Carbopol 910 than for glycerol.

Figure 8.2 shows the way in which the Power number N_p varies with gap size. N_p is seen to vary in a similar way to the couple as expected, since the quantities are proportionally related by equation 4.33.

8.2 Variation of Numerical Couple and Power Number with Step Size h.

The numerical couple and Power numbers obtained from the computer program for the cylindrical stirrer for varying step size h are given in Table 8.1. It can be seen that as the step size increases, the couple values and Power numbers decrease for both fluids. A change such as this is expected and we assume that the smaller the step size the more accurate are the values of couple and Power number. The rate of decrease of both the couple and Power number is seen to be greater for Carbopol 910 than for glycerol. Similar results (not presented) to those above were obtained for the disc rotor.

8.3 Variation of Numerical Couple and Power Number with Reynolds Number.

Table 8.2 shows the way in which the numerical couple values and Power numbers vary with the speed or Reynolds number Re for a cylindrical

or disc stirrer rotating in glycerol. At low speeds, the couple values double when the speed doubles. If, for a Newtonian fluid, only primary flow occurs at all Re, the couple values would double everytime the speed of the rotor doubles as shown by the line joining the dots in Figure 8.3. However, this is not the case in reality, since at higher speeds secondary flow also occurs and, therefore, the couple increases more rapidly with speed due to the extra circulation in the flow as shown by the curve joining the squares in Figure 8.3. It should be noted here that for convenience and reasonable run time of the computer, a step size of 0.1 was chosen.

The couples are seen to be higher for the small gap geometry than the large gap for both stirrers and may be explained by the same reasons as those given in section 8.1. Comparison of the two stirrers show that generally the values are higher for the cylindrical stirrer than the disc rotor as expected and in accordance with the comments made in section 8.1. Also the value M_{sec}/M_{pri} is greater for the disc stirrer than for the cylindrical stirrer for increasing Re due to the extra circulation generated by the disc.

At low speeds the Power number (Table 8.2) is seen to decrease by half when the speed doubles. At higher speeds when secondary flow also occurs, the Power number decreases less rapidly in agreement with Figure 1.3.

The variation of the couple and Power number with the speed for either the cylindrical or disc stirrer rotating in Carbopol 910, is shown in Table 8.3. In this case, the couple values do not double when speed doubles, since Carbopol 910 is a shear-thinning fluid. Instead, the couple values increase by a factor which decreases roughly by a constant amount each time for primary flow. The presence of only

primary flow at all speeds may be represented by the estimated line joining the dots in Figure 8.4. However, due to the presence of secondary flows at higher speeds, the factor by which the couple values increase does not decrease by the same amount as with primary flow, but decreases by a smaller amount, resulting in higher couple values than expected from primary flow. This deviation from the primary flow is shown by the curve joining the squares in the same diagram. There is a sharper rise in this curve than that for glycerol due to the shear-thinning nature of Carbopol 910.

Again the couples values are higher for the small gap than the large gap for both stirrers and for corresponding gap sizes the couples are generally higher for the cylindrical stirrer than the disc rotor. The Power numbers are seen to decrease with increasing speed for both the glycerol and Carbopol 910 as expected.

8.4 Numerical Discharge Efficiencies.

Table 8.4 gives the ratio of the Power number to the Pumping number (from equation 4.68) which shows some indication of the discharge efficiency of the arrangement under consideration. From Nagata [59] a small value of this ratio shows that the rotor is superior in discharge efficiency, whereas a large value indicates inferior discharge efficiency.

From the values it can be seen that the disc stirrer is generally better in discharging than the cylindrical rotor as expected. Furthermore, the small gap geometry shows weak discharging properties than the corresponding large gap geometry again as expected, since there is more freedom of movement.

8.5 Comparison of Theoretical Couples with Experimental Couples.

Table 8.5 gives the theoretical and experimental couple values for the cylindrical or disc stirrer rotating in glycerol. We can see that for the cylindrical stirrer the theoretical couple values are higher than their corresponding experimental couple values, whereas for the disc stirrer the theoretical couples are lower.

Representative plots of couple versus speed showing both theoretical and experimental values for the cylindrical and disc stirrers are shown in Figures 8.5 and 8.6 respectively. Although it is apparent from Table 8.5 that secondary flow effects start to occur at about Re = 1.6, this is not easily visible from Figure 8.5 due to the very small extra increase in couple at this Reynolds number. In Figure 8.6, the experimental line shows secondary flow effects occurring at approximately Re = 1.6, but again no effects are visible from the theoretical line.

The error in the scale reading on the Haake Rotovisco viscometer is ± 1, and a maximum error of~10% in the experimental value is generally accepted. Experimental error bars are shown in Figures 8.5 and 8.6. At low scale readings, such as 1 or 2, an error of ± 1 would mean upto 100% error in the actual couple values. This explains the relatively high differences in the experimental couple values at low Re shown in the tables. Further contribution to the error may be given by a slight 'wobble' in the rotor which is more pronounced for the disc rotor than the cylindrical rotor. This is expected since the disc stirrer is less sturdy due to the inner radius above the disc being smaller. Divergence is seen to occur at higher Re and may be explained due to secondary flow effects

Table 8.6 gives the experimental and theoretical couple values for the two stirrers rotating in Carbopol 910. Relatively high errors are seen to occur at low Reynolds numbers which can be explained partly by the reasons given above. Contribution to the error is also given by the fluid model not being exactly correct for Carbopol 910, since approximation methods were used to find the best model to fit the viscometric data. Comparison with the corresponding glycerol results show that generally the error is slightly higher for Carbopol 910.

Figures 8.7 and 8.8 show representative plots of couple against speed for Carbopol 910 together with experimental error bars. It is evident from these plots that the agreement between the experimental and theoretical couple values is better for the cylindrical rotor than for the disc stirrer - probably again due to the extra 'shake' in the disc stirrer. Again divergence is seen to occur at higher Re due to secondary flow effects.

8.6 Conclusions

The above results show that the general trends for the variation of numerical couples and Power numbers with the gap (y_b) and step size h (=K) and also speeds are as expected. The various arrangements are also found to discharge as one would expect. The experimental couple values are seen to compare relatively well with the predicted values, within experimental errors. The couple results for the cylindrical stirrer obtained here are generally similar to those obtained in our preliminary experiments [8] for both glycerol and Carbopol 910 for corresponding speeds.

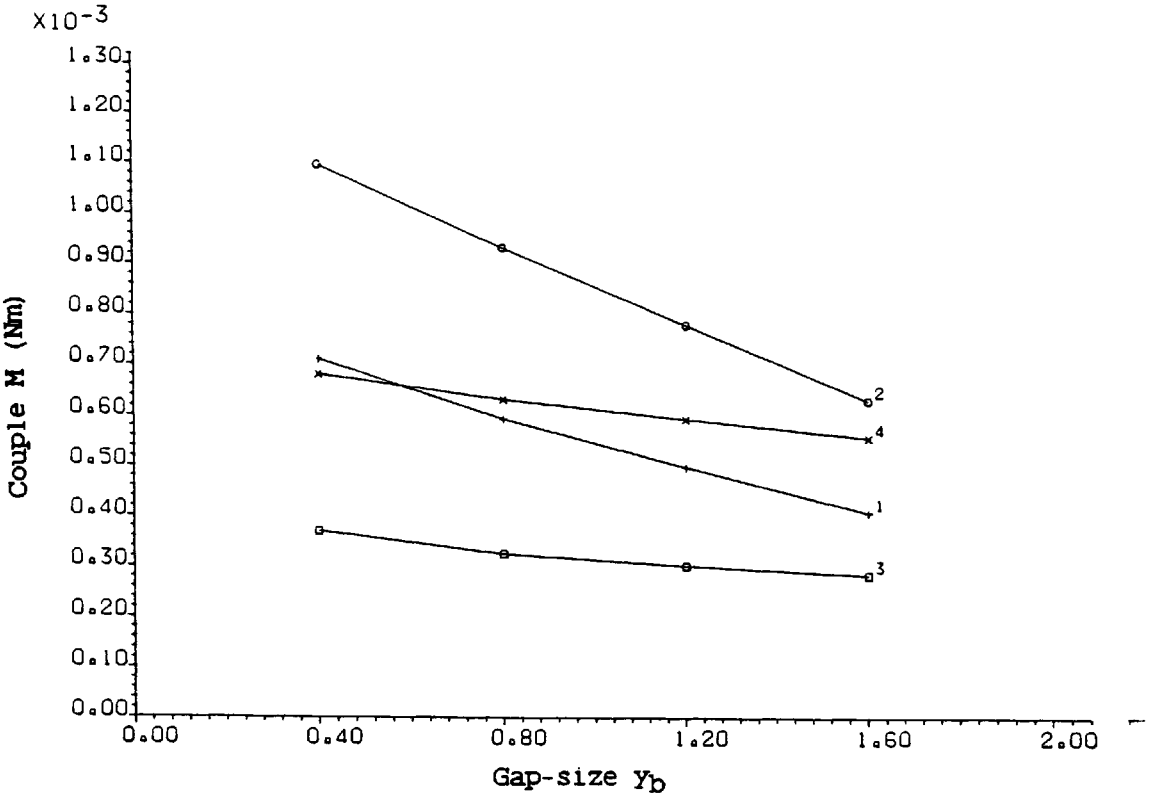

Figure 8.1 Variation of numerical couple values with gap-size for the cylindrical rotor in glycerol (1) or Carbopol 910 (2) and the disc rotor in glycerol (3) or Carbopol 910 (4).

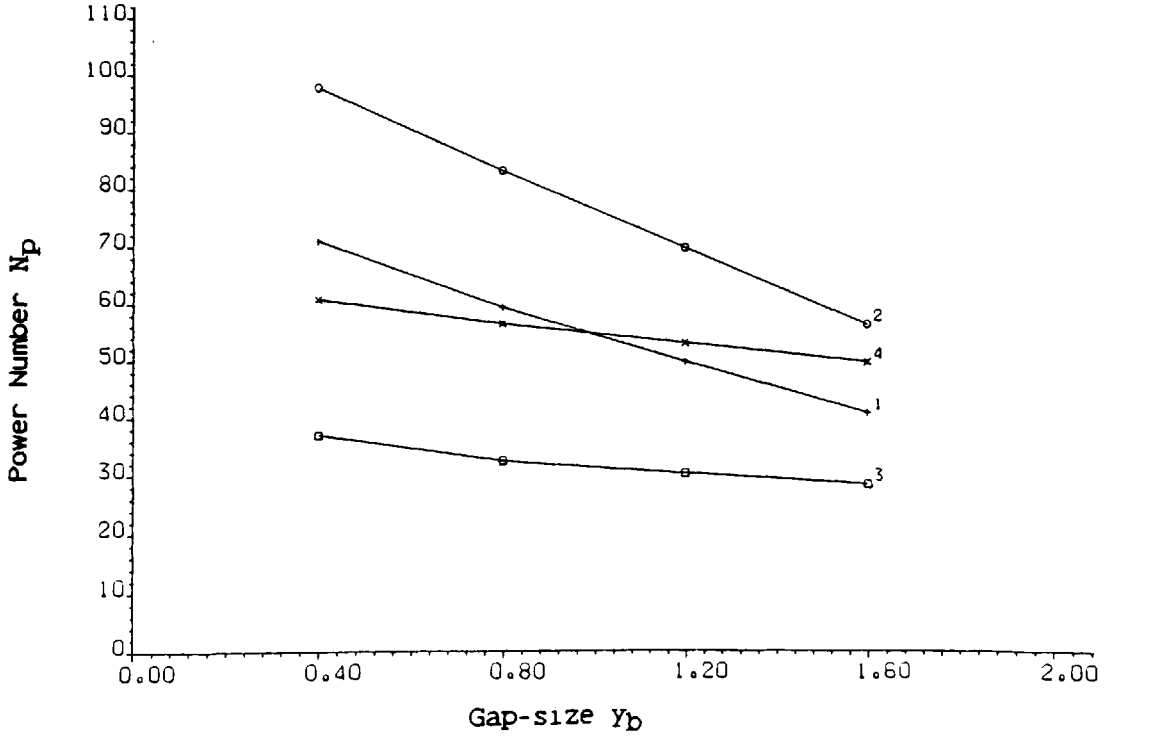

Figure 8.2 Variation of numerical Power number with gap-size for the cylindrical rotor in glycerol (1) or Carbopol 910 (2) and the disc rotor in glycerol (3) or Carbopol 910 (4).

Step-size h = K	Glycerol		Carbopol 910	
	Couple M x 10^7 Nm	Power Number	Couple M x 10^7 Nm	Power Number
0.025	3651	31.5	5460	48.7
0.05	3360	29.5	5324	41.8
0.1	3191	28.0	4821	37.9
0.125	3128	27.5	4614	36.2
0.2	2944	25.9	4070	32.0

Table:8.1 Variation of Couple and Power Number with Step-size for the Cylindrical Stirrer with y_b=1, y_c=2, x_c=2

Cylindrical Stirrer

Speed (rads per sec)	Reynolds Number Re	Small Gap y_b=0.8, y_c=3.1, x_c=1.9		Large Gap y_b=1.3, y_c=3.1, x_c=1.9	
		Couple M x 10^7 Nm	Power Number	Couple M x 10^7 Nm	Power Number
0.105	0.05	373.00	952.0	299.6	764.0
0.21	0.10	746.00	476.0	599.1	382.0
0.42	0.20	1492.00	238.0	1198.2	19.0
0.84	0.40	2984.00	119.0	2396.4	95.6
1.68	0.80	5968.00	60.0	4793.0	47.8
3.36	1.60	11936.00	30.0	9586.2	24.0
6.72	3.20	23872.00	15.0	19173.5	12.0
13.44	6.40	47782.00	7.5	38377.0	6.0
26.88	12.80	95565.00	3.7	77051.0	3.0
53.76	25.60	192260.00	1.9	157396.0	1.5

Disc Stirrer

Speed (rads per sec)	Reynolds Number Re	Small Gap y_b=0.8, y_c=1.4, x_c=3.1 x_g=0.5, x_c=0.9		Large Gap y_b=1.3, y_c=2.0, x_c=3.1 x_g=0.5, x_c=1.9	
		Couple M x 10^7 Nm	Power Number	Couple M x 10^7 Nm	Power Number
0.105	0.05	204.12	521.2	198.5	506.8
0.21	0.01	408.23	260.6	397.0	253.4
0.42	0.20	816.46	130.3	794.0	126.7
0.84	0.40	1632.93	65.1	1588.3	63.4
1.68	0.80	3265.91	32.6	3176.6	31.7
3.36	1.60	6532.17	16.4	6353.5	16.0
6.72	3.20	13067.20	8.3	12710.8	8.0
13.44	6.40	26157.00	4.1	25440.2	4.0
26.88	12.80	52666.75	2.1	51269.4	2.0
53.76	25.60	108140.70	1.1	107153.6	1.0

Table: 8.2 Variation of the Numerical Couple and Power Number with the Speed/Reynolds Number for the Cylindrical or Disc Stirrer Rotating in Glycerol

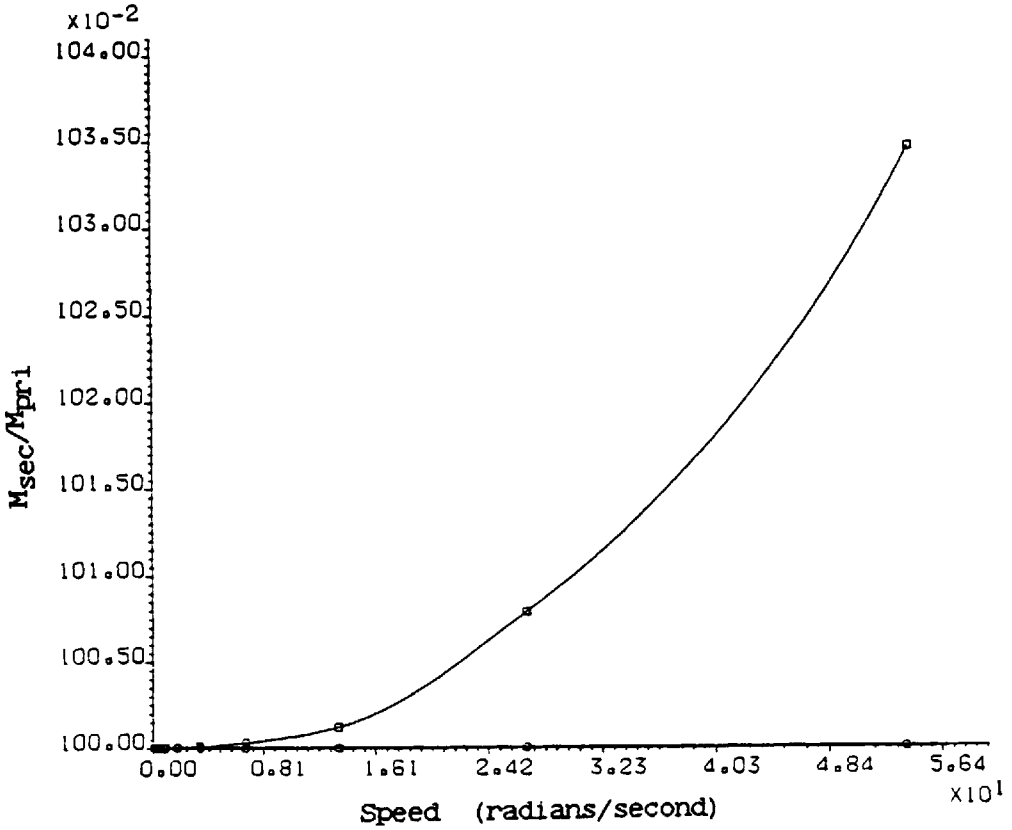

Figure 8.3 The ratio of secondary flow couple to the primary flow couple as a function of speed for glycerol.

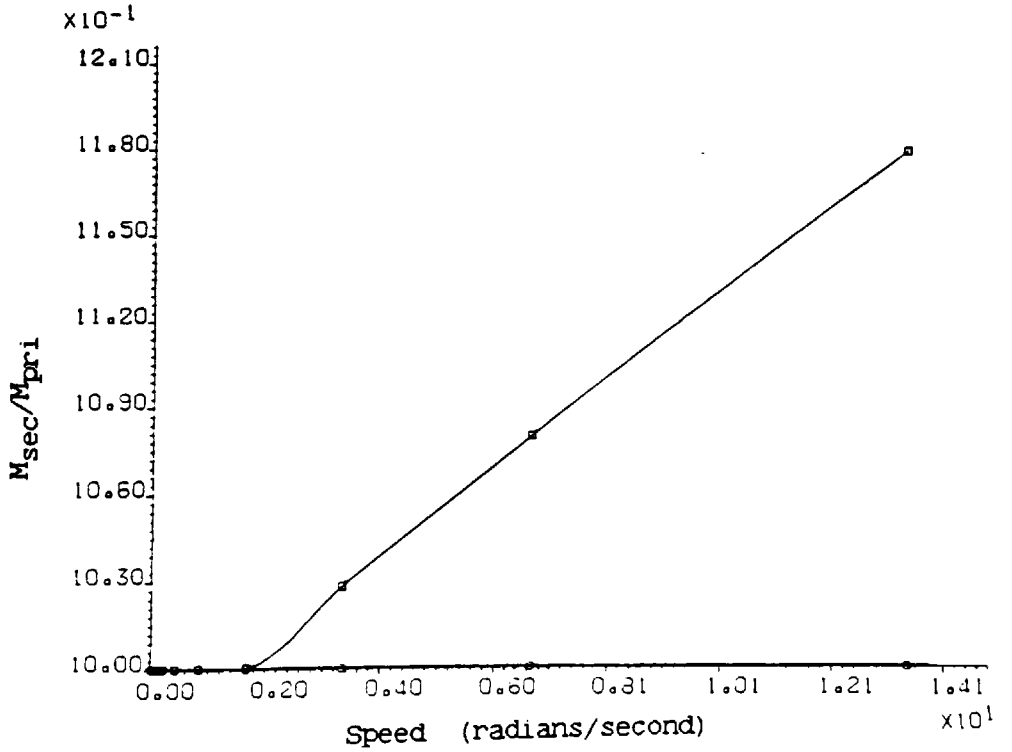

Figure 8.4 The ratio of secondary flow couple to the primary flow couple as a function of speed for Carbopol 910.

Cylindrical Stirrer					
Speed (rads per sec)	Reynolds Number Re	Small Gap y_b=0.8, y_c=3.1, x_c=1.9		Large Gap y_b=1.3, y_c=3.1, x_c=1.9	
		Couple M x 10^7 Nm	Power Number	Couple M x 10^7 Nm	Power Number
0.105	0.01	1426.2	2964.8	1130.9	2350.9
0.21	0.02	2458.0	1402.2	1951.8	1113.3
0.42	0.04	4037.9	575.8	3211.0	457.9
0.84	0.08	6308.6	224.9	5026.2	179.2
1.68	0.16	9371.8	83.5	7476.2	66.6
3.36	0.32	13564.2	30.4	10830.5	24.3
6.72	0.64	18962.3	10.6	15171.6	8.3
13.44	1.28	25966.0	3.6	20783.3	2.9
Disc Stirrer					
Speed (rads per sec)	Reynolds Number Re	Small Gap y_b=0.8, y_c=1.4, x_c=3.1 x_g=0.5, x_c=0.9		Large Gap y_b=1.3, y_c=2.0, x_c=3.1 x_g=0.5, x_c=1.9	
		Couple M x 10^7 Nm	Power Number	Couple M x 10^7 Nm	Power Number
0.105	0.01	780.1	1621.6	759.2	1578.2
0.21	0.02	1386.2	790.7	1348.2	769.0
0.42	0.04	2377.1	339.0	2311.4	329.6
0.84	0.08	3940.9	140.5	3844.0	136.6
1.68	0.16	6350.7	56.6	6184.0	55.1
3.36	0.32	10197.3	22.9	9951.4	22.3
6.72	0.64	16381.0	9.2	16031.5	9.0
13.44	1.28	26744.0	3.7	26156.8	3.7

Table: 8.3 Variation of the Numerical Couple and Power Number with the Speed/Reynolds Number for the Cylindrical or Disc Stirrer Rotating in Carbopol 910

	Power Number N_p	Pumping Number N_q	$DE = \frac{N_p}{N_q}$
Cylindrical Stirrer Glycerol			
-Small Gap (0.8)	2.05	7.48	3.65
-Large Gap (1.3)	2.58	6.01	2.33
Carbopol 910			
-Small Gap (0.8)	4.15	3.64	0.87
-Large Gap (1.3)	3.92	2.90	0.74
Disc Stirrer Glycerol			
-Small Gap (0.8)	3.01	4.11	1.37
-Large Gap (1.3)	3.71	3.98	1.07
Carbopol 910			
-Small Gap (0.8)	5.67	3.74	0.66
-Large Gap (1.3)	5.54	3.68	0.66

Table: 8.4 Theoretical Discharge Efficiencies for the Arrangements Studied.

Cylindrical Stirrer

Speed (rads per secs)	Small Gap		Large Gap	
	Theoretical Couple M x 10^7 Nm	Experimental Couple M x 10^7 Nm	Theoretical Couple M x 10^7 Nm	Experimental Couple M x 10^7 Nm
0.105	372.96	368.00	299.60	245.25
0.21	745.92	735.75	599.12	490.50
0.42	1491.84	1471.50	1198.24	981.50
0.84	2983.68	2943.00	2396.49	1962.00
1.68	5967.37	5886.00	4793.00	4169.25
3.36	11934.85	11772.00	9586.16	8583.75
6.72	23870.52	23544.00	19173.50	17412.80
13.44	47745.00	47088.00	38377.40	35561.25

Disc Stirrer

Speed (rads per secs)	Small Gap		Large Gap	
	Theoretical Couple M x 10^7 Nm	Experimental Couple M x 10^7 Nm	Theoretical Couple M x 10^7 Nm	Experimental Couple M x 10^7 Nm
0.105	204.12	245.25	198.50	245.25
0.21	408.23	490.50	397.10	490.50
0.42	816.46	981.00	794.20	981.00
0.84	1632.93	1962.00	1588.30	1716.75
1.68	3265.91	3679.00	3176.60	3433.50
3.36	6532.17	7602.75	6353.50	7112.25
6.72	13067.19	15696.00	12710.80	14960.25
13.44	26157.35	32863.50	25440.20	31146.75

Table: 8.5 A Comparison Between the Theoretical and Experimental Couple Values for the Cylindrical and Disc Stirrers Rotating in Glycerol.

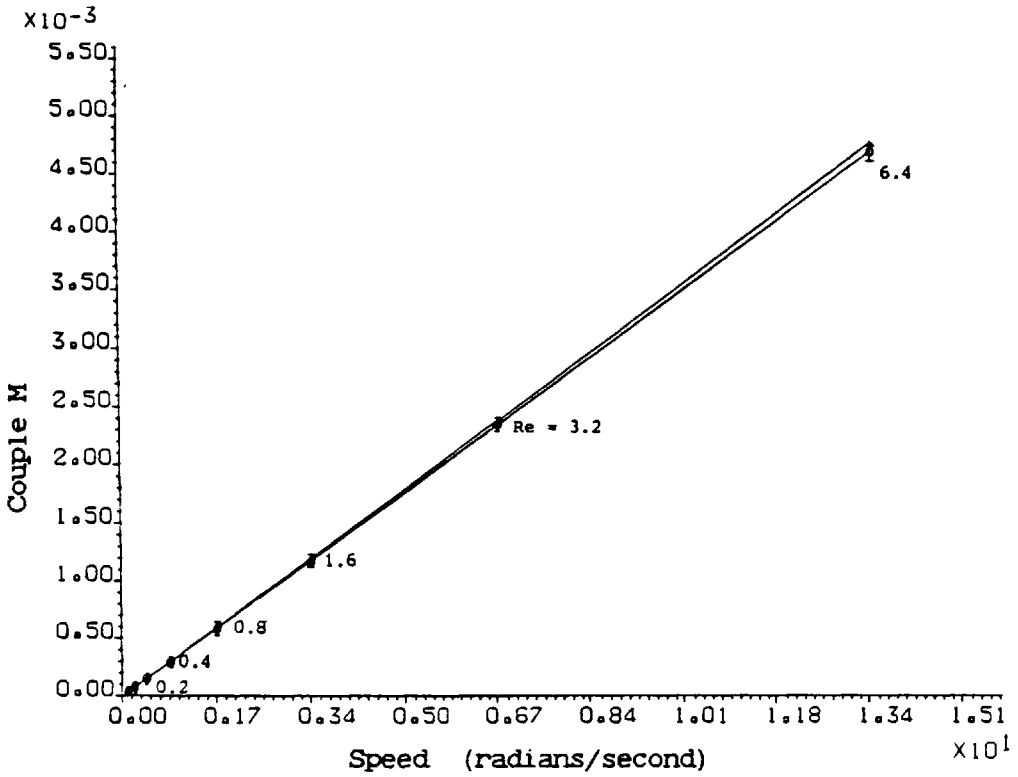

Figure 8.5 A variation of numerical (×) and experimental (o) couple values with speed for the cylindrical stirrer in glycerol, gap =0.8.

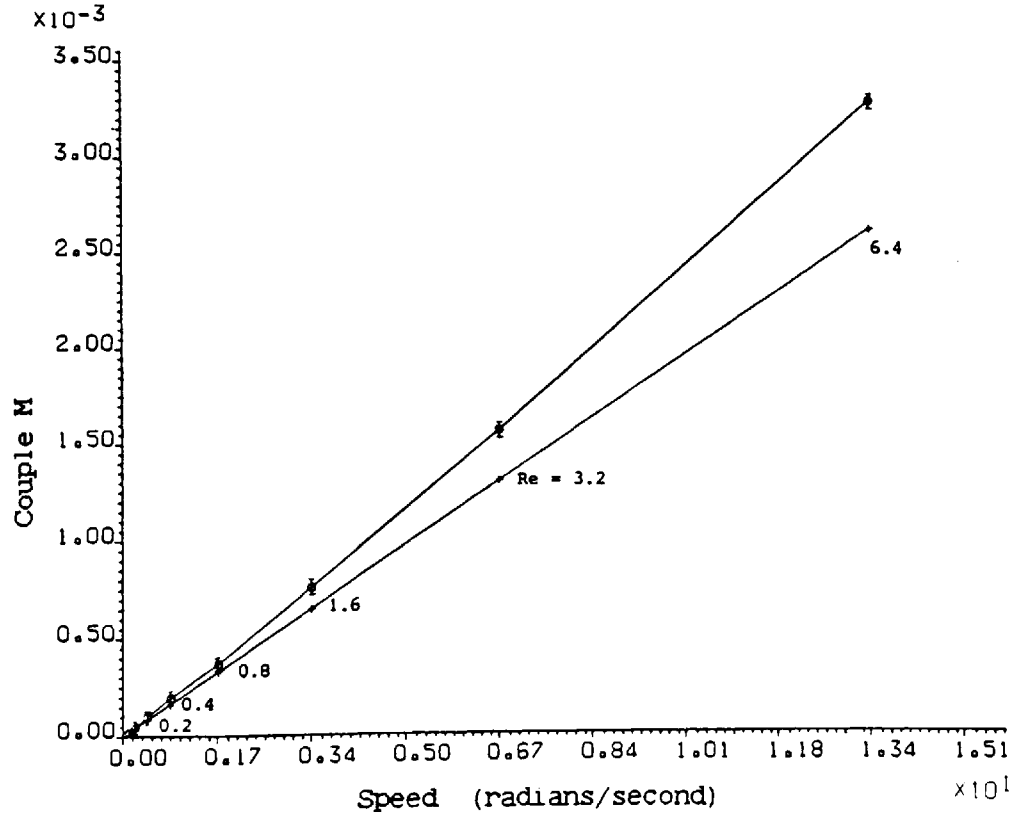

Figure 8.6 A variation of numerical (×) and experimental (o) couple values with speed for the disc stirrer in glycerol, gap = 0.8.

Cylindrical Stirrer

Speed (rads per secs)	Small Gap		Large Gap	
	Theoretical Couple M x 10^7 Nm	Experimental Couple M x 10^7 Nm	Theoretical Couple M x 10^7 Nm	Experimental Couple M x 10^7 Nm
0.105	1426.2	1349.00	1130.85	1226.25
0.21	2458.3	2452.50	1951.80	2207.25
0.42	4037.9	3924.50	3211.00	3678.75
0.84	6308.6	6131.25	5026.20	5395.50
1.68	9371.8	8583.75	7476.20	7602.75
3.36	13564.2	12017.25	10830.50	11281.50
6.72	18962.3	16677.00	15171.60	15205.50
13.44	25966.8	24279.25	20783.30	21336.75

Disc Stirrer

Speed (rads per secs)	Small Gap		Large Gap	
	Theoretical Couple M x 10^7 Nm	Experimental Couple M x 10^7 Nm	Theoretical Couple M x 10^7 Nm	Experimental Couple M x 10^7 Nm
0.105	780.20	981.00	759.15	981.00
0.21	1386.20	1716.75	1348.20	1716.75
0.42	2377.10	2943.00	2311.40	2943.00
0.84	3940.90	4414.50	3833.00	4414.50
1.68	6350.70	6867.00	6184.00	7602.00
3.36	10197.37	11772.00	9951.40	12262.50
6.72	16380.95	16677.00	16031.50	17658.00
13.44	26744.00	27223.00	26256.75	20846.00

Table: 8.6 A Comparison Between the Theoretical and Experimental Couple Values for the Cylindrical and Disc Stirrers Rotating in Carbopol 910.

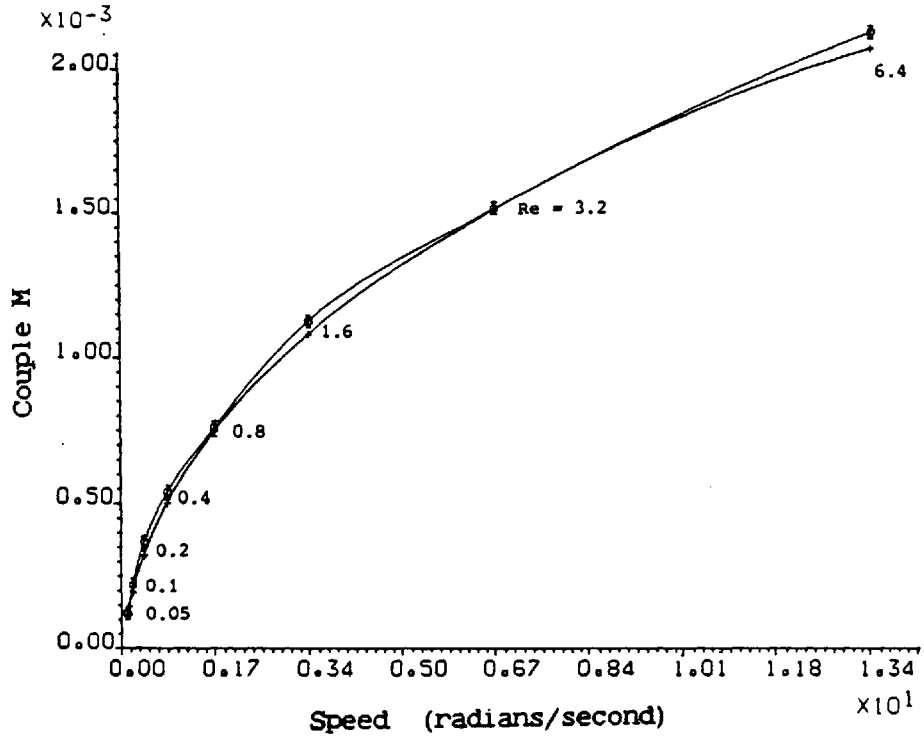

Figure 8.7 A variation of numerical (*) and experimental (o) couple values with speed for the cylindrical stirrer in Carbopol 910, gap = 1.3.

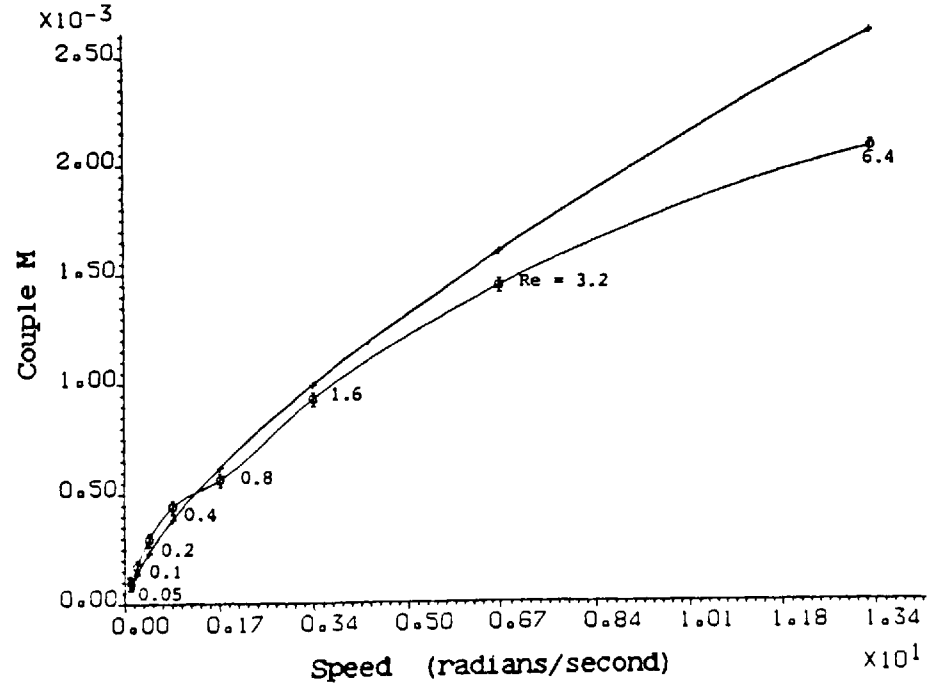

Figure 8.8 A variation of numerical (*) and experimental (o) couple values with speed for the disc stirrer in Carbopol 910, gap = 1.3.

CHAPTER 9

CONCLUSIONS AND SUGGESTIONS FOR FUTURE WORK

9.0 CONCLUSIONS

A novel flow visualisation technique has been developed which is relatively cheap, easy to use and moderately efficient for obtaining good clear simultaneous pictures of fluid flows in the horizontal and vertical planes of the apparatus. This ensures an instantaneous three-dimensional view of the flows. A permanent record of the flows can be taken, stored on a video cassette and studied at leisure whenever required using the freeze-frame and playback facilities. The freeze-frame facility allows relatively more accurate timing of flows and determination of particle positions than the stop watch, which was used in preliminary experimentation on primary flows. A number of recordings of the flows can be stored on one video cassette thus giving lower costs. Futhermore, the technique enables flow patterns to be determined as well as various primary and secondary flow parameters and torque values. In fact, more information about the flows can be obtained from this technique than from any other method used previously. In principle, a full three-dimensional analysis of flows due to stirrers, such as anchors, gates and Rushton Turbines can be carried out.

The advantage of the use of large tracer particles is that they are easy to track individually and can be removed from the fluid hence enabling the fluid to be reused. However, inaccuracies occur with the usage of large particles as was seen with the experimental angular velocities being generally lower in most cases (especially for secondary flows) than the corresponding theoretical values. Moreover, the tracking of individual tracer particles' positions and manual input of data into the computer for analysis proved extremely time-consuming.

A suggestion to overcome the above problems is to use smaller particles which are highly reflective and which are more likely to travel at the same speed of the fluid. These would obviously be more difficult to visualise and track. Therefore, a touch sensitive screen or computer scan method is recommended with the former working on the principle that the particle on the TV screen is touched with a sensitive pen and its position directly recorded into the computer. This would also be rather time-consuming although more accurate, since no human reading of particle positions and time is involved. This is where the computer scan method would be extremely helpful. Here, the computer would automatically scan the TV screen every frame, if required, and the positions of all the particles would be recorded into the computer and direct analysis would then be carried out. This would save much time and effort and give much more accurate results with the use of smaller tracer particles. Obviously, this technique can only be installed and used if large sums of money is available since it is a very expensive technique.

Another limitation involved with our flow visualisation technique is the speed used to obtain secondary flow. We are confined to a speed of 128 rpm for good resolution of the tracer particles, since above this speed even with the freeze-frame facility, the particles cannot be seen clearly. The above computer scan method would also help to overcome this problem so that flows at higher speeds can be studied experimentally.

For comparison with experimental results, theoretical prediction of more complex flows and for eventual scale-up, a numerical technique using finite difference methods has been developed similar to that used by Pao to model both primary and secondary flows induced by

rotating stirrers. The theoretical couple values, Power numbers, Pumping numbers and discharge efficiencies can all be determined. Flows for Reynolds numbers upto 400 can be simulated successfully, but it was not found necessary to simulate flows for Re>400. However, in view of the ease with which the results for Re=400 were obtained, we see no difficulty in simulating flows for Re>400 or even for Re ≥ 1000 as carried out by Pao [67] and Hyun [38].

The method is relatively easy to use with no complicated matrix involved and enables each parameter to be iterated individually unlike the method used by Paddon. Furthermore, comparison of the results obtained from our method with those of other workers for similar arrangements show encouraging agreement enabling us to feel confident in using our method to simulate flows investigated in this study.

9.0.1 Comparison of Theoretical Results with Experimental Results

Numerical and experimental angular velocities for primary flow generally give good quantitative agreement for both the cylindrical and disc stirrers rotating in either glycerol or Carbopol 910. Primary flow shear rates give good qualitative and fair quantitative agreement for all arrangements.

For secondary flows, there is relatively good quantitative agreement between the experimental and theoretical angular velocities for glycerol and only fair quantitative agreement for Carbopol 910. The shear rates are highly scattered and give only fair qualitative agreement between theoretical and experimental values. For both glycerol and Carbopol 910 the experimental and numerical values of the stream function and vorticity agree well qualitatively. However, the

experimental and theoretical streamlines are of opposite directions for Carbopol 910 due to its slight elastic property not being present in the theoretical model.

9.0.2 Couple Values, Power Numbers and Discharge Efficiencies.

Numerical and experimental couple values generally agree well quantitatively for the cylindrical stirrer rotating in either glycerol or Carbopol 910 at all Reynolds numbers. However, for the disc stirrer rotating in either fluid, the agreement between the experimental and theoretical couple values is relatively good at low Re but divergence is seen to occur at higher Re due to secondary flow effects. Numerical couple values and Power numbers vary with speed, gap size and step size as expected. The various geometries discharge fluid also as expected.

From the above comments it can be safely concluded that we have achieved our aim of contributing to the field of the low speed mixing of viscous fluids by developing experimental and theoretical techniques which generally give good results for primary flows. For secondary flows, the comparison of the results are better for glycerol than for Carbopol 910 as expected. However, we feel confident that had a more realistic fluid model been used with the elastic behaviour of Carbopol 910 being incorporated, better agreement of the results would have been obtained. Also, a better characterisation of the fluids to include a wider shear rate region is required so that more accurate fluid models can be used in the various equations which would give better agreement of the theoretical results with those obtained experimentally for non-Newtonian fluids.

The experimental method can be used as it stands, but if funding is available, modifications as those mentioned earlier, to the technique are welcome to give improved results. Modifications to the mathematical method would include non-axisymmetric flows as well as axisymmetric flows, more appropriate fluid models for the fluids studied and also changes to the computer program for the wide range of geometries investigated.

9.1 Suggestions For Future Work.

The work carried out in this study has provided a basis for future work in the field of mixing. It is hoped that the techniques developed here will be used to aid in the investigation of flows generated by more complicated stirrers, such as the Rushton Turbine in more complex fluids e.g. those which exhibit elasticity or 'yield stress' behaviour. We hope that eventually the various types of mixers, fluids and conditions under they are used in 'real life' industrial applications can be modelled theoretically. As mentioned earlier, this would inevitably save time, money and effort as experimental work would not need to be carried out. Obviously much work needs to be carried out before this stage is reached. Below are suggestions for future work which will help to give a better understanding of the mixing flows involved.

(i) The theoretical and experimental study of more complex arrangements of stirrers in a range of fluids of more industrial relevance. This would include the determination of both primary and secondary flow parameters, power consumption and discharge efficiencies. In fact, a study of various stirrers in elastic fluids is the subject of ongoing work.

(ii) A study of the effect of baffles on flows and power consumption.

(iii) A theoretical and experimental investigation of colour band and dispersive mixing where part of the fluid is coloured and the concentration of colour in the fluid measured as it changes with time until a homogeneous mixture is obtained. This would include determination of circulation, mixing and residence times.

(iv) A study of how two particles which are initially adjacent disperse through the fluid.

(v) A determination of stagnant regions in mixing vessels using powder, dye or particle techniques.

(vi) A study of transient flows i.e. from start-up.

(vii) A prediction of the most suitable mixing geometries for various industrial fluids examined.

(viii) A determination of how various geometries studied can be scaled up to manufacture level.

REFERENCES

[1] AMES A.F.
Numerical Method for Particle Differential Equations
Nelson, London 1977

[2] AYAZI SHAMLOU P. and EDWARDS M.F.
Chem. Eng. Sci. 1985 40 1773

[3] BARNES H.
Unilever Research, Port Sunlight Laboratory, Bebington
Private Communication

[4] BARTELA M. and GORI F.
J. of Fluids Eng. 1982 104 31

[5] B.F. GOODRICH CHEMICAL (U.K.) LIMITED
Hounslow, Middlesex

[6] BINNINGTON R.J. et al.
J of non-Newt. Fluid Mech. 1983 12 255

[7] BIRD R.B. et al
Dynamics of Polymeric Liquids: Volume 1 - Fluid Mechanics
John Wiley, New York, 1977

[8] BODALIA V. et al
Proceedings of the Fourth International Conference on
Numerical Methods in Laminar and Turbulent Flows - Volume 1,
C. Taylor et al (Editor), Pineridge Press, Swansea, 1985.

[9] BORNE J.R.
Brit. J. Appl. Phys. 1965 16 1411

[10] CAIRNCROSS E.K and HANSFORD G.S
B.S.R. Conference,Exeter, Sept.1971

[11] CHAVAN et al
Al Che 1975 21 613

[12] CHENG D.C-H
Chem. Soc. Lecture, Aberystwyth, 1979

[13] CHENG D.C-H
First European Conference on Mixing and Centrifugal Separation
Coles N.G. (Editor), Bedford, BHRA, 1974

[14] CHENG D.C-H
A Comparison of 14, Commercial Viscometers and a Hand Made Instrument
W.S.L. Report, Stevenage 1978

[15] CHHABRA R.P. and UHLERR P.H.T.
Chem. Eng. Commun. 1980 5 115

[16] COCHRANE T. et al.
J. of Non-Newt Fluid Mech. 1982 10 95

[17] COCHRANE T.
Phil. Trans. Royal Soc. London 1981 301 163

[18] COLLIAS D.J. and PRUD'HOMME R.K.
Chem. Eng. Sci. 1985 40 1495

[19] COULSON J.M. and RICHARDSON J.F.
Chemical Engineering, Volume 2, Third Edition
Permagon Press, Oxford, 1978

[20] COURTAULDS LIMITED
Foleshill Road, Coventry.

[21] DEMBEK G.
Flow Vis. Proc. Int. Sym. 1982

[22] DESOUZA A.
Can. J. Chem. Eng 1972 50 15

[23] DIJKSTRA D. and VAN HEIJST G.J.F.
J. Fluid mech. 1983 128 123

[24] DOREMUS P. and PIAU J.M.
J. of Non-Newt. Fluid Mech. 1983 13 279

[25] FORESTI R. and LIU T.
Ind. Eng. Chem. 1959 51 860

[26] FOSDICK K.L. and KAO B.G.
Rheol. Acta. 1980 19 675

[27] GAD-EL-HAK M.
Trans. of the ASME, 1986 108 34

[28] GIESEKUS H.
Rheol. Acta. 1967 6 339

[29] GRIFFITHS D.F. et al
J. Fluid Mech. 1969 36 161

[30] GRIFFITHS D.F. and WALTERS K.
J. Fluid Mech. 1970 42 379

[31] HAVARD S.
Final Year Project, 1985 , Polytechnic of Wales
Private communication

[32] HEADING J.
Mathematical Methods in Science and Engineering
Arnold 1976

[33] HILL C.T. et al
Chem. Eng. Sci. 1966 21 815

[34] HOCKER H. et al
Ger. Chem. Eng. 1981 4 113

[35] HONJI H. and TANEDA S.
J.Phy.Soc. Japan 1969 27 1668

[36] HOLLAND F.A.
Fluid Flow
Reinhold, New York, 1966

[37] HYDRAULICS & SUPREME PLASTICS ENGINEERING LTD.
Holbrook Lane, Coventry

[38] HYUN J.M.
Trans. of the ASME, 1985 107 92

[39] HYMAN D.
Advances in Chemical Engineering: Volume 3 - Mixing and Agitation
Academic Press 1962 119-202

[40] JAKSIC M.M. and TOBIAS C.W.
Flow.Vis.Proc.Int.Sym.1982 647

[41] JEFFREY G.B.
Proc. London maths Soc.1915 14 327

[42] KALE D.D et al
Rheol. Acta. 1975 14 631

[43] KEENTOK et al
J.of Non-Newt.Fluid Mech 1985 17 23

[44] KNIGHT D.G.
Polytechnic of Wales
Private Communication

[45] KRAMER J.M. and JOHNSON M.W.
Trans. Rheol. 1972 16 197

[46] KURIYAMA et al
AIChE 1982 28 385

[47] KUWAHARA K. et al
J. Phy. Soc. Japan 1978 45

[48] LAN A. and ANGELINO H.
First European Conference on Mixing and Centrifugal Seperation
Coles N.G. (Editor), Bedford, B.H.R.A., 1974

[49] MANN R. and KNYSH P.
I. Chem. E. Symposium Series - Fluid Mixing II No. 89

[50] MENA B. et al
J. of Non-Newt. Fluid Mech 1979 5 427

[51] METZNER A.B. and OTTO R.E.
AIChE 1957 3 3

[52] METZNER A.B. and OTTO R.E.
AIChE 1961 1 3

[53] METZNER A.B. and NORWOOD K.W.
AIChE Sept. 1960 432

[54] METZNER A.B. and TAYLOR J.S.
AIChE 1960 6 107

[55] MITCHELL A.R.
Computational Methods in Partial Differential Equations
John Wiley, London, 1969

[56] MITCHKA P.
Appl. Sci. Res. 1966 15 345

[57] NAG FORTRAN LIBRARY MANUAL MARK 10
Numerical Algorithms Group, Oxford, 1983

[58] NAGATA S.
Mixing: Principles and Applications
John Wiley and Sons, London, 1975

[59] NIENOW A.W. et al
Chem. Eng. Commun. 1983 19 273

[60] NIENOW A.W. et al
Chem. Eng. Commun. 1983 22 29

[61] NIRSCHL J.P. and STEWART W.E.
J. of Non-Newtonian Fluid Mech. 1984 16 233

[62] O' KANE K.
First European Conference on Mixing and Centrifugal Separation
Coles N.G. (Editor), Bedford, B.H.R.A., 1974

[63] OLDROYD J.G.
Proc. Roy. Soc. 1958 4 278

[64] OLDSHUE J.Y
Fluid Mixing Technology
McGraw-Hill Publications Company, New York, 1983

[65] PADDON D.J.
Ph.D Thesis U.C. Wales 1980

[66] PADDON D.J. and WALTERS K.
Rheol. Acta. 1979 18 565

[67] PAO, H-P
The Physics of Fluids 1972 15 4

[68] PASQUALI G. and FAJNER D.
Chem. Eng. Commun. 1983 22 371

[69] POULTER R. and SNADDON R.W.L.
J.Phys.D: Appl. Phys. 1978 11 1387

[70] PETERS D.C.
Ph.D. Thesis, Univ. of Wales, 1966

[71] PETERS D.C. and SMITH J.M.
Trans. Inst. Chem. Engrs. 1967 45 360

[72] PETERS D.C. and SMITH J.M.
Can. J. of Chem. Eng. 1969 47 268

[73] PHYSICAL PROPERTIES DATA SERVICE
National Engineering Laboratory
East Kilbride, Glasgow

[74] PLOT 10 ROUTINES
Computer Centre, Polytechnic Of Wales
Pontypridd

[75] QUILLEN C.S.
Chem. Eng., 1954 61 6

[76] QURAISHI M.S. and FAHIDY T.Z.
Chem, Eng. Sci. 1982 37 775

[77] ROTZ C.A. and SUH N.
Trans. ASME J. Fluids Eng. June 1979 101 186

[78] RUSHTON J.H.
Ind. Eng. Chem., 1955 47 582

[79] SACH and RUSHTON J.H.
Chem. Eng. Prog., 1954 50 597

[80] SATO K.
Chem. Eng. Commun. 1980 7 45

[81] SESTAK J. et al
J. Rheology 1982 26 459

[82] SHAN-SHENG Z.
Flow Vis. Proc. Int. Sym. 1982

[83] SHIH and HWANG
J. Chin. Inst. Chem. Eng.

[84] SMITH G.D.
Numerical Solution of Partial Differential Equations: Finite Difference Methods, Oxford University Press, 1978

[85] SPRAGG et al
Proceedings of the Fourth International Conference on Numerical Methods in Laminar and Turbulent Flows - Volume 1, C. Taylor et al (Editor), Pineridge Press, Swansea, 1985.

[86] TALBOTT W.H. and GODDARD J.D.
Rheol. Acta. 1979 18 505

[87] THOMAS R.S. and WALTERS K.
Q. Jl. Mech. Appl. Math. 1964 17 39

[88] TOWNSEND P. et al
J. of Non-Newt. Fluid Mech. 1976 1 107

[89] ULBRECHT J.
Chem. Eng. 1974 347

[90] ULBRECHT J. and GASPARETTO
J. Rheol. 1980 24 551

[91] VAN AKEN J.A et al
Rheol. Acta. 1980 19 159

[92] VAN WAZER J.R. et al
Viscosity and Flow Measurement
Interscience, London 1963

[93] VARGA R.S.
Matrix Iterative Analysis
Prentice Hall, Englewood Cliffs, N.J. 1962

[94] VON KARMAN T.H.
Z.A.M.M. 1921 1 233

[95] WALTERS K.
Rheometry
Chapman and Hall, London 1975

[96] WALTERS K.
J. Fluid Mech. 1970 40 191

[97] WALTERS K. and SAVINS J.G.
Trans. Soc. Rheol. 1965 9 407

[98] WALTERS K. and WATERS N.D.
Brit. J. Appl. Phy. 1963 14 667

[99] WALTERS K. and WATERS N.D.
Polymer Systems - Deformation and
Flow - Macmillon, London 1968

[100] WANG J.H. and YANG W.J.
Laminar and Turbulent Flow Conference 1983

[101] WATERS N.D. and KING M.J.
Q. Jl. Mech. Appl. Math. 1971 24 331

[102] WATERS N.D. and GOODEN D.K.
Q. Jl. Mech. Appl. Math. 1980 33 190

[103] WEIN O.
J. of Non-Newt. Fluid Mech. 1976 1 357

[104] WEIN O.
Rheol. Acta. 1977 16 248

[105] WEIN O.
J. of Non-Newt. Fluid Mech. 1979 5 297

[106] WHITE J.L. et al
Trans. Soc. Rheol 1977 21 1

[107] WHITE J.L. and IDE Y.
J. of Non-Newt. Fluid Mech. 1976 1 57

[108] WILLIAMS E.W.
J. of Non-Newt. Fluid Mech. 1976 1 57

[109] WILLIAMS R.W.
Ph.D. Thesis U.C. Wales 1979

[110] WILLIAMS R.W.
Rheol. Acta. 1979 18 345

[111] WILLIAMS R.W.
Rheol. Acta. 1980 19 448

[112] WILLIAMS R.W.
Polytechnic of Wales
Private Communication

NOMENCLATURE

a, b, c, d, e	coefficients of the matrix given in equation (4.36)
a_N, b_N	defined by equations (3.4) and (3.5) respectively
A, B	defined by equation (4.41)
A^X, A^Y, A^{XY}, A^{XX}, A^{YY}	defined by equations (4.58)
e_{ik}	rate of strain tensor
F	periodic function in equation (3.3)
F_p, F_s	defined by equations (4.52) and (4.53)
g	gravitational constant in equation (4.3) or shear rate
G_D, G_H	defined by equations (4.42) and (4.47) respectively
h, k	finite difference grid width and height
I	incompressibility
I_1, I_2, I_3 I_4, I_5	defined by equations (4.21), (4.22), (4.29), (4.30), and (4.31)
K_1, K_2	defined by equations (4.23) and (4.32) respectively
M	couple
n	parameter in Cross and Carreau models
N	number of data points
N_p	Power number
N_q	Pumping number
p	arbitrary isotropic pressure
P	defined by equation (4.17)
q	deformation rate
r	radius
r_b	outer radius of disc or cylindrical stirrer
r_c	radius of cylindrical container
r_g	inner radius of disc stirrer
Re	Reynolds number

t	time
T	time to complete one cycle of stream pattern
u	dimensionless angular velocity
V_r, V_θ, V_z	fluid velocities in r, θ, and z directions
V_x, V_y	dimensionless fluid velocities in x and y directions
V_{xq}, V_{yq}	velocity of particle q in x and y directions
W, W1	defined by equations (4.66)
x	dimensionless radius
x_b	dimensionless radius of rotor
x_c	dimensionless radius of cylindrical container
x_g	dimensionless inner radius of disc stirrer
y	dimensionless height
y_b	dimensionless height of fluid between base of container and base of rotor
y_c	dimensionless height of fluid in container
y_g	dimensionless height of upper part of disc rotor
z	height of tracer particle from bottom of container
z_b	height of fluid between base of container and base of rotor
z_c	height of fluid in container
α	dimensionless stream function
α_1	defined by equation (4.38)
β	defined by equation (4.56)
Ψ	stream function
ρ	density of the fluid
γ	strain rate
λ	parameter in Cross and Carreau equations
τ_{ij}	physical components of the extra stress tensor due to the structure of the fluid
η	Newtonian viscosity
$\eta(q)$	apparent viscosity

η_0	zero shear viscosity
η_∞	infinite shear viscosity
$\mu(\dot{\gamma})$	reduced viscosity
ω	rotational angular speed of the fluid
Ω	angular speed of the rotor
Γ	defined by equation (4.44)
χ	vorticity

APPENDICES

APPENDIX 1

A copy of the paper showing results from preliminary work on the solid aluminium cylindrical stirrer.

COMPARISON OF THEORETICAL AND EXPERIMENTAL FLOWS ABOUT A FINITE ROTATING CYLINDER

V. Bodalia, T.H. Hammond, D.G. Knight and R.W. Williams
Polytechnic of Wales, Pontypridd, CF37 1DL, U.K.

SUMMARY

The laminar flow of Newtonian and shear-thinning non-Newtonian fluids between a finite rotating cylinder and an outer cylindrical container is studied theoretically and experimentally. Numerical solutions for the primary flow velocity, shear rate and couple on the rotating cylinder are obtained using finite differences and the Strongly Implicit iterative method to model the governing non-linear partial differential equation. A flow visualisation technique is used to obtain experimental results for glycerol (Newtonian) and an aqueous solution of Carbopol 910 (non-Newtonian) which are found to be at least in reasonable agreement with theoretical predictions.

1. INTRODUCTION

This paper aims to make a contribution to the study of the low-speed mixing of viscous fluids. Such mixing is a commonly used but little understood industrial process. For simplicity our preliminary investigations are confined to the symmetric steady flow induced by a finite cylinder rotating with angular velocity Ω radians/sec in a fluid contained in a stationary flat bottomed outer cylinder (fig. 1a).

Both Newtonian and non-Newtonian fluids are considered, and since in this type of flow the usual dominant practical effect is the shear-thinning nature of the fluid (as opposed to properties such as elasticity or thixotropy) the non-Newtonian behaviour is taken to be a non-linear dependence of viscosity on shear rate. As relatively "thick" materials are considered attention need only be focussed on low Reynolds number flow. Results for fluid particle speed and rotor drag are obtained both by numerical simulation and experiment.

2. THEORY

Cylindrical polar coordinates (r, θ, z) are taken with the z-axis along the axis of rotation (fig. 1a). The base of the container (radius r_c) is at z=0 and the base of the rotor (radius r_b) is at $z=z_b$. The fluid surface is at $z=z_c$.

FIGURE 1

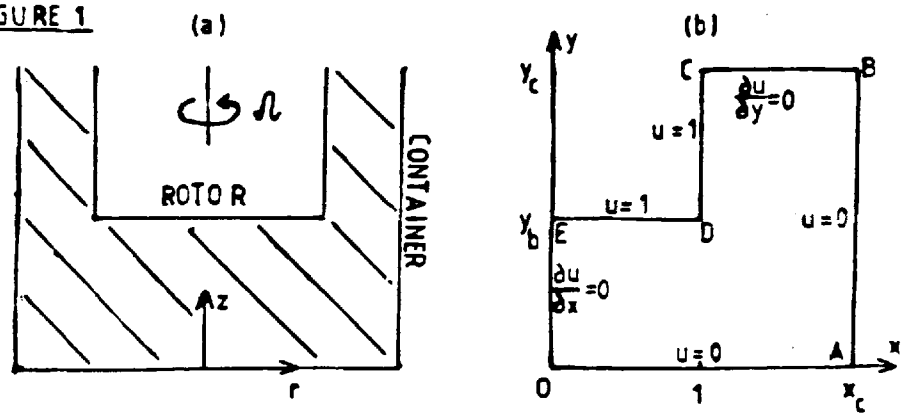

Non-dimensionalising by writing

$$z=r_b y \quad , \quad r=r_b x \tag{1}$$

and assuming inertial forces and secondary flow effects are negligible, we take the physical components of the axially symmetric primary flow velocity as

$$v_x=0 \quad , \quad v_\theta=r_b x\Omega u(x,y) \quad , \quad v_y=0. \tag{2}$$

The boundary conditions are (fig. 1b)

$u = 0$ on OA, AB ; $u = 1$ on DE, CD ;

$\partial u/\partial y = 0$ on BC (no normal flow); (3)

$\partial u/\partial x = 0$ on OE (symmetry),

where $x_c = r_c/r_b$, $y_b=z_b/r_b$, $y_c=z_c/r_b$. (4)

For the relation between the stress tensor p_{ik} and the velocity we choose the purely viscous generalised Newtonian fluid with equation of state

$$p_{ik} = -p\delta_{ik} + 2\eta(q)\,\overset{(1)}{e}_{ik} \quad , \tag{5}$$

where p is an arbitary isotropic pressure and the shear rate q is the second invariant of the first rate-of-strain tensor $\overset{(1)}{e}_{ik}$ [1,2].

Depending on the precise form of the variable viscosity $\eta(q)$ equation (5) yields fluid models [2] such as the Cross and Carreau models with

$$\eta(q)=\eta_\infty + (\eta_o-\eta_\infty) \; / \; (1+(\lambda q)^{1-n}), \lambda>0 \tag{6}$$

$$\eta(q)=\eta_\infty + (\eta_o-\eta_\infty) \; (1+\lambda^2 q^2)^{(n-1)/2} \tag{7}$$

respectively, where η_o (the zero-shear viscosity), η_∞ the infinite shear viscosity), λ and n are constants.

Substituting (2) into the stress equations of motion in their cylindrical polar form [1,2] and noting that $\partial/\partial\theta \equiv 0$ yields

$$\frac{\partial}{\partial x}\left(P(x,y)\frac{\partial u}{\partial x}\right) + \frac{\partial}{\partial y}\left(P(x,y)\frac{\partial u}{\partial y}\right) = 0 \tag{8}$$

where $P(x,y) = x^3 \mu(\gamma)$ (9)

$$\mu(\gamma) = \eta(\Omega\gamma)/\eta_o \tag{10}$$

and $$\gamma = x\left((\partial u/\partial x)^2 + (\partial u/\partial y)^2\right)^{\frac{1}{2}} . \tag{11}$$

The problem now centres on solving (8) for u subject to (3).

The couple M on the rotor is given by

$$M = 2\pi\Omega\eta_o r_b^3 \left[\int_0^1 x^3 \mu(\gamma) \left|\frac{\partial u}{\partial y}\right| dx + \int_{y_b}^{y_c} \mu(\gamma) \left|\frac{\partial u}{\partial x}\right| dy \right] \tag{12}$$

but since each derivative of u has a singularity at D there is some difficulty in using (12) as it stands. Following the standard technique [3] for removing such singularities we can evaluate M as

$$M = 2\pi\Omega\eta_o r_b^3 \; [\, I + J + K \,] \tag{13}$$

where

$$I = \int_0^1 x^3 \left[\mu(\gamma) \left|\frac{\partial u}{\partial y}\right| - \frac{2}{3}\mu_\infty G \, (1-x)^{-1/3}\right] dx \tag{14}$$

$$J = \int_{y_b}^{y_c} \left[\mu(\gamma) \left|\frac{\partial u}{\partial x}\right| - \frac{2}{3}\mu_\infty G \, (y-y_b)^{-1/3}\right] dy \tag{15}$$

$$K = \mu_\infty G \, (81/220 + (y_c - y_b)^{2/3}) \tag{16}$$

Both integrands are taken to be zero at the corner. G is a constant to be determined from a knowledge of u near the corner.

3. FINITE DIFFERENCE APPROXIMATION

Taking a grid defined by

$$x_i = ih, (i=0,1..n,n+1,..N); \; y_j = jk, (j=0,1..m,m+1..M) \tag{17}$$

$$\text{where} \quad nh=1, \; Nh=x_c, \; mk=y_b, \; Mk=y_c \tag{18}$$

then (8) can be discretised [4,5] at interior grid points by

$$-a_{ij}u_{i,j-1} - b_{ij}u_{i-1,j} + c_{ij}u_{i,j} - d_{ij}u_{i+1,j} - e_{ij}u_{i,j+1} = 0 + O(h^3) \tag{19}$$

where

$$a_{ij} = \frac{1}{\alpha} P_{i,j-\frac{1}{2}}, \; b_{ij} = \alpha P_{i-\frac{1}{2},j}; \; d_{ij} = \alpha P_{i+\frac{1}{2},j}, \; e_{ij} = \frac{1}{\alpha} P_{i,j+\frac{1}{2}} \tag{20}$$

$$\alpha = k/h, \quad c_{ij} = a_{ij} + b_{ij} + d_{ij} + e_{ij} . \tag{21}$$

From boundary OE and BC we have

$$u_{o,j} = (4/3)u_{1,j} - (1/3)u_{2,j} + O(h^3) \tag{22}$$

$$u_{i,M} = (4/3)u_{i,M-1} - (1/3)u_{i,M-2} + O(h^3). \tag{23}$$

Equations (19),(22),(23) give a set of simultaneous equations

$$AU = B \tag{24}$$

in which B is a known vector of length (N-1)(M-1), U is the unknown and A is a block tri-diagonal (N-1)(M-1) by (N-1)(M-1) matrix. We solve (24) iteratively using the Strongly Implicit Method [6,7] . As our initial approximation for u we take a Newtonian Couette flow [1] above D, a linear approximation directly beneath the rotor and in the remaining region a linear combination of both the Couette and below-rotor approximations.

Provision was made within the program to obtain u(x,y) for a particular non-Newtonian fluid by starting from a Newtonian solution. The required non-Newtonian solution could be reached via a sequence of steps in which the non-Newtonian parameters were incremented from Newtonian towards those of the required fluid. However it was found that the same non-Newtonian solution could be obtained in one direct step from

the initial approximation described above.

The shear rate $\gamma(x,y)$ was also iteratively calculated (to $O(h^2)$) from $u(x,y)$ until converged values were obtained and Richardson extrapolation was used to improve the accuracy of u and γ. Convergence was typically obtained within 150 iterations (80 seconds run-time on a DEC-20 mainframe) for a suitable choice of the iteration acceleration factor [6] even for quite markedly shear-thinning fluids such as the Carreau model with $\eta_o = 10$, $\eta_\infty = 0.1$, $\lambda=1$, $n=0.5$, and with $h = k = 0.05$ when $y_b=1$ $x_c = 2$ $y_c = 2$.

Typical u and γ contours are presented (Figs. 2,3). For fluids with the same η_o the more shear-thinning fluid has the fluid motion confined closer to the rotor - a typical pseudoplastic effect.

FIGURE 2-u Contours

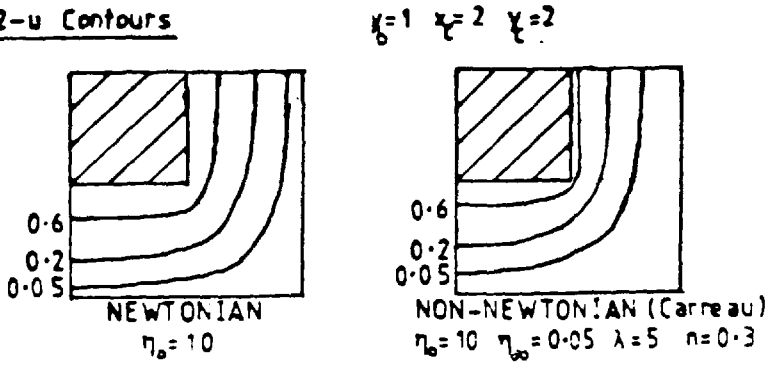

FIGURE 3-$\dot{\gamma}$ Contours

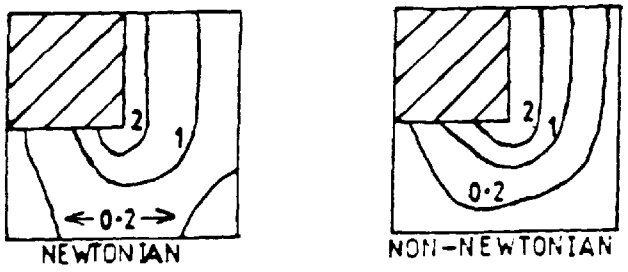

Geometry and Fluid as in Figure2

The couple M was calculated from u and γ using the trapezium rule and equation (12), where G is given[3] by

$$G = (2/\sqrt{3})k^{-2/3}\left[\alpha^{4/3}(u_{n+1,m}-1)+(u_{n,m-1}-1)\right] / (\alpha^{2/3}+1) + O(h^{8/3}) \qquad (25)$$

Typical results are given in Section 4.

4. COMPARISION WITH EXPERIMENT

4.1 Description

A blackened aluminium rotor turned by a Haake Rotovisco viscometer and perspex container (with r_b=2cm, r_c=3.8 cm, y_b= 1·2 (small gap) or 2·1 cm (large gap)) were used. Coloured tinsel particle positions were recorded as functions of time by video cameras viewing the (r,z) and (r, θ)planes. From the radius and period of each particle orbit a primary flow velocity was found. At a chosen Ω (16 rpm) the particles maintained fixed orbits for many minutes without settling and no significant secondary flow was seen. The couple was determined by a dynamometer in the viscometer.

The test fluids were a 10 poise (glycerol/water) Newtonian fluid and an aqueous solution of Carbopol 910 of nominal viscosity 9 poise. The Carbopol was markedly shear-thinning but did not show any significant thixotropic, elastic or yield stress behaviour. The model parameters η_o, η_∞, λ and n were obtained (to an error <1.5%) from the viscometer viscosity curve using a non-linear minimization technique, and then used in the program for finding u, γ and M.

The Reynolds number Re (incorporating the gap z_b) used to determine the speed of flow for a fluid of density ρ is

$$Re = \rho r_b^2 \Omega^2 / \bar{q}n(\bar{q}) \quad , \quad \bar{q} = r_b\Omega/z_b. \tag{26}$$

4.2 Results

(a) In Fig. 4 numerically computed u-values are plotted against experimental u-values. The data points lie reasonably near the bold line signifying the expected values. The scatter for small u-values can be assumed due to inherent experimental error.

FIGURE 4 – u values

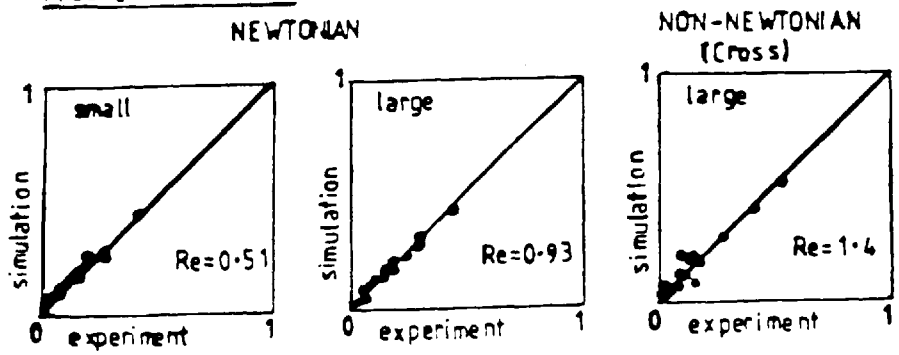

Small gap Carbopol results were adversely affected by thermal currents generated by camera illumination and are not presented. In agreement with Fig. 3 Carbopol fluid speed at a fixed position near the cylinder is faster than for glycerol.

(b) Fig. 5 compares numerical and experimental couples and includes experimental error bars and Reynolds numbers. There is remarkable small gap Newtonian agreement and higher speed divergence is due to secondary flow effects [8-10] .

FIGURE 5-Couples

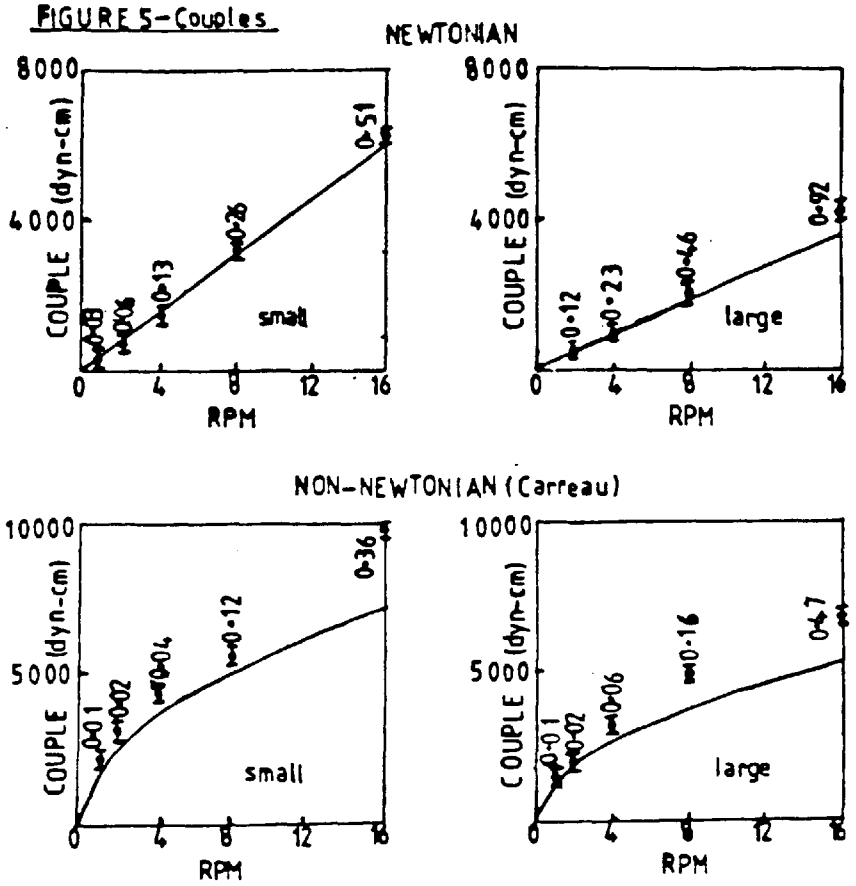

A quantitative comparison of Carbopol results is probably affected by extrapolation of viscosity data outside the measured viscosity range when using fluid model parameters.

5. CONCLUSION

(a) Numerical and experimental u-values are in reasonable agreement for all fluids.

(b) Numerical and experimental couple values agree well quantitatively for Newtonian flow with secondary flow effects apparent for $Re > 0.2$. For non-Newtonian flow there is good qualitative and fair quantitative agreement with secondary flow effects apparent for $Re \geq 0.1$.

(c) Secondary flow in the present geometry, primary and secondary flow in polygonal geometries and the incorporation of slightly elastic fluid models are the subject of ongoing work.

ACKNOWLEDGEMENT

The authors thank Dr. H.A. Barnes of Unilever Research for his interest and encouragement.

REFERENCES

1. WALTERS, K. - Rheometry, Chapman and Hall, London, 1975.

2. BIRD, R.B., ARMSTRONG, R.C. and HASSAGER, O. - Dynamics of Polymeric Liquids : Vol.1. Fluid Mechanics, John Wiley, New York, 1977.

3. MITCHELL, A.R. - Computational Methods in Partial Differential Equations, John Wiley, London, 1969.

4. AMES, W.F. - Numerical Methods for Partial Differential Equations, Nelson, London 1977.

5. PADDON, D.J. and WALTERS, K. - 'On edge effects and related sources of error in rotational rheometry', Rheol.Acta., 1979, 18, 565.

6. SMITH, G.D. - Numerical Solution of Partial Differential Equations : Finite Difference Methods, Oxford University Press, 1978.

7. NAG Fortran Library Manual Mark 10, Numerical Algorithms Group, Oxford, 1983.

8. WILLIAMS, R.W. - 'On the secondary flow induced by spheres and discs rotating in elastico-viscous liquids'. Rheol.Acta., 1980, 19, 548.

9. WEIN, O. - 'Rotational quasi-viscometric flows around a rotating sphere', J. non-Newtonian Fluid Mechanics, 1979, 5, 297.

10. WATERS, N.D. and GOODEN D.K. - 'The couple on a rotating oblate spheroid in an elastico-viscous', Q.Jl.Mech. Appl. Math., 1980, 33, 189.

APPENDIX 2

Listings of computer programs used for the calculation of experimental primary and secondary flow parameters.

```
C*************** PRIMARY FLOW EXPERIMENT DATA PROCESSING *****************

      character*12, datain,rotor,fluid,gapsiz,
     &              temp,date,ugout,
     &              thu,thg,vel,shear

      character*1,answer

      dimension t(100),t1(100),t2(100),h(100),h1(100),h2(100),sd(100),
     &          yn1(100),xn(100),yp(100),xp(100),yn2(100),sp(100),
     &          x(100),y(100),x2(100),y2(100),r(100),u(100),gam(100),
     &          xf(100),yf(100),u1(100),u2(100),u3(100),u4(100),
     &          g1(100),g2(100),g3(100),g4(100),udiff(100),gdiff(100),
     &          um1(100),um2(100),uth(100),gm1(100),gm2(100),gth(100)

      integer srevs
      real meanu,meang

      type*;type*,'do you want to create x-y files?  (y/n)'
      accept 'a1',answer
      if ((answer.eq.'y').or.(answer.eq.'Y'))call filexy
5     type*,'input the number of data points,n'
      accept*,n
      type*,'input speed in revs per min. srevs'
      accept*,srevs
      type*,'input radius of rotor rb in mm'
      accept*,rb
      type*,'input xo,yo'
      accept*,xo,yo
      type*,'input tolh'
      accept*,tolh

      type*,'insert name of input file'
      read(5,100)datain
      type*,'insert name of thu input file'
      read(5,100)thu
      type*,'insert name of thg input file'
      read(5,100)thg
      type*,'insert name for u output file'
      read(5,100)vel
      type*,'insert name for g output file'
      read(5,100)shear
      type*,'insert name for output file'
      read(5,100)ugout

      type*,'input type of rotor'
      read(5,100)rotor
      type*,'input name of fluid'
      read(5,100)fluid
      type*,'input gap-size'
      read(5,80)gapsiz
      type*,'input temperature'
      read(5,80)temp
      type*,'input date of experiment'
      read(5,100)date

      open(unit=30,file=datain,status='old')

      do 10 i=1,n
      read(30,*),t1(i),yn1(i),h1(i),xn(i),xp(i),yp(i),t2(i),yn2(i),
     & h2(i)

      yn1(i) = yn1(i)+yo;   yn2(i) = yn2(i)+yo;   yp(i) = yp(i)-yo
      xn(i) = xn(i)+xo;     xp(i) = xp(i)-xo

      r(i) = (yn1(i)+xn(i)+xp(i)+yp(i)+yn2(i))*0.8
      x(i) = r(i)/rb
      h(i) = 0.5*((h1(i)+h2(i))*4)
      y(i) = h(i)/rb
      t(i) = t2(i)-t1(i)
      sp(i)= 60/t(i)
      u(i) = sp(i)/srevs

10    continue

      toll=0.1

c     ********** particle sorting **********

c     for each particle
      do 30 i=1,n

c     search through the particles
      kmin=0;   gama=0.0;  gamas=0.0;  gamasq=0.0

      do 20 j=1,n

      dx=abs(x(j)-x(i));   dy=abs(y(j)-y(i))
      if((dx.lt.toll).or.(dx.gt.tolh)) go to 20
      if((dy.lt.toll).or.(dy.gt.tolh)) go to 20
```

```
      kmin=kmin+1
      du=u(j)-u(i)
      gama=x(i)*sqrt((du/dx)**2+(du/dy)**2)
      gamas= gamas + gama
      gamasq= gamasq + gama**2
20    continue

      if(kmin.gt.1) then
         gam(i)= gamas/kmin
         first= kmin / (kmin-1)
         second= gamasq / kmin
         third= (gamas/kmin)**2
         sd(i)= sqrt((second-third)*first)     ! standard deviation
      else
         gam(i)=0.0
         if(kmin.eq.1) gam(i)=gamas/kmin
         sd(i)= 0.0
      end if
30    continue


c     ********** theoretical u & g values **********
c     *** u values ***

      open(unit=41,file=thu,status='old')
         icount=0; sum=0.0; sumsq=0.0
         do 60 i=1,n
         read(41,*),xf(i),yf(i),u1(i),u2(i),u3(i),u4(i)
         um1(i) = ((x(i)-xf(i))*(u2(i)-u1(i))/0.1)+u1(i)
         um2(i) = ((x(i)-xf(i))*(u4(i)-u3(i))/0.1)+u3(i)
         uth(i) = ((y(i)-yf(i))*(um2(i)-um1(i))/0.1)+um1(i)
         udiff(i)'= ((uth(i)-u(i))/uth(i))*100.

         icount=icount+1
         sum=sum+udiff(i)
         sumsq=sumsq+udiff(i)*udiff(i)
60    continue
         first= icount/(icount-1)
         second= sumsq/icount
         third= (sum/icount)**2
         stdu= sqrt((second-third)*first)  !std. dev. of udiff(i)

         meanu = sum/icount


c     *** g values ***
      open(unit=42,file=thg,status='old')
         icount=0; sum=0.0; sumsq=0.0
         do 70 i=1,n
         read(42,*),xf(i),yf(i),g1(i),g2(i),g3(i),g4(i)
         gm1(i) = ((x(i)-xf(i))*(g2(i)-g1(i))/0.1)+g1(i)
         gm2(i) = ((x(i)-xf(i))*(g4(i)-g3(i))/0.1)+g3(i)
         gth(i) = ((y(i)-yf(i))*(gm2(i)-gm1(i))/0.1)+gm1(i)
         gdiff(i) = ((gth(i)-gam(i))/gth(i))*100.

         icount=icount+1
         sum=sum+gdiff(i)
         sumsq=sumsq+gdiff(i)*gdiff(i)
70    continue
         first= icount/(icount-1)
         second= sumsq/icount
         third= (sum/icount)**2
         stdg= sqrt((second-third)*first)  !std. dev. of gdiff(i)

         meang = sum/icount


      open(unit=69,file=ugout,status='new')
      open(unit=43,file=vel,status='new')
      open(unit=45,file=shear,status='new')

      write(69,200)ugout
      write(69,250)datain
      write(69,300)rotor,fluid,gapsiz
      write(69,400)srevs
      write(69,500)temp,date
      write(69,600)tolh,xo,yo
      write(69,930),meanu,stdu,meang,stdg
      write(69,900),n
      write(69,800)
      write(43,650)datain
      write(45,700)datain

      do 55 i=1,n
      write(69,900),i,x(i),y(i),u(i),gam(i),sd(i),udiff(i),gdiff(i)
      write(43,910),u(i),uth(i)
      write(45,920),gam(i),gth(i)
55    continue

80    format(a7)
100   format(a12)
```

```
200     format(' THIS OUTPUT IS FROM ',A12)
250     format(' DATA INPUT FILE IS ',A12,/)
300     format(' ROTOR = ',A12,'     FLUID = ',A12,
     &        '      GAP-SIZE = ',A7)
400     format(' SPEED OF ROTOR = ',I3,'RPM',' TYPE OF FLOW = PRIMARY')
500     format(' TEMPERATURE = ',A7,'    DATE OF EXPT. ',A12)
600     format(' TOLH = ',F4.1,'  XO = ',F5.2,'  YO = ',F5.2,/)
650     format(' COMPARISON OF U VALUES FOR ',A12,/,
     &        ' EXPERIMENTAL U',/,' THEORETICAL U')
700     format(' COMPARISON OF G VALUES FOR ',A12,/,
     &        ' EXPERIMENTAL G',/,' THEORETICAL G')
800     format('    I     X(I)      Y(I)      U(I)
     &      GAM(I)      SDG(I)     UDIFF(I)     GDIFF(I)   ')
900     format(1x,i4,3(3x,f7.3),f13.6,(3x,f7.3),2(1x,f13.6))
910     format(1x,2(f7.3))
920     format(1x,2(f13.6))
930     format(1X,'FOR UDIFF(I), MEAN = ',F7.3,'   STANDARD DEVIATION '
     &,'= ',F7.3,
     &      /,' FOR GDIFF(I), MEAN = ',F7.3,'   STANDARD DEVIATION = ',
     &  F7.3,//)

        close(unit=30,status='keep')
        close(unit=69,status='keep')
        close(unit=41,status='keep')
        close(unit=42,status='keep')
        close(unit=43,status='keep')
        close(unit=45,status='keep')
        type*;type*;type*,'run the program again?  (y/n)'
        accept '(a1)',answer
        if((answer.eq.'y').or.(answer.eq.'Y')) go to 5
        stop
        end


        subroutine filexy
        character*12, datain,ugout,answer

        dimension t1(100),t2(100),h(100),h1(100),h2(100),
     &            yn1(100),xn(100),yp(100),xp(100),yn2(100),
     &            x(100),y(100),r(100)

10      type*;type*,'       *****   create  xy files    *****'
        type*;type*
        type*,'input the number of data points,n'
        accept*,n
        type*,'input xo,yo'
        accept*,xo,yo
        rb=19.5; srevs=16; tolh=0.4

        type*,'input name of input file'
        read(5,100)datain
        type*,'input name for  xy  output file'
        read(5,100)ugout
        open(unit=30,file=datain,status='old')

        do 20 i=1,n
        read(30,*),t1(i),yn1(i),h1(i),xn(i),xp(i),yp(i),t2(i),yn2(i),
     &  h2(i)

        yn1(i) = yn1(i)+yo;   yn2(i) = yn2(i)+yo;   yp(i) = yp(i)-yo
        xn(i) = xn(i)+xo;     xp(i) = xp(i)-xo
        r(i) = (yn1(i)+xn(i)+xp(i)+yp(i)+yn2(i))*0.8
        x(i) = r(i)/rb
        h(i) = 0.5*((h1(i)+h2(i))*4)
        y(i) = h(i)/rb

20      continue

        open(unit=49,file=ugout,status='new')
        write(49,200)ugout
        write(49,250)datain
        do 50 i=1,n
        write(49,*),x(i),y(i)
50      continue

80      format(a7)
100     format(a12)
200     format(' THIS OUTPUT IS FROM ',A12)
250     format(' DATA INPUT FILE IS ',A12,/)

        close(unit=30,status='keep')
        close(unit=49,status='keep')
        type*;type*,'create another  xy  file?  (y/n)'
        accept 'a1',answer
        if ((answer.eq.'y').or.(answer.eq.'Y')) goto 10
        stop
        end
```

```
C****************** SECONDARY FLOW PART 1 *************************
C***************** EXPERIMENT DATA PROCESSING *********************
C***** SMOOTHING OF RAW DATA & CALCULATION OF VELOCITIES **********

      character*12, datain,rotor,fluid,gapsiz,sxy,xy,reply1,
     &              date,temp,vel,master,xbyb,reply,mxsys

      dimension t(500),xb(500),yb(500),th(500),x(500),y(500),
     &          xg(500),yg(500),h(500),xd(500),yd(500),thd(500),
     &          ys(500),ths(500),ax(500),bx(500),ay(500),by(500),
     &          xs(500),ath(500),bth(500)
      real k,kk
      integer srev,d,f

      iddum=1
      iround=1
5     type*,'input the number of data points,d'
      accept*,d
      type*,'input speed in revs per min. srevs'
      accept*,srev
      type*,'input xo,yo'
      accept*,xo,yo
      type*,'input f for d/f'
      accept*,f

      type*,'input name of input file'
      read(5,100)datain
      type*,'input name for vel output file'
      read(5,100)vel
      type*,'input name for sxy output file'
      read(5,100)sxy
      type*,'input name for xy output file'
      read(5,100)xy
      type*,'input name for  xbyb  output file'
      read(5,100)xbyb

      if (iround.eq.1)then
          type*,'do you want to open a xsys master file ?   (y/n)'
          accept '(a1)',reply1

          if ((reply1.eq.'y').or.(reply1.eq.'Y')) then
              type*,'input name of the xsys master file'
              accept 100,mxsys
              open(unit=50,file=mxsys,status='new')

              if (iround.eq.1) then
                  write(50,125)datain
                  write(50,110)mxsys
                  write(50,250)
                  iround=0
              end if
          end if
      end if

      if (iddum.eq.1)then
          type*,'do you want to open a general master file ?   (y/n)'
          accept '(a1)',reply

          if ((reply.eq.'y').or.(reply.eq.'Y')) then
              type*,'input name of the general master file'
              accept 100,master
              open(unit=42,file=master,status='new')
              iddum=0
          end if
      end if
      type*,'input type of rotor'
      read(5,100)rotor
      type*,'input name of fluid'
      read(5,100)fluid
      type*,'input gap-size'
      read(5,90)gapsiz
      type*,'input temperature in deg. celsius'
      read(5,90)temp
      type*,'input date of experiment'
      read(5,100)date

      s=srev*0.1047
      open(unit=30,file=datain,status='old')

        do 10 i=1, d
        read(30,*),xg(i),yg(i),h(i)
        xb(i) = ((xg(i)-xo)*4)/19.5
        yb(i) = ((yg(i)-yo)*4)/19.5
        x(i) = sqrt(xb(i)**2 + yb(i)**2)
        y(i) = (h(i)*4)/19.5
10      continue
```

```
      th(1)=0.0
      t(1)=0.0

        do 20 i = 2, d
        t(i) = t(i-1) + 0.4
        tile = (xb(i-1)*xb(i)+yb(i-1)*yb(i))/(x(i)*x(i-1))
        tile = acos(tile)
        type*,i,'theta = ',tile
        check = yb(i-1)*xb(i)-xb(i-1)*yb(i)
        if(check.lt.0.0) tile = 6.283185308-tile
        th(i) = th(i-1)+tile
        type*,th(i)
20      continue

      p=t(d)
      k=6.2832/p
      nmax=d/f
      xxx=th(d)
      do 25 i=1,d
         th(i)=th(i)+xxx*(1.0-t(i)/p)
25    continue

      do 40 n = 0 ,nmax+1
         sax=0
         say=0
         sbx=0
         sby=0
         sath=0
         sbth=0
         do 30 i=2 , d
              t1=t(i-1)
              t2= t(i)
              dt= t2-t1
              a1= k*n*t1
              a2= k*n*t2
              c1=cos(a1)
              c2=cos(a2)
              s1=sin(a1)
              s2=sin(a2)

              x1=x(i-1)
              x2=x(i)
              y1=y(i-1)
              y2= y(i)
              th1=th(i-1)
              th2=th(i)

              sax = sax + dt*(x1*c1 + x2*c2)
              say = say + dt*(y1*c1 + y2*c2)
              sath = sath + dt*(th1*c1 + th2*c2)
              if (n.lt.1) goto 30

              sbx = sbx + dt*(x1*s1 + x2*s2)
              sby = sby + dt*(y1*s1 + y2*s2)
              sbth = sbth + dt*(th1*s1 + th2*s2)
30       continue

         ax(n+1) = sax/p
         ay(n+1) = say/p
         ath(n+1) = sath/p
         if (n .lt. 1) go to 40
         bx(n+1) = sbx/p
         by(n+1) = sby/p
         bth(n+1) = sbth/p
40    continue

c     ***** calc. smoothed x, y, th, xd, yd, thd *****

      do 60 i = 1,d
         xsn = ax(1)/2
         ysn = ay(1)/2
         thsn = ath(1)/2
         xd1 = 0
         yd1 = 0
         thd1 = 0
         t1 = t(i)

         do 50 n = 1, nmax
              kk  = k*n*t1
              c1 = cos(kk)
              s1 = sin(kk)
```

```
              xsn = xsn + ax(n+1)*c1 + bx(n+1)*s1
              ysn = ysn + ay(n+1)*c1 + by(n+1)*s1
              thsn = thsn + ath(n+1)*c1 + bth(n+1)*s1

              xd1 = xd1 + n*(bx(n+1)*c1 - ax(n+1)*s1)
              yd1 = yd1 + n*(by(n+1)*c1 - ay(n+1)*s1)
              thd1 = thd1 + n*(bth(n+1)*c1 - ath(n+1)*s1)
50          continue

            xs(i) =xsn
            ys(i) =ysn
            ths(i) =thsn-xxx*(1.0-t(i)/p)
            xd(i) = k*xd1/s
            yd(i) = k*yd1/s
            thd(i) =abs((k*thd1+xxx/p)/s)
            th(i) = th(i)-xxx*(1.0-t(i)/p)
60        continue

          open(unit=25,file=vel,status='new')
          open(unit=31,file=sxy,status='new')
          open(unit=43,file=xy,status='new')
          open(unit=41,file=xbyb,status='new')

          write(25,110)vel
          write(25,120)datain
          write(25,130)rotor,fluid,gapsiz
          write(25,140)srev
          write(25,150)temp,date
          write(25,155)xo,yo
          write(25,160)
          write(31,125)datain
          write(41,125)datain
          write(43,125)datain
          write(31,170)f
          write(41,210)
          write(31,175)
          write(41,220)
          write(43,230)
          write(43,240)

          do 70 i=1,d
             write(25,180),i,xs(i),ys(i),xd(i),yd(i),thd(i),xs(i)*thd(i)
             write(31,*),xs(i),ys(i)
             write(41,*),xb(i),yb(i)
             write(43,*),x(i),y(i)
             if((reply1.eq.'y').or.(reply1.eq.'Y'))write(50,*),xs(i),ys(i)
             if ((reply.eq.'Y').or.(reply.eq.'y')) write(42,*),
     &       xs(i),ys(i),xd(i),yd(i),thd(i)
70        continue

90        format(a7)
100       format(a12)
110       format(' THIS OUTPUT IS FROM ',A12)
120       format(' DATA INPUT FILE IS ',A12,/)
125       format(' DATA INPUT FILE IS ',A12)
130       format(' ROTOR = ',A12,'     FLUID = ',A12,
     &    '      GAP-SIZE = ',A7)
140       format(' SPEED OF ROTOR = ',I3,' RPM',' TYPE OF FLOW = SECONDARY')
150       format(' TEMPERATURE = ',A7,'    DATE OF EXPT. ',A12,/)
155       format(' XO = ',F6.2,'   YO = ',F6.2,/)
160       format('    I       XS(I)         YS(I)         XD(I)
     &    YD(I)       THD(I)      XS(I)*THD(I)')
170       format(' SMOOTHED X  (F = ',I3,')')
175       format(' SMOOTHED Y')
180       format(1X,I4,6(F13.6))
210       format(' XB')
220       format(' YB')
230       format(' X(I)')
240       format(' Y(I)')
250       format(' MASTER XSYS')

          close(unit=25,status='keep')
          close(unit=30,status='keep')
          close(unit=31,status='keep')
          close(unit=41,status='keep')
          close(unit=43,status='keep')

          type*,'want to analyse another file?   (y/n)'
          accept '(a1)',reply
          if((reply.eq.'y').or.(reply.eq.'Y'))goto 5
          close(unit=42,status='keep')
          close(unit=50,status='keep')
          stop
          end
```

```
C******************** SECONDARY FLOW PART 2 ************************
C***************** EXPERIMENT DATA PROCESSING ********************
C******* CALCULATE SHEAR-RATES, VORTICITY, INCOMPRESSIBILITY ******

      character*12, datain,fluid,gapsiz,flow,date,thu,thg,thv,
     &              rotor,temp,vort,inco,shear,vel,
     &              comu,comg,comv

      dimension x(500),y(500),sdg(500),gam(500),
     &          xd(500),yd(500),xinc(500),sdv(500),
     &          sdx(500),vor(500),u(500),xf(500),yf(500),
     &          u1(500),u2(500),u3(500),u4(500),udiff(500),
     &          g1(500),g2(500),g3(500),g4(500),gdiff(500),
     &          v1(500),v2(500),v3(500),v4(500),vdiff(500),
     &          um1(500),um2(500),uth(500),vth(500),v(500),g(500),
     &          gm1(500),gm2(500),gth(500),vm1(500),vm2(500)

      integer srevs
      real meanu,meang,meanv,meani

      type*,'input the number of data points,n'
      accept*,n
      type*,'input speed in revs per min. srevs'
      accept*,srevs
      type*,'input xo,yo'
      accept*,xo,yo
      type*,'input tolh'
      accept*,tolh

      type*,'insert name of master input file'
      read(5,100)datain
      type*,'insert name for  thu  input file'
      read(5,100)thu
      type*,'insert name for  thg  input file'
      read(5,100)thg
c     type*,'insert name for  thv  input file'
c     read(5,100)thv
      type*,'insert name for  vel  output file'
      read(5,100)vel
      type*,'insert name for  shear  output file'
      read(5,100)shear
c     type*,'insert name for  vort  output file'
c     read(5,100)vort
      type*,'insert name for  inco  output file '
      read(5,100)inco
      type*,'insert name for comparison of u output file '
      read(5,100)comu
      type*,'insert name for comparison of g output file '
      read(5,100)comg
c     type*,'insert name for comparison of v output file '
c     read(5,100)comv

      type*,'input type of rotor'
      read(5,100)rotor
      type*,'input name of fluid'
      read(5,100)fluid
      type*,'input gap-size'
      read(5,90)gapsiz
      type*,'input temperature in deg. celsius'
      read(5,90)temp
      type*,'input date of experiment'
      read(5,100)date


c     open(unit=31,file=vort,status='new')
      open(unit=41,file=inco,status='new')
      open(unit=25,file =shear,status='new')
      open(unit=45,file=vel,status='new')
      open(unit=30,file=datain,status='old')
      open(unit=51,file=comu,status='new')
      open(unit=52,file=comg,status='new')
c     open(unit=53,file=comv,status='new')

      do 30 i=1,n
      read(30,*),x(i),y(i),xd(i),yd(i),u(i)
30    continue
```

```
c       ***** x(i), y(i), u(i) ARE SMOOTHED VALUES FROM sec1.for *****
          toll=0.1
        do 60 i=1, n

c       ***** SEARCH THROUGH PARTICLES *****
        sg=0.0
        sqg=0.0
        sv=0.0
        sqv=0.0
        sx=0.0
        sqx=0.0
        kmin=0

        do 40 j=1,n
              dx=abs(x(j)-x(i))
              dy=abs(y(j)-y(i))
              if ((dx.lt.toll).or.(dx.gt.tolh)) go to 40
              if ((dy.lt.toll).or.(dy.gt.tolh)) go to 40

              kmin=kmin + 1
              du=u(j)-u(i)
              dxd=xd(j)-xd(i)
              dyd=yd(j)-yd(i)
              dx=(x(j)-x(i))
              dy=(y(j)-y(i))

              gap=2*(((dxd/dx)**2)+((dyd/dy)**2)+((xd(i)/x(i))**2))
              gap=gap+(x(i)**2)*(((du/dx)**2)+((du/dy)**2))
              gap=sqrt(gap+(((dxd/dy)+(dyd/dx))**2))
              sg=sg+gap
              sqg=sqg+gap**2

              vop=((dxd/dy) - (dyd/dx))
              sv=sv+vop
              sqv=sqv+vop**2

              xip=x(i)*((dxd/dx) + (dyd/dy)) + xd(i)
              xpi=x(i)*(abs(dxd/dx) + abs(dyd/dy)) + abs(xd(i))
              xip=xip/xpi*100
              sx=sx+xip
              sqx=sqx+xip**2


40      continue

           if (kmin.gt.1) then
                cmin=float(kmin)
                gam(i)=sg/cmin
                vor(i)=sv/cmin
                xinc(i)=sx/cmin
                one=cmin/(cmin-1)
                twog=sg/cmin
                twov=sv/cmin
                twox=sx/cmin
                threeg=sqg/cmin
                threev=sqv/cmin
                threex=sqx/cmin
                sdg(i)=sqrt((threeg-twog**2)*one)
                sdv(i)=sqrt((threev-twov**2)*one)
                sdx(i)=sqrt(abs((threex-twox**2)*one))
           else
                gam(i)=0
                vor(i)=0
                xinc(i)=0
                sdg(i)=0
                sdv(i)=0
                sdx(i)=0
                   if (kmin.eq.1) then
                      gam(i)=sg
                      vor(i)=sv
                      xinc(i)=sx
                   end if
           end if
60      continue

        open(unit=42,file=thu,status='old')
        icount=0
        sum=0.0
        sumsq=0.0
        do 62 i=1,n
              read(42,*),xf(i),yf(i),u1(i),u2(i),u3(i),u4(i)
              um1(i)=((x(i)-xf(i))*(u2(i)-u1(i))/0.1)+u1(i)
              um2(i)=((x(i)-xf(i))*(u4(i)-u3(i))/0.1)+u3(i)
              uth(i)=((y(i)-yf(i))*(um2(i)-um1(i))/0.1)+um1(i)
              udiff(i)=((uth(i)-u(i))/uth(i))*100.0
```

```
            icount=icount+1
            sum=sum+udiff(i)
            sumsq=sumsq+ udiff(i)*udiff(i)
62      continue

        count=float(icount)
        first=count/(count-1)
        second= sumsq/count
        third= (sum/count)**2
        stdu= sqrt((second-third)*first)   ! std.dev of udiff(i)
        meanu = sum/count

        open(unit=43,file=thg,status='old')
        icount=0
        sum=0.0
        sumsq=0.0
        do 65 i=1,n
             read(43,*),xf(i),yf(i),g1(i),g2(i),g3(i),g4(i)
             gm1(i)=((x(i)-xf(i))*(g2(i)-g1(i))/0.1)+g1(i)
             gm2(i)=((x(i)-xf(i))*(g4(i)-g3(i))/0.1)+g3(i)
             gth(i)=((y(i)-yf(i))*(gm2(i)-gm1(i))/0.1)+gm1(i)
             gdiff(i)=((gth(i)-gam(i))/gth(i))*100.0

             icount=icount+1
             sum=sum+gdiff(i)
             sumsq=sumsq+ gdiff(i)*gdiff(i)
65      continue

        count=float(icount)
        first=count/(count-1)
        second= sumsq/count
        third= (sum/count)**2
        stdg= sqrt((second-third)*first)   ! std.dev of gdiff(i)


        meang = sum/count
c       open(unit=44,file=thv,status='old')
        icount=0
        sum=0.0
        sumsq=0.0
        do 67 i=1,n
c            read(44,*),xf(i),yf(i),v1(i),v2(i),v3(i),v4(i)
             vm1(i)=((x(i)-xf(i))*(v2(i)-v1(i))/0.1)+v1(i)
             vm2(i)=((x(i)-xf(i))*(v4(i)-v3(i))/0.1)+v3(i)
             vth(i)=((y(i)-yf(i))*(vm2(i)-vm1(i))/0.1)+vm1(i)
c            vdiff(i)=((vth(i)-vor(i))/vth(i))*100.0

             icount=icount+1
c            sum=sum+vdiff(i)
c            sumsq=sumsq+ vdiff(i)*vdiff(i)
67      continue

        count=float(icount)
        first=count/(count-1)
        second= sumsq/count
        third= (sum/count)**2
c       stdv= sqrt((second-third)*first)   ! std.dev of vdiff(i)
c       meanv = sum/count

        sumfi=0.0
        do 68 i=1,n
        sumfi=sumfi+xinc(i)
        fn=float(n)
68      continue
        meani=sumfi/fn

        write(25,110)shear
c       write(31,110)vort
        write(41,110),inco
        write(45,110)vel

        do 70 i=1,4
            if (i.eq.1)   j=25
c           if (i.eq.2)   j=31
            if (i.eq.3)   j=41
            if (i.eq.4)   j=45
            write(j,120)datain
            write(j,130)rotor,fluid,gapsiz
            write(j,140)srevs
            write(j,150)temp,date
            write(j,160)tolh
70      continue
```

```
      write(45,210)meanu,stdu
      write(25,220)meang,stdg
c     write(31,230)meanv,stdv
      write(41,240)meani
      write(25,170)
c     write(31,180)
      write(41,190)
      write(45,165)

      write(51,250)datain
      write(52,260)datain
c     write(53,270)datain


      do 80 i= 1, n
          write(45,200)i,x(i),y(i),u(i),udiff(i)
          write(25,200)i,x(i),y(i),gam(i),sdg(i),gdiff(i)
c         write(31,200)i,x(i),y(i),vor(i),sdv(i),vdiff(i)
          write(41,200)i,x(i),y(i),xinc(i),sdx(i)
          write(51,280)u(i),uth(i)
          write(52,290),gam(i),gth(i)
c         write(53,290)vor(i),vth(i)
80    continue


90    format(a7)
100   format(a12)
110   format(' THIS OUTPUT IS FROM ',A12)
120   format(' DATA INPUT FILE IS ',A12,/)
130   format(' ROTOR = ',A12,'     FLUID = ',A12,
     & '      GAP-SIZE = ',A7)
140   format(' SPEED OF ROTOR = ',I3,'RPM',' TYPE OF FLOW = SECONDARY')
150   format(' TEMPERATURE = ',A7,'    DATE OF EXPT. ',A12)
160   format(' TOLH = ',f3.2,/)
165   format('    I     XS(I)     YS(I)          U(I)
     &          UDIFFI(I)')
170   format('    I     XS(I)     YS(I)         GAM(I)
     &         SIG(I)        GDIFF(I)')
c     format('    I     XS(I)     YS(I)         VOR(I)
c    &          SDV(I)        VDIFF(I)')
190   format('    I     XS(I)     YS(I)        XINC(I)
     &         SDX(I)')
200   format(1X,I4,2(3X,F7.3),2(3X,F13.6),(3X,F13.6))
210   format(' FOR UDIFF(I), MEAN = ',F9.3,'   STANDARD DEVIATION'
     & ,' = ',F9.3,/)
220   format(' FOR GDIFF(I), MEAN = ',F9.3,'   STANDARD DEVIATION'
     & ,' = ',F7.3,/)
c     format(' FOR VDIFF(I), MEAN = ',F9.3,'   STANDARD DEVIATION'
c    & ,' = ',F9.3,/)
240   format(' MEAN OF XINC(I) = ',F7.3,/)
250   format(' COMPARISON OF U VALUES FOR ',A12,/,
     &        ' EXPERIMENTAL U',/,' THEORETICAL U')
260   format(' COMPARISON OF G VALUES FOR ',A12,/,
     &        ' EXPERIMENTAL G ',/,' THEORETICAL G ')
c     format(' COMPARISON OF V(XI) VALUES FOR ',A12,/,
c    &        ' EXPERIMENTAL V(XI)',/,' THEORETICAL V(XI)')
280   format(1x,2(f7.3))
290   format(1x,2(f13.6))

      close(unit=25,status='keep')
      close(unit=41,status='keep')
      close(unit=30,status='keep')
c     close(unit=31,status='keep')
      close(unit=42,status='keep')
      close(unit=43,status='keep')
c     close(unit=44,status='keep')
      close(unit=45,status='keep')
      close(unit=51,status='keep')
      close(unit=52,status='keep')
c     close(unit=53,status='keep')
      stop
      end
```

APPENDIX 3

Typical computer printouts of

a) tabulated experimental results

b) numerical shear rate values.

G-VALUES,starting row j=M(i=1..N)

```
j=          11
 0.000 0.000 0.000 0.000 0.000 2.480 1.981 1.419 1.058 0.818 0.596
j=          10
 0.000 0.000 0.000 0.000 0.000 2.490 1.986 1.418 1.054 0.812 0.590
j=           9
 0.000 0.000 0.000 0.000 0.000 2.521 2.001 1.416 1.042 0.796 0.574
j=           8
 0.000 0.000 0.000 0.000 0.000 2.594 2.034 1.409 1.016 0.765 0.543
j=           7
 0.000 0.000 0.000 0.000 0.000 2.765 2.104 1.387 0.964 0.710 0.495
j=           6
 0.000 0.274 0.585 0.978 1.574 3.207 2.283 1.304 0.862 0.621 0.429
j=           5
 0.000 0.246 0.512 0.818 1.211 1.830 1.343 0.952 0.677 0.497 0.350
j=           4
 0.000 0.214 0.432 0.653 0.870 1.033 0.866 0.666 0.494 0.365 0.263
j=           3
 0.000 0.180 0.352 0.506 0.624 0.669 0.586 0.463 0.342 0.244 0.172
j=           2
 0.000 0.156 0.297 0.412 0.484 0.493 0.432 0.336 0.234 0.142 0.085
j=           1
 0.000 0.139 0.260 0.352 0.400 0.398 0.353 0.275 0.183 0.089 0.000
```

ROTOR = CYLINDER FLUID = GLYCEROL GAP-SIZE = 15 MM
SPEED OF ROTOR = 16RPM TYPE OF FLOW = PRIMARY
TEMPERATURE = 23 C DATE OF EXPT. 11/10/85
TOLH = 0.4 XO = 0.25 YO = 0.50

FOR UDIFF(I), MEAN = 0.741 STANDARD DEVIATION = 13.579
FOR GDIFF(I), MEAN = -61.030 STANDARD DEVIATION = 59.204

57

I	X(I)	Y(I)	U(I)	GAM(I)	UDIFF(I)	GDIFF(I)
1	0.205	0.308	0.357	0.439696	-7.907790	-83.920077
2	0.369	0.308	0.351	0.746007	-9.418236	-76.242690
3	0.913	0.667	0.775	2.415018	-12.475591	-25.968916
4	0.728	0.667	0.854	2.173096	-13.070540	-71.466489
5	0.246	0.154	0.137	0.422835	14.175488	-61.522271
6	0.523	0.667	0.837	1.264088	-6.547506	-55.000454
7	0.533	0.359	0.351	1.148746	3.401380	-83.213056
8	0.667	0.179	0.156	1.308299	1.483050	-109.537096
9	0.113	0.667	0.919	0.307462	-14.117950	-89.731542
10	0.441	0.667	0.854	1.050526	-7.811105	-56.897075
11	0.400	0.103	0.109	0.744858	-6.874777	-85.052117
12	1.385	0.615	0.158	1.559471	15.206491	-62.367818
13	0.574	0.513	0.558	1.240816	-1.386745	-55.562972
14	0.513	0.615	0.803	1.332811	-13.457284	-72.892203
15	0.431	0.718	0.876	1.035009	-0.558072	-54.940602
16	0.790	0.667	0.810	2.279402	-9.377431	-58.396150
17	0.708	0.462	0.516	1.333133	-13.560151	-43.485440
18	1.200	0.333	0.139	1.740231	7.372571	-133.274910
19	0.256	0.513	0.576	0.606297	1.418264	-75.774858
20	0.790	0.385	0.346	1.480883	-2.005061	-64.392311
21	0.995	0.667	0.673	2.210162	-6.809942	7.674166
22	1.097	0.564	0.356	2.139537	4.648402	-47.917959
23	0.667	0.359	0.371	1.561188	-8.858743	-104.630178
24	1.118	0.513	0.291	2.090512	6.186765	-71.161500
25	0.769	0.436	0.372	1.487659	7.890910	-54.579211
26	0.513	0.359	0.399	0.952361	-8.961186	-57.422301
27	1.477	0.872	0.188	0.694191	2.228923	36.083596
28	1.467	0.974	0.178	1.131690	17.410031	3.874047
29	1.159	0.256	0.124	1.219186	-0.883433	-79.927834
30	0.831	0.564	0.618	1.559426	-11.611834	-18.806003
31	0.903	0.308	0.239	1.731753	-4.081415	-106.917034
32	0.267	0.487	0.594	0.607044	-8.134255	-72.087840
33	1.477	1.051	0.193	1.726372	11.209696	-45.422764
34	1.200	0.256	0.116	1.275813	-2.996087	-96.643464
35	1.124	0.923	0.676	2.008798	-2.518979	22.250517
36	0.708	0.205	0.207	1.191689	-17.138306	-80.202404
37	1.703	1.179	0.054	1.632601	34.831227	-89.858824
38	1.477	0.538	0.111	1.206781	6.437128	-70.673256
39	0.882	0.103	0.071	1.277353	2.523049	-97.618442
40	0.841	0.513	0.533	1.651598	-12.441516	-37.936610
41	1.149	0.949	0.229	1.536334	62.848742	35.980045
42	1.344	0.744	0.224	1.144680	15.099674	11.060550
43	1.579	1.333	0.156	0.870151	3.048252	18.484106
44	1.333	0.641	0.192	1.261668	16.861892	-12.958393
45	1.262	0.564	0.224	2.651139	8.247043	-139.824522
46	1.518	0.513	0.069	0.817745	8.374639	-30.672226
47	1.395	0.538	0.154	2.111240	0.589933	-157.134872
48	0.113	0.615	0.775	0.206259	-5.789368	-29.647113
49	1.118	0.821	0.573	1.921348	8.668170	33.692941
50	0.851	0.615	0.730	1.811287	-16.852842	-20.716414
51	1.344	0.333	0.099	1.468714	6.236561	-142.191263
52	1.262	0.718	0.300	1.673803	9.540965	-10.829650

APPENDIX 4

A listing of the computer program used for numerical determination of flow parameters for the disc stirrer.

```
c       program d10.for

c  Flow of a variable viscosity fluid between a rotating disc and a cylinder.
c  The governing pde's are:
c                    R[VxTx+VyTy]=MU[Txx+Tyy-Tx/x]+MUx[Tx-2T/x]+MUy[Ty]
c                                 x*XI=ALFAxx+ALFAyy-ALFAx/x
c   R[VxXIx+VyXIy-VxXI/x-2TTy/xΔ3]=MU[XIxx+XIyy+XIx/x-XI/x 2]+MUx[2XIx+XI/x]
c              +MUy[2XIy]+MUxy[4ALFAxy/x-2ALFAy/x 2]+(MUxx-MUyy)[XI-2ALFAyy/x]
c  where Vx=ALFAy/x,Vy=-ALFAx/y,MU=viscosity,R=Reynolds number,
c                                              XI=vorticity= (Vx)y-(Vy)x
c  and we want ALFA (the stream-function) and T(=x*x*u)
c                                        (which defines the theta-velocity)
c  Execute using @ex d10,d10p,d10pp,@ng,teklib where D10 is the main program,
c          D10P, D10PP hold subprograms, NG holds NAG graphics
c
c  Diagram of geometry:
c                                          Ty=0 XI=0
c  y=yc    j=M=mm   -   T  -  -  -  C--------------------------B
c                       |                                     |
c                       |                                     |
c                       |                                     |
c                       |       T=x*x                         |
c                       |  XI=ALFAxx/x                        |
c                       |                                     |
c                       |  T=x*x                              |  T=0
c  y=yg    j=m          L  -  -    G-------------H            |  XI=ALFAxx/x
c                       |  XI=ALFAyy/x                        |
c                T=0    |                       |  T=1        |
c                XI=0   |                       |  XI=ALFAxx/x|
c                       E  XI=ALFAyy/x          D             |
c                       |-------T=x*x-----------|             |
c                       |                       |             |
c                       |                       |             |
c                       |                       |             |
c                       |                       |             |
c                       |                       |             |
c                       O-----------K-----------F-------------A
c       origin i=1,j=1          T=0   XI=ALFAyy/x
c    ALFA=0 on all boundaries    at F:x=xb=1,i=n     at A:x=xc,i=N=nn
c
c  parameters and declaration   nm: main program parameter for setting array
c                bounds, maxits: max.no. of sweeps allowed through equations
      parameter (nm=81,maxits=1000)
      real x(nm),y(nm) ,k ,mu(nm,nm) !grid points;step in y direction;viscosity
      real ts(nm,nm),t(nm,nm),xis(nm,nm),xi(nm,nm),als(nm,nm) ! old & new T,XI,ALFA values
      real  al(nm,nm),u(nm,nm),gs(nm,nm),g(nm,nm),wl(nm,nm)   ! u ,old & new shear-rates
      real params(10)                                          ! fluid parameters
      logical unused(nm,nm)                                    ! used in graphics
      character store, geo                          ! used in storing alfa values on file
      logical notcvg                                ! used in convergence tests
      common n,m,nl,ml,n2,m2,nn,mm,yb,yg,yc,xg,xc,h,k,alfa ! geometrical quantities
      al=1.0/3.0;a2=2*al;a4=4*al; pi=3.14159; small=2.0e-4 ! some useful constants
      a5=5*al;a8=8*al;all=11*al
c  input section
5     type*;type*,'geometrical dimensions'
      type*,'enter (S)mall gap, (L)arge gap, (I)nput from keybd'
      accept 'al',geo
      if((geo.eq.'s').or.(geo.eq.'S')) then
         yb=0.8; yg=1.4; yc=3.1; xg=0.5; xc=1.9
      else
         if((geo.eq.'l').or.(geo.eq.'L'))then
            yb=1.3; yg=2.0; yc=3.1; xg=0.5; xc=1.9
         else
            if((geo.eq.'i').or.(geo.eq.'I'))then
               type*;type*,'input yb, yg, yc, xg, xc'
               accept*,yb,yg,yc,xg,xc
            else goto 5
      end if; end if; end if
      type*;type*,'yb= ',yb;type*,'yg= ',yg;type*,'yc= ',yc
      type*,'xg= ',xg; type*,'xc= ',xc; type*
      type*,'input step size h'; accept*,h; k=h
      type*,'input final Reynolds number & increment';accept*,Rend,Rstep
      type*,'ALFA storage required? y or n'; accept'(a1)',store
      type*,'conv.crit=',small
      type*,'input smoothing parameter';accept*,sg

c  calculate k/h(=alpha), numbers of steps n,nn,m,mm,nl,ml,n2,m2 and
c  check if h,k are compatible with geometrical dimensions.
c  Also,check if array sizes are big enough and print some initial output.
      call STEPS(nm,Rend,Rstep)

c  generate mesh points
      do i=1,nn; x(i)=(i-1)*h; end do
      do j=1,mm; y(j)=(j-1)*k; end do

c  specify the fluid
      call FLUID(iflow,params)
```

```
********************** PRIMARY FLOW ************************
c  find primary flow
        call TGUESS(ts,x,y,nm); call TGUESS(t,x,y,nm)
        do i=1,nn; do j=1,mm
         als(i,j)=0;xis(i,j)=0;g(i,j)=0;gs(i,j)=0;al(i,j)=0;xi(i,j)=0;
        enddo;enddo
        R=0;       notcvg=.true.  ;       isweep=0
         type*,'isweep   dmaxt       dmaxg'
        call MUFIND(mu,g,params,iflow,nm)
        do while (notcvg)
        isweep=isweep+1
         call TFIND(t,ts,als,gs,mu,R,x,nm)
         call UGFIND(g,u,t,xis,x,y,nm,al)
         call MUFIND(mu,g,params,iflow,nm)
         call MAXDIF(t,ts,dmaxt,nm,nn,mm)
         if(mod(isweep,20).eq.0)then
          call MAXDIF(g,gs,dmaxg,nm,nn,mm)
          type 2,isweep,dmaxt,dmaxg
         endif
         if(dmaxt<small)notcvg=.false.
         do i=1,nn;do j=1,mm; ts(i,j)=t(i,j);gs(i,j)=g(i,j); enddo; enddo
        end do

c  output section for primary flow
        type*,'isweep=',isweep
        type*;type*,'*** primary flow solution (R=0) available ***';type*
c       type*,'mu';call pprint(mu,nm,nn,mm)
        call XPRINT(t,u,g,xi,al,x,R,iflow,params,store,nm)
        call COUPLE(u,g,x,y,params,iflow,wl,al,a2,a4,a5,a8,all,pi,nm)
        call GRAFIX(x,y,u,t,g,params,iflow,nm,al,xi,mu,unused)
        type*;type*

c********************** SECONDARY FLOW ***********************

        call FLUID(iflow,params)
        type*,'input conv.crit. for secondary flow'
        accept*,small
        type*,'conv.crit=',small
        DO WHILE(R<Rend)   !*********************************************
         isweep=0;R=R+Rstep;type*,'R=',R;notcvg=.true.
         type*,'isweep   dmaxt       dmaxg       dmaxi      dmaxal'
         DO while (notcvg)
          isweep=isweep+1
          do i=1,nn; do j=1,mm;
           ts(i,j)=t(i,j);xis(i,j)=xi(i,j);gs(i,j)=g(i,j)
          enddo;enddo
c  find latest approximation to solutions
          call XIFIND(xi,xis,al,ts,als,mu,x,R,nm,sg)
          do i=1,nn;do j=1,mm;als(i,j)=al(i,j);enddo;enddo
          call ALFIND(al,als,xi,x,nm)
          call TFIND(t,ts,al,gs,mu,R,x,nm)
          call UGFIND(g,u,t,xi,x,y,nm,al)
          call MUFIND(mu,g,params,iflow,nm)
c  check for convergence
          if(mod(isweep,2).eq.0)then
          call MAXDIF(t,ts,dmaxt,nm,nn,mm)
          call MAXDIF(g,gs,dmaxg,nm,nn,mm)
          call MAXDIF(al,als,dmaxal,nm,nn,mm)
          call MAXDIF(xi,xis,dmaxi,nm,nn,mm)
          if(mod(isweep,20).eq.0)then
           type 1,isweep,dmaxt,dmaxg,dmaxi,dmaxal
          end if
          if((max(dmaxt,dmaxal)<small).or.(isweep.eq.maxits)) notcvg=.false.
         endif
         END DO

         type*,'isweep=',isweep
         if(isweep.eq.maxits)then
           type*,'R=',R,'no convergence';stop
         end if
        type*;type*,'*** secondary flow solution available ***';type*
c  solutions available at latest R-value
         type*;type*,'---------------------'
         type*,'R=',R,' converged solutions available for output'
         type*,'-------------------'
         call XPRINT(t,u,g,xi,al,x,R,iflow,params,store,nm)
         call COUPLE(u,g,x,y,params,iflow,wl,al,a2,a4,a5,a8,all,pi,nm)
         call GRAFIX(x,y,u,t,g,params,iflow,nm,al,xi,mu,unused)
        END DO          !*************************************************
        type*;type*;type*,'final Reynolds number reached';type*;type*
        call XPRINT(t,u,g,xi,al,x,R,iflow,params,store,nm)
        call COUPLE(u,g,x,y,params,iflow,wl,al,a2,a4,a5,a8,all,pi,nm)
        call GRAFIX(x,y,u,t,g,params,iflow,nm,al,xi,mu,unused)
        type*;type*
 1      format(1x,i3,4f12.5)
 2      format(1x,i3,2f12.5)


        end ! d10
```

```
c file           DIOP.FOR


        subroutine TFIND(t,ts,al,g,mu,R,x,nm)
c  finds t from ts etc.
        real t(nm,nm),ts(nm,nm),x(nm),al(nm,nm),g(nm,nm),mu(nm,nm),k
        real mux,muy
        common n,m,n1,m1,n2,m2,nn,mm,yb,yg,yc,xg,xc,h,k,alpha
c interior
        hh2=.5*h*h; hh=.5*h
        do i=2,n1;  x1=x(i);  do j=2,m1
         if((i>n).or.(j<m).or.((i>n2).and.(j>m2)))then
          mux=.5*(mu(i+1,j)-mu(i-1,j))/h
          muy=.5*(mu(i,j+1)-mu(i,j-1))/k
c  avoid corner at D
          if((i.eq.n+1).and.(j.eq.m))mux=.25*(
        2   mu(n+2,m+1)-mu(n,m+1)+mu(n+2,m-1)-mu(n,m-1))/h
              if((i.eq.n).and.(j.eq.m-1))muy=.25*(
        2   mu(n-1,m)-mu(n-1,m-2)+mu(n+1,m)-mu(n+1,m-2))/k
c  avoid corner at H
          if((i.eq.n+1).and.(j.eq.m2))mux=.25*(mu(n+2,m2-1)
     2         -mu(n,m2-1)+mu(n+2,m2+1)-mu(n,m2+1))/h
              if((i.eq.n).and.(j.eq.m2-1))muy=.25*(
        2   mu(n-1,m2)-mu(n-1,m2+2)+mu(n+1,m2)-mu(n+1,m2+2))/k
c  end of corners
          dtx=ts(i+1,j)-ts(i-1,j);  dty=ts(i,j+1)-ts(i,j-1)
          denom=4*(mu(i,j)+hh2*mux/x1)
          t1=mu(i,j)*(ts(i+1,j)+ts(i-1,j)+ts(i,j+1)+ts(i,j-1))
          t2=(mux-mu(i,j)/x1)*dtx+muy*dty; t2=hh*t2
         t3=R*(dtx*(al(i,j+1)-al(i,j-1))-dty*(al(i+1,j)-al(i-1,j)))/x1/4.
          t(i,j)=(t1+t2-t3)/denom
         endif
        enddo;enddo
c  top boundary
        j=mm;do i=n2+1,n1;t(i,j)=(4*t(i,j-1)-t(i,j-2))/3.0;enddo
        end ! tfind



        subroutine ALFIND(al,als,xi,x,nm)
c  finds al from als etc
        real al(nm,nm),als(nm,nm),xi(nm,nm),x(nm),k
        common n,m,n1,m1,n2,m2,nn,mm,yb,yg,yc,xg,xc,h,k,alpha
c interior only
        do i=2,n1; do j=2,m1
         if((i>n).or.(j<m).or.((i>n2).and.(j>m2))) then
          al(i,j)=0.25*(als(i+1,j)+als(i-1,j)+als(i,j+1)+als(i,j-1)
        2          -(.5*h/x(i))*(als(i+1,j)-als(i-1,j))
        3           -h*h*x(i)*xi(i,j))
         endif
        enddo;enddo
        end ! alfind


        subroutine xifind(xi,xis,al,t,als,mu,x,R,nm,sg)
        real xi(nm,nm),xis(nm,nm),al(nm,nm),x(nm),k,t(nm,nm)
        real als(nm,nm),mu(nm,nm),kk,mux,muy,muxx,muyy,muxy
        common n,m,n1,m1,n2,m2,nn,mm,yb,yg,yc,xg,xc,h,k,alpha
c  boundaries
        hh2=2*h*h
c     CG:
        i=n2;do j=m2+1,m1;xi(i,j)=(8*al(i+1,j)-al(i+2,j))/hh2/x(i);end do
c     GH:
        j=m2;do i=n2,n-1;xi(i,j)=(8*al(i,j+1)-al(i,j+2))/hh2/x(i);end do
c     HD:
        i=n;do j=m+1,m2-1;xi(i,j)=(8*al(n+1,j)-al(n+2,j))/hh2;end do
        j=m;do i=2,n-1;xi(i,j)=(8*al(i,m-1)-al(i,m-2))/hh2/x(i);enddo
        j=1;do i=2,nn;xi(i,j)=(8*al(i,2)-al(i,3))/hh2/x(i);enddo
        i=nn;do j=2,m1;xi(i,j)=(8*al(n1,j)-al(nn-2,j))/hh2/x(i);enddo
c  interior
        hh=h*h; kk=k*k
        do i=2,n1; x1=x(i); xx=x1*x1; do j=2,m1
         if((i>n).or.(j<m).or.((i>n2).and.(j>m2)))then
c  find vorticity for corner D
         if((i.eq.n+1).and.(j.eq.m)) xis(n,m)=(
     2       8*als(n+1,m)-als(n+2,m))/hh2
         if((i.eq.n).and.(j.eq.m-1)) xis(n,m)=(
     2    8*als(n,m-1)-als(n,m-2))/hh2
c  find vorticity for corner H
          if ((i.eq.n+1).and.(j.eq.m2))xis(n,m2)=(
     2        8*als(n+1,m2)-als(n+2,m2))/hh2
          if ((i.eq.n).and.(j.eq.m2+1)) xis(n,m2)=(
     2        8*als(n,m2+1)-als(n,m2+2))/hh2
          mux=.5*(mu(i+1,j)-mu(i-1,j))/h
          muy=.5*(mu(i,j+1)-mu(i,j-1))/k
          muxx=(mu(i+1,j)-2*mu(i,j)+mu(i-1,j))/hh
          muyy=(mu(i,j+1)-2*mu(i,j)+mu(i,j-1))/kk
          muxy=.25*(mu(i+1,j+1)+mu(i-1,j-1)-mu(i-1,j+1)-mu(i+1,j-1))/h/k
```

```
c  avoid corner D
       if((i.eq.n+1).and.(j.eq.m))then
        mux=.25*(mu(n+2,m+1)-mu(n,m+1)+mu(n+2,m-1)-mu(n,m-1))/h
        muxx=.5*(mu(n+2,m+1)-2*mu(n+1,m+1)+mu(n,m+1)
     2   +mu(n+2,m-1)-2*mu(n+1,m-1)+mu(n,m-1))/hh
       end if
       if((i.eq.n).and.(j.eq.m-1))then
        muy=.25*(mu(n-1,m)-mu(n-1,m-2)+mu(n+1,m)-mu(n+1,m-2))/k
        muyy=.5*(mu(n-1,m)-2*mu(n-1,m-1)+mu(n-1,m-2)
     2       +mu(n+1,m)-2*mu(n+1,m-1)+mu(n+1,m-2))/kk
       end if
       if((i.eq.n+1).and.(j.eq.m+1))muxy=.125*(
       2   mu(n+2,m+3)+mu(n,m+1)-mu(n,m+3)-mu(n+2,m+1)
       3   +mu(n+2,m+1)+mu(n,m-1)-mu(n,m+1)-mu(n+2,m-1))/h/k
       if((i.eq.n+1).and.(j.eq.m-1))muxy=.0625*(
       2   mu(n+2,m+1)-mu(n,m+1)+mu(n,m-3)-mu(n+2,m-3)
       3  +mu(n+3,m)-mu(n+3,m-2)+mu(n-1,m-2)-mu(n-1,m))/h/k
       if((i.eq.n-1).and.(j.eq.m-1))muxy=.125*(
       2   mu(n-1,m)+mu(n-3,m-2)-mu(n-3,m)-mu(n-1,m-2)
       3  +mu(n+1,m)+mu(n-1,m-2)-mu(n-1,m)-mu(n+1,m-2))/h/k
c  avoid corner H
       if ((i.eq.n+1).and.(j.eq.m2))then
       mux=0.25*(mu(n+2,m2-1)-mu(n,m2-1)+mu(n+2,m2+1)-mu(n,m2+1))/h
       muxx=.5*(mu(n+2,m2-1)-2*mu(n+1,m2-1)+mu(n,m2-1)
     2  +mu(n+2,m2+1)-2*mu(n+1,m2+1)+mu(n,m2+1))/hh
       end if

       if ((i.eq.n).and.(j.eq.m2+1)) then
       muy=.25*(mu(n-1,m2)-mu(n-1,m2+2)+mu(n+1,m2)-mu(n+1,m2+2))/k
       muyy=.5*(mu(n-1,m2)-2*mu(n-1,m2+1)+mu(n-1,m2+2)
     2  +mu(n+1,m2)-2*mu(n+1,m2+1)+mu(n+1,m2+2))/kk
       end if

       if ((i.eq.n+1).and.(j.eq.m2-1))muxy=.125*(
     2    mu(n+2,m2-3)+mu(n,m2-1)-mu(n,m2-3)-mu(n+2,m2-1)
     3    +mu(n+2,m2-1)+mu(n,m2+1)-mu(n,m2-1)-mu(n+2,m2+1))/h/k

       if ((i.eq.n+1).and.(j.eq.m2+1))muxy=0.0625*(
     2    mu(n+2,m2-1)-mu(n,m2-1)+mu(n,m2+3)-mu(n+2,m2+3)
     3    +mu(n+3,m2)-mu(n+3,m2+2)+mu(n-1,m2+2)-mu(n-1,m2))/h/k

       if ((i.eq.n-1).and.(j.eq.m2+1))muxy=0.125*(
     2    mu(n-1,m2)+mu(n-3,m2+2)-mu(n-3,m2)-mu(n-1,m2+2)
     3    +mu(n+1,m2)+mu(n-1,m2+2)-mu(n-1,m2+2))/h/k
         dax=al(i+1,j)-al(i-1,j); day=al(i,j+1)-al(i,j-1)
         dxix=xis(i+1,j)-xis(i-1,j); dxiy=xis(i,j+1)-xis(i,j-1)
                                     dty=t(i,j+1)-t(i,j-1)
         denom=mu(i,j)*(1+.125*hh2/xx)-.125*hh2*(mux/x1+muxx-muyy)
     2        -.125*R*h*day/x1
         t1=.25*mu(i,j)*(xis(i+1,j)+xis(i-1,j)+xis(i,j+1)+xis(i,j-1)
     2                  +.5*h*dxix/x1)
         t2=.25*h*(muy*dxiy+mux*dxix)
         t3=.25*muxy*(al(i+1,j+1)+al(i-1,j-1)-al(i-1,j+1)-al(i+1,j-1)
     2               -h*day/x1)/x1
         t4=-.5*(muxx-muyy)*(al(i,j+1)-2*al(i,j)+al(i,j-1))/x1
         t5=.0625*R*(day*dxix-dax*dxiy-4*h*t(i,j)*dty/xx)/x1
         xi(i,j)=(t1+t2+t3+t4-t5)/denom
         end if
       enddo;enddo
       xi(n,m)=0;xis(n,m)=0;xi(n,m2)=0;xis(n,m2)=0
c  global smoothing
       sgm1=1-sg
       do i=1,nn;do j=1,mm;
        xi(i,j)=sgm1*xis(i,j)+sg*xi(i,j)
       end do;enddo
       end ! xifind



       subroutine MUFIND(mu,g,params,iflow,nm)
c  finds viscosity values
       real mu(nm,nm),g(nm,nm),params(10),k
       common n,m,n1,m1,n2,m2,nn,mm,yb,yg,yc,xg,xc,h,k,alpha
       do i=1,nn;do j=1,mm; mu(i,j)=VIS(params,g(i,j),iflow);enddo;enddo
c      mu(n,m)=VIS(params,10000.0,iflow)
       end ! mufind


       subroutine UfromT(u,t,x,nm)
c  finds u from t ( u=t/x/x )
       real u(nm,nm),t(nm,nm),x(nm)
       common n,m,n1,m1,n2,m2,nn,mm,yb,yg,yc,xg,xc,h,k,alpha
       do i=2,nn;a=x(i)*x(i);do j=1,mm;u(i,j)=t(i,j)/a;enddo;enddo
       i=1;do j=1,m;u(i,j)=u(2,j);enddo
       do i=1,n-1; do j=m+1,m2-1;u(i,j)=1;enddo;enddo
       do i=1,n2;do j=m2,mm;u(i,j)=1;enddo;enddo
       end ! ufromt
```

```
      subroutine FLUID(iflow,s)
c  sets fluid parameters s(i),i=1,2..
c  it's recommended that s(1)..s(5) be reserved for up to 5 parameters which are
c  actually input during a program run, and s(6)..s(10) used for combinations of s(1)..s(5)
c  which are useful in VIS; s(1)..s(5) are printed in graphical output
c  note program lambda = model lambda * angular speed omega
      real s(*)
      do i=1,10; s(i)=0; end do ! initialise s

      type*,'input an integer (iflow) specifying fluid model required'
      type*,'0=Newtonian,2=Carreau,3=Cross,4..',
     2          '(not yet specified)'
      accept*,iflow

      if(iflow.eq.0)then
        s(1)=1
        type*,'Newtonian fluid with non-dimensional viscosity=1'

      else if (iflow.eq.2) then
        type*,'Carreau model:input etazero,etainfinity,n,lambda'
        type*,'                          (0<n<1,lambda>0)'
        accept*,s(1),s(2),s(3),s(4)
        s(9)=s(2)/s(1);  s(10)=0.5*(s(3)-1)

      else if(iflow.eq.3) then
        type*,'Cross model:input etazero,etainfinity,n,lambda'
        type*,'                        (0<n<1,lambda>0)'
        accept*,s(1),s(2),s(3),s(4)
        s(8)=1-s(3);s(9)=s(2)/s(1)

      else if(iflow.eq.4) then
        ! to be specified

      end if
      end ! fluid



      function VIS(s,g,iflow)
c  calculates viscosity at a grid-point i.e mu at (i,j)
c  s is the array of fluid parameters, g is shear-rate at (i,j)
      real s(*)

      if(iflow.eq.0)then
        vis=s(1)

      else if(iflow.eq.2)then
        vis=(s(9)+(1-s(9))*(1+s(4)*s(4)*g*g)**s(10))

      else if(iflow.eq.3)then
        vis=(s(9)+(1-s(9))/(1+s(4)**s(8)*g**s(8)))

      else if(iflow.eq.4)then
        ! vis for some other fluid etc.

      end if
      end ! vis



      subroutine UGFIND(g,u,t,xi,x,y,nm,alfa)
c  creates g and u from t,alfa,xi
      real g(nm,nm),u(nm,nm),x(nm),y(nm),k,alfa(nm,nm),t(nm,nm)
      real xi(nm,nm)
      common n,m,n1,m1,n2,m2,nn,mm,yb,yg,yc,xg,xc,h,k,alpha
c  find u
      call UfromT(u,t,x,nm)
      twoh=2*h;twok=2*k;fourhk=twoh*twok;sqh=h*h;sqk=k*k
c  initialise to zero & then set values
      do i=1,nn;do j=1,mm;g(i,j)=0;end do;end do
c  interior points
      do i=2,n1; x2=x(i)*x(i); x6=x2*x2*x2;  do j=2,m1
       if((i>n).or.(j<m).or.((i>n2).and.(j>m2)))then
      ax=(alfa(i+1,j)-alfa(i-1,j))/twoh
      ay=(alfa(i,j+1)-alfa(i,j-1))/twok
      axx=(alfa(i-1,j)-2*alfa(i,j)+alfa(i+1,j))/sqh
      ayy=(alfa(i,j-1)-2*alfa(i,j)+alfa(i,j+1))/sqk
      axy=(alfa(i+1,j+1)-alfa(i+1,j-1)+alfa(i-1,j-1)-alfa(i-1,j+1))
      axy=axy/fourhk
      uxij=(u(i+1,j)-u(i-1,j))/twoh
      uyij=(u(i,j+1)-u(i,j-1))/twok
      gterm=4*ay*ay+ax*ax
      gterm=gterm+2*x(i)*(ax*(ayy-axx)-2*ay*axy)
      gterm=gterm+x2*(4*axy*axy+(ayy-axx)*(ayy-axx))
        g(i,j)=(1/x2)*sqrt(x6*(uxij*uxij+uyij*uyij)+gterm)
       end if
      end do; end do
```

```
c  on OE: x=0,i=1
        do j=1,m; g(1,j)=0; end do
c  on OA: y=0,j=1,U=0,Ux=0
        do i=2,n1; x2=x(i)*x(i); x6=x2*x2*x2;
          uyij=(4*u(i,2)-u(i,3))/twok
          g(i,1)=(1/x2)*sqrt(x6*uyij*uyij+x2*x2*xi(i,1)*xi(i,1))
        end do
          g(nn,1)=0 ! (corner at A)
c  on AB: x=xc,i=nn,U=0,Uy=0  taking B on AB
        xc2=xc*xc; xc6=xc2*xc2*xc2
        do j=2,m1
          uxij=(u(nn-2,j)-4*u(nn-1,j))/twoh
          g(nn,j)=(1/xc2)*sqrt(xc6*uxij*uxij+xc2*xc2*xi(nn,j)*xi(nn,j))
        end do
          g(nn,mm)=xc*abs(u(nn-2,mm)-4*u(nn-1,mm))/twoh
c  on BC: y=yc,j=mm,Uy=0
        do i=n2+1,n1; x2=x(i)*x(i); x6=x2*x2*x2 ! B,C not taken to be on BC
          uxij=(u(i+1,mm)-u(i-1,mm))/twoh
          g(i,mm)=(1/x2)*sqrt(x6*uxij*uxij)
        end do
c  on CG: x=xg,i=n2,U=1; Uy=0(except at G)
        xg2=xg*xg; xg6=xg2*xg2*xg2
        do j=m2+1,mm
          uxij=(4*u(n2+1,j)-3-u(n2+2,j))/twoh
          g(n2,j)=(1/xg2)*sqrt(xg6*uxij*uxij+xg2*xg2*xi(n2,j)*xi(n2,j))
        end do
c  on GH:y=yg, j=m2, U=1; Ux=0 (include G but not H)
        do i=n2,n-1
          uyij=(-u(i,m2+2)-3+4*u(i,m2+1))/twok
          x2=x(i)*x(i);x6=x2*x2*x2
          g(i,m2)=(1/x2)*sqrt(x6*uyij*uyij+x2*x2*xi(i,m2)*xi(i,m2))
        end do
        g(n2,m2)=0
c  on HD: x=1, i=n, U=1, Uy=0 (except at H and D)
        do j=m+1,m2-1
        uxij=(4*u(n+1,j)-3-u(n+2,j))/twoh
          g(n,j)=sqrt(uxij*uxij+xi(n,j)*xi(n,j))
        end do
c  on ED: y=yb,j=m,U=1; Ux=0(except at D)
        do i=2,n-1
          uyij=(u(i,m-2)+3-4*u(i,m-1))/twok
          x2=x(i)*x(i); x6=x2*x2*x2
          g(i,m)=(1/x2)*sqrt(x6*uyij*uyij+x2*x2*xi(i,m)*xi(i,m))
        end do
c  at D i=n,j=m
c  discontinuity in shear-rate.
c  taking D on HD we pick a convenient value for a shear-rate map
        g(n,m)=abs((4*u(n+1,m)-3-u(n+2,m))/twoh)
c   at H i=n,j=m2
c   discontinuity in shear-rate.
c   taking H on HD we pick a convenient value for a shear-rate map
        g(n,m2)=abs((4*u(n+1,m2)-3-u(n+2,m2))/twoh)
        end ! ugfind



c  end of d10p
```

```
c file      d10pp.for


        subroutine STEPS(nm,Rend,Rstep)
c  performs some essential initial tasks e.g finding how many steps
        common n,m,n1,m1,n2,m2,nn,mm,yb,yg,yc,xg,xc,h,k,alpha
        real k
c  calculate k/h and numbers of steps n,nn,m,mm,n1,m1,n2,m2
        alpha=k/h
        n=anint(1.0/h)+1;m=anint(yb/k)+1;nn=anint(xc/h)+1;mm=anint(yc/k)+1
        n1=nn-1;m1=mm-1;n2=anint(xg/h)+1;m2=anint(yg/k)+1
        if(m.lt.5)type*,'care..k too big?'
        if((nn-n).lt.4)type*,'care..h too big?'
c  check if h,k are compatible with geometrical dimensions
        if(abs((n-1)*h-1)>.1*h)then;type*,'1 not dvsbl by h';stop;endif
        if(abs((m-1)*k-yb)>.1*k)then;type*,'yb not dvsbl by k';stop;endif
        if(abs((nn-1)*h-xc)>.1*h)then;type*,'xc not dvsbl by h';stop;endif
        if(abs((mm-1)*k-yc)>.1*k)then;type*,'yc not dvsbl by k';stop;endif
        if (abs((n2-1)*h-xg)>0.1*h) then;type*,'xg not dvsbl by h';
     2  stop;endif
        if (abs((m2-1)*k-yg)>0.1*k)then;type*,'yg not dvsbl by by k';
     2  stop;endif
c  check if array sizes are big enough
        if(nm<nn)then;type*,'need larger h or nm';stop;endif
        if(nm<mm)then;type*,'need larger k or nm';stop;endif
c  an initial output section
        type*;type*,' h= ',h,'   k= ',k,'   k/h= ',alpha
        type*,'yb= ',yb,'   yg= ',yg,'     yc= ',yc,'    xg= ',xg,
     2  '    xc= ',xc
        type*,' n= ',n,'  m= ',m,'  N= ',nn,'  M= ',mm
     2  ,'    n2= ',n2,'    m2= ',m2
        type*;type*,'Rend= ',Rend,'   Rstep= ',Rstep
        type*;type*
        end ! steps



        subroutine TGUESS(ts,x,y,nm)
c  sets bc's for ts and zeros elsewhere ( except rotor )
        real ts(nm,nm),x(nm),y(nm),k
        common n,m,n1,m1,n2,m2,nn,mm,yb,yg,yc,xg,xc,h,k,alpha
        do i=1,nn; do j=1,mm; ts(i,j)=0; enddo;enddo
        j=m; do i=1,n; ts(i,j)=x(i)*x(i); end do
        j=m2;do i=n2,n; ts(i,j)=x(i)*x(i);enddo
        i=n; do j=m,m2; ts(i,j)=1;          end do
        i=n2;do j=m2,mm;ts(i,j)=x(i)*x(i);enddo
                t=1-xc
        j=mm; do i=n2+1,nn; ts(i,j)=(x(i)-xc)/t; enddo
        do i=1,n-1;do j=m+1,m2-1;ts(i,j)=1;enddo;enddo
        do i=1,n2-1;do j=m2,mm; ts(i,j)=1;enddo;enddo
        end ! tguess



        subroutine XPRINT(t,u,g,xi,alfa,x,R,iflow,params,store,nm)
c  options for printing t,u,g,xi,alfa
        real t(nm,nm),u(nm,nm),alfa(nm,nm),xi(nm,nm),params(10),x(nm)
        real g(nm,nm)
        character answer,store
        character*12, filenm
        common n,m,n1,m1,n2,m2,nn,mm,yb,yg,yc,xg,xc,h,k,alpha,mu

        type*;type*,'print converged t-VALUES ? type y for yes,n for no'
        accept '(a1)',answer
        if(answer.ge.'y')then
        type*;type*,'interpolation file name for t-values ?'
        accept 'a12',filenm
          type*;type*,'t(i,j),starting row j=M(i=1..N)';type*
          call PPRINT(t,nm,nn,mm,65,filenm)
        end if

        type*;type*,'print converged U-VALUES ? type y for yes,n for no'
        accept '(a1)',answer
        if(answer.ge.'y')then
        type*;type*,'interpolation file name for u-values ?'
        accept 'a12',filenm
          type*;type*,'u(i,j),starting row j=M(i=1..N)';type*
          call PPRINT(u,nm,nn,mm,66,filenm)
        end if
        type*,'print converged G-VALUES ? : y for yes, n for no'
        accept'(a1)',answer
        if(answer.ge.'y') then
        type*;type*,'interpolation file name for g-values ?'
        accept 'a12',filenm
          type*,' G-VALUES,starting row j=M(i=1..N)';type*
          call PPRINT(g,nm,nn,mm,67,filenm)
        end if
        type*
```

```
      type*,'print converged XI-VALUES ? : y for yes, n for no'
      accept'(a1)',answer
      if(answer.ge.'y') then
      type*;type*,'interpolation file name for xi-values ?'
      accept 'a12',filenm
        type*,' XI-VALUES,starting row j=M(i=1..N)';type*
        call PPRINT(xi,nm,nn,mm,68,filenm)
      end if
      type*
      type*;type*,'print latest ALPHA values? y for yes,n for no'
      accept '(a1)',answer
      if(answer.ge.'y')then
      type*;type*,'interpolation file name for alfa-values ?'
      accept 'a12',filenm
        type*;type*,'alfa(i,j) starting row j=M (i=1,..N)';type*
        call PPRINT(alfa,nm,nn,mm,69,filenm)
      end if
      type*
      if(store.eq.'y')then
       type*,'store latest ALPHA-values,fluid & geometry on file?'
       type*,'NO? input 9      YES? input ialfa, 30<=ialfa<=99'
       accept*,ialfa
       if(ialfa>29)then
        write(ialfa),R,iflow,(params(i),i=1,5)
        write(ialfa),n,m,n1,m1,n2,m2,nn,mm,yb,yg,yc,xg,xc,h,k,alpha
        do i=1,nn; do j=1,mm; write(ialfa),alfa(i,j); enddo;enddo
       close(ialfa)
        type*,'file FOR',ialfa,'.DAT created'
       end if
      type*
      endif
      type*
      type*,'print converged MU-VALUES ? : y for yes, n for no'
      accept'(a1)',answer
      if(answer.ge.'y') then
      type*;type*,'interpolation file name for mu-values ?'
      accept 'a12',filenm
        type*,' MU-VALUES,starting row j=M(i=1..N)';type*
        call PPRINT(mu,nm,nn,mm,70,filenm)
      end if
      end ! xprint



      subroutine PPRINT(u,nm,nn,mm,iunit,filenm)
c  prints array u , starting row j=M(i=1..N)
      real u(nm,nm)
      character*12, filenm
      open(unit=iunit,file=filenm,status='new')
        do j=mm,1,-1
                type*,'j=',j
                type 1,(u(i,j),i=1,nn)
              write(iunit,2),(u(i,j),i=1,nn)
        end do
 1    format(1x,22f6.3)
2     format(19(f5.3,','),f5.3)
      close(unit=iunit,status='keep')
      end ! PPRINT



      subroutine MAXDIF(uold,unew,dmax,nm,nn,mm)
c  finds max. difference between old u and new u
      real uold(nm,nm),unew(nm,nm)
      dmax=0
      do i=1,nn;do j=1,mm
        diff=abs(abs(uold(i,j))-abs(unew(i,j)))
        if(diff>dmax)dmax=diff
      end do; end do
      end ! maxdif



      subroutine couple(u,g,x,y,params,iflow,a,a1,a2,a4,a5,a8,a11,pi,nm)
c  calculates couple and power number
      real u(nm,nm),g(nm,nm),x(nm),y(nm),params(10),a(nm,nm),k
      common n,m,n1,m1,n2,m2,nn,mm,yb,yg,yc,xg,xc,h,k,alpha
      character answer
      type*;type*,'couple required? y for yes, n for no'
      accept '(a1)',answer

      IF(answer.ge.'y')THEN

      type*,'input inner radius ri, outer radius ro & angular speed '
      accept*,ri,ro,omega
      type*,'input fluid density,zero shear & infinite shear viscosity'
      accept*,rho,etazer,etainf
      xmuinf=etainf/etazer
      absg1=alpha**a4*(u(n+1,m)-1)+(u(n,m-1)-1)
```

```
        absg1=abs(absg1/(alpha**a2+1))
        absg1=2*absg1/(k**a2*sqrt(3.0))
        absg2=alpha**a4*(u(n+1,m2)-1)+(u(n,m2+1)-1)
        absg2=abs(absg2/(alpha**a2+1))
        absg2=2*absg2/(k**a2*sqrt(3.0))
c  fill elements a(1,1)..a(n,1) with function values & integrate to find
c  first integral in couple equation
          twoh=2*h; twok=2*k
        a(1,1)=0 ;a(n,1)=0
        do i=2,n-1
          a(i,1)=x(i)*x(i)*x(i)*vis(params,g(i,m),iflow)
          a(i,1)=a(i,1)*abs(u(i,m-2)+3-4*u(i,m-1))/twok
          a(i,1)=a(i,1)-a2*x(i)*x(i)*x(i)*xmuinf*absg1*(1-x(i))**(-a1)
        end do
        call trapz(a,1,n,h,firsti,nm)
c  now repeat to find second integral in couple
        a(m,1)=0; a(m2,1)=0
        do i=m+1,m2-1
          a(i,1)=vis(params,g(n,i),iflow)*abs(4*u(n+1,i)-3-u(n+2,i))/twoh
          a(i,1)=a(i,1)-a2*xmuinf*absg1*((y(i)-yb)**(-a1))
          a(i,1)=a(i,1)-a2*xmuinf*absg2*((yg-y(i))**(-a1))
        end do
        call trapz(a,m,m2,k,secndi,nm)
c  now repeat to find third integral in couple
        a(n2,1)=0; a(n,1)=0
        do i=n2,n-1
          a(i,1)=x(i)*x(i)*x(i)*vis(params,g(i,m2),iflow)
          a(i,1)=a(i,1)*abs(4*u(i,m2+1)-3-u(i,m2+2))/twok
          a(i,1)=a(i,1)-a2*x(i)*x(i)*x(i)*xmuinf*absg2*(1-x(i))**(-a1)
        end do
        call trapz(a,n2,n,h,thirdi,nm)
c  now repeat to find fourth integral in couple
        a(m2,1)=0
        do i=m2,mm
        a(i,1)=vis(params,g(n2,i),iflow)*abs(4*u(n2+1,i)-3-u(n2+2,i))/twoh
        a(i,1)=a(i,1)*((ri**3)/(ro**3))
        end do
        call trapz(a,m2,mm,k,forthi,nm)
        gterm=xmuinf*absg1*(81.0/220.0)+xmuinf*(yg-yb)**a2*(absg1+absg2)
        gterm=gterm-((2.0/11.0)*(1-xg)**a11)+((3.0/4.0)*(1-xg)**a8)-
     2              ((6.0/5.0)*(1-xg)**a5)+((1-xg)**a2)
        couple=2*pi*omega*etazer*ro**3*(firsti+secndi+thirdi+forthi+gterm)
        powrno=couple/(rho*omega*omega*ro**5)
        type*;type*;type*,'couple=',couple,'   power no.=',powrno
        type*

        end IF
        end ! couple



        subroutine trapz(f,istart,iend,stpsiz,sum,nm)
c  uses trapezium rule with stepsize stpsiz to evaluate the integral of the
c  function values f(istart,1)..f(iend,1)
c  a 2D array f is used to avoid declaring a new 1D array in the main program
        real f(nm,nm)
        sum=f(istart,1)+f(iend,1)
        do i=istart+1,iend-1; sum=sum+2*f(i,1); end do
        sum=0.5*stpsiz*sum
        end ! trapz

        subroutine GRAFIX(x,y,u,t,g,params,iflow,nm,alfa,xi,mu,unused)
c  graphical output options
        real x(nm),y(nm),u(nm,nm),t(nm,nm),g(nm,nm),params(10),
     &       xpts(5),ypts(5),contor(10),alfa(nm,nm),xi(nm,nm),mu(nm,nm)
        real k,xu(81,81)
        logical unused(nm,nm)
        common n,m,n1,m1,n2,m2,nn,mm,yb,yg,yc,xg,xc,h,k,alpha
        external j06gbz,j06gbu;   character answer
c  j06gbz(or j06gby),j06gbu(or j06gbv,j06gbw) are for graphics section
        type*;type*,'graphical output? y for yes ,n for no'
        accept'(a1)',answer
        IF(answer.ge.'y')THEN

          xpts(1)=0;xpts(2)=1;xpts(3)=1;xpts(4)=xg;xpts(5)=xg
          ypts(1)=yb;ypts(2)=yb;ypts(3)=yg;ypts(4)=yg;ypts(5)=yc

          type*;type*,'graphs on same or different sheets? type s or d'
          accept '(a1)',answer; type*

          IF(answer.eq.'d')then ! graphs on different sheets

          type*,'write R-values by hand on graphs';type*
          type*;type*,'graph of u? type y or n'
          accept '(a1)',answer; type*

          if(answer.eq.'y')then ! plot u
            type*;type*,'how many u-contours? (max.=10)';accept*,nu
            type*,'which u-values? '; accept*,(contor(i),i=1,nu);type*
```

```
            call setdev(2)                              ! set up graph-plotter
            call j06waf                                 ! initialise graphics
            call j06wbf(0.0,xc,0.0,yc,1)
            call j06wcf(0.05,0.85,0.05,0.85)            ! define viewport
            call j06xgf(1.0,0.6)
            call j06aef                                       ! axes,border
            call j06baf(xpts,ypts,5,1,2,ifail)                ! draw rotor
            call j06gdf(u,x,y,nm,1,nn,1,mm,nu,contor,1,
     2                  j06gbz,1,0,j06gbu,0,unused,ifail)  ! draws contours
            call j06wzf
c
c           call subroutine to plot headings using plot10
c
            call plothd('U (VELOCITY)',12,iflow,params(1),params(2),
     2      params(3),params(4),h,k,r,yb,nu,contor,yg,yc)
          end if

          type*;type*,'graph of xu? type y or n'
          accept '(a1)',answer; type*

          if(answer.eq.'y')then ! plot xu
             do i=1,nn; do j=1,mm
                xu(i,j)= x(i) * u(i,j)
             end do; end do
c  adjust t in rotor
            do i=1,n-1;do j=m+1,m2-1;xu(i,j)=9;enddo;enddo
            do i=1,n2-1;do j=m2,mm;xu(i,j)=9;end do;end do
            type*;type*,'how many xu-contours? (max.=10)';accept*,nxu
            type*,'which xu-values? '; accept*,(contor(i),i=1,nxu);type*

            call setdev(2)                              ! set up graph-plotter
            call j06waf                                 ! initialise graphics
            call j06wbf(0.0,xc,0.0,yc,1)
            call j06wcf(0.05,0.85,0.05,0.85)            ! define viewport
            call j06xgf(1.0,0.6)
            call j06aef                                 ! axes,border
            call j06baf(xpts,ypts,5,1,2,ifail)               ! draw rotor
            call j06gdf(xu,x,y,nm,1,nn,1,mm,nxu,contor,
     2             1,j06gbz,1,0,j06gbu,0,unused,ifail)   ! draws contours
            call j06wzf
c
c           call subroutine to plot headings using plot10
c
            call plothd('XU (x.u) CONTOURS',17,iflow,params(1),params(2)
     2      ,params(3),params(4),h,k,r,yb,nxu,contor,yg,yc)
c  re-adjust in rotor
            do i=1,n-1;do j=m+1,m2-1;xu(i,j)=0;enddo;enddo
            do i=1,n2-1;do j=m2,mm;xu(i,j)=0;end do;enddo
          end if

          type*;type*,'graph of T ? type y or n'
          accept '(a1)',answer; type*

          if(answer.eq.'y')then ! plot t
c  adjust t in rotor
            do i=1,n-1;do j=m+1,m2-1;t(i,j)=9;enddo;enddo
            do i=1,n2-1;do j=m2,mm;t(i,j)=9;end do;end do
            type*;type*,'how many t-contours ? (max=10)'; accept*,nu
            type*,'which t-values ? '; accept*,(contor(i),i=1,nu);type*

            call setdev(2)                               ! set up graph-plotter
            call j06waf
            call j06wbf(0.0,xc,0.0,yc,1)
            call j06wcf(0.05,0.85,0.05,0.85)            ! define viewport
            call j06xgf(1.0,0.6)
            call j06aef
            call j06baf(xpts,ypts,5,1,2,ifail)
        TYPE*,'IFAIL=', IFAIL
            call j06gdf(t,x,y,nm,1,nn,1,mm,nu,contor,1,
     2                  j06gbz,1,0,j06gbu,0,unused,ifail)
            call j06wzf
c
c           call subroutine to plot headings using plot10
c
            call plothd('T (X.X.U)',9,iflow,params(1),params(2),
     2      params(3),params(4),h,k,r,yb,nu,contor,yg,yc)
c  re-adjust in rotor
            do i=1,n-1;do j=m+1,m2-1;t(i,j)=0;enddo;enddo
            do i=1,n2-1;do j=m2,mm;t(i,j)=0;end do;enddo
          end if

          type*;type*,'graph of g ? type y or n'
          accept '(a1)',answer; type*

          if(answer.eq.'y')then ! plot g
c  adjust g values inside rotor
            do i=1,n-1;do j=m+1,m2-1; g(i,j)=999; end do; end do
            do i=1,n2-1;do j=m2,mm;g(i,j)=999;end do;end do
            type*;type*,'how many g-contours? (max.=10)';accept*,ng
```

```
            type*,'which g-values? '; accept*,(contor(i),i=1,ng);type*
            call setdev(2)                          ! set up graph-plotter
            call j06waf
            call j06wbf(0.0,xc,0.0,yc,1)
            call j06wcf(0.05,0.85,0.05,0.85)        ! define viewport
            call j06xgf(1.0,0.6)
            call j06aef
            call j06baf(xpts,ypts,5,1,2,ifail)
            call j06gdf(g,x,y,nm,1,nn,1,mm,ng,contor,1,
     2                  j06gbz,1,0,j06gbu,0,unused,ifail)
            call j06wzf
c
c           call subroutine to plot headings using plot10
c
            call plothd('G (SHEAR-RATE)',14,iflow,params(1),params(2),
     2      params(3),params(4),h,k,r,yb,ng,contor,yg,yc)
c  reset rotor  values to zeros
            do i=1,n-1; do j=m+1,m2-1; g(i,j)=0; end do; end do
            do i=1,n2-1;do j=m2,mm;g(i,j)=0; end do;end do
          end if

        type*;type*,'graph of xi ? type y or n'
          accept '(a1)',answer; type*

          if(answer.eq.'y')then ! plot xi
c  adjust xi values inside rotor
            do i=1,n-1;do j=m+1,m2-1; xi(i,j)=999; end do; end do
            do i=1,n2-1;do j=m2,mm;xi(i,j)=999;end do;end do
            type*;type*,'how many xi-contours? (max.=10)';accept*,nxi
            type*,'which xi-values?';accept*,(contor(i),i=1,nxi);type*

            call setdev(2)                          ! set up graph-plotter
            call j06waf
            call j06wbf(0.0,xc,0.0,yc,1)
            call j06wcf(0.05,0.85,0.05,0.85)        ! define viewport
            call j06xgf(1.0,0.6)
            call j06aef
            call j06baf(xpts,ypts,5,1,2,ifail)
            call j06gdf(xi,x,y,nm,1,nn,1,mm,nxi,contor,1,
     2                  j06gbz,1,0,j06gbu,0,unused,ifail)
            call j06wzf
c
c           call subroutine to plot headings using plot10
c
            call plothd('XI (VORTICITY)',14,iflow,params(1),
     2      params(2),params(3),params(4),h,k,r,yb,nxi,contor,yg,yc)
c  reset rotor  values to zeros
            do i=1,n-1; do j=m+1,m2-1; xi(i,j)=0; end do; end do
            do i=1,n2-1;do j=m2,mm;xi(i,j)=0; end do;end do
          end if

          type*;type*,'graph of alfa ? type y or n'
          accept '(a1)',answer; type*

          if(answer.eq.'y')then ! plot alfa
            type*;type*,'how many alfa-contours? (max.=10)';accept*,nalfa
            type*,'which alfa-values?';accept*,(contor(i),i=1,nalfa);type*

            call setdev(2)                          ! set up graph-plotter
            call j06waf
            call j06wbf(0.0,xc,0.0,yc,1)
            call j06wcf(0.05,0.85,0.05,0.85)        ! define viewport
            call j06xgf(1.0,0.6)
            call j06aef
            call j06baf(xpts,ypts,5,1,2,ifail)
            call j06gdf(alfa,x,y,nm,1,nn,1,mm,nalfa,contor,1,
     2                  j06gbz,1,0,j06gbu,0,unused,ifail)
            call j06wzf
c
c           call subroutine to plot headings using plot10
c
            call plothd('ALFA (STREAMLINES)',18,iflow,params(1),
     2      params(2),params(3),params(4),h,k,r,yb,nalfa,contor,yg,yc)
          end if

          type*;type*,'graph of mu ? type y or n'
          accept '(a1)',answer; type*

          if(answer.eq.'y')then ! plot mu
c  adjust mu in rotor
            do i=1,n-1;do j=m+1,m2-1;mu(i,j)=9;enddo;enddo
            do i=1,n2-1;do j=m2,mm;mu(i,j)=9;end do;end do
            type*;type*,'how many mu-contours? (max.=10)';accept*,nmu
            type*,'which mu-values?';accept*,(contor(i),i=1,nmu);type*

            call setdev(2)                          ! set up graph-plotter
            call j06waf
            call j06wbf(0.0,xc,0.0,yc,1)
            call j06wcf(0.05,0.85,0.05,0.85)        ! define viewport
```

```
            call j06xgf(1.0,0.6)
            call j06aef
            call j06baf(xpts,ypts,5,1,2,ifail)
            call j06gdf(mu,x,y,nm,1,nn,1,mm,nmu,contor,1,
     2                  j06gbz,1,0,j06gbu,0,unused,ifail)
            call j06wzf
c
c           call subroutine to plot headings using plot10
c
            call plothd('mu (VISCOSITY)',14,iflow,params(1),
     2      params(2),params(3),params(4),h,k,r,yb,nmu,contor,yg,yc)
c  re-adjust in rotor
            do i=1,n-1;do j=m+1,m2-1;mu(i,j)=0;enddo;enddo
            do i=1,n2-1;do j=m2,mm;mu(i,j)=0;end do;enddo
          end if

          ELSE ! graphs on same sheet

        type*,'write fluid details,contour keys etc by hand on graphs'
c  plot u
            type*;type*,'how many u-contours? (max.=10)';accept*,nu
            type*,'which u-values? '; accept*,(contor(i),i=1,nu);type*

            call setdev(2)                          ! set up graph-plotter
            call j06waf
            call j06wbf(0.0,xc,0.0,yc,1)
            call j06wcf(0.00,0.50,0.50,1.00)
            call j06xgf(1.0,0.6)
            call j06ylf(0.8,0.0)
            call j06aef
            call j06baf(xpts,ypts,5,1,2,ifail)
            call j06gdf(u,x,y,nm,1,nn,1,mm,nu,contor,1,
        2                 j06gbz,1,0,j06gbu,0,unused,ifail)
            call j06yaf(0.0,yc-0.5)
            call j06zaf(8h       u ,8)
c  plot t
            type*;type*,'how many t-contours ? (max=10)'; accept*,nu
            type*,'which t-values ? '; accept*,(contor(i),i=1,nu)

            call j06wcf(0.50,1.00,0.50,1.00)
            call j06aef
            call j06baf(xpts,ypts,5,1,2,ifail)
            call j06gdf(t,x,y,nm,1,nn,1,mm,nu,contor,1,
        2                 j06gbz,1,0,j06gbu,0,unused,ifail)
            call j06yaf(0.0,yc-0.5)
            call j06zaf(8h     T    ,8)
c  plot g
c  adjust g values inside rotor
            do i=1,n-1; do j=m+1,m2-1; g(i,j)=999; end do; end do
            do i=1,n2-1; do j=m2,mm;g(i,j)=999; end do;end do
            type*;type*,'how many g-contours? (max.=10)';accept*,ng
            type*,'which g-values? '; accept*,(contor(i),i=1,ng)
            call j06wcf(0.00,0.50,0.00,0.50)
            call j06aef
            call j06baf(xpts,ypts,5,1,2,ifail)
            call j06gdf(g,x,y,nm,1,nn,1,mm,ng,contor,1,
        2                 j06gbz,1,0,j06gbu,0,unused,ifail)
            call j06yaf(0.0,yc-0.5)
            call j06zaf(8h        g,8)
c  reset rotor g-values to zeros
            do i=1,n-1; do j=m+1,m2-1; g(i,j)=0; end do;end do
            do i=1,n2-1; do j=m2,mm; g(i,j)=0;end do;end do
c  plot alfa
            type*;type*,'how many alfa-contours? (max.=10)';accept*,nalfa
            type*,'which alfa-values? '; accept*,(contor(i),i=1,nalfa)
            call j06wcf(0.50,1.00,0.00,0.50)
            call j06aef
            call j06baf(xpts,ypts,5,1,2,ifail)
            call j06gdf(alfa,x,y,nm,1,nn,1,mm,nalfa,contor,1,
        2                 j06gbz,1,0,j06gbu,0,unused,ifail)
            call j06yaf(0.0,yc-0.5)
            call j06zaf(8h a l f a,8)
            call j06wzf

          end IF
        type*,'stop program now ? y or n';accept'(a1)',answer
        if(answer.eq.'y')stop
        end IF

        end ! graphix



        subroutine TITLE(iflow,params,h,k)
c  attempts to print a graph title
        real params(*),k

            call j06wcf(0.05,0.20,0.85,1.0)      ! prepare fluid details
            call j06yaf(0.05,0.9)                ! move pen to top of sheet
```

```
            call j06zaf(5hiflow,5)              ! prints iflow
            call j06zbf(iflow,3)
            call j06wcf(0.1,0.35,0.85,1.0)
            call j06yaf(0.18,0.9)
            call j06zaf(3h : ,3)                ! prints params
            xx=.1
            do i=1,5
                xx=xx+.1
                call j06wcf(xx-.03,xx+.18,.85,1.0)
                call j06yaf(xx,.9)
                call j06zdf(params(i),9,3)
            end do
            call j06wcf(0.7,0.90,0.85,1.0)
            call j06yaf(0.6,0.9)
            call j06zaf(3h  h,3)                                    ! prints h
            call j06zdf(h,8,5)
            call j06wcf(0.85,1.00,0.85,1.0)
            call j06yaf(0.55,0.9)
            call j06zaf(3h  k,3)                                    ! prints k
            call j06zdf(k,8,5)

        end ! title


c  plot10 based subroutines

c  subroutine tvtext - plots n characters starting at ix,iy

            subroutine tvtext(k,ix,iy,text,n)
            dimension text(16),ichx(80)

c           break up string of characters in text and store individually

            decode(80,1000,text)ichx
 1000       format(80R1)

c           set character size to 1 (maximum)
            call swchar(1)
            call chrsiz(K)

c           move pen to ix,iy if either of these is non zero
c           leave pen in current position if both ix,iy are zero
            IF(ix.ne.0.or.iy.ne.0)call movabs(ix,iy)
c           repeat loop n times plotting one character each time
c           each character is plotted using plot10 subroutine ancho
            do i=1,N
            call ancho(ichx(i))
            enddo
            return
            end


c  subroutine plothd - plots headings and boxes using plot10 subroutines
            subroutine plothd(c,n,iflow,x1,x2,x3,x4,x5,x6,x7,yb,nc,z,yg,yc)
            dimension z(8),c(4),buff(2)
c           initialise plot10 graphics
            call initt(1200)
c           plot variable part of top heading (passed in call statement)
            call tvtext(1,100,700,c,n)
c           plot fixed part of top heading
            call tvtext(1,0,0,' CONTOURS FOR ',14)
c           plot variable part of top heading (dependent on iflow)
            IF(iflow.eq.0)call tvtext(1,0,0,'NEWTONIAN FLUID ',16)
            IF(iflow.eq.1)call tvtext(1,0,0,'POWER FLUID ',12)
            IF(iflow.eq.2)call tvtext(1,0,0,'CARREAU FLUID ',14)
            IF(iflow.eq.3)call tvtext(1,0,0,'CROSS FLUID ',12)
c           plot fixed part of top heading
            call tvtext(1,0,0,'(GAP =',6)
c           plot gap size in top heading
            encode(4,1003,buff)yb
            call tvtext(1,0,0,buff,4)
            call tvtext(1,0,0,')',1)
c           move pen to 100,690
            call movabs(100,690)
c           draw underline for top heading - length variable and
c           dependent on iflow and n
            IF(iflow.eq.0)call drwabs(655+n*15,690)
            IF(iflow.eq.1)call drwabs(595+n*15,690)
            IF(iflow.eq.2)call drwabs(625+n*15,690)
            IF(iflow.eq.3)call drwabs(595+n*15,690)
c           plot x-axis heading
            call tvtext(1,200,10,'DIMENSIONLESS RADIUS X',22)
c           character to achieve vertical plot of heading
            id=20
            call tvtext(1,10,560,'D',1)
            call tvtext(1,10,560-id,'I',1)
            call tvtext(1,10,560-2*id,'M',1)
            call tvtext(1,10,560-3*id,'E',1)
```

```
            call tvtext(1,10,560-4*id,'N',1)
            call tvtext(1,10,560-5*id,'S',1)
            call tvtext(1,10,560-6*id,'I',1)
            call tvtext(1,10,560-7*id,'O',1)
            call tvtext(1,10,560-8*id,'N',1)
            call tvtext(1,10,560-9*id,'L',1)
            call tvtext(1,10,560-10*id,'E',1)
            call tvtext(1,10,560-11*id,'S',1)
            call tvtext(1,10,560-12*id,'S',1)
            call tvtext(1,10,560-14*id,'H',1)
            call tvtext(1,10,560-15*id,'E',1)
            call tvtext(1,10,560-16*id,'I',1)
            call tvtext(1,10,560-17*id,'G',1)
            call tvtext(1,10,560-18*id,'H',1)
            call tvtext(1,10,560-19*id,'T',1)
            call tvtext(1,10,560,21*id,'Y',1)
c           calculate y-position for plotting of "DISC ROTOR" in ky
            ky=int((yb+yg)/(2.0*yc)*0.7*783.0+0.10*783.0)
c           plot "DISC ROTOR"
            call tvtext(1,140,ky,'DISC ROTOR',10)

c           draw box lines for contour key
            call movabs(760,625)
            call drwabs(960,625)
            call drwabs(960,565)
            call drwabs(760,565)
            call drwabs(760,625)
            call tvtext(1,784,560,'CONTOUR KEY',11)
            call movabs(760,565)
            call drwabs(760,565-nc*30)
            call movabs(820,565)
            call drwabs(820,565-nc*30)
            call movabs(960,565)
            call drwabs(960,565-nc*30)
            call movabs(760,565-nc*30)
            call drwabs(960,565-nc*30)
c           plot nc contour key values
            do 1100 i=1,nc
            encode(2,1001,buff)i
            call tvtext(1,770,548-i*30,buff,2)
            encode(7,1002,buff)z(i)
            call tvtext(1,840,buff)z(i)
            call tvtext(1,840,548-i*30,buff,7)
 1100       continue

c           draw box lines for parameters
            call movabs(760,340)
            call drwabs(960,340)
            call drwaba(960,280)
            call drwabs(760,280)
            call drwabs(760,340)
            call tvtext(1,792,300,'PARAMETERS',10)
            call movabs(760,280)
            call drwabs(760,70)
            call movabs(820,280)
            call drwabs(820,70)
            call movabs(960,280)
            call drwabs(960,70)
            call movabs(760,70)
            call drwabs(960,70)
c           plot parameter values
            encode(8,1000,buff)x1
            call tvtext(1,830,260,buff,8)
            encode(8,1000,buff)x2
            call tvtext(1,830,230,buff,8)
            encode(8,1000,buff)x3
            call tvtext(1,830,200,buff,8)
            encode(8,1000,buff)x4
            call tvtext(1,830,170,buff,8)
            encode(8,1000,buff)x5
            call tvtext(1,830,140,buff,8)
            encode(8,1000,buff)x6
            call tvtext(1,830,110,buff,10)
            encode(8,1000,buff)x7
            call tvtext(1,830,80,buff,10)

c           terminate plot10 graphics
            call finitt(0,0)
            return

 1000       format(F8.3)
 1001       format(I2)
 1002       format(F7.3)
 1003       format(F4.1)
            end


c  end of d10pp.for
```